

AD A074047

LEVEL

2/2



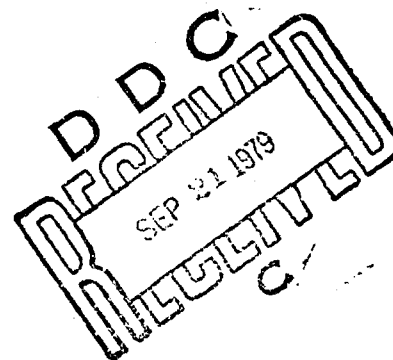
RADC-TR-79-56

Final Technical Report
August 1979

LINEAR MODULATION TECHNIQUES FOR DIGITAL MICROWAVE

Harris Corporation

Robert C. Davis



APPROVED FOR PUBLIC RELEASE; DISTRIBUTION UNLIMITED

Reproduced From
Best Available Copy


DDC FILE COPY

ROME AIR DEVELOPMENT CENTER
Air Force Systems Command
Griffiss Air Force Base, New York 13441

This report has been reviewed by the RADC Information Office (OI) and is releasable to the National Technical Information Service (NTIS). At NTIS it will be releasable to the general public, including foreign nations.

RADC-TR-79-56 has been reviewed and is approved for publication.

APPROVED:




FREDERICK D. SCHMANDT
Project Engineer

APPROVED:



FRED I. DIAMOND
Technical Director
Communications and Control Division

FOR THE COMMANDER:



JOHN P. HUSS
Acting Chief, Plans Office

If your address has changed or if you wish to be removed from the RADC mailing list, or if the addressee is no longer employed by your organization, please notify RADC (DCCT) Griffiss AFB NY 13441. This will assist us in maintaining a current mailing list.

Do not return this copy. Retain or destroy.

UNCLASSIFIED

SECURITY CLASSIFICATION OF THIS PAGE (When Data Entered)

19 REPORT DOCUMENTATION PAGE		READ INSTRUCTIONS BEFORE COMPLETING FORM
1. REPORT NUMBER RADC TR-79-56	2. GOVT ACCESSION NO.	3. RECIPIENT'S CATALOG NUMBER
4. TITLE (and Subtitle) LINEAR MODULATION TECHNIQUES FOR DIGITAL MICROWAVE	5. TYPE OF REPORT & PERIOD COVERED Final Technical Report, Mar 77 - Nov 78	6. PERFORMING ORG. REPORT NUMBER N/A
7. AUTHOR(s) Robert C. Davis	8. CONTRACT OR GRANT NUMBER(s) F30602-77-C-0039	
9. PERFORMING ORGANIZATION NAME AND ADDRESS Harris Corporation/Electronic Systems Division P O Box 37 Melbourne FL 32901	10. PROGRAM ELEMENT, PROJECT, TASK AREA & WORK UNIT NUMBERS 62702F 45192106	
11. CONTROLLING OFFICE NAME AND ADDRESS Rome Air Development Center (DCCT) Griffiss AFB NY 13441	12. REPORT DATE August 1979	13. NUMBER OF PAGES 338
14. MONITORING AGENCY NAME & ADDRESS (if different from Controlling Office) Same	15. SECURITY CLASS. (of this report) UNCLASSIFIED	15a. DECLASSIFICATION/DOWNGRADING SCHEDULE N/A
16. DISTRIBUTION STATEMENT (of this Report) Approved for public release; distribution unlimited.		
17. DISTRIBUTION STATEMENT (of the abstract entered in Block 20, if different from Report) Same		
18. SUPPLEMENTARY NOTES RADC Project Engineer: Frederick D. Schmandt (DCCT)		
19. KEY WORDS (Continue on reverse side if necessary and identify by block number) Digital Microwave Modulation		
20. ABSTRACT (Continue on reverse side if necessary and identify by block number) The objective of this program was to study and develop modulation techniques and implementation methods applicable to a linear digital microwave radio operating in the 4 and 8 GHz frequency bands. Modulation techniques capable of providing 3 to 4.5 bits/sec/Hz under the FCC Docket 19311 spectral criterion are developed and included herein. Techniques for the practical implementation of spectrally efficient linear modulation (AM-PM) signal designs in conjunction with presently available microwave power amplifiers are developed. An adaptive predistortion technique for linearizing nonlinear power amplifiers.		

DD FORM 1 JAN 73 1473

UNCLASSIFIED

SECURITY CLASSIFICATION OF THIS PAGE (When Data Entered)

408972

UNCLASSIFIED

SECURITY CLASSIFICATION OF THIS PAGE(When Data Entered)

(e.g., TWT's) for the purpose of counteracting AM/AM and AM/PM conversion effects is presented which is useful for linear digital signal designs. A new baseband adaptive equalization scheme which is suited to high rate digital modems is presented. M-ary Quadrature Amplitude Modulation (M-QAM) is chosen as the most efficient scheme for obtaining 3 to 5 bits/sec/Hz under FCC Docket 19311. Waveguide filtering is used to provide FCC Docket 19311 compliance with the M-QAM schemes. An error correction coding/decoding strategy which is applicable to M-QAM signal formats is presented. On the theoretical side, techniques for determining spectral and performance properties for constrained bandwidth digital signaling are discussed.

Accession For	
NTIS GRA&I	<input checked="checked" type="checkbox"/>
DDC TAB	<input type="checkbox"/>
Unann need	<input type="checkbox"/>
Just cation	<input type="checkbox"/>
By _____	
Distribution/	
Availability G & S	
Dist	Avail and/or special
A	

UNCLASSIFIED

SECURITY CLASSIFICATION OF THIS PAGE(When Data Entered)

TABLE OF CONTENTS

<u>Paragraph</u>	<u>Title</u>	<u>Page</u>
1.	INTRODUCTION AND GUIDE TO THE MAJOR RESULTS OF THIS STUDY	1-1
2.	THE ANALYTICAL CHARACTERIZATION OF DIGITAL SIGNALLING	2-1
2.1	Discussion of the Analytical Characterization	2-7
2.2	Some General Properties of Filters Consisting of a Transversal Filter and a Square Root Nyquist Filter in Tandem	2-10
2.2.2	Ratio of Peak-to-Average Pulse Energy With Transversal Filter and Square Root Nyquist Filter Combination	2-12
2.2.3	The Noise Bandwidth of Shaping Filters	2-15
2.2.4	Spectral Characteristics of Shaping Filters	2-17
2.2.5	Optimal Partial Response for Maximizing Percent Power in a Given Band	2-20
2.2.6	Performance Characteristics Of Systems Using Shaping Filters	2-23
2.2.6.1	Linear Equalizer Processors	2-24
2.2.6.1.1	Calculating the Noise Enhancement Factor in Perfect Equalizers ...	2-27
2.2.6.1.2	Performance With Perfect Equalization	2-30
2.2.6.2	How Performance is Determined For Viterbi Algorithm Sample Processors	2-33
2.2.7	A Technique For Converting a Given Filter to a Square-Root Nyquist Filter	2-35
2.2.7.1	Frequency Response Characteristics of the Converted Square Root Nyquist Filter	2-37
3.	THE SPECTRAL REQUIREMENTS OF FCC DOCKET 19311	3-1
3.1	Effect of Authorized Bandwidth on Capacity Under FCC Docket 19311	3-1
3.2	How the FCC Docket 19311 Spectral Mask Is Determined for a Given Signal Spectrum	3-6
4.	PERFORMANCE OF IDEAL DIGITAL COMMUNICATIONS SYSTEMS	4-1
4.1	Ideal M-PSK Systems	4-2
4.2	Ideal M-QAM Systems	4-4
4.2.1	Modified 6-QAM Signaling	4-8
4.2.1.1	Performance of Modified 6-QAM	4-9
4.3	Capacity of Ideal Systems Compared to Shannon Capacity	4-12
5.	THE SUSCEPTIBILITY OF BANDWIDTH EFFICIENT MODEMS TO INTERFERENCE AND OTHER OUTSIDE DISTURBANCES	5-1
6.	PERFORMANCE OF PRACTICAL DIGITAL COMMUNICATION SYSTEMS	6-1
6.1	Introduction	6-1
6.2	Systems Using Square Root Nyquist Shaping Filters	6-2
6.3	Partial Response in Conjunction With Square Root Nyquist Filters	6-13

TABLE OF CONTENTS (Continued)

<u>Paragraph</u>	<u>Title</u>	<u>Page</u>
6.3.1	Some Optimal Partial Response Results	6-17
6.3.1.1	Optimal Length Two Partial Response	6-18
6.3.1.2	Near-Optimal Length Three Partial Response	6-28
6.4	Performance of Systems Using Prolate Spheroid Pulse Shaping Filters	6-36
6.4.1	Discrete Characterization of the Prolate Spheroid Shaping Filter	6-41
6.4.2	Capacity of the Prolate Spheroid Pulse Shape Under FCC Docket 19311	6-44
6.4.3	Performance of the Prolate Spheroid Shaping Filter Scheme With Perfect Nyquist Equalization at Receiver	6-47
6.4.4	Performance of Prolate Spheroid Shaping Filter With Viterbi Algorithm Receiver	6-51
6.5	Performance of Transmitter-Filtered and Receiver-Equalized Systems	6-57
6.5.1	Introduction	6-57
6.5.2	Equalization Results for Impulse Signalling Through Butterworth Baseband Filters	6-58
6.5.2.1	M-QAM Results	6-70
6.5.2.2	M-PSK Results	6-73
6.5.3	Filtered and Equalized Square-Pulse Signaling	6-73
6.5.3.1	Spectrum Results	6-76
6.5.3.2	Performance Results	6-84
6.5.3.3	General Capacity Curve	6-84
6.6	Comparing Digital Transmission Schemes When the Power Amplifier is Peak Power Limited	6-90
6.6.1	Specific Cases - Power Amplifier Peak-Limited Performance	6-95
6.6.1.1	Nyquist Signaling	6-95
6.6.1.1.1	M-QAM, Nyquist Shaping	6-98
6.6.1.2	Duobinary Partial Response Shaping	6-100
6.6.1.2.1	Case 1: Duobinary-All Partial Response Filter at Transmitter	6-100
6.6.1.2.2	Case 2: duobinary Partial Response with Equal Division of Filtering	6-103
6.6.1.3	Peak Amplifier Power Limited M-QAM Signaling With 5-Pole Butterworth Transmit Waveguide Filter	6-107
6.6.2	Trade-Offs of Primary Candidate Schemes on Basis of Peak Power	6-110
6.6.2.1	Comments on the Peak Power Performance Trade-Offs	6-112
6.6.3	The Relative Theoretical Efficiencies of Preamplifier and Passive Postamplifier Spectral Shaping When the Amplifier is Peak Power Limited	6-117
6.7	Performance of Preamplifier Filtered M-QAM in Conjunction With a Linear Amplifier	6-122
6.7.1	Introduction	6-122
6.7.2	Performance Simulation Results for Filtered M-QAM Systems When Used With the Ford Linear Amplifier	6-128

TABLE OF CONTENTS (Continued)

<u>Paragraph</u>	<u>Title</u>	<u>Page</u>
6.7.3	Comparison Between Butterworth Waveguide Filtering and Baseband Filtering When the Ford Linear Amplifier is Used ...	6-140
6.8	Adaptive Predistortion Linearization of Power Amplifiers for Digital Signaling	6-144
6.8.1	Introduction	6-144
6.8.2	The effect of AM/AM and AM/PM Conversion	6-146
6.8.3	Implementing an Adaptive Predistortion Digital Modulator	6-148
6.8.4	Results Obtained for the Adaptive Predistortion Amplifier Linearization Scheme	6-152
6.8.4.1	Introduction	6-152
6.8.4.2	Signal Space Predistortion Results	6-152
6.8.4.3	Effect of Predistortion of Spectrum	6-158
6.9	Computer Simulations of M-QAM Modem Performance	6-170
6.9.1	Introduction	6-170
6.9.2	M-QAM Demodulator Description	6-170
6.9.2.1	Adaptive Equalization Technique	6-171
6.9.2.1.1	Performance Results Obtained With the Adaptive Baseband Equalization Technique	6-175
6.9.3	M-QAM Simulation Results for Various Implementation Imperfections	6-176
6.9.3.1	Performance of Nominal M-QAM Modem with TWT Amplifier	6-184
6.9.3.2	Performance Sensitivity to Receiver Phase Reference Jitter	6-184
6.9.3.3	Performance Sensitivity to Receiver Symbol Timing	6-184
6.9.3.4	Performance Sensitivity to AGC Variation	6-190
6.9.4	Performance of Modem with SAW Device Receive IF Filters	6-190
6.9.5	Computer Simulations - Summary and Conclusions	6-200
7.	AN APPLICATION OF ERROR CORRECTION CODING TECHNIQUES TO A SPECTRALLY-EFFICIENT DIGITAL MODEM	7-1
8.	SUMMARY AND MAJOR CONCLUSIONS OF THIS STUDY	8-1

APPENDICES

A1	Channel Capacity Bounds and Their Relevance to Signal Design ..	A1-2
A2	Minimum Bandwidth Pulse Shape	A2-2
A3	Coding Gain For High Bit Packing Density Signalling Schemes ...	A3-2
A3.1	Introduction	A3-2
A3.2	Channel Capacity	A3-2
A3.3	One Bit/Symbol Code Example	A3-4
A3.4	Importance of Considering Coding and Modulation Jointly	A3-6
A4	Bibliography and References	A4-2

LIST OF ILLUSTRATIONS

<u>Figure</u>	<u>Title</u>	<u>Page</u>
2-1	General Optimum Receiver	2-1
2-2	An Equivalent Representation for $h(t)$ Filter	2-3
2-3	Proof That Filter 2 is Square root Nyquist	2-4
2-4	An Equivalent Representation of the Digital System of Figure 2-1	2-5
2-5	Equivalent Representation of Arbitrary Pulse-Shaped digital system With Optimum Receiver	2-5
2-6	Discrete Characterization for Digital Signalling Scheme ...	2-6
2.1-1	The Pulse Shaping Filter	2-8
2.2	Tandem Combination of Transversal Filter and Square Root Nyquist Filter	2-10
2.2.4	General Transversal Filter Spectrum	2-19
2.2.6-1	General Optimum Receiver Structure for Digital Signaling ..	2-24
2.2.6-2	Discrete Characterization of System in Figure 2.2.6-1	2-24
2.2.6-3	Perfectly Equalized Systems Under Consideration	2-30
2.2.6-4	Equivalent to Figure 2.2.6-3 as Far as Performance of Decision Device is Concerned	2-31
2.2.6.2	Discrete Representation of Digital Transmission Scheme With a Viterbi Algorithm Processor	2-33
2.2.7-1	An Analytical Representation of Filter With Impulse Response, $h(t)$	2-36
2.2.7-2	Conversion of $h(t)$ into Square Root Nyquist	2-37
3.1-1	FCC Docket 19311 Spectrum Masks	3-2
3.1-2	A Typical Spectrum	3-5
3.1-3	Approximate Factor r by Which the Capacity of a System Operating in Authorized Bandwidth of B_a MHz Exceeds that of the Same System in 3.5 MHz Bandwidth	3-7
3.1-4	Showing How FCC 19311 Mask is Produced for a Typical Spectrum	3-9
4-1	Ideal Digital Communication System Using Quadrature Modulation	4-1
4-2	Specific Signal Designs	4-3
4.1	Ideal M-ARY PSK Performance	4-5
4.2	Ideal M-QAM Performance	4-7
4.2.1	Modified 6-QAM Signal Design	4-8
4.2.1.1	Modified 6-QAM Performance	4-12
4.3	Channel Capacity Comparisons M-QAM and M-PSK Ideal System .	4-13
5-1	4-QAM Signal Design	5-2
5-2	Worst-Case Degradation for M-ARY PAM on Quadrature Carriers Versus Interference	5-6
6.2-1	Systems With Square Root Nyquist Shaping Filters	6-2
6.2-2	Spectra With Square root Raised Cosine Filters	6-4
6.2-3	Spectrum for $\alpha = 0.2$ Square Root Raised Cosine Filter	6-6
6.2-4	Spectrum for $\alpha = 0.5$ Square Root Nyquist Shaping Filter ...	6-7

LIST OF ILLUSTRATIONS (Continued)

Figure	Title	Page
6.2-5	Spectrum for $\alpha = 1.0$ Square root Raised Cosine Filter	6-8
6.2-6	Symbols/Sec/Hz for Square Root Raised Cosine Shaping Filters	6-9
6.2-7	Capacity Versus Performance With M-QAM Signaling for Square Root Raised Cosine Shaping Filters, $\alpha =$ Rolloff Parameter, $P(E) = 10^{-5}$	6-10
6.2-8	Capacity Versus Performance With M-PSK Signaling for Square Root Raised Cosine Shaping Filters	6-12
6.3.1	Partial Response Signaling System	6-17
6.3.1.1-1	Duobinary Partial Response With $\alpha = 0$ Filter	6-19
6.3.1.1-2	Duobinary Partial Response With $\alpha = 0.2$	6-20
6.3.1.1-3	Duobinary Partial Response With $\alpha = 0.5$	6-21
6.3.1.1-4	Duobinary Partial Response With $\alpha = 1.0$	6-22
6.3.1.1-5	Performance of M-ARY Signaling Through Duobinary Transmit Filter for Viterbi Algorithm Demodulation	6-24
6.3.1.1-6	Symbols/s/Hz for Duobinary Partial Response Through Square Root Cosine Filter With Rolloff Parameter, α	6-25
6.3.1.1-7	Capacity Versus Performance of Duo M-ARY Partial Response Shaping With Viterbi Algorithm Receiver $P(E) = 10^{-5}$	6-26
6.3.1.1-8	Comparison of Systems Using No Partial Response and Duobinary Partial Response for $\alpha = 0.2$	6-27
6.3.1.2-1	$f(D) = 0.4723 + 0.74422d + 0.4723D^2$ PR 3, $\alpha = 0.5$, BT = 0.3	6-29
6.3.1.2-2	$f(D) = 0.43216 + 0.7915D + 0.43216D^2$ PR 3, $\alpha = 0.5$, BT = 0.4	6-30
6.3.1.2-3	Optimum Length 3 Partial Response for BT = 0.5 for = 0.5 for $\alpha = 0.5$ $\sqrt{\text{Raised Cosine Filter}}$	6-31
6.3.1.2-4	Optimum Length 3 Partial Response for BT = 0.6 for = 0.6 for $\alpha = 0.5$ $\sqrt{\text{Raised Cosine Filter}}$	6-32
6.3.1.2-5	Performance of M-ARY Signaling Through Partial Response $f(D) = 0.4723 + 0.74422 D + 0.4723 D^2$ With Viterbi Algorithm Demodulation	6-34
6.3.1.2-6	Capacity Versus Performance for Optimal Length 3 Partial Response Through $\alpha = 0.5$ Square Root Raised Cosine Shaping Filter, Viterbi Demodulation	6-35
6.3.1.2-7	Capacity Versus Performance for Optimum Partial Responses Used With $\alpha = 0.5$ Rolloff Square Root Cosine Filter Viterbi Demodulation, $P(E) = 10^{-5}$	6-37
6.4-1	Digital System With Prolate Spheroid Shaping Filters	6-38
6.4-2	Prolate Spheroid Spectrum for $BT_p = 1.9$ Out-of- Band Power = -40 dB	6-39
6.4-3	Prolate Spheroid Spectrum for $B_m T_p = 2.2$ Out-of-Band Power = -50 dB	6-40
6.4-4	-50 dB Spectral Occupancy Prolate Spheroid Pulse Shape	6-42
6.4.1	Pulse Autocorrelation Function for Prolate Spheroid -50 dB Pulse	6-43

LIST OF ILLUSTRATIONS (Continued)

<u>Figure</u>	<u>Title</u>	<u>Page</u>
6.4.2	Capacity in Symbols/s/Hz for -50 dB Prolate Spheroid Function	6-46
6.4.3-1	Degradation Versus μ for Prolate Spheroid Shaping Filter With Perfect Nyquist Equalization at Receiver	6-48
6.4.3-2	Combinations of Symbols/s/Hz and Degradation for Prolate Spheroid Shaping Filter With Perfect Receiver Equalization	6-49
6.4.3-3	Capacity Versus Performance of Nyquist Equalized Prolate Spheroid Pulse Shape for M-QAM Signaling $P(E) = 10^{-5}$	6-50
6.4.3-4	Capacity Versus Performance of Nyquist Equalized Prolate Spheroid Pulse Shape for M-PSK Signaling $P(E) = 10^{-5}$	6-52
6.4.4-1	Viterbi Algorithm Performance for Prolate Spheroid Pulse Shaped M-QAM	6-53
6.4.4-2	Viterbi Algorithm Performance for Prolate Spheroid Pulse Shaped M-QAM	6-54
6.4.4-3	Viterbi Algorithm Performance for Prolate Spheroid Pulse Shaped M-QAM	6-55
6.4.4-4	Capacity Versus Performance for Viterbi Algorithm Processor for Prolate Spheroid Pulse Shaped M-QAM $P(E) = 10^{-5}$	6-56
6.5.1	Digital System with Transmit Shaping Filter and Receiver Equalization	6-57
6.5.2-1	Butterworth Spectra $f_0 = 3$ dB BW	6-59
6.5.2-2	Five-Pole Butterworth Transmit and Receiver Filters 3 dB BW = $\beta \times$ Symbol Rate Performance With Ideal Nyquist Equalization	6-60
6.5.2-3	Five-Pole Butterworth Transmit and Receiver Filters 3 dB BW = $\beta \times$ Symbol Rate Ideal Equalization to Duobinary	6-61
6.5.2-4	Degradation for Five-Pole Butterworth Transmit and Receiver Filters	6-62
6.5.2-5	Eight-Pole Butterworth Transmit and Receive Filters 3 dB BW = $\beta \times$ Symbol Rate Ideal Nyquist Equalization	6-63
6.5.2-6	Eight-Pole Butterworth Transmit and Receive Filters 3 dB BW = $\beta \times$ Symbol Rate Ideal Duobinary Equalization ..	6-63
6.5.2-7	Eight-Pole Butterworth Transmit and Receive Filters Ideal Equalization to Designated Partial Response	6-64
6.5.2-8	Symbols/s/Hz Under FCC 19311 for Butterworth Spectra Versus Filter Bandwidth	6-67
6.5.2-9	Combinations of Symbols/s/Hz and Degradation for Equalized Five-Pole Butterworth Filters	6-68
6.5.2-10	Combinations of Symbols/s/Hz and Degradation for Equalized Eight-Pole Butterworth Filters	6-69
6.5.2.1.1	Capacity Versus Performance of Equalized Five-Pole Butterworth Filters for M-QAM Signaling $P(E) = 10^{-5}$	6-71
6.5.2.1-2	Capacity Versus Performance of Equalized Eight-Pole Butterworth Filters for M-QAM Signaling $P(E) = 10^{-5}$	6-72

LIST OF ILLUSTRATIONS (Continued)

<u>Figure</u>	<u>Title</u>	<u>Page</u>
6.5.2.2-1	Capacity Versus Performance of Nyquist Equalized Five-Pole Butterworth Filters for M-PSK Signaling $P(E) = 10^{-5}$	6-74
6.5.2.2-2	Capacity Versus Performance of Nyquist Equalized Eight-Pole Butterworth Filters for M-PSK Signaling $P(E) = 10^{-5}$	6-75
6.5.3	Digital Transmission With Square Pulse Signalling Shaping Filter and Equalized Receiver	6-76
6.5.3.1-1	$\beta = 0.3$ Five-Pole Butterworth Filter on PAM	6-78
6.5.3.1-2	$\beta = 0.35$ Five-Pole Butterworth Filter on PAM	6-79
6.5.3.1-3	$\beta = 0.14$ Five-Pole Butterworth Filter on PAM	6-80
6.5.3.1-4	$\beta = 0.5$ Five-Pole Butterworth Filter on PAM	6-81
6.5.3.1-5	$\beta = 0.6$ Five-Pole Butterworth Filter on PAM	6-82
6.5.3.1-6	Symbols/s/Hz Possible Under FCC 19311 for Square Pulse Signalling Through Five-Pole Butterworth Filter	6-83
6.5.3.2	Five-Pole Butterworth Filters on PAM With Receiver Equalization	6-85
6.5.3.3-1	Combinations of Symbols/s/Hz and Performance for Square Pulse Signalling Through Five-Pole Butterworth Filters With Receive Equalization	6-86
6.5.3.3-2	Capacity Versus Performance of Equalized Five-Pole Butterworth Filters for M-QAM Signalling $P(E) = 10^{-5}$	6-88
6.5.3.3-3	Capacity Versus Performance of Equalized Five-Pole Butterworth Filters for M-PSK Signalling $P(E) = 10^{-5}$	6-89
6.6	General Digital Transmission Scheme	6-90
6.6.1.1	Transfer Functions for Square Root Raised Cosine Filters Compensated for $\text{SIN}(\pi f T)/\pi f T$ Rolloff	6-97
6.6.1.1.1-1	Amplifier Peak-Limited M-QAM Nyquist Signaling Performance Equal Transmit-Receive Filtering	6-99
6.6.1.1.1-2	Amplifier Peak-Limited M-QAM Nyquist Signaling Performance	6-101
6.6.1.2.1-1	Full Duobinary Transmit Filter With $\text{Sin}(\pi f T)/\pi f T$ Compensation	6-102
6.6.1.2.1-2	Amplifier Peak Limited M-QAM With Duobinary Partial Response Shaping Filter All at Transmitter	6-104
6.6.1.2.2-1	Transfer Function of Transmit Filter for Equal Division of Duobinary Signaling	6-105
6.6.1.2.2-2	Amplifier Peak Limited M-QAM With Duobinary Partial Response Shaping Filter Equally Divided Between Transmitter and Receiver	6-106
6.6.1.3-1	dB Power Loss Due to Filtering PAM With 5-Pole Butterworth Filters	6-108
6.6.1.3-2	Peak Power Limited Filtered M-QAM With Receiver Equalization	6-109
6.6.2-1	Comparison of Equalized Butterworth Performance With Cosine Rolloff (Duobinary) and Raised Cosine Rolloff (Nyquist) Performance	6-111
6.6.2-2	Peak Power Limited Comparison Between Ideal Sharp Cutoff M-QAM and 5-Pole Butterworth Filtered-and-Equalized M-QAM	6-113

LIST OF ILLUSTRATIONS (Continued)

Figure	Title	Page
6.6.3a	System Employing Preamplifier Filtering	6-118
6.6.3b	System Employing Passive Postamplifier Filtering	6-118
6.7-1	IMD Versus RF Power Output, Two Signal	6-123
6.7-2	Power Transfer Curve (AM-AM)	6-124
6.7-3	Relative Phase Versus RF Input Power	6-125
6.7-4	Relative Phase Versus RF Input Power	6-126
6.7.2-1	Modelled System	6-129
6.7.2-2	4-ary QAM Ford Linear AMP	6-130
6.7.2-3	4-ary Ford Linear AMP	6-131
6.7.2-4	4-ary QAM Ford Linear AMP	6-133
6.7.2-5	4-ary QAM Ford Linear AMP	6-134
6.7.2-6	4-ary QAM - Ford Linear AMP	6-135
6.7.2-7	Ford Linear AMP 8-QAM 0 dB Backoff	6-137
6.7.2-8	8-QAM with Ford AMP 1 dB Backoff	6-138
6.7.2-9	Power Versus Backoff for 10^{-7} , 8-QAM, $\alpha = 0.5$	6-139
6.7.3	Comparison Between M-QAM Schemes Using Ford Linear AMP $P(E) = 10^{-5}$	6-142
6.8.1	Model Nonlinear TWT Amplifier Input-Output Characteristics	6-145
6.8.2-1	A Representative Digital Modulation Signal Point	6-146
6.8.2-2	Predistorted Input Signal Point	6-147
6.8.3	Adaptive Power Amplifier Linearization Scheme for Digital AM/PM Modulator	6-149
6.8.4.2-1	TWT Output Signal Points With Predistortion Correction - Arbitrary Peak Power Backoff	6-154
6.8.4.2-2	TWT Predistorted Inputs to Produce No Distortion on Output	6-155
6.8.4.2-3	TWT Output Signal Points With No Predistortion Correction	6-156
6.8.4.2-4	TWT Predistorted Input for Zero Output Distortion	6-157
6.8.4.2-5	TWT Output Signal Points With No Predistortion Correction	6-159
6.8.4.3-1	Sinc Spectrum	6-160
6.8.4.3-2	Five-Pole Waveguide Filter Insertion Loss	6-162
6.8.4.3-3	Ford Linear Amp	6-164
6.8.4.3-4	Ford Linear Amp	6-165
6.8.4.3-5	Ford Linear Amp	6-167
6.8.4.3-6	Ford Linear Amp	6-168
6.9.2.1	M-QAM Demodulator With Adaptive RAM Equalization	6-172
6.9.2.1.1-1	Performance of 8-QAM Demodulator	6-177
6.9.2.1.1-2	Performance of 4-QAM Demodulator With Baseband Equalizer ..	6-178
6.9.3-1	Receiver Equalizer Filter	6-181
6.9.3-2	Performance of M-QAM 5-Pole Butterworth Transmitter Filter 3 dB BW = $0.5 \times SR$	6-182
6.9.3.1	8-QAM Performance With TWT Amplifier	6-185
6.9.3.2-1	8-QAM Sensitivity to Phase Reference Jitter	6-186
6.9.3.2-2	4-QAM Sensitivity to Phase Reference Jitter	6-187
6.9.3.3-1	8-QAM Sensitivity to Symbol Timing Variation	6-188
6.9.3.3-2	4-QAM Sensitivity to Symbol Timing Variation	6-189
6.9.3.4-1	8-QAM Sensitivity to AGC Variation	6-191
6.9.3.4-2	4-QAM Sensitivity to AGC Variation	6-192
6.9.4-1	$\alpha = 0.25$ Raised Cosine Frequency Response	6-193

LIST OF ILLUSTRATIONS (Continued)

<u>Figure</u>	<u>Title</u>	<u>Page</u>
6.9.4-2	8-QAM - Sensitivity to AGC	6-194
6.9.4-3	8-QAM Performance	6-196
6.9.4-4	8-QAM SAW Filter Performance	6-197
6.9.4-5	8-QAM Performance	6-198
6.9.4-6	4-QAM Performance	6-199
7-1	Error Correction Coding, Rate = 5/6, Applied to 8-Level Modulation	7-2
7-2	8-QAM Performance With Rate 5/6 Coding	7-4
7-3	Rate 4/6 Error Correction Coding Applied to an 8-Level Modulator	7-5
7-4	Performance of Rate 2/3 Coding With 8-QAM Modulator	7-7
8-1	Overall LMT System Block Diagram	8-5
8-2	LMT Modem Spectrum	8-6
8-3	LMT Practical Hardware Modem Performance	8-8
A1	Theoretical Bound $\frac{R}{W}$ Versus ρ	A1-5
A2-1	Normalized Spectral Occupancy, $f_b T$ Versus R Optimum Pulse	A2-5
A2-2	Optimum Pulse Shape for 40 dB Spectral Occupancy	A2-6
A2-3	Slepian and Pollak's $\psi_0(t)$	A2-7
A2-4	μ Versus B_s/B_A for Constant In-Band Power Using Prolate Spheroidal Functions	A2-9
A2-5	Out-of-Band Power Versus B_s/B_A for Constant μ Using Prolate Spheroidal Functions	A2-10
A3-1	Comparison of Capacity Curves with Actual System Performance (Systems Have $P(e) = 10^{-5}$)	A3-3
A3-2a	4-ary PAM Baseband Voltages	A3-4
A3-2b	Rate One-Half Constraint Length 3 Convolution Code	A3-5

LIST OF TABLES

<u>Title</u>	<u>Title</u>	<u>Page</u>
6.4.1	R(D), f(D), and Roots of f(D) for System Using Prolate Spheroid μ Symbols Long	6-44
6.6.1.1	Spectral Truncation Power Loss when Equal Transmit Receive Raised cosine Nyquist Signaling is Used	6-98
6.9.2.1.1-1	Nominal Conditions Simulated (8-QAM)	6-175
6.9.2.1.1-2	Nominal Conditions Simulated (4-QAM)	6-179
6.9.3'	Nominal Conditions for Sensitivity Simulations	6-183

EVALUATION

The attainment of bandwidth efficient digital communication over line-of-sight (LOS) had been limited by non-linear power amplifiers. The optimal signals for bandwidth efficiency are those wherein information is stored in the signal amplitude. In order to perform well, such signal structures require linear operation and the linearity requirements increase as bandwidth efficiencies increase. Linearization of the amplifier by backing it off results in lower power output and thus lower system gain which can reduce system availability.

An alternative approach is to use techniques which store the information entirely in phase or frequency and which consequently are not affected by non-linearities. Above 2 bits/sec/Hz efficiencies the performance of such techniques rapidly decreases, mitigating against their use at higher efficiencies.

The above restricted the development of practical modems to bandwidth efficiencies of approximately 2 bits/sec/Hz. Advances in the development of microwave linear power amplifiers (RADC contract F30602-76-C-0271 for example) reduced amplifier backoff requirements and caused this new focus on signal structures involving amplitude modulation for attaining higher bandwidth efficiencies.

As a result of this study it is concluded that practical modem designs can achieve spectral efficiencies in the 3 to 5 bits/sec/Hz range under the FCC Dockett 19311 spectral criterion. M-QAM signalling is concluded to be the most desirable modulation technique of those considered: a design plan for such a modem has been obtained. The novel adaptive predistortion technique developed for linearizing the power amplifier almost totally removes

the amplifier as a degrading influence in the system - even for peak drive levels approaching single signal saturation. The employment of this technique allows the use of presently available power amplifiers (usually TWT's) for high spectral efficiency modems. It can also remove the pressure on microwave amplifier designers to attain increasingly stringent distortion levels in order to support digital signalling at increasing spectral efficiencies. A linear amplifier, like that developed under contract F30602-76-C-0271, can be used with the modem but the peak input drive levels must be limited to 2.5 to 3.5 dB below signal saturation to prevent severe distortion unless the amplifier linearization technique is utilized. If the linearization technique is utilized the additional expense of a more linear amplifier is not needed.

The demodulator design incorporates a new baseband equalization technique which represents a considerable improvement from a complexity standpoint over standard transversal equalizer techniques.

The techniques uncovered under this effort are considered prime candidates for incorporation into the design of the future DCS III microwave system being investigated under TPO R4A. Provided this promise is borne out during the investigations to be carried out under the "ECCM for the DCS" contractual effort, a breadboard implementation of the designed modem should be undertaken to prove out the practicality of the developments (particularly the amplifier linearization and baseband equalization techniques) of this contractual effort. These techniques are expected to be significant factors in future line-of-sight digital microwave designs investigated under TPO's R3B and R4A.


FREDERICK D. SCHMANDT
Project Engineer

1. INTRODUCTION AND GUIDE TO THE MAJOR RESULTS OF THIS STUDY

This final technical report represents the culmination of the study effort on linear modulation techniques for digital microwave. This study effort was performed in response to the growing pressure for increased capacity digital transmission schemes for the line-of-sight microwave military communication system.

Prior efforts to achieve high spectral efficiency digital transmission over microwave systems have generally adopted constant envelope signal designs.¹²⁻¹⁹ The reason for the adoption of these constant envelope schemes has, in the past, been because of the lack of a practical, operational, linear amplifier of sufficient power output at the microwave frequencies. For example, traveling wave tube (TWT) amplifiers are generally used at the microwave frequencies and the TWT amplifiers have rather severe distortion characteristics (unless backed off rather drastically) that are inconsistent with the requirements of most linear modulation schemes. The restriction of the digital signal design to a constant envelope variety, while making efficient use of the peak power amplifier capability, cuts the designer off from the greater theoretical spectral efficiencies available with signal designs which also use amplitude as a degree of freedom. (See Paragraph 4.3.)

Ongoing developments of "linear" amplifiers for microwave are providing improved power output and linearity characteristics. (See Paragraph 6.7.1.) It was therefore a purpose of this study to determine the effectiveness with which a realistic "linear" amplifier could be used in conjunction with linear digital modulation formats. (See Paragraph 6.7.2.) It was found in this study (as expected) that the linearity requirements for high spectral efficiency modems are quite stringent. For a range of spectral efficiencies from 3 to 5 bits/sec/Hz, it is felt that 30 to 45 dB down distortion levels (third order intermod's, for example) are required to avoid rather severe performance degradation (see Section 5). For compliance with the FCC Docket 19311 spectral mask

through the use of only preamplifier filtering, the intermod distortion levels required of a "linear" amplifier are likely to be even more stringent than from the performance degradation standpoint. Perhaps 50 dB down third-order intermods may be required to comply with the stringent FCC Docket 19311 mask when compliance is attempted using only preamplifier filtering (see Paragraph 6.8.4.3).

The attainment of 40 to 50 dB down intermod distortion at respectable power output levels for the operational microwave application is an extremely difficult task to assign to the amplifier analog designer. Consequently, we felt that a more realistic, robust, digital linear modulation scheme would involve adaptation to the presently available amplifier characteristics. From the digital signaling viewpoint, it was recognized that basically the power amplifier need only output the correct combinations of amplitude and phase at a relatively small set of discrete signal format points. A means was discovered on this study to adaptively "predistort" the combinations of input amplitude and phase to force the proper output combinations of amplitude and phase. Thus, for the purposes of digital data transmission, the amplifier is rendered free of distortion. This scheme has been shown to be effective in conjunction with even TWT amplifiers having rather severe AM/AM and AM/PM conversion characteristics. The discovery and development of this adaptive predistortion linearization technique is felt to be a major result of the present study. The technique is described in Paragraph 6.8.

An apparently new technique for adaptive baseband receiver equalization was also developed on this study. The effectiveness of this technique is demonstrated for an M-QAM (QASK) signal format in Paragraph 6.9.2.1. The technique offers performance within 1.5 dB of ideal M-QAM at 10^{-9} error rate using realistic filters, but is not so complex to implement as an adaptive IF equalizer.

New coding concepts for obtaining improved performance with spectrally efficient modems are presented in Section 7. Results indicating up to 5 dB coding gain over uncoded performance at 3 bits/sec/Hz are presented there.

Computer simulation performance results are presented for a variety of equipment imperfections in an M-QAM modem design in Paragraph 6.9.3. The M-QAM design is chosen (see Paragraph 6.6.2) as the most efficient technique for obtaining 3 to 5 bits/sec/Hz spectral efficiencies under FCC Docket 19311 criteria. This selection is made on the basis of peak power amplifier capability required; which, as argued in Paragraph 6.6, is the proper selection criterion for the microwave environment.

From a theoretical standpoint, the unifying analytical characterization for linear digital modulation schemes presented in Section 2. and due to Forney,¹ provides many useful analytical tools for the evaluation of performance and spectral characteristics. We feel that this analytical characterization provides a theoretical framework within which to work that is indispensable to any research activity concerned with spectrally-efficient digital modem development. We have made use of this characterization throughout this study to obtain many of the specific results presented in ensuing sections.

The culmination, from a practical viewpoint, of this study is the presentation in Paragraph 6.8.3 and Paragraph 6.9.2 of block diagrams for an M-QAM modulator/demodulator incorporating all the major results and conclusions of this study. The modulator employs the adaptive predistortion amplifier linearization technique. Consequently, it can be used in conjunction with TWT amplifiers driven near saturation on peaks. The demodulator adopts the baseband equalization technique alluded to previously. A waveguide filter is employed to provide FCC Docket 19311 mask compliance.

In summary, we believe that this study provides many results of interest to most workers in the field of spectrally-efficient digital linear modulation techniques for line-of-sight microwave.

2. THE ANALYTICAL CHARACTERIZATION OF DIGITAL SIGNALLING

Here we will discuss a viewpoint for the general digital signalling pulse-shaping filter problem that is useful in analyzing the performance of such systems. Most of this viewpoint is directly attributable to Forney's¹ excellent paper, "Maximum Likelihood Sequence Estimation of Digital Sequences in the Presence of Intersymbol Interference." This paper is highly recommended and we feel it is necessary to any researcher in the constrained bandwidth digital communication area.

Suppose one has a pulse-shaping filter with impulse response, $h(t)$. Forney shows that the optimum receiver for digital signalling in the presence of additive white Gaussian noise (AWGN) with such a shaping filter is as shown in Figure 2-1. The optimum receiver under any criterion of optimality whatsoever is representable as in Figure 2-1. The receiver consists of a filter matched to the transmit pulse shape, the output of which is sampled at the baud rate, followed by a processor for these samples. The structure of the sample processor is the only variable as one changes the criterion of optimality.

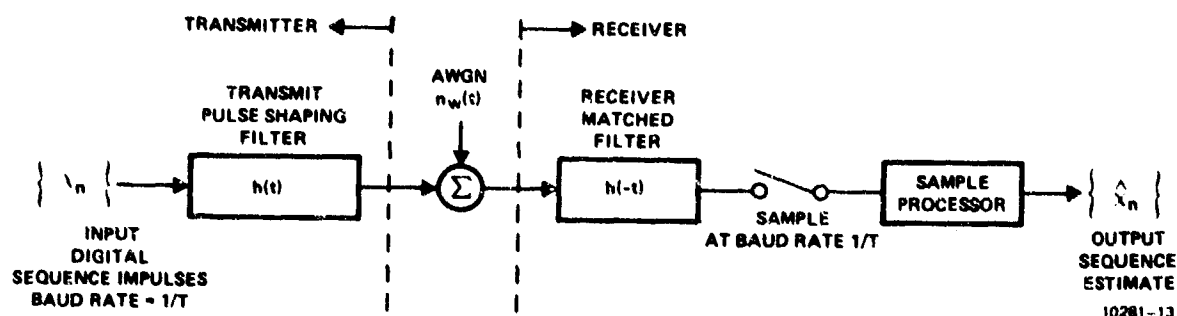


Figure 2-1. General Optimum Receiver

A point of interest in this system is the overall impulse response of the tandem combination of the transmit pulse-shaping filter and the receiver matched filter. This impulse response is given by

$$R_{hh}(t) = \int_{-\infty}^{+\infty} h(x) h(x+t) dx, \quad (2-1)$$

i.e., the autocorrelation function of the transmit shaping filter impulse response. Following Forney, a polynomial $R(D)$ is defined such that

$$R(D) = \sum_{i=-\infty}^{+\infty} R_{hh}(iT) D^i \quad (2-2)$$

The coefficients of $R(D)$ are symmetrical, i.e.,

$$R_{hh}(iT) = R_{hh}(-iT) \quad (2-3)$$

Hence, if β is a root of $R(D)$, then β^{-1} is also. This implies that one can factor $R(D)$ as

$$R(D) = f(D)f(D^{-1}) \quad (2-4)$$

where $f(D)$ contains all factors arising from β roots and $f(D^{-1})$ contains all factors arising from β^{-1} roots. It is noted that if $f(D)$ is thought of as the tap gain polynomial for a transversal filter then $f(D^{-1})$ corresponds to a transversal filter with reversed tap gains.

The polynomial $R(D)$ describes an equivalent transversal filter that filters the input data sequence to provide the sampled data output from the overall tandem combination of transmit and receive filters of Figure 2-1.

An interesting viewpoint is produced when one chooses to represent the original transmit filter with impulse response $h(t)$ by the scheme shown in Figure 2-2. Here, we have placed two cancelling transversal filters in series ahead of the original filter.

For arbitrary $f(D)$, the impulse response of the overall combination is unchanged by the incorporation of the two transversal filters shown in Figure 2-2. Here, $f(D)$ will be chosen as defined in Eq. (2-4). Under this condition it will be shown that Filter (2) in Figure 2-2 is a square root of Nyquist filter. This then will imply that an arbitrary filter, $h(t)$, can be viewed exactly as the tandem combination of a transversal filter, $f(D)$, and a square-root of Nyquist filter.

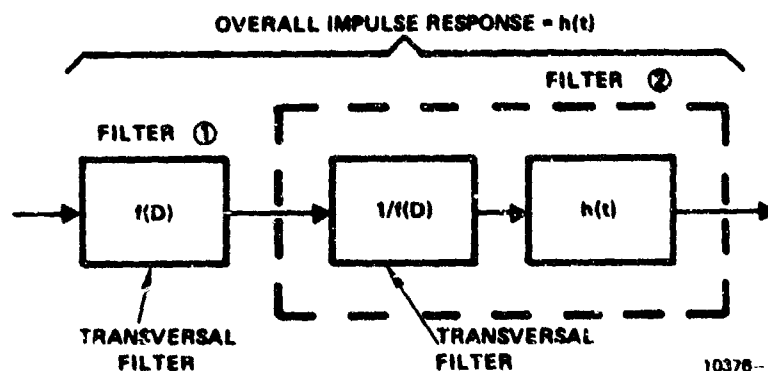


Figure 2-2. An Equivalent Representation for $h(t)$ Filter

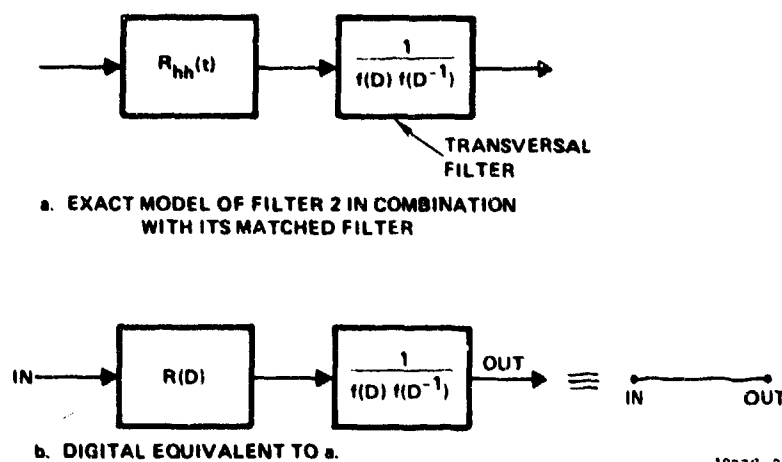
First, we define what is meant by a "square root of Nyquist filter."

Definition: A filter, which in tandem with its matched filter, produces no crosstalk with impulse signalling at baud time sampling intervals is a square root of Nyquist filter.

The frequency response of such a filter is the square root of the frequency response of a Nyquist filter, hence the name.

The tandem combination of filter (2) in Figure 2-2 and its matched filter is shown in Figure 2-3a. Here a filter with impulse response $R_{hh}(t)$ represents the combination of $h(t)$ and its matched filter, $h(-t)$. The transversal filter, $1/(f(D)f(D^{-1}))$ represents the

combination of the $1/f(D)$ transversal filter and its matched (reversed tap gains) counterpart, $1/f(D^{-1})$. With baud time sampling, the filter of Figure 2-3a has the digital equivalent of Figure 2-3b. By the definition of $f(D)$ as given in Equation (2-4), it is obvious that zero intersymbol interference results. Therefore, Filter 2 of Figure 2-2 represents a square root of Nyquist filter, by the previous definition.



10378 2

Figure 2-3. Proof that Filter 2 is Square Root Nyquist

With the partitioning of the pulse-shaping filter in the manner described above, the digital transmission scheme of Figure 2-1 can be drawn as in Figure 2-4. The matched square root of Nyquist receiver front-end filter is in fact Forney's¹ whitened matched filter. With additive white Gaussian noise (AWGN) having two-sided spectral density $N_0/2$ at the input, the output noise samples from any $\sqrt{\text{Nyquist}}$ filter are uncorrelated and have variance $= N_0/2$. It is therefore seen that the transversal filter, $1/f(D^{-1})$, serves to whiten the noise (at sample times) from the matched filter, $h(-t)$.

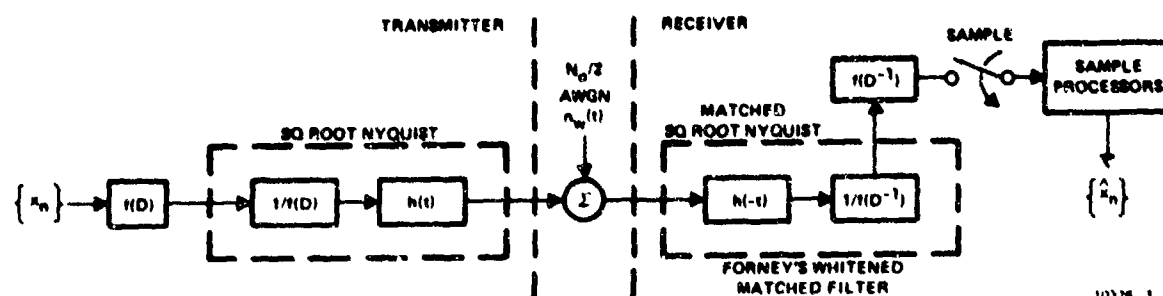


Figure 2-4. An Equivalent Representation of the Digital System of Figure 2-1

Obviously no change is incurred at the receiver if the sampling is done directly at the output of the whitened matched filter (WMF), and the transversal filter, $f(D^{-1})$, conceptually incorporated into the sample processor, if needed. One thus arrives at the totally equivalent representation of the digital signalling scheme shown first in Figure 2-1 as now shown in Figure 2-5.

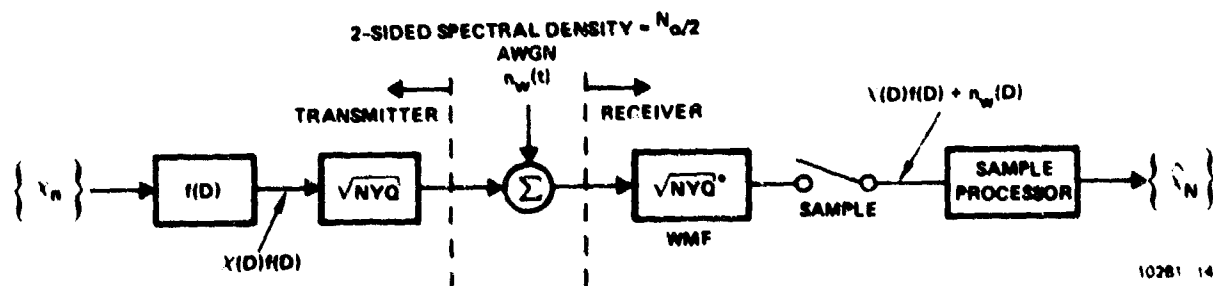


Figure 2-5. Equivalent Representation of Arbitrary Pulse-Shaped Digital System With Optimum Receiver

The combination of the transmitter and receiver $\sqrt{\text{Nyquist}}$ filters is transparent to the digital impulses passing through them since they form a Nyquist channel. If the input sequence $\{x_n\}$, at the transmitter is characterized by a polynomial, $x(D)$, where

$$x(D) = x_0 + x_1 D + x_2 D^2 + \dots, \quad (2-5)$$

then the input sequence to the sample processor at the receiver is characterized by the polynomial, $z(D)$, where

$$z(D) = x(D)f(D) + n_w(D) \quad (2-6)$$

The polynomial, $n_w(D)$, represents the effect of noise on the received samples. The coefficients of $n_w(D)$ are uncorrelated Gaussian and have variance $N_0/2$.

Thus one has the totally discrete characterization of the general digital transmission system with optimum receiver shown in Figure 2-6.

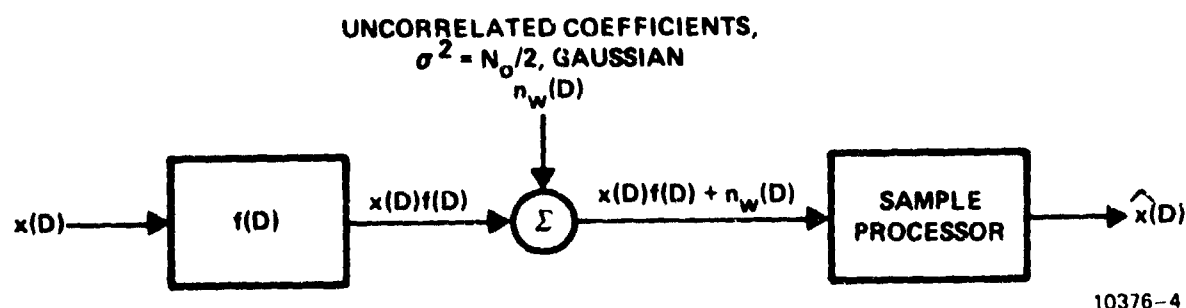


Figure 2-6. Discrete Characterization for Digital Signalling Scheme

The only element required from the given system in order to perform this characterization is $f(D)$. The polynomial $f(D)$ is determined

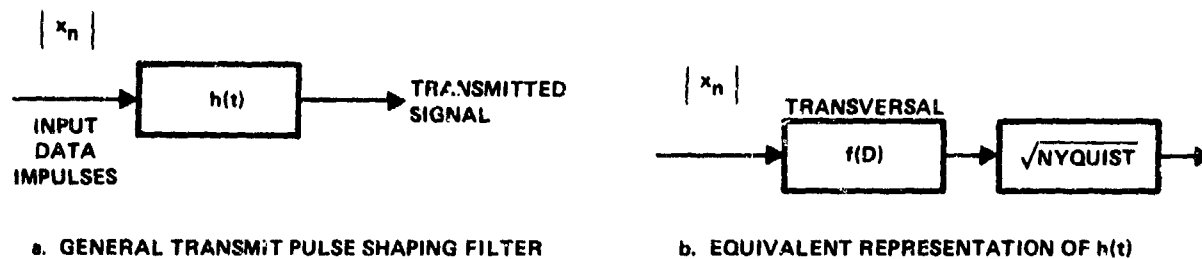
from the original pulse-shaping filter through Equations (2-1), (2-2), and (2-4).

2.1 Discussion of the Analytical Characterization

In this section we discuss the engineering impact of the analytical characterization for the general pulse-shaping digital transmission scheme presented in the preceding section. We shall discuss its impact from a couple of viewpoints relevant to the present study. First, what are its implications on the problem of pulse-shaping for spectral containment? Second, of what use is this characterization in predicting performance for such systems?

The system engineer is confronted with a very challenging problem when he tries to determine the optimal pulse shaping filter to employ in a digital signalling scheme that allows maximum bits/s/Hz operation. Generally he understands that he must reconcile the conflicting requirements of minimizing some measure of bandwidth while maximizing some measure of performance. The fundamental mechanism by which he exercises control over both these measures is through the choice of the pulse shaping filter characterized in the previous section. The problem is that there are an infinite number of choices for such a filter. How does he go about deciding which is right for his application? We feel that the analytical characterization presented in the previous section provides a framework within which the system designer can operate and obtain some meaningful answers to that question. As we shall be discussing in the model developed above attributable to Forney,¹ the performance is solely determined by the polynomial, $f(D)$. The radiated spectrum is jointly determined by $f(D)$ and the particular $\sqrt{\text{Nyquist}}$ filter employed in the characterization.

Figure 2.1-1a shows the transmit shaping filter at the control of the system designer for affecting spectral containment. Figure 2.1-1b shows its analytical equivalent.



10376-5

Figure 2.1-1. The Pulse Shaping Filter

From the system design viewpoint, the decision on what $h(t)$ impulse response to use is rather overwhelming. Should it be of infinite or finite duration? In either case what should its particular functional form be? If a particular choice is made, what is its spectrum, performance, and sensitivity to practically encountered perturbations from ideal? Has a choice been made that places unattainable requirements on the hardware designer?

We submit that finding the answers to such questions is made more tractable to the system designer if he recognizes that he can equivalently ask questions about what $f(D)$ and square root Nyquist filter combinations to choose in the representation of Figure 2.1-1b. It is not clear but that from implementation viewpoints the designer might even wish to build the shaping filter as shown in Figure 2.1-1b, i.e., as a transversal filter followed by a square root Nyquist filter. Certainly the practical problems of implementing square root Nyquist filters for digital signalling are better understood than those associated with building general partial response filters. Also, the implementation of the transversal filter specified by $f(D)$ is a relatively easy task.

For the system designer to adopt the position that he will perform a search for good shaping filters for implementation as shown in Figure 2.1-1b he needs to convince himself that he has not removed any "practically interesting" filters from consideration. By "practically interesting," we mean a shaping filter that lends itself to practical implementation and is tolerant to practically-encountered perturbations from the ideal specified pulse shape.

What we have shown in the previous section is that any shaping filter -- "practically interesting" or not -- is representable as shown in Figure 2.1-1b. Although we cannot conclusively prove it, it seems reasonable to assume that a practically interesting general pulse shape, $h(t)$, in Figure 2.1-1a will have a practically interesting $f(D)$ and square root Nyquist representation in Figure 2.1-1b. Conversely, it is certainly true that interesting filters implemented as in Figure 2.1-1b is not overly-constrained as a practical matter. The belief is that once one has located a good transversal filter - square root Nyquist filter combination to use from performance/spectrum viewpoints, it can be theoretically bettered only by a filter corresponding to more complex $f(D)$ (longer crosstalk span for example) and/or more complex square root Nyquist filter (steeper response rolloff for example) and thus more practical problems will probably be encountered with such a theoretically "better" filter. In any case, in the next few sections we will be restricting ourselves to an investigation of the characteristics associated with filters implemented as a tandem combination of transversal filter and square root Nyquist filter as in Figure 2.1-1b.

2.2

Figure 2.2 shows the type of filter considered here. One series element of the overall filter is a transversal filter characterized by the impulse response, $h_1(t)$, given by

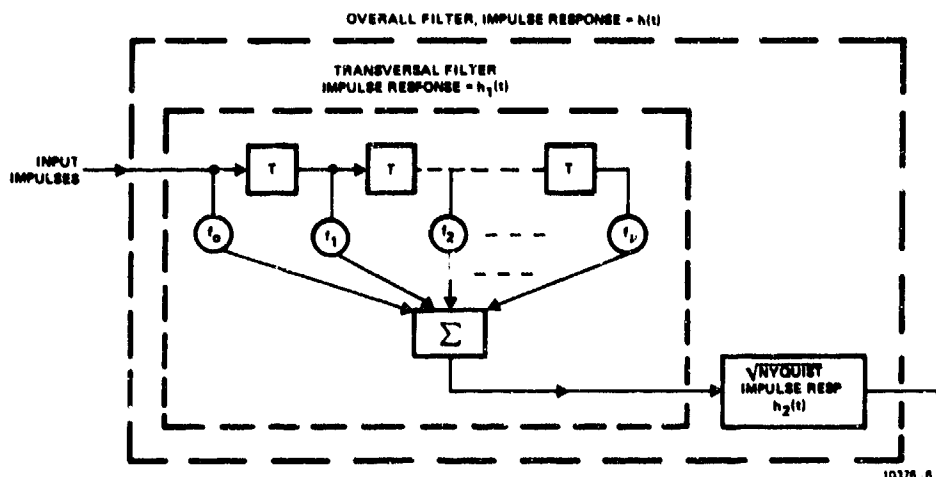


Figure 2.2. Tandem Combination of Transversal Filter and Square Root Nyquist Filter

$$h_1(t) = \sum_{i=0}^{\nu} f_i \delta(t - iT) \quad (2.2-1)$$

The other series element of the overall filter is a square root Nyquist filter characterized by impulse response, $h_2(t)$. We assume here that the impulse response, $h_2(t)$, is normalized to have energy, E_n , i.e.,

$$\int_{-\infty}^{+\infty} h_2^2(t) dt = E_n \quad (2.2-2)$$

The overall impulse response of the tandem combination of filters is given by

$$h(t) = \int_{-\infty}^{+\infty} h_1(x) h_2(t-x) dx \quad (2.2-3)$$

that is, the convolution of the two impulse responses. From Equations (2.2-1) and (2.2-3)

$$h(t) = \int_{-\infty}^{+\infty} \sum_{i=0}^{\nu} f_i \delta(x - iT) h_2(t - x) dx$$

$$h(t) = \sum_{i=0}^{\nu} f_i h_2(t - iT) \quad (2.2-4)$$

2.2.1 The Energy in the Overall Filter Impulse Response

The pulse energy of the overall filter impulse response is given by

$$E = \int_{-\infty}^{+\infty} h^2(t) dt \quad (2.2-5)$$

From Equations (2.2-4) and (2.2-5) we obtain

$$E = \sum_{i=0}^{\nu} \sum_{j=0}^{\nu} f_i f_j \int_{-\infty}^{+\infty} h_2(t - iT) h_2(t - jT) dt \quad (2.2-6)$$

Making a change of variable, $x = t - iT$, Equation (2.2-6) can be written as

$$E = \sum_{i=0}^{\nu} \sum_{j=0}^{\nu} f_i f_j \int_{-\infty}^{+\infty} h_2(x) h_2(x - (j - i)T) dx \quad (2.2-7)$$

The integral of Equation (2.2-7) is recognized as the impulse response at $t = (j - i)T$ of the square root Nyquist filter in combination with its matched filter counterpart. By the previously given definition of a square root Nyquist filter, the integral is thus zero except for $j = i$. Thus, Equation (2.2-7) becomes

$$E = \int_{-\infty}^{+\infty} h_2^2(x) dx \sum_{i=0}^{\nu} f_i^2 \quad (2.2-8)$$

By the definition of Equation (2.2-2), Equation (2.2-8) becomes

$$E = E_n \sum_{i=0}^{\nu} f_i^2 \quad (2.2-9)$$

Therefore, the impulse energy of the overall filter is simply the sum of the squares of the tap gains in the transversal filter times the energy of the square root Nyquist filter's impulse response.

2.2.2 Ratio of Peak-to-Average pulse Energy With Transversal Filter and Square Root Nyquist Filter Combination

We wish to demonstrate the fact that the use of partial response in a transmit filter of the type shown in Figure 2.2 results in an increase of peak output pulse energy over the peak pulse energy for no partial response.

Obviously, peak output of the transversal filter of Figure 2.2 is given by

$$T_{pk} = p_d \sum_{i=0}^{\nu} |f_i| \quad (2.2-10)$$

where T_{pk} = transversal filter peak output

p_d = peak data input magnitude

f_i = i th gain in transversal filter

It has been assumed that the data has symmetrical peaks at $\pm p_d$ and the sign on each peak data entry in the transversal filter has been chosen to correspond to the sign of the associated tap gain.

When this peak transversal filter output is input to the square root Nyquist filter, a pulse of peak energy, E_p , where

$$E_p = (T_{pk})^2 E_n \quad (2.2-11)$$

is produced. The average pulse energy on the other hand is given by E_a :

$$E_a = \sigma_d^2 E \quad (2.2-12)$$

where σ_d^2 = data mean square value

E = Overall filter pulse energy from Equation (2.2-9)

Using Equation (2.2-9) in Equation (2.2-12) we have

$$E_a = \sigma_d^2 E_n \sum_{i=0}^{\nu} f_i^2 \quad (2.2-13)$$

The ratio of peak-to-average energy is thus given by

$$\frac{E_p}{E_a} = \frac{(T_{pk})^2}{\sigma_d^2 \sum_{i=0}^{\nu} f_i^2} \quad (2.2-14)$$

Using Equation (2.2-10) in Equation (2.2-14), we have

$$\frac{E_p}{E_a} = \left(\frac{p_d^2}{\sigma_d^2} \right) \frac{\sum_{i=0}^{\nu} \sum_{k=0}^{\nu} |f_i f_k|}{\sum_{i=0}^{\nu} f_i^2} \quad (2.2-15)$$

Equation (2.2-15) can also be written as

$$\frac{E_p}{E_a} = \left(\frac{P_d}{\sigma_d^2} \right)^2 \left\{ 1 + \frac{\left[\sum_{i=0}^{\nu} \sum_{k \neq i}^{\nu} |f_i f_k| \right]}{\sum_{i=0}^{\nu} f_i^2} \right\} \quad (2.2-16)$$

The factor, $(P_d/\sigma_d^2)^2$, in Equation (2.2-16) is the ratio of peak-to-average energy of the data input. The term in brackets is never less than unity. The only case for which it is unity is for $\nu = 0$, that is, for no partial response filtering. Thus we see that the use of partial response generally always increases the ratio of peak-to-average transmitted pulse energy or power.

As an example, the factor in brackets is computed for duobinary partial response where $\nu = 1$ and $f_0 = 1$ and $f_1 = 1$. In this case,

$$\begin{aligned} \sum_{i=0}^1 \sum_{k \neq i}^1 |f_i f_k| &= f_0 f_1 + f_1 f_0 \\ &= 2 \end{aligned}$$

and

$$\sum_{i=0}^1 f_i^2 = 2$$

These quantities used in Equation (2.2-16) yield

$$\left(\frac{E_p}{E_a} \right)_{\text{duobinary}} = \left(\frac{P_d}{\sigma_d^2} \right)^2 (2) \quad (2)$$

Thus we see that duobinary partial response results in a peak-to-average power ratio that is 3 dB higher than the corresponding ratio for the input data (or for a system using no partial response).

A situation where consideration of peak-to-average power ratio becomes important is when operating over a peak power limited channel, as opposed to an average power limited channel. Suppose two different digital transmission schemes require the same average signal-to-noise ratio for a prescribed performance. But further suppose that one uses partial response and requires 3 dB higher peak-average power ratio than the other. Even though the performance of the two systems is identical on the basis of average power, the system with 3 dB higher peak-average power ratio is at a 3 dB disadvantage when used on the peak power limited channel.

Microwave power amplifiers tend to be peak power limited devices as opposed to average power limited. That is, there tends to be an output power level above which the distortion incurred becomes excessive or at which the output power saturates. The output power level of a typical TWT amplifier even decreases as the drive level exceeds saturation drive. The microwave power amplifier can be driven on peaks up to and including saturated power output. It can usually even be driven continuously at saturation output power without encountering any device limitation such as excessive power dissipation in the amplifier. That is to say, the power amplifier is designed to operate continuously at saturated power output. In this situation, it seems clear that one should make comparisons among systems based upon peak power required for a given performance level. In this situation, no particular merit should be attached to one system operating at a lower average power than another if they both provide the same performance for the same peak power.

2.2.3 The Noise Bandwidth of Shaping Filters

Here we determine the white noise bandwidth of a filter with the representation shown in Figure 2.2. The one-sided white noise bandwidth of a given filter is defined by the relationship

$$N_0 G_0^2 B_N = \sigma_n^2 \quad (2.2-17)$$

Where B_N = One-sided noise bandwidth
 N_0 = One-sided spectral density of white noise
 σ_n^2 = Mean-square output noise from the given filter
 G_0 = Given filter's dc response

It is well-known³ that for a filter with impulse response $h(t)$, σ_n^2 is given by

$$\sigma_n^2 = \frac{N_0}{2} \int_{-\infty}^{+\infty} h^2(t) dt \quad (2.2-18)$$

In our case, $h(t)$ is the impulse response of the overall filter shown in Figure 2.2. Equations (2.2-5) and (2.2-8) show that Equation (2.2-18) can be written as:

$$\sigma_n^2 = \frac{N_0}{2} \left(\int_{-\infty}^{+\infty} h_2^2(x) dx \right) \sum_{i=0}^{\nu} f_i^2 \quad (2.2-19)$$

where f_i = Transversal tap gain
 $h_2(t)$ = Impulse response of the square root Nyquist Filter

Assuming unit energy in the square root Nyquist filter impulse response Equation (2.2-19) becomes

$$\sigma_n^2 = \frac{N_0}{2} \sum_{i=0}^{\nu} f_i^2 \quad (2.2-20)$$

From Equations (2.2-20) and (2.2-17) we obtain

$$B_N = \frac{1}{2G_0} \sum_{i=0}^{\nu} f_i^2 \quad (2.2-21)$$

Usually, for unit energy in the square root Nyquist filter impulse response, its dc response is \sqrt{T} . Thus, G_0 is given by:

$$G_o = \sqrt{T} G_{oT} \quad (2.2-22)$$

Where:

G_{oT} = dc gain of the transversal filter.

Obviously,

$$G_{oT} = \sum_{i=0}^{\nu} f_i \quad (2.2-23)$$

Therefore, from Equations (2.2-22) and (2.2-23)

$$G_o = \sqrt{T} \sum_{i=0}^{\nu} f_i \quad (2.2-24)$$

Substituting Equation (2.2-24) into Equation (2.2-21), we finally obtain

$$B_N = \left[\sum f_i^2 / (\sum f_i)^2 \right] (1/2T) \quad (2.2-25)$$

Thus the noise bandwidth of a general filter with the analytical representation shown in Figure 2.2 is the bracket factor times the Nyquist bandwidth, $1/2T$ as shown by Equation (2.2-25). It is interesting to note that when $f(D) = 1$, i.e., the original filter is square root Nyquist, the noise bandwidth is the Nyquist bandwidth, $1/2T$. Thus, all square root Nyquist filters have $B_N = 1/2T$, independent of their particular functional form.

2.2.4 Spectral Characteristics of Shaping Filters

In the equivalent representation of a general shaping filter as shown in Figure 2.1-1b, it is obvious that under the assumption that the input digital sequence, $\{x_n\}$, has uncorrelated symbols, the overall output spectrum, $S(w)$, is given by the equation:

$$S(w) = |T(w)H_{\sqrt{N}}(w)|^2 \quad (2.2-26)$$

where:

$T(w)$ = Fourier Transform of transversal Filter

and

$H_{\sqrt{N}}(w)$ = Fourier transform of square root Nyquist filter

Equation (2.2-26) can also be written as

$$S(w) = T(w)T^*(w)N(w) \quad (2.2-27)$$

where:

$N(w)$ = A real Nyquist filter transform

If the polynomial, $f(D)$, describing the transversal filter tap gains is expressed as

$$f(D) = \sum_{i=0}^{\infty} f_i D^i \quad (2.2-28)$$

then the impulse response, $p(t)$, of the filter is given by:

$$p(t) = \sum_{i=0}^{\infty} f_i \delta(t-iT) \quad (2.2-29)$$

where: T = tap gain spacing,

= baud time.

$T(w)$ is therefore given by

$$\begin{aligned} T(w) &= \int_{-\infty}^{+\infty} p(t)e^{-jwt} dt \\ &= \sum_{i=0}^{\infty} f_i \int_{-\infty}^{+\infty} \delta(t-iT)e^{-jwt} dt \\ T(w) &= \sum_{i=0}^{\infty} f_i e^{-jiwT} \end{aligned} \quad (2.2-30)$$

or from Equations (2.2-28) and (2.2-30)

$$T(w) = f(e^{-jwT}).$$

(2.2-31)

The contribution of the transversal filter to the output spectrum of Equation (2.2-27) - namely $T(w)T^*(w)$ - is seen from Equation (2.2-31) to be periodic in w . The shape of the quantity $T(w)T^*(w)$ goes through one period as w moves over the interval $(-\pi/T, +\pi/T)$ and repeats on every other $2\pi/T$ interval as representatively shown by Figure 2.2.4. We will call the frequency interval $(-\pi/T, +\pi/T)$ the basic Nyquist band segment. From the spectral containment viewpoint then the choice of a particular $f(D)$ transversal filter can only determine the shape over the basic Nyquist band segment. The transversal filter will produce periodic side lobes centered on all multiples of $1/T$ in frequency. The magnitude of these side lobes are all equal to the main lobe. It, therefore, remains as a task for the square root Nyquist filter to reduce these side lobes. Obviously, then, a necessary condition for low side lobe levels on the radiated spectrum of Equation (2.2-27) is that the square root Nyquist filter implemented must have low response at frequencies that are nonzero multiples of $1/T$. As a practical matter, this essentially implies that the rolloff of the square root Nyquist filter must be relatively rapid in the frequency interval from $w = \pi/T$ to $w = 2\pi/T$ and

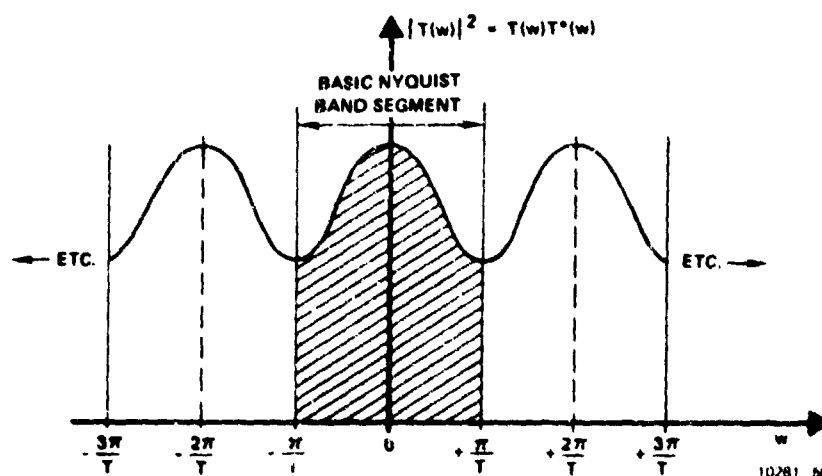


Figure 2.2.4. General Transversal Filter Spectrum

retain high attenuation characteristics at higher frequencies. The transversal filter can provide help for spectral shaping in and around the Nyquist band edge at π/T by providing a dip as shown in Figure 2.2.4 (or even a null) but the side lobe level at $2\pi/T$ will be just as large as the main lobe and the square root Nyquist filter must reduce it to acceptable levels under the given spectral criterion.

It seems clear that partial response schemes (i.e., $f(D)$ polynomials) which place the main lobe peak in the basic Nyquist band segment at $w = 0$ are to be desired since this places the periodic side lobe levels farthest removed from the Nyquist band edge at π/T and hence will allow the gentlest rolloff square root Nyquist filter (which is desirable from practical viewpoints). We will not prejudice the case for such partial response schemes, however. Instead we now turn to the determination of optimum partial response $f(D)$'s to employ for maximizing a measure of spectral containment.

2.2.5 Optimal Partial Response for Maximizing Percent Power in a Given Band

The problem we now solve is to find the optimum $f(D)$ polynomial of a given length (degree) for maximizing the percent energy contained in a given bandwidth, w_B , once a square root Nyquist filter has been chosen by the system designer for the implementation shown in Figure 2.1-1b. Thus we wish to maximize the quantity

$$P(w_B) = \frac{\int_{-w_B}^{+w_B} S(w)dw}{\int_{-\infty}^{+\infty} S(w)dw} \quad (2.2-32)$$

where $S(w)$ is as given in Equation (2.2-27). For a transversal filter of finite length $= (\nu + 1)$, Equation (2.2-30) becomes

$$T(w) = \sum_{i=0}^{\nu} f_i e^{-jiwt} \quad (2.2-33)$$

Substituting Equations (2.2-27) and (2.2-33) in (2.2-32), we obtain for percent power in band:

$$P(w_B) = \frac{\sum_{i=0}^{\nu} \sum_{k=0}^{\nu} f_i f_k \int_{-w_B}^{+w_B} e^{j(i-k)wT} N(w) dw}{\int_{-\infty}^{+\infty} S(w) d(w)} \quad (2.2-34)$$

The term in the denominator of Equation (2.2-34) represents the total energy in the shaping filter pulse. Since baud time translates of a square root Nyquist filter impulse response are orthonormal, the denominator is given by:

$$\int_{-\infty}^{+\infty} S(w) dw = \sum_{i=0}^{\nu} f_i^2 \quad (2.2-35)$$

i.e., the total pulse energy of the pulse shaping filter shown in Figure 2.1-1b is given by the sum of the squares of the transversal tap gains.

Thus maximizing the ratio in Equation (2.2-34) is equivalent to maximizing the numerator under the constraint that $\sum_{i=0}^{\nu} f_i^2 = \text{a constant}$

which we choose to be unity.

The fractional power in band $\pm w_B$ is then given by:

$$P(w_B) = \sum_{i=0}^{\nu} \sum_{k=0}^{\nu} f_i f_k \int_{-w_B}^{+w_B} e^{j(i-k)wT} N(w) dw, \quad (2.2-36a)$$

$$\text{under constraint: } \sum_{i=0}^{\mu} f_i^2 = 1 \quad (2.2-36b)$$

If we define a quantity

$$m_{ik} = \int_{-w_B}^{+w_B} e^{j(i-k)wT} N(w) dw, \quad (2.2-37)$$

then Equation (2.2-36a) can be written as the quadratic form:

$$P(w_B) = \vec{f}^T M \vec{f} \quad (2.2-38)$$

where M is the $(v+1) \times (v+1)$ real, symmetric matrix with elements defined by Equation (2.2-37) and f is a vector of tap gains,

$$\vec{f} \triangleq [f_0, f_1, \dots, f_v] \quad (2.2-39)$$

The maximization of the quadratic form in Equation (2.2-38) under the constraint Equation (2.2-36b) is a well-known³⁵ problem and has the solution that \vec{f} be the eigenvector of the matrix, M , having largest eigenvalue.

If we call this eigenvector \vec{f}_M , then \vec{f}_M represents the tap gains to use in the transversal equalizer to maximize percent energy in band $\pm w_B$. If the eigenvalue associated with this eigenvector is λ_M then from Equation (2.2-38) the maximum fractional power in band is

$$P_M(w_B) = \lambda_M = \text{maximum eigenvalue of } M \quad (2.2-40)$$

Since f_M and λ_M are functions of the matrix, M , and hence through Equation (2.2-37), of w_B and $N(w)$ the optimum spectral concentrating transversal filter is in general a function of the bandwidth within which energy is to be maximized and of the particular square root Nyquist filter employed in Figure 2.1-1b.

2.2.6 Performance Characteristics Of Systems Using Shaping Filters

In previous Section 2. it has been shown that an arbitrary shaping filter is representable as a tandem combination of a transversal filter characterized by a polynomial $f(D)$ and a square root Nyquist filter as shown in Figure 2.1-1b. In this section, it is shown that the polynomial $f(D)$ plays the central role in determining the performance of many digital receiver structures.

For digital signalling, Forney¹ has shown that the optimum receiver under any criterion of optimality has the form shown in Figure 2.2.6-1. It was demonstrated previously¹ that the sample sequence input to the sample processor can be represented by the polynomial, $a(D)$, given

$$a(D) = x(D) f(D) f(D^{-1}) + n_w(D) f(D^{-1}) \quad (2.2.6-1)$$

where

$a(D)$ = Sequence of samples input to sample processor

$x(D)$ = Sequence of transmitted symbols

$n_w(D)$ = Sequence of uncorrelated noise samples with
variance $N_0/2$.

$f(D)$ as defined in Section 2.

The discrete time characterization of the digital system shown in Figure 2.2.6-1 can thus be drawn as in Figure 2.2.6-2. In this section we shall be concerned with the performance of some specific sample processors - perfect linear equalizers and Viterbi algorithm processors.

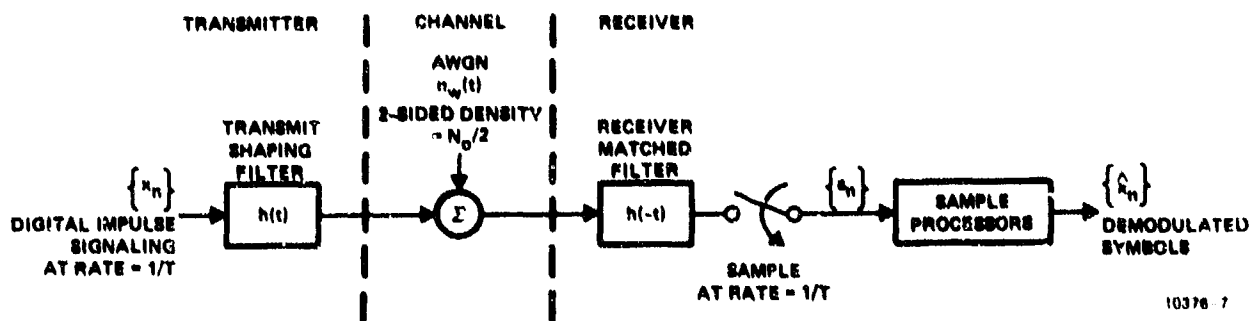


Figure 2.2.6-1. General Optimum Receiver Structure for Digital Signaling

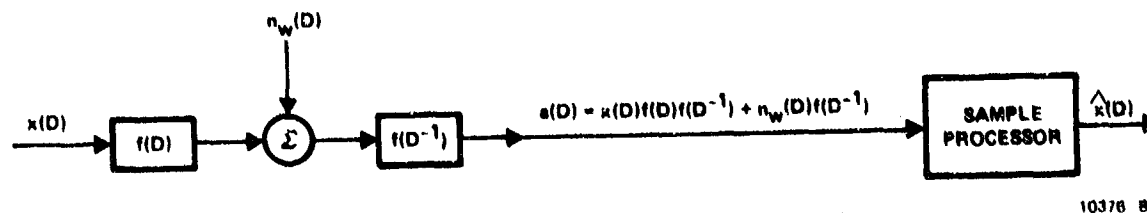


Figure 2.2.6-2. Discrete Characterization of System in Figure 2.2.6-1.

2.2.6.1 Linear Equalizer Processors

We will view here that the function performed by linear equalizers is to convert the intersymbol interference that exists on the input samples into some desired partial response represented by the polynomial, $g(D)$. As can be seen in Equation (2.2.6-1) the partial response presented to the sample processor as a natural action of the transmit-receive matched filtering is represented by the polynomial.

$$R(D) = f(D)f(D^{-1}) \quad (2.2.6-2)$$

Thus, the equalizer must be a device which processes the sample sequence $a(D)$ given in Equation (2.2.6-1) by multiplying $a(D)$ by a polynomial, $t(D)$, (which may be of infinite degree), given by

$$t(D) = \frac{g(D)}{f(D)f(D^{-1})} \quad (2.2.6-3)$$

If we designate the equalized output sequence by polynomial $e(D)$, then from Equations (2.2.6-1) and (2.2.6-3) we have

$$\begin{aligned} e(D) &= a(D) t(D) \\ e(D) &= x(D)g(D) + n_{\omega}(D) \frac{g(D)}{f(D)} \end{aligned} \quad (2.2.6-4)$$

Since $x(D)$, the transmitted input sequence, is multiplied by the desired partial response, $g(D)$, the desired equalization is effected. We include equalizers which totally remove intersymbol interference by including in our general partial response polynomial $g(D)$, the case of $g(D) = 1$.

In general, as can be seen from Equation (2.2.6-3), the length of the transversal equalizer, $t(D)$, is infinite. This is the case unless the desired partial response, $g(D)$, contains as a factor, the channel's "natural" partial response, $f(D)f(D^{-1})$, i.e., unless

$$g(D) = f(D)f(D^{-1})p(D). \quad (2.2.6-5)$$

The situation represented by Equation (2.2.6-5) virtually never occurs in practice. Usually one wishes to equalize to a partial response which is shorter than that occurring as a natural action in the channel. In this case, the length of the required transversal filter, $t(D)$, is theoretically infinite. This may not be catastrophic from practical viewpoints, however, if the high degree coefficients of the polynomial, $t(D)$, diminish rapidly enough such that the effects of truncation are not severe.

The effect of the equalization on noise is shown by Equation (2.2.6-4). The noise sequence, $n(D)$, with uncorrelated Gaussian coefficients of variance $N_0/2$, is multiplied by $g(D)/f(D)$. Thus, the noise variance at the equalizer output is

$$\sigma_e^2 = (N_0/2) \left\| \frac{g(D)}{f(D)} \right\|^2 \quad (2.2.6-6)$$

where

$$\|z(D)\|^2 \triangleq \sum_{i=0}^{\infty} z_i^2 \quad (2.2.6-7)$$

i.e., the noise variance is $N_0/2$ times the sum of the squared coefficients of the polynomial (generally of infinite degree) defined by $z(D) = g(D)/f(D)$. We will assume that the polynomials of interest to us have square-summable coefficients. In general, those situations that produce a $z(D)$ such that $\|z(D)\|^2$ is not finite occur when equalization of a channel having naturally-produced frequency response nulls inside the Nyquist band to a partial response not having nulls at the same frequencies is attempted.

The quantity, $\left\| \frac{g(D)}{f(D)} \right\|^2$, will be called N_e , the noise enhancement factor for perfect $g(D)$ partial response equalization, i.e.,

$$N_e = \left\| \frac{g(D)}{f(D)} \right\|^2 \quad (2.2.6-8)$$

We turn for the moment to a discussion of techniques for calculating the noise enhancement factor.

2.2.6.1.1 Calculating the Noise Enhancement Factor in Perfect Equalizers

The noise enhancement factor as shown in Equation (2.2.6-7) is a function of the channel - through the polynomial $f(D)$ - and the desired partial response, $g(D)$. Here we wish to determine N_e given by Equation (2.2.6-8). We will assume that the desired partial response polynomial $g(D)$ is of degree less than the degree of $f(D)$. Further, we assume that $f(D)$ has a set of roots for $D \in \{\beta_i\}$. The β_i are in general complex numbers. Thus $f(D)$ can be written as

$$f(D) = K \prod_i (1 - \beta_i^{-1} D). \quad (2.2.6-9)$$

The polynomial $z(D)$, where

$$z(D) = \frac{g(D)}{f(D)}, \quad (2.2.6-10)$$

has the partial fraction expansion

$$z(D) = \sum_k \frac{r_k}{1 - \beta_k^{-1} D} \quad (2.2.6-11)$$

where

$$r_k = (1 - \beta_k^{-1} D) \left. \frac{g(D)}{f(D)} \right|_{D = \beta_k} \quad (2.2.6-12)$$

If each root β_k has magnitude greater than unity (the root lies outside the unit circle in the D complex plane) and hence β_k^{-1} has magnitude less than unity then each term of Equation (2.2.6-11) can be written

$$\frac{r_k}{1 - \beta_k^{-1} D} = r_k \sum_{i=0}^{\infty} (\beta_k^{-1})^i D^i \quad (2.2.6-13)$$

From Equations (2.2.6-11) and (2.2.6-13) we have

$$z(D) = \sum_k r_k \sum_{i=0}^{\infty} (\beta_k^{-1})^i D^i \quad (2.2.6-14)$$

or interchanging the order of summations in Equation (2.2.6-14) we obtain

$$z(D) = \sum_{i=0}^{\infty} \left[\sum_k r_k (\beta_k^{-1})^i \right] D^i \quad (2.2.6-15)$$

The noise enhancement factor N_e is given by

$$N_e = \|z(D)\|^2$$

$$N_e = \sum_{i=0}^{\infty} \left[\sum_k r_k (\beta_k^{-1})^i \right]^2 \quad (2.2.6-16)$$

The infinite sum on i in Equation (2.2.6-16) can usually be closed to yield a calculated N_e in specific cases. For example, consider a channel for which

$$f(D) = (1 - aD)(1 + D) = 1 + (1-a)D - aD^2$$

where $a < 1$

and the desired response, $g(D) = 1 + D$, i.e., duobinary equalization is to be effected. In this case

$$\begin{aligned} z(D) &= \frac{g(D)}{f(D)} \\ &= \frac{1 + D}{(1 - aD)(1 + D)} \\ z(D) &= \frac{1}{1 - aD} = \sum_{i=0}^{\infty} a^i D^i \end{aligned}$$

The noise enhancement factor is given by

$$N_e = \sum_{i=0}^{\infty} (a^2)^i$$

or closing the sum we have

$$N_e = \frac{1}{1 - a^2}$$

Although in the above example we chose a case having only a single uncanceled root between $f(D)$ and $g(D)$, the principle is the same in the multiple uncanceled root case. Generally, given the uncanceled roots, the term in brackets in Equation (2.2.6-16) must be squared and then each component term closed separately in the fashion used in the example.

This technique for finding the noise enhancement factor for perfect equalizers was used in performance evaluations of specific equalizer cases presented in later sections.

2.2.6.1.2 Performance with Perfect Equalization

In the following development we make use of the noise enhancement factor of the preceding section to determine the performance of a type of a perfectly equalized system.

Let us be specific about the type of perfectly equalized system we consider here. The system considered is shown in Figure 2.2.6-3. The output of the receiver matched filter is sampled and input to the equalizer characterized by the generally infinite degree polynomial, $t(D)$, found in the preceding section. The output of the

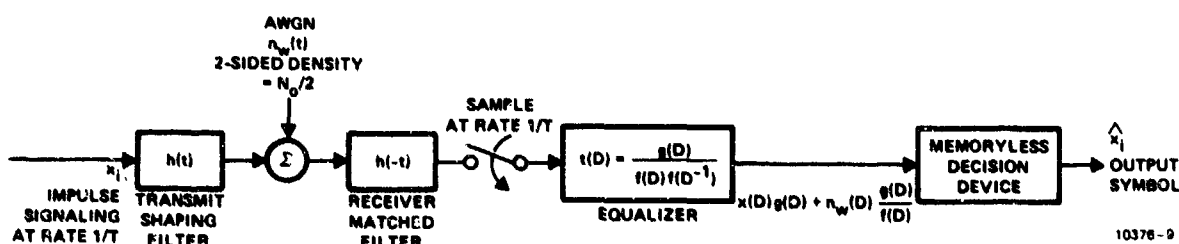


Figure 2.2.6-3. Perfectly Equalized Systems Under Consideration

equalizer is input to a memoryless decision device where each equalizer output sample is observed in turn. A decision is made upon the transmitted symbol based solely on the observation of the present input symbol from the equalizer. Typically, the decision device takes the form of a (possibly multilevel) threshold detector. The performance (probability of symbol error) with such a memoryless decision device is a function of the ratio of the mean square signal input to the variance of the Gaussian noise at the input. The performance depends only on this ratio and is not influenced by correlation between successive input noise samples. From the noise enhancement factor discussions of the preceding sections, we know that the noise variance at the input to the decision

device is given by Equation (2.2.6-6). Thus, as far as the performance of the memoryless decision device is concerned the system of Figure 2.2.6-4 is equivalent to the system of Figure 2.2.6-3. Note that the additive white Gaussian noise in Figure 2.2.6-4 has been increased in spectral density by the noise enhancement factor, N_e , from Equation (2.2.6-8).

Suppose one knows D_0 , the degradation relative to one-shot performance of the signalling scheme shown in Figure 2.2.6-4 for $N_e = 1$. The scheme shown in Figure 2.2.6-4 thus has an additional degradation factor due to noise enhancement resulting in total degradation relative to one-shot performance for that system of

$$D = D_0 N_e \quad (2.2.6-17)$$

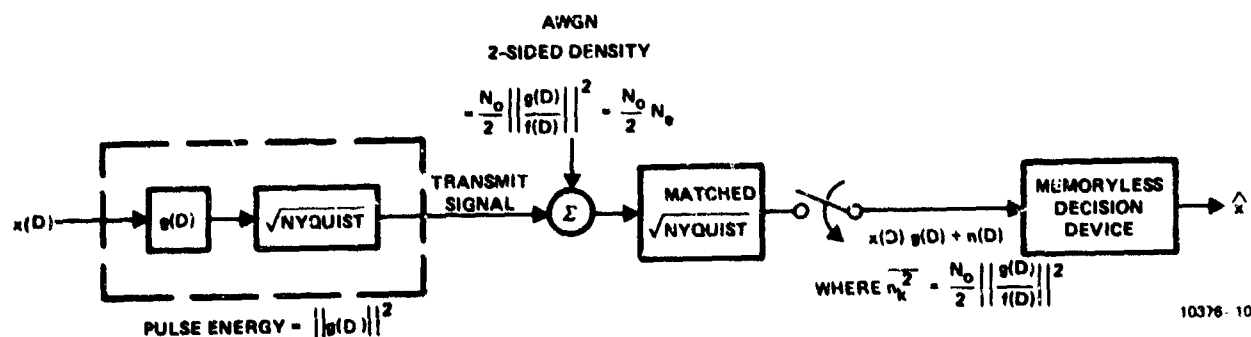


Figure 2.2.6-4. Equivalent to Figure 2.2.6-3 as far as Performance of Decision Device is Concerned

Further, the system of Figure 2.2.6-4 uses $g(D)$ as the transmit transversal filter in conjunction with square root Nyquist filter resulting in transmitted pulse energy of $\|g(D)\|^2$ whereas the system in Figure 2.2.6-3 has assumed $f(D)$ as the transversal component of the transmit filter resulting in transmitted pulse energy of $\|f(D)\|^2$. Thus to obtain D_T , the total degradation relative to one-shot performance for the system of Figure 2.2.6-3, an additional normalizing factor of $\|f(D)\|^2 / \|g(D)\|^2$ must be included resulting in

$$D_T = D_0 N_e \left[\|f(D)\|^2 / \|g(D)\|^2 \right]$$

or

$$D_T = D_0 \left\| \frac{g(D)}{f(D)} \right\|^2 \left[\|f(D)\|^2 / \|g(D)\|^2 \right] \quad (2.2.6-18)$$

The degradation in dB relative to one-shot is thus

$$D_T(\text{dB}) = D_0(\text{dB}) + 10 \log_{10} \left\{ \left\| \frac{g(D)}{f(D)} \right\|^2 \left[\|f(D)\|^2 / \|g(D)\|^2 \right] \right\} \quad (2.2.6-19)$$

The first term, D_0 , in Equation (2.2.6-19) which is a function only of $g(D)$ represents a fundamental inefficiency relative to one-shot (Nyquist) performance of using the partial response, $g(D)$, and a memoryless decision device receiver of the type shown in Figure 2.2.6-4. The second term represents an additional toll extracted for having to perfectly equalize the actually transmitted partial response, $f(D)$, to the desired form, $g(D)$. In the case $g(D) = 1$ (Nyquist Equalization) the degradation factor, D_0 , is 0 dB.

The degradation expression of Equation (2.2.6-19) shows the functional manner in which the $f(D)$ polynomial from the analytical characterization of the shaped pulse digital transmission system enters into and is central to the determination of performance for a type of perfectly equalized receivers. The result of Equation (2.2.6-19) has been used to produce results presented elsewhere in this report for equalized receivers.

2.2.6.2 How Performance is Determined for Viterbi Algorithm Sample Processors

In the preceding section, we have indicated the manner in which the performance of certain types of perfectly equalized receivers depends upon the $f(D)$ polynomial from the analytical characterization of digital signaling schemes presented in Section 2. In this section we do the same for Viterbi Algorithm sample processors.

The system under consideration is that shown in Figure 2.2.6.2. This system was taken from Figure 2-6 but with the sample processor taking the form of a Viterbi algorithm processor. Forney¹ shows that such a processor provides a maximum likelihood sequence estimation, $\hat{x}(D)$ given the received sequence $z(D)$.

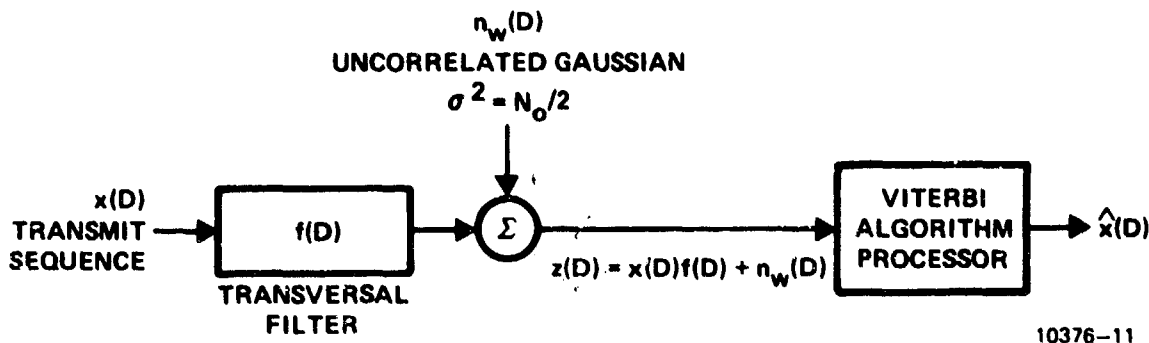


Figure 2.2.6.2. Discrete Representation of Digital Transmission Scheme with a Viterbi Algorithm Processor

Those familiar with the Viterbi algorithm will note that when the polynomial $f(D)$ is of finite degree $= \nu$ and the sequence $x(D)$ has coefficients taken from a finite set of M discrete levels then the signal $x(D)f(D)$ represents a finite state signal where the number of states, N_s , is given by

$$N_s = (M^\nu) \quad (2.2.6.2-1)$$

A different state is assigned to each of the M^V combinations of the V most recent coefficients possible in the sequence, $x(D)$. This finite state signal, $x(D)f(D)$, is perturbed by the uncorrelated Gaussian noise sequence, $n_w(D)$, to produce the sequence $z(D)$ input to the Viterbi algorithm processors, i.e.,

$$z(D) = x(D)f(D) + n_w(D) \quad (2.2.6.2-2)$$

This finite state signal, encumbered by uncorrelated Gaussian noise samples, is the type of signal for which the Viterbi algorithm produces a maximum-likelihood estimate, $\hat{x}(D)$, of the transmitted sequence, $x(D)$. Those unfamiliar with the Viterbi algorithm processor are referred to the various literature references⁹⁻¹¹ describing its operation.

Although we will not go into the detailed computation of performance for the Viterbi algorithm (see Forney¹), we will briefly indicate the central role of the polynomial $f(D)$ in determining the performance. As shown by Forney the performance of the Viterbi algorithm processor is determined by the "distance," d_{ij}^2 , between pairs of sequences, $x_i(D)$ and $x_j(D)$, are conveyed over the channel where

$$\begin{aligned} d_{ij}^2 &\triangleq \|x_i(D)f(D) - x_j(D)f(D)\|^2 \\ &= \|\epsilon_{ij}(D)f(D)\|^2 \end{aligned} \quad (2.2.6.2-3)$$

$$\text{where } \epsilon_{ij}(D) \triangleq x_i(D) - x_j(D)$$

Forney obtains a Union Bound on the probability of symbol error given the set of distances (in his paper, the line before Equation (82)) for all possible error sequences, $\epsilon_{ij}(D)$.

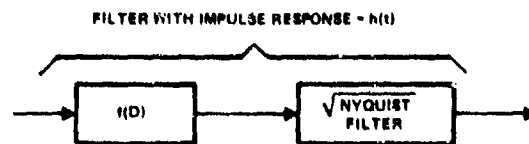
During the course of this contract, a computer program was written to search out and determine the distances specified by Equation (2.2.6.2-3) for all paths having distance less than some specifiable level for M-ary equispaced coefficients in $x(D)$ (i.e., M-ary PAM transmission) for

an arbitrary $f(D)$ polynomial. The computer program computes Forney's Union Bound on symbol error rate versus E_b/N_0 , including all the effects of these paths. This computer program was used to generate all the performance results for Viterbi algorithm receivers presented in this report.

Equation (2.2.6.2-3) above indicates the central role played by the polynomial $f(D)$ in determining distance between sequences, hence in determining the performance of digital systems using Viterbi algorithm processors.

2.2.7 A Technique for Converting a Given Filter to a Square-Root Nyquist Filter

The analytical characterization of an arbitrary filter as a cascade of a transversal filter and a square root Nyquist filter as described in Section 2., suggests a possible technique for converting a given filter which is not square root Nyquist to one which is. As shown in Section 2., a filter having impulse response $h(t)$ can be represented as shown in Figure 2.2.7-1.



$f(D)$ DEFINED BY RELATIONSHIP:

$$R(D) = f(D)f(D^{-1})$$

$$\text{WHERE: } R(D) = \sum_{i=-\infty}^{+\infty} r_i D^i$$

$$\text{AND: } r_i = r_{-i} = \int_{-\infty}^{+\infty} h(t)h(t+iT)dt$$

T = BAUD TIME OF DIGITAL IMPULSES
TRANSMITTED THROUGH $h(t)$

10376 12

Figure 2.2.7-1. An Analytical Representation of Filter with Impulse Response, $h(t)$

From Figure 2.2.7-1 it can be seen that if one wishes to remove the effect of the transversal filter component of the filter with impulse response $h(t)$, one can place a recursive filter, $1/f(D)$, ahead of the original filter as in Figure 2.2.7-2. Thus one obtains the square root Nyquist filter component of the original filter. We assume that the $f(D)$ polynomial of the original filter is of finite degree so that $1/f(D)$ is practically realizable as a finite length recursive filter. The polynomial $f(D)$ is of finite degree, ν , whenever the autocorrelation function of the original filter is zero for $t = \pm nT$ for all $n > \nu$. This can be ascertained from the equations defining $R(D)$ in Figure 2.2.7-1. This condition for $f(D)$ to have finite degree is equivalent to a requirement that the original filter in cascade with its matched filter counterpart have finite span intersymbol interference at sample times. Note that this condition does not require that the original filter impulse response be of finite duration, only the stated condition on the pulse autocorrelation function must be met.

2.2.7.1 Frequency Response Characteristic of the Converted Square Root Nyquist Filter

We find here the frequency response characteristic of the converted square root Nyquist filter of Figure 2.2.7-2. The original filter has frequency response, $H_0(\omega)$, given by

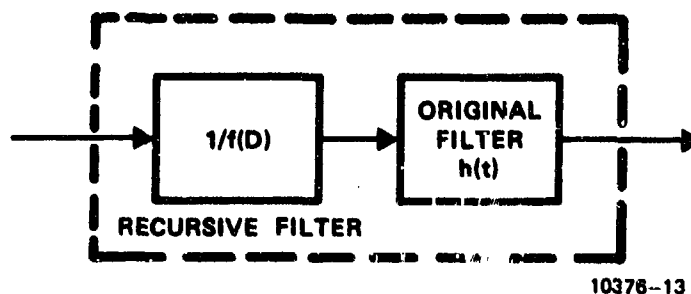


Figure 2.2.7-2. Conversion of $h(t)$ into Square Root Nyquist

$$H_0(\omega) = \int_{-\infty}^{+\infty} h(t)e^{-j\omega t} dt \quad (2.2.7.1-1)$$

Assuming that the recursive filter has a frequency response given by $X(\omega)$, then obviously the square root Nyquist filter has frequency response, $H_N(\omega)$, given by

$$H_N(\omega) = X(\omega)H_0(\omega) \quad (2.2.7.1-2)$$

It can be shown that under certain conditions, the frequency response of the recursive filter is given by

$$X(\omega) = 1/f(e^{-j\omega T}) \quad (2.2.7.1-3)$$

Thus, from Equations (2.2.7.1-2) and (2.2.7.1-3), the frequency response of the square root Nyquist filter is given by

$$H_N(\omega) = H_0(\omega)/f(e^{-j\omega T}) \quad (2.2.7.1-4)$$

The conditions under which Equation (2.7.7.1-4) gives the frequency response of the converted square root Nyquist filter are met when

$$f(e^{-j\omega T}) \neq 0 \text{ for any } \omega \quad (2.2.7.1-5)$$

This condition means that the original filter has no frequency response nulls inside the Nyquist bandwidth. This also means that the polynomial $f(D)$ has no roots on the unit circle as can be seen from equation (2.2.7.1-5). This also implies that the infinite polynomial $t(D)$, where

$$t(D) = 1/f(D) \quad (2.2.7.1-6)$$

has square-summable coefficients, and consequently, the response of the recursive filter, $1/f(D)$, to an input sufficiently remote in the past goes to zero. This is comforting (and necessary) if one is to implement the recursive filter and have finite energy in the pulses from the recursive filter.

Thus, in the case that the original filter has no nulls in its frequency response inside the Nyquist band, $\pm 1/2T$, one can convert the filter to square root Nyquist by building an appropriate recursive filter to place ahead of the original filter. The frequency response of the resultant square root of Nyquist filter one creates by this implementation shown in Figure 2.2.7-2 is given by equation (2.2.7.1-4).

3. THE SPECTRAL REQUIREMENTS OF FCC DOCKET 19311

The spectral constraint under which this study has operated is embodied in FCC Docket 19311.⁶ The spectral requirements are defined in this Docket as follows:

"When using transmissions employing digital modulation techniques--for operating frequencies below 15 GHz, in any 4 kHz band, the center frequency of which is removed from the assigned frequency by 50 percent or more of the authorized bandwidth: Attenuation shall be as specified by the following equation but in no event less than 50 dB.

$$A = 35 + 0.8(P-50) + 10 \log_{10} B \quad (3-1)$$

(Attenuation greater than 80 dB is not required.)

Where:

A = attenuation (in decibels) below the mean output power level

P = percent removed from the carrier frequency

B = authorized bandwidth in MHz."

3.1 Effect of Authorized Bandwidth on Capacity Under FCC Docket 19311

The spectral requirements of FCC 19311 translate into the masks shown in Figure 3.1-1 for the authorized bandwidths from 3.5 to 20 MHz of interest in this study.

One of the difficult aspects of meeting FCC 19311 requirements across this range of authorized bandwidths is the constant -50 dB corner on all the masks at ± half the authorized bandwidth. The specification is stated in terms of the relative power in a constant 4-kHz bandwidth independent of the authorized bandwidth. A particular manifestation

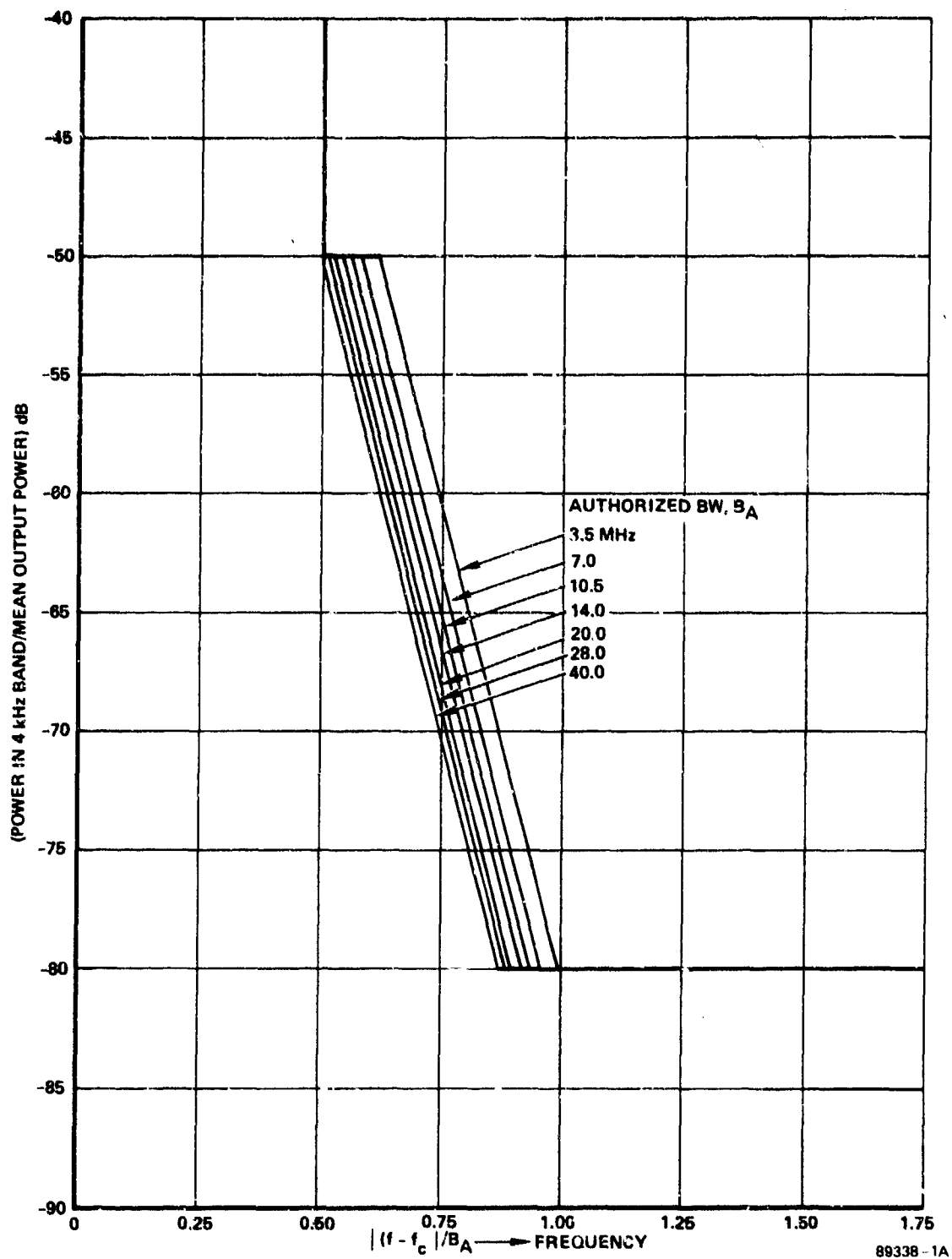


Figure 3.1-1. FCC Docket 19311 Spectrum Masks

of the difficulty is that a particular modulation scheme meeting the -50 dB corner for an authorized bandwidth of 20 MHz may not comply for an authorized bandwidth of 3.5 MHz. This is because the power in a fixed 4 kHz band is 7.6 dB higher for 3.5 MHz than for 20 MHz authorized bandwidth. The difference in 4 kHz band power is allowed for in the linear rolloff portions of the masks but not in the corners. Because of this "corner problem," the choice of the signal for meeting the spectral mask for an authorized bandwidth of 3.5 MHz is the most critical. A signaling scheme meeting the requirements of the 3.5 MHz mask is guaranteed to meet the masks for all other bandwidths. If one uses the 3.5 MHz authorized bandwidth case as the spectral mask against which all modulation schemes are referenced to compute bits/sec/Hz capacity then the capacity will in general be slightly higher than the computed capacity for larger authorized bandwidth cases. This occurs whenever the 3.5 MHz authorized bandwidth spectral compliance is dictated by the -50 dB (or -80 dB) corner. That is, when the signal spectrum just touches one of these corners. In the 20 MHz authorized bandwidth case such a spectrum would pass 7.6 dB below the corners and consequently the symbol rate could be increased slightly and still comply with the 20 MHz mask.

If the 3.5 MHz FCC 19311 compliance is dictated by the signal spectrum just touching the mask in the linear rolloff region, then it will also touch the linear rolloff part of the mask for 20 MHz also (or for any other authorized bandwidth). In this case there is no difference in capacity in bits/sec/Hz for any of the authorized bandwidths.

In most of the signal spectra examined in this study, FCC 19311 spectral compliance is dictated by the signal spectra just touching the -50 dB mask corner. Since we base the computed capacity for most schemes examined in this study on the 3.5 MHz authorized bandwidth case, we examine here the potential increase in capacity for the higher authorized bandwidth cases. We shall argue here that the bias is usually small and that one is thus justified in computing the capacity for all

schemes based only on the 3.5 MHz authorized bandwidth case. As noted above, a signaling scheme meeting the mask for 3.5 MHz authorized bandwidths is guaranteed to meet the mask for higher bandwidths. Thus, the bits/sec/Hz capacity computed on the basis of the 3.5 MHz mask is certainly achievable at higher authorized bandwidths.

Figure 3.1-2 shows a typical spectrum chosen to just touch the -50 dB corner of the spectral mask for an authorized bandwidth of 3.5 MHz. Also shown is the spectrum that would result for a higher authorized bandwidth, B_a , with the same signaling scheme when the symbol rate is increased by the factor $(B_a/3.5)$. That is, for both authorized bandwidths, the symbol (or bit) rate is the same factor times the authorized bandwidth and hence both systems have the same bits/sec/Hz capacity. As shown, both spectra have the identical shape under this condition when plotted versus frequency normalized by authorized bandwidth. The only difference between the two curves is the $10 \log_{10}(B_a/3.5)$ db lower power in a 4 KHz spectrum analyzer bandwidth for the higher authorized bandwidth system. Because of the drop in 4 KHz power, the higher authorized bandwidth system spectrum passes below the -50 dB corner on the FCC 19311 mask. Consequently, the symbol rate (hence capacity) can be increased somewhat for the higher bandwidth system. We now approximate the factor by which the capacity can be increased.

We assume that the 3.5 MHz authorized bandwidth spectrum has a slope of $-\Delta$ dB per 3.5 MHz in the vicinity of the -50 dB mask corner. That is, a line drawn tangent to the spectrum at the corner frequency has a slope of $-\Delta$ dB per authorized bandwidth. The curve for the higher authorized

bandwidth, B_a MHz, also has the same slope per authorized bandwidth in the vicinity of the mask corner. From Figure 3.1-2, the slope of the higher bandwidth (dotted) curve is approximated by

$$\Delta \approx \frac{10 \text{ Log}(B_a/3.5)}{\Delta f/B_a} \quad \text{dB}/B_a \text{ Hz}$$

or

$$\Delta f \approx \frac{10 \text{ Log}(B_a/3.5)}{\Delta} B_a \quad (3-2)$$

From Figure 3.1-2 and Equation (3-2), the RF 50 dB bandwidth for the higher authorized bandwidth is given by β_{50} , where

$$\beta_{50} = 2(.5B_a - \Delta f) \quad (3-3)$$

$$= 2 \left(.5B_a - \frac{10 \text{ Log}(B_a/3.5)}{\Delta} B_a \right)$$

$$\beta_{50} = [1 - (20/\Delta) \text{ Log}(B_a/3.5)] B_a \quad (3-4)$$

Equation(3-4) shows that the 50 dB corner on the spectrum is reduced below the higher authorized bandwidth by the bracketed factor. Thus, the symbol rate, hence capacity in bits/sec/Hz, can be increased by a factor, r , given by

$$r = 1/[1 - (20/\Delta) \text{ Log}(B_a/3.5)], \quad (3-5)$$

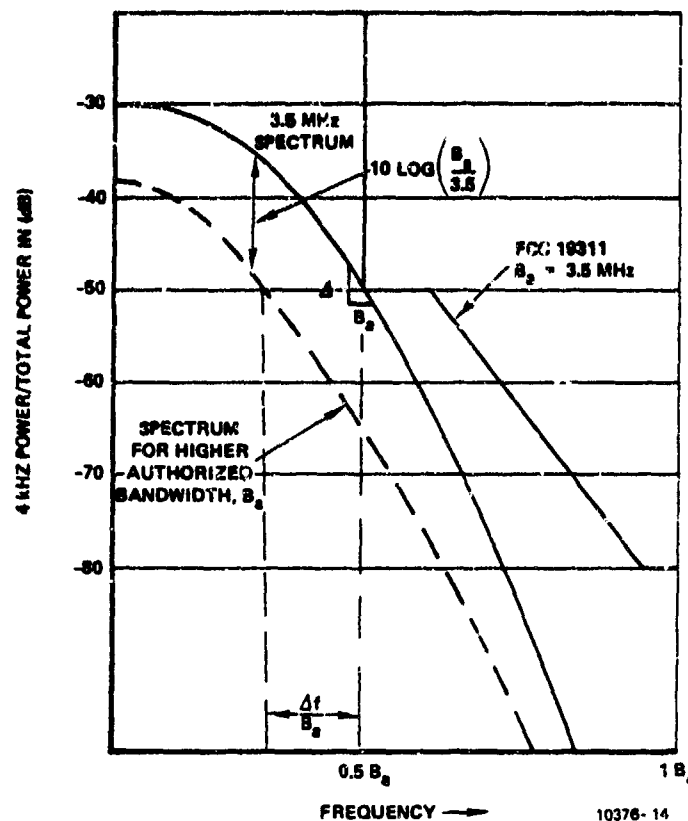


Figure 3.1-2. A Typical Spectrum

where r = Factor by which capacity for authorized bandwidth B_a system can be increased over that available for an authorized bandwidth of 3.5 MHz

B_a = Actual authorized bandwidth in MHz.

Δ = Slope of 3.5 MHz spectrum at the 50 dB corner in dB per B_a hertz.

Virtually none of the spectra examined in this study have a Δ less than 100 dB per B_a hertz.

We have plotted the quantity r in Equation (3-5) versus $10 \log_{10}(B_a/3.5)/\Delta$ in Figure 3.1-3. In the remainder of this report, for simplicity, an authorized bandwidth of 3.5 MHz is assumed when generating capacity curves. If one wishes to find the corresponding capacity for a system operating in a larger authorized bandwidth of B_a

MHz he may note the slope, Δ in dB per B_a hertz for the signal spectrum, compute the quantity $10 \log_{10}(B_a/3.5)/\Delta$ and find the factor r on Figure 3.1-3 by which to multiply the 3.5 MHz authorized bandwidth capacity in bits/sec/Hz. As mentioned, Δ is virtually never less than 100 and for worst-case $B_a = 20$ MHz this factor is rarely larger than 1.18. That is, the capacity for a 20 MHz authorized bandwidth might be as much as 18 percent greater than a plotted capacity for a 3.5 MHz authorized bandwidth.

3.2 How the FCC Docket 19311 Spectral Mask Is Determined for a Given Signal Spectrum

In general we have a signal spectrum denoted by $S(f)$. This signal spectrum is usually the magnitude squared of some shaping filter transfer function, i.e.,

$$S(f) = |H_T(f)|^2 \quad (3.2-1)$$

However the spectrum is determined we assume that the total radiated power is normalized to unity:

$$\int_{-\infty}^{+\infty} S(f) df = 1 \quad (3.2-2)$$

Usually it is more convenient to work with a normalized frequency variable, f/f_R where f_R is some reference frequency such as symbol rate or filter 3 dB bandwidth. In terms of the arbitrary normalized frequency variable, Equation (3.2-2) can be written:

$$\int_{-\infty}^{+\infty} f_R S(f/f_R) d(f/f_R) = 1 \quad (3.2-3)$$

In most cases it becomes obvious what the scaling of the quantity $f_R S(f/f_R)$ must be for the integral in Equation (3.2-3) to equal unity. A simple example is the case where the spectrum is assumed flat over the Nyquist band, $-\frac{1}{2T} < f < \frac{1}{2T}$, and the reference frequency f_R

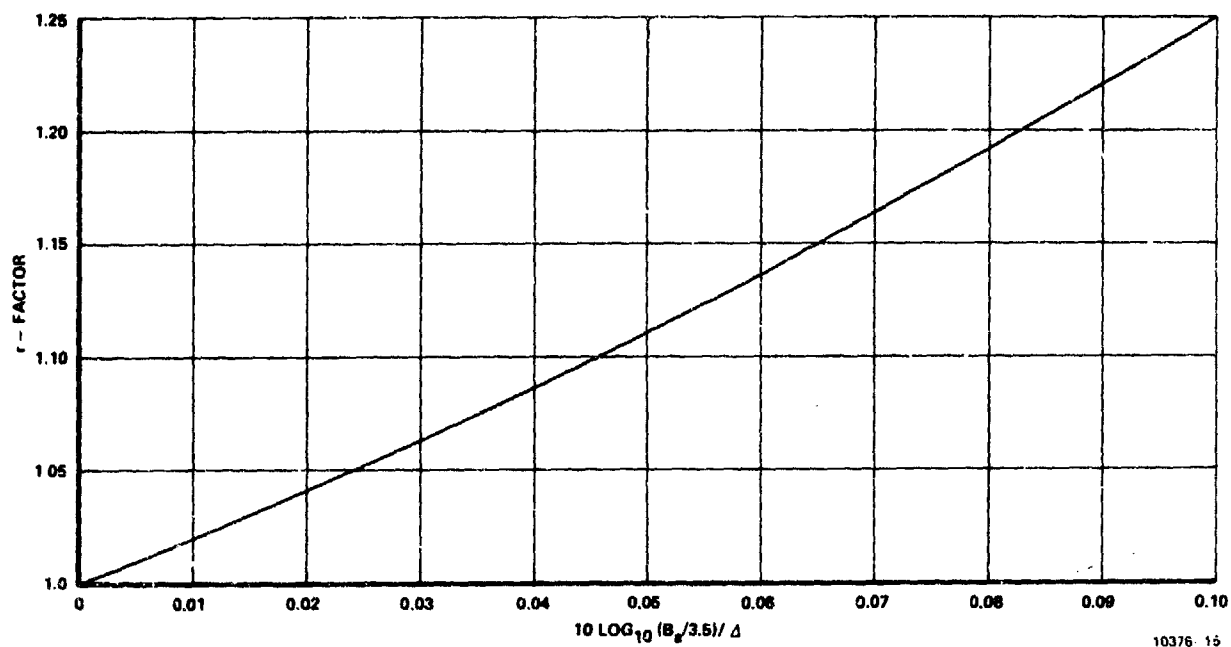


Figure 3.1-3. Approximate Factor r by Which the Capacity of a System Operating in Authorized Bandwidth of B_a MHz Exceeds That of the Same System in 3.5 MHz Bandwidth

is chosen as the Nyquist frequency $1/T$. In this case Equation (3.2-3) becomes

$$\int_{-\frac{1}{T}}^{+\frac{1}{T}} \frac{1}{T} [S(fT)] d(fT) = 1 \quad (3.2-4)$$

and it is obvious that:

$$\frac{1}{T} S(fT) = 1, \quad -\frac{1}{2T} < f < \frac{1}{2T}$$

In any case, one usually computes and plots the quantity $f_R S(f/f_R)$ versus the normalized frequency variable, f/f_R , with the normalization such that Equation (3.2-3) hence Equation (3.2-2) holds, i.e., the total radiated power equals unity. Figure 3.1-4 shows a typical plot of $f_R S(f/f_R)$ in dB. (Figure 3.1-4 is actually the spectrum produced by a square-root raised cosine $\alpha = 0.5$ shaping filter where the reference frequency $f_R = 1/T$, the Nyquist rate.) Given the spectrum shown, we wish to find the most restrictive FCC 19311 spectral mask with which this spectrum will comply.

Usually it is the -50 dB corner of the FCC 19311 spectral mask which first touches the spectrum and hence dictates the mask. For FCC 19311 the mask is stated in terms of the power in a 4 kHz bandwidth relative to total power. This quantity is given by

$$P_4(f) = (4 \text{ kHz}) \times S(f) \quad (3.2-5)$$

where $P_4(f)$ = power (relative to total power) in a 4 kHz bandwidth centered at frequency = f

$S(f)$ = Signal spectrum at f

Here it is assumed that 4 kHz is such a small bandwidth that $S(f)$ is essentially constant across 4 kHz. Equation (3.2-5) can also be written as

$$P_4(f) = \left(\frac{4 \text{ kHz}}{f_R} \right) \left[f_R S(f) \right]. \quad (3.2-6)$$

If we are trying to locate the -50 dB (fractional power = 10^{-5}) corner on the FCC 19311 mask now we want

$$P_4(f) = 10^{-5} = \left(\frac{4 \text{ kHz}}{f_R} \right) \left[f_R S(f) \right] \quad (3.2-7)$$

Furthermore, the frequency f at which this occurs is $f = B_a/2$, i.e.,

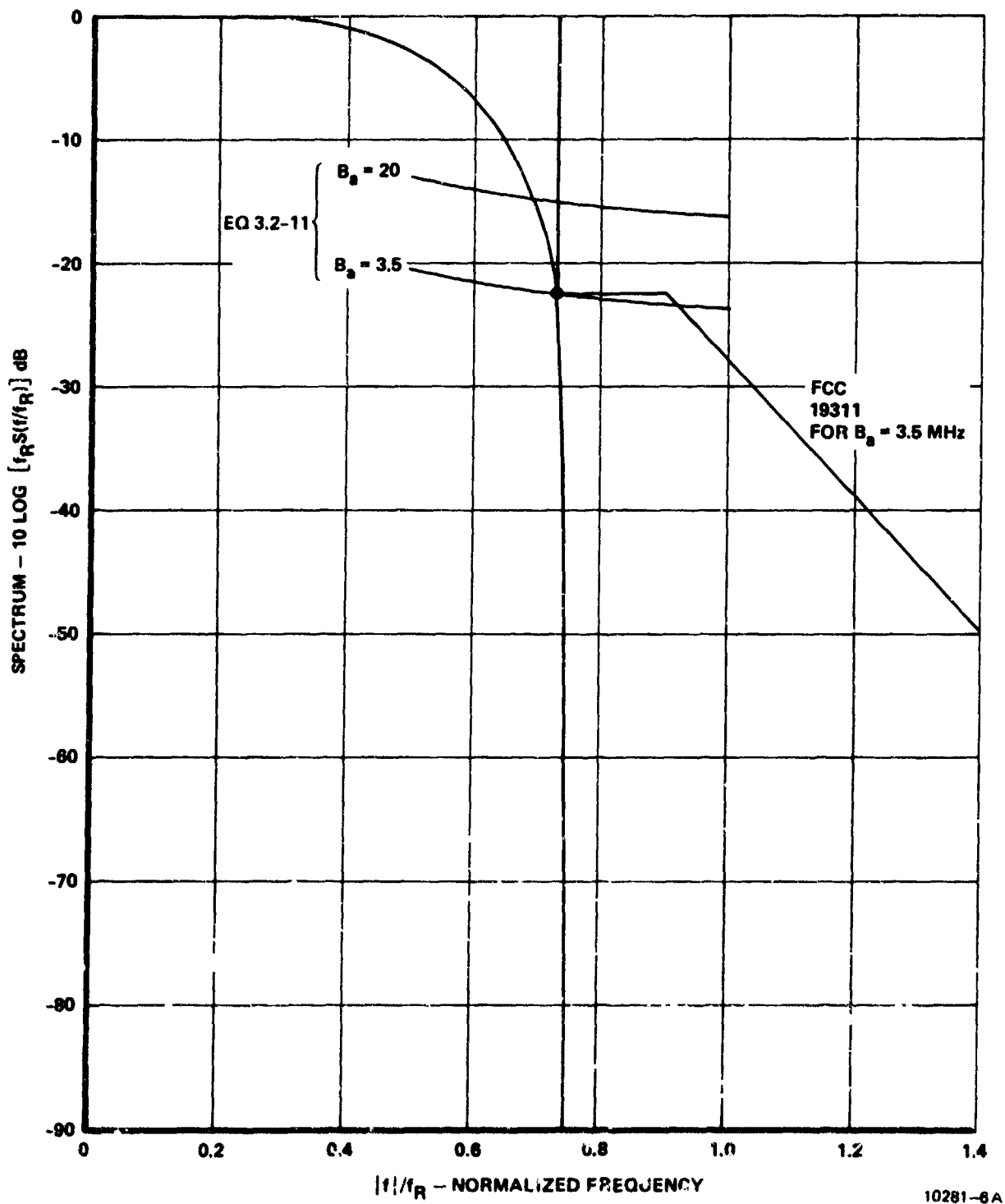


Figure 3.1-4. Showing How FCC 19311 Mask is Produced for a Typical Spectrum

the frequency of the -50 dB corner is at $\pm B_a/2$ from center frequency. Thus the normalized frequency of the corner is

$$\left(\frac{f}{f_R}\right) = \frac{B_a}{2f_R} \quad (3.2-8)$$

Equation (3.2-7) can be rearranged to give

$$\left[f_R S(f)\right] = 10^{-5} \left(\frac{f_R}{B_a}\right) \left(\frac{B_a}{4 \text{ kHz}}\right) \quad (3.2-9)$$

and Equation (3.2-8) can be used in (3.2-9) to yield

$$\left[f_R S(f)\right] = 10^{-5} \frac{(B_a/4 \text{ kHz})}{2(f/f_R)} \quad (3.2-10)$$

or

$$10 \log \left[f_R S(f)\right] = -53 + 10 \log (B_a/4 \text{ kHz}) - 10 \log (f/f_R) \quad (3.2-11)$$

Equation (3.2-11) defines the maximum allowable value of the spectrum in Figure 3-4 at a normalized frequency, f/f_R , such that the spectrum at that frequency complies with the -50 dB corner on an FCC 19311 mask for an authorized bandwidth of B_a . Equation (3.2-11) is plotted on Figure 3-4 for authorized bandwidths of $B_a = 3.5 \text{ MHz}$ and $B_a = 20 \text{ MHz}$. The point of intersection of Equation (3.2-11) with the actual spectrum shows the location of the most restrictive FCC 19311 - 50 dB mask corner for each authorized bandwidth. From Equation (3.2-8) the authorized bandwidth for this intersection is

$$\frac{B_a}{f_R} = 2 \left(\frac{f}{f_R}\right) \text{ at intersection} \quad (3.2-12)$$

Having located the -50 dB corner on the spectral mask one can then produce the 19311 mask in its entirety from Equation (3-1) of the prior section. This has been done on Figure 3-4 for the $B_a = 3.5$ MHz case.

This technique has been implicitly employed throughout this report to produce FCC 19311 spectral masks given the signal spectrum.

4. PERFORMANCE OF IDEAL DIGITAL COMMUNICATIONS SYSTEMS

In this section the performance of ideal digital communication systems of the type shown in Figure 4-1 will be displayed. The performance obtainable by these ideal systems will serve as performance references with which to compare the performances of nonideal systems investigated in later sections.

The system of Figure 4-1 is ideal in the sense that the filters used are ideally bandlimited to the Nyquist band $\pm 1/2T$. The

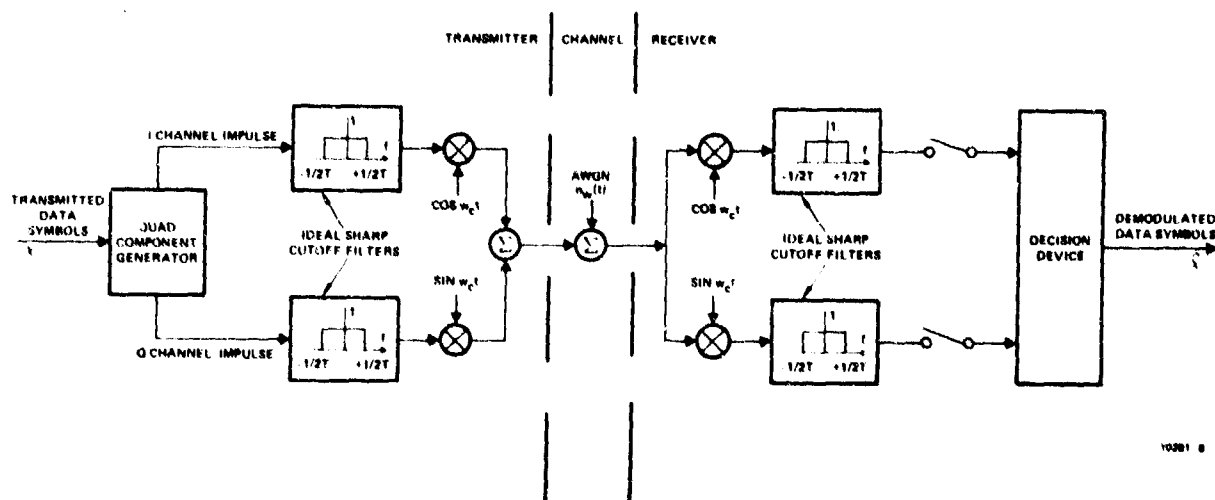


Figure 4-1. Ideal Digital Communication System Using Quadrature Modulation

transmitted RF spectrum resulting from the use of such filter is thus ideally bandlimited to a band of width $= 1/T$, where T is the symbol rate, i.e., the rate of choosing a pair of impulses to input to the baseband filters is $1/T$. Further, it is presumed that each pair of impulses carries B bits of information, i.e., there are 2^B distinct pairs of impulse weights, one pair of which is chosen for transmission each symbol

time. The bit rate is thus B/T in such a system. The bits/s per Hertz of RF bandwidth capacity, C_I is thus

$$C_I = B \quad (4-1)$$

where C_I = Ideal system capacity in bits/s/Hz,

B = Number of bits carried per RF symbol.

As shown in Figure 4-1, the two baseband signals resulting from the pair of impulses are used to modulate quadrature carriers. At the receiver, the RF signal is downconverted back to baseband by the use of coherent quadrature mixer references. Because of the ideal Nyquist character of the channel, samples of the baseband signals will be the transmitted impulse weights corrupted by the channel noise, but with zero intersymbol interference.

The sampled quadrature components are fed to a decision device which optimally decides which quadrature pair was transmitted given the received pair of samples.

The performance of the system described above is well known for many sets of the 2^B quadrature transmitted pairs. A given set of quadrature pairs is known as the digital signal design. Some specific signal designs that fit into the format implied by Figure 4-1 are shown in Figure 4-2.

4.1 Ideal M-PSK Systems

Figure 4-2a shows the eight pairs of impulse weights employed for 8-ary PSK. Here the pairs are chosen equispaced around a circle in the quadrature two-dimensional signal space. At the symbol sample times, the RF amplitude is a constant and the phase is one of the eight phases. At the receiver, the decision device decides the transmitted pair is that nearest in phase to the received pairs' phase and outputs the corresponding 3 bits of information. It is to be noted that the RF

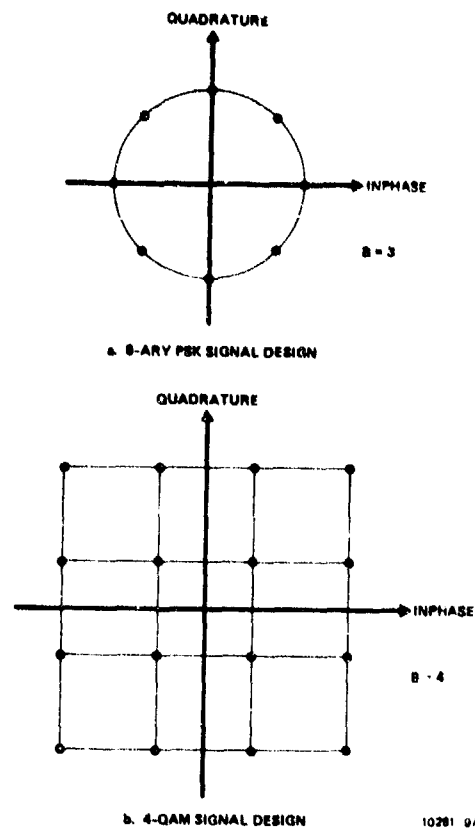


Figure 4-2. Specific Signal Designs

envelope is constant only at the symbol sampling times - at other times between samples, the envelope fluctuates in a complex manner. Figure 4-2a shows the 8-ary PSK case, but in general there can be any number of points equispaced around the circle. The performance in the general M-ary PSK case (M equispaced phases) is well known.²⁴

Tight upper and lower bounds for low error rates of the probability of symbol error are given by

$$Q\left(\sqrt{(E_s/N_0)\sin^2(\pi/M)}\right) < P(E) < 2Q\left(\sqrt{(E_s/N_0)\sin^2(\pi/M)}\right) \quad (4.1-1)$$

for M-ary PSK where

$P(E)$ = Probability of symbol error
 E_s = Energy per symbol = $E_b \log_2 M$
 E_b = Energy per bit
 N_o = One-sided noise spectral density
 M = Number of equispaced phases

The upper bound of Equation (4.1-1) is plotted in Figure 4.1 for several values of M . The curves are plotted versus E_b/N_o , the signal to noise ratio in a bandwidth equal to the bit rate. From Equation (4-1), the ideal bandlimited system capacity in bits/sec/Hz is given by

$$C_I = \log_2 M \text{ bits/sec/Hz} \quad (4.1-2)$$

and each curve in Figure 4.1 is labelled with the appropriate ideal capacity. Of course, the ideal system performance and bits/sec/Hz capacity cannot be achieved in practice. One cannot achieve the ideal bandlimited spectrum. Another point of impracticality, as an example, is the $M = 128$ PSK case. Here, the phases are separated by only $(360/128) = 2.8^\circ$ and certainly no one would attempt to implement a demodulator with the capability of resolving signal points that close together.

4.2 Ideal M-QAM Systems

Figure 4.2b shows another example of a signal design for the modulation scheme shown in Figure 4-1. Here the 16 pairs of quadrature components generated at the transmitter fall on a 4×4 square grid. These points would be generated if 4-ary PAM impulses were conveyed on each of the two quadrature channels. We shall call this type of signal design Quadrature Amplitude Modulation (QAM), with a prefix number designating the number of PAM levels on each quadrature component. Thus, the modulation of Figure 4-2b would be designated 4-QAM. In general, we have M-QAM. M-QAM signal designs are well known in the literature and the performance is given by

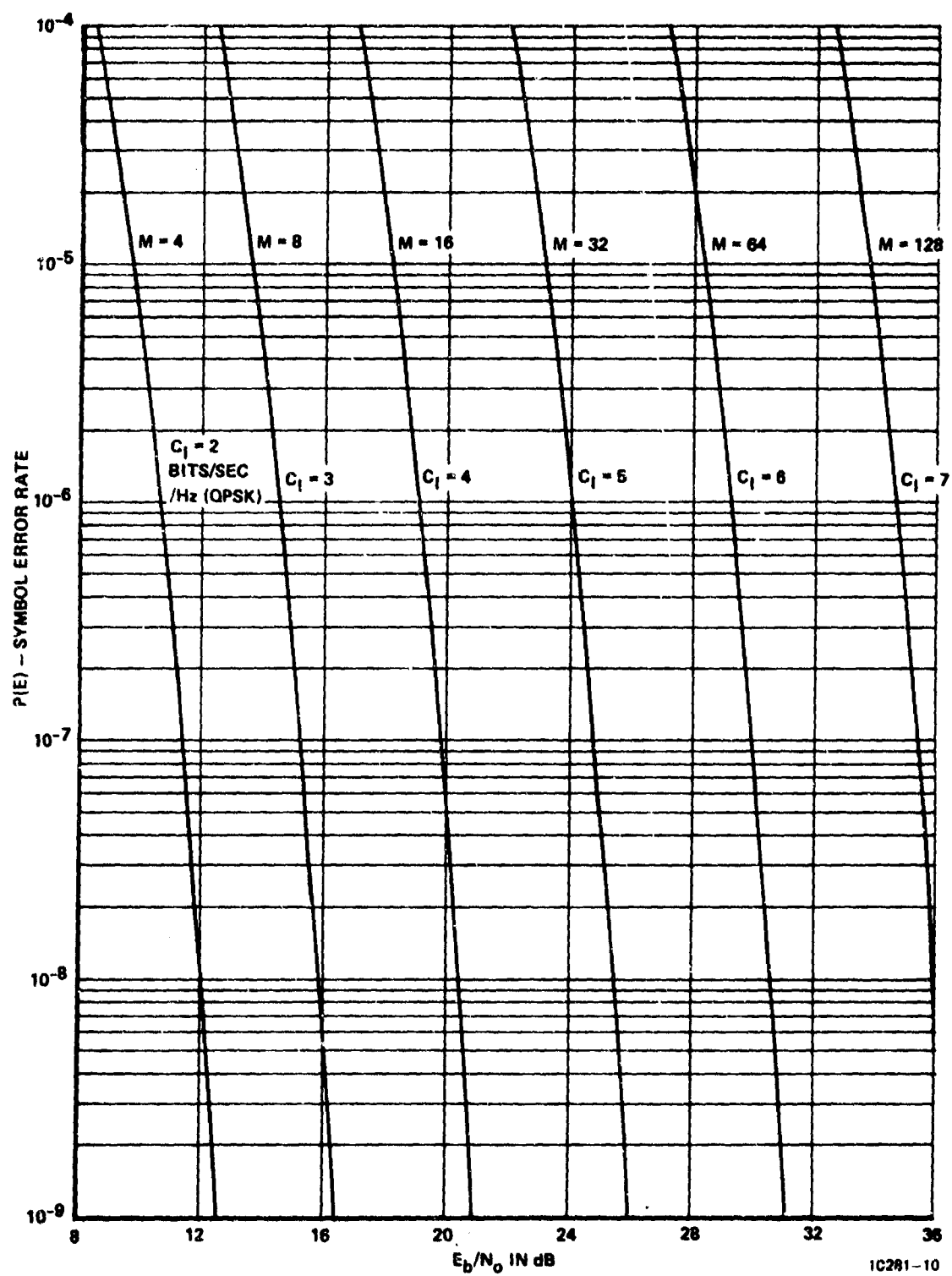


Figure 4.1. Ideal M-ARY PSK Performance

$$P(E) = \frac{4(M-1)}{M} Q\left(\sqrt{\frac{2E_b}{N_0} \left(\frac{3 \log_2 M}{M^2 - 1}\right)}\right) \left[1 - \left(\frac{M-1}{M}\right) Q\left(\sqrt{\frac{2E_b}{N_0} \left(\frac{3 \log_2 M}{M^2 - 1}\right)}\right)\right] \quad (4.2-1)$$

for M-QAM:

where E_b = Average energy per bit
 N_0 = One-sided noise density
 M = Number PAM levels on each quadrature component
 $P(E)$ = Probability of Symbol Error

The performance for M-QAM schemes is plotted in Figure 4.2. Since there are M^2 signal points for M-QAM, the number of bits, B , carried per RF symbol is

$$B = 2 \log_2 M. \quad (4.2-2)$$

and Equations (4-1) and (4.2-2) give the capacity of the ideally bandlimited M-QAM modulation as

$$C_I = 2 \log_2 M \text{ bits/sec/Hz} \quad (4.2-3)$$

The C_I for each curve is also noted in Figure 4.2.

Comparing Figure 4.2 with Figure 4.1, one notes the increasing theoretical superiority of M-QAM over M-PSK schemes for the same theoretical capacity in bits/sec/Hz as capacity increases.

Again, the same comments made previously in reference to M-PSK about the impracticality of the large bits/sec/Hz schemes hold also for the M-QAM schemes. For example, 16-QAM, used to obtain near 8 bits/sec/Hz bandwidth efficiency, would require transmitters and receivers capable of maintaining good resolution amongst the 256 signal points in the 16 x 16 grid. This generally is too stringent a requirement on all the system distorting effects and would be beyond the present state of the communications art.

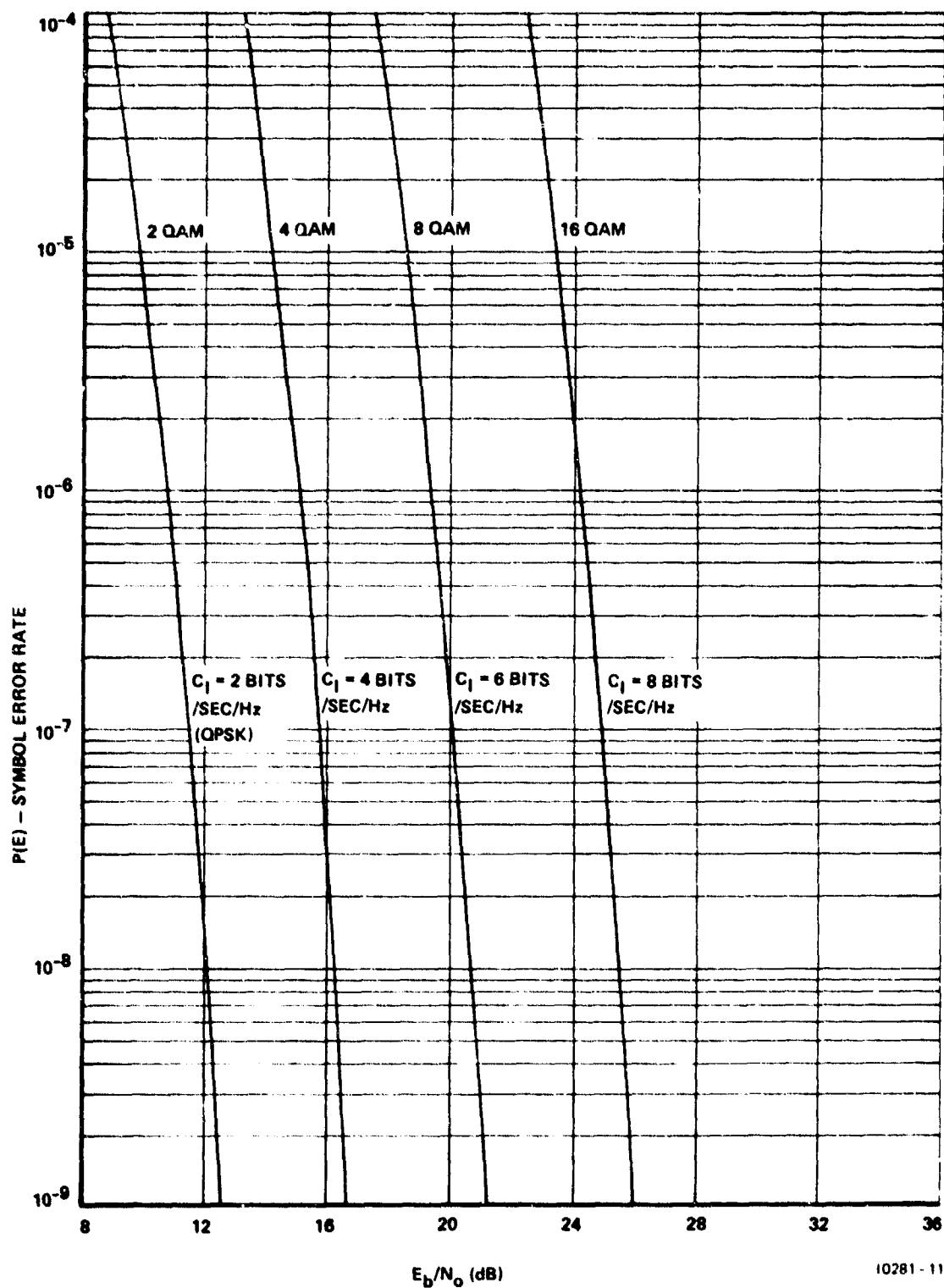


Figure 4.2. Ideal M-QAM Performance

The curves of Figures 4.1 and 4.2 will serve in following sections as references against which we compare the performance of many different nonideal modulation schemes examined during the course of this study.

4.2.1 Modified 6-QAM Signaling

It is advantageous with the M-QAM signaling format at the 4 bits/sec/Hz capacity level to use the modified 6-QAM format shown in Figure 4.2.1. As shown, this signal design is basically 6-QAM but with the four corner signals omitted. There are thus 32 possible signal points and consequently, 5 bits of information can be conveyed per RF symbol. This signal design can fill in the gap of capacities between that of 4-QAM (which carries 4 bits per symbol) and 8-QAM (which carries 6 bits per symbol).

In the remainder of this section we compute the performance and peak-to-average power ratio for the modified 6-QAM signal design.

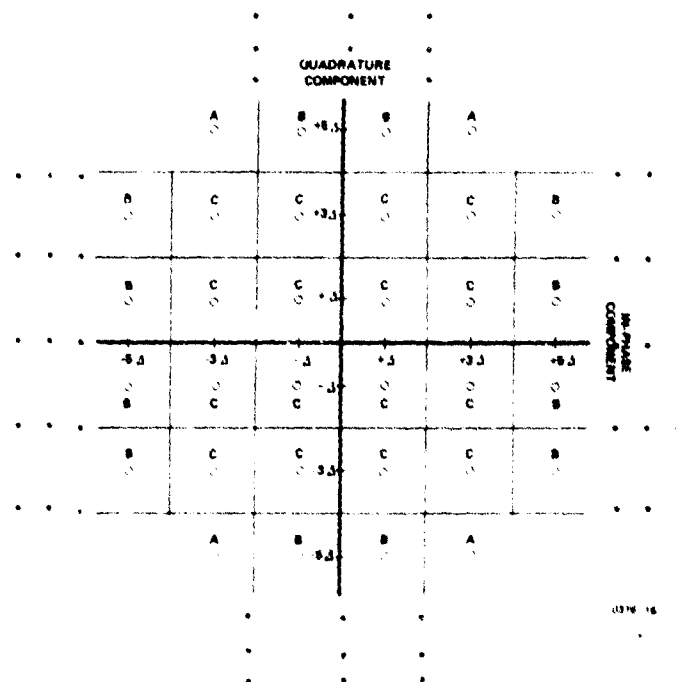


Figure 4.2.1. Modified 6-QAM Signal Design

4.2.1.1 Performance of Modified 6-QAM

As shown in Figure 4.2.1, the spacing between adjacent quadrature levels is 2Δ . For random data, the probability of transmitting each of the indicated 32 signal points is equal to $1/32$. The average energy per symbol, E_s , in terms of Δ for this signal format is found by computing the average vector length squared for the 32 signal points, i.e.,

$$E_s = \frac{\Delta^2}{32} [8(34) + 8(26) + 4(18) + 8(10) + 4(2)] \quad (4.2.1.1-1)$$

$$E_s = 20 \Delta^2 \quad (4.2.1.1-2)$$

or

$$\Delta = \sqrt{E_s/20} \quad (4.2.1.1-3)$$

for Δ in terms of E_s .

From Figure 4.2.1, the peak signal energy in terms of Δ is given by

$$E_p = (5^2 + 3^2) \Delta^2$$

or

$$E_p = 34 \Delta^2 \quad (4.2.1.1-4)$$

Taking the ratio of Equation (4.2.1.1-4) to Equation (4.2.1.1-2) we find that the ratio of peak-to-average power for the modified 6-QAM format is given by

$$\frac{P_p}{P_a} = \frac{E_p}{E_s} = 1.7 \Rightarrow 2.3 \text{ dB} \quad (4.2.1.1-5)$$

This ratio will be needed in later conversions of average power performance to peak power performance curves.

The lines in Figure 4.2.1 represent the locations of receiver decision thresholds. With these thresholds we note that there are three basic types of decisions regions labeled A, B, and C in Figure 4.2.1. The probability of symbol error given each of these types of decision regions is given by the following expressions:

$$\text{Letting } q = Q\left(\frac{\Delta}{\sqrt{N_0/2}}\right), \quad (4.2.1.1-6)$$

$$\text{where } Q(x) = \int_x^{\infty} \frac{e^{-y^2/2}}{\sqrt{2\pi}} dy, \quad (4.2.1.1-7)$$

we have:

$$P(E/A) = 1 - (1-q)^2 = 2q - q^2 \quad (4.2.1.1-8)$$

$$P(E/B) = 1 - (1-q)(1-2q) = 3q - 2q^2 \quad (4.2.1.1-9)$$

$$P(E/C) = 1 - (1-2q)^2 = 4q - 4q^2 \quad (4.2.1.1-10)$$

The average symbol error rate $P(E)$ is given by

$$P(E) = P(E/A)P(A) + P(E/B)P(B) + P(E/C)P(C) \quad (4.2.1.1-11)$$

From Figure 4.2.1 given equal probability for each signal point, we see that

$$P(A) = 4/32 \quad (4.2.1.1-12)$$

$$P(B) = 12/32 \quad (4.2.1.1-13)$$

$$P(C) = 16/32 \quad (4.2.1.1-14)$$

Substituting Equations (4.2.1.1-12) to (4.2.1.1-14) and (4.2.1.1-8) to (4.2.1.1-10) into Equation (4.2.1.1-11) we obtain

$$P(E) = \frac{27}{8} q - \frac{23}{8} q^2 \quad (4.2.1.1-15)$$

$$P(E) = 3.4q - 2.9q^2 = 3.4q (1 - 0.85q) \quad (4.2.1.1-16)$$

From Equations (4.2.1.1-3) and (4.2.1.1-6) we have

$$q = Q \left(\sqrt{E_s / 10N_0} \right) \quad (4.2.1.1-17)$$

Since 5 bits of information are carried by each symbol,

$$E_s = 5 E_b \quad (4.2.1.1-18)$$

where E_b = average energy per bit.

Substituting Equation (4.2.1.1-18) into Equation (4.2.1.1-17) we have

$$q = Q \left(\sqrt{(1/4) 2E_b / N_0} \right) \quad (4.2.1.1-19)$$

Equations (4.2.1.1-19) and (4.2.1.1-16) give the probability of symbol error for modified 6-QAM in terms of average E_b/N_0 as:

$$P(E) = 3.4Q \left(\sqrt{\frac{1}{4} \frac{2E_b}{N_0}} \right) \left[1 - 0.85Q \left(\sqrt{\frac{1}{4} \left(\frac{2E_b}{N_0} \right)} \right) \right] \quad (4.2.1.1-20)$$

For high E_b/N_0 this represents performance roughly 6 dB worse than binary PSK.

The symbol error rate given by Equation (4.2.1.1-20) is plotted versus E_b/N_0 in Figure 4.2.1.1. Also shown for comparison are the curves for 4- and 8-QAM.

For 10^{-5} symbol error rate, the modified 6-QAM scheme requires average E_b/N_0 of 16.1 dB.

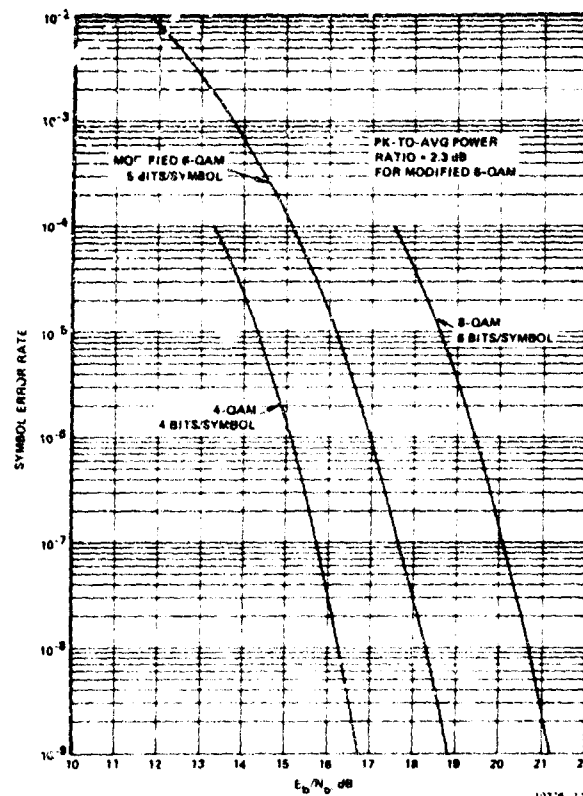


Figure 4.2.1.1. Modified 6-QAM Performance

The performance of modified 6-QAM is used in later performance trade-offs.

4.3 Capacity of Ideal Systems Compared to Shannon Capacity

The data presented in the previous section for the ideal systems can be presented in the useful form shown in Figure 4.3. Here, for the ideally bandlimited systems discussed above, we have plotted the capacity, C_I , for each system versus the required E_b/N_0 for error rate of 10^{-5} , 10^{-7} , and 10^{-9} . Also plotted is Shannon's channel capacity curve (see Appendix 1). Shannon's curve represents a theoretical bound on the absolute maximum capacity at zero error rate for a given E_b/N_0 for an infinitely complex modulation/demodulation digital transmission system. As such, it represents a goal to strive for in practical system design, but it represents essentially unattainable performance in a practical system.

Note in Figure 4.3 that the ideal M-QAM schemes track parallel to Shannon's capacity bound - being about 8 dB away at 10^{-5} error rate. Generally, this is an indication of good efficiency for a system not employing error-correction coding. By using some type of multilevel error-correction coding scheme, one could hope to buy some of the 8 dB back. See, for example, the coding/decoding technique in Section 7.

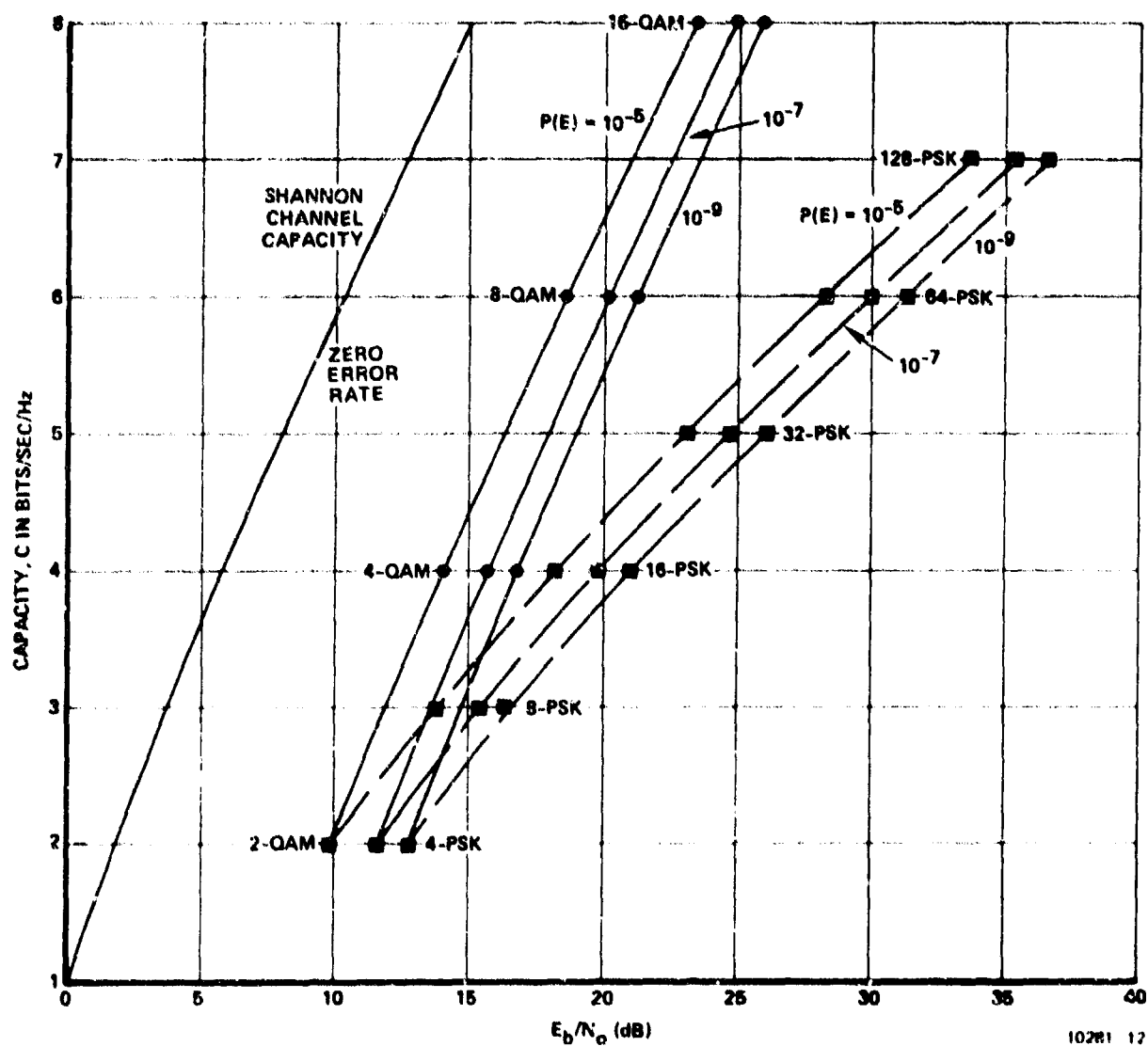


Figure 4.3. Channel Capacity Comparisons M-QAM and M-PSK Ideal Systems

Also, note in Figure 4.3, the increasing theoretical inefficiency of the M-PSK schemes relative to Shannon capacity and to M-QAM schemes at the higher capacity regions. This occurs because the signal design points are constrained to all lie on a circle as in Figure 4-2a. The M-QAM schemes on the other hand disperse the points over the signal space as in Figure 4-2b and thus achieve better nearest-neighbor structure for the same signal power.

The curves of Figure 4.3 are used throughout this report for comparison purposes to gauge the performance/bandwidth efficiency of many types of modulation schemes. In the ensuing sections, we almost always use the 10^{-5} error probability curve for comparison purposes between two systems. If one wishes to convert from 10^{-5} to 10^{-9} error rate on these curves, for most systems examined, it is necessary to add approximately 3 dB to the E_b/N_0 plotted, as exemplified by the spread between the 10^{-5} and 10^{-9} curves of Figure 4.3.

5. THE SUSCEPTIBILITY OF BANDWIDTH EFFICIENT MODEMS TO INTERFERENCE AND OTHER OUTSIDE DISTURBANCES

The vulnerability of bandwidth efficient modems to interference is particularly severe. This is an inescapable theoretical consequence of forcing transmitted symbols to carry many bits of information - the only way to obtain high b/s/Hz operation through modem signal design. The number of symbols/s that can be transmitted with no intersymbol distortion through a channel having ideal low pass bandwidth of W Hertz was first determined by Nyquist⁴ to be $2W$ symbols/s. Practical channels tend to verify that such a limit exists in that severe degradation is incurred as this value of symbols/s is approached. It turns out that one of the most effective ways of increasing the data throughput once this limit is approached is to increase the number of bits carried per transmitted symbol. This forces the transmitted signal points in signal space to be closer together for a given transmitter power limit. At the receiver, the problem of resolving which signal point was transmitted (i.e., demodulation) becomes more difficult in the face of outside disturbances.

The outside disturbances can be of many types. One type is additive Gaussian noise. The bandwidth efficient modem consequently requires a higher signal-to-noise ratio for a given symbol error rate as the number of b/s/Hz is increased.

Another type of outside disturbance is created by cochannel or adjacent channel interference. The bandwidth efficient modem is thus more vulnerable to interference since less interference power is required to push the transmitted signal point closer to an adjacent point, thus resulting in an error at the receiver. The outside disturbance can also result from loss of cross polarization discrimination in a dual polarization system.

To gain an appreciation for the increasing intolerance to outside disturbances as the number of bits/symbol is increased to obtain more b/s/Hz, we shall consider the effect of interference on M-QAM signaling. "M-QAM" denotes M-ary Quadrature Amplitude Modulation and is also known as Quadrature Amplitude Shift Keying or QASK.²⁰ The signal design for 4-QAM is shown in Figure 5-1. Here, four-level amplitudes

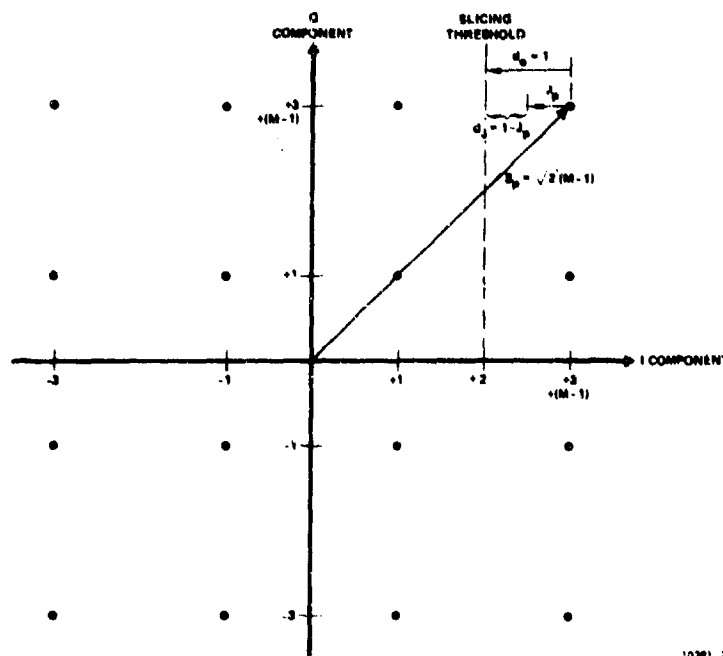


Figure 5-1. 4-QAM Signal Design

occur on each quadrature component of the transmitted signal. Each transmitted symbol can carry 4 information bits (2 bits on each of the two quadrature components). The 16 circles show the 16 allowable combinations of inphase and quadrature components. For general M-QAM, the quadrature components are given by

$$C_i = -(M - 1) + 2(i - 1), \quad i = 1, 2, \dots, M \quad (5-1)$$

The peak quadrature component is thus $(M-1)$. The peak signal amplitude is thus given by

$$S_p = \sqrt{2} (M-1) \quad (5-2)$$

We will assume the peak interference amplitude is J_p .

At the receiver, slicing thresholds are established at the midpoint between quadrature component levels as shown for the 4-QAM example in Figure 5-1. The distance to the threshold with no jamming is 1, i.e., as shown in Figure 5-1,

$$d_0 = 1, \quad (5-3)$$

The symbol error rate in the absence of jamming is approximated by

$$P_0 \approx Q \left(\frac{d_0}{\sigma_n} \right) \quad (5-4)$$

where

$$Q(x) = \frac{1}{2} \int_x^\infty e^{-y^2/2} dy$$

and σ_n = rms Gaussian noise at the receiver.

If we now presume that the interfering signal, with amplitude J_p , is so arranged as to reduce the distance to the threshold the maximum amount as shown in Figure 5-1, the distance to the threshold with interference is given by:

$$d_j = 1 - J_p. \quad (5-5)$$

The probability of error with worst-case interference is thus approximated by

$$P_J \approx Q\left(\frac{d_j}{\sigma_n}\right) \quad (5-6)$$

Comparing Equation (5-4) and Equation (5-6) the worst-case degradation caused by the interferer is

$$D \text{ (dB)} = 20 \text{ Log } \left(\frac{d_o}{d_j}\right) \quad (5-7)$$

From Equation (5-5), Equation (5-3), and Equation (5-7)

$$D(\text{dB}) = 20 \text{ Log } \left(\frac{1}{1 - J_p}\right) \quad (5-8)$$

$$\text{or } D(\text{dB}) = 20 \text{ Log } \left(\frac{1}{1 - \left(\frac{J_p}{S_p}\right)} S_p\right) \quad (5-9)$$

Substituting Equation (5-2) into Equation (5-9) we obtain

$$D(\text{dB}) = 20 \text{ Log } \left[\frac{1}{1 - \left(\frac{J_p}{S_p}\right) \sqrt{2(M-1)}} \right] \quad (5-10)$$

Eye-closure at the demod is caused by the interferer when the denominator in Equation (5-10) equals zero. In this case, the distance to the slicing threshold is reduced to zero by the interferer.

This worst-case degradation is plotted in Figure 5-2 for various values of M versus the ratio of peak signal to peak interference power ratio, i.e., $20 \text{ Log } (S_p/J_p)$. The case for $M = 2$ corresponds to QPSK. From these curves one estimates that 16-QAM requires approximately 25 dB higher signal-to-interference-ratio for a given level of degradation compared to QPSK. 8-QAM requires approximately 17 dB higher signal/interference ratio than QPSK. Thus we have a quantitative evaluation of the increased susceptibility of the higher spectral efficiency M-QAM schemes to interference.

Although we have called the source of outside disturbance an interferer in the above development, the disturbance could come from any source. The disturbance could arise because of equipment imperfection for example. The requirement that mixers and amplifiers used at the receiver hold all distortions to below 40 dB down relative to the signal is starting to press the equipment designers. As indicated in Figure 5-2, however, it is necessary to do so to hold degradation in performance below 1 dB with 8-QAM. This tends to argue that one should not go much above the spectral efficiency of 8-QAM if significant design problems are to be avoided. From work done on this study, 8-QAM can provide around 4.5 b/s/Hz under FCC 19311 in a practical implementation. Thus, from practical viewpoints, it seems to us that 4.5 b/s/Hz should be about the upper limit of spectral efficiency sought at the present time. An attempt to push spectral efficiencies much higher than this should be looked upon with a good deal of skepticism because of the implementation problems that arise above that level. Consequently, in the remainder of this report we have placed primary emphasis on schemes capable of 3 to 5 b/s/Hz.

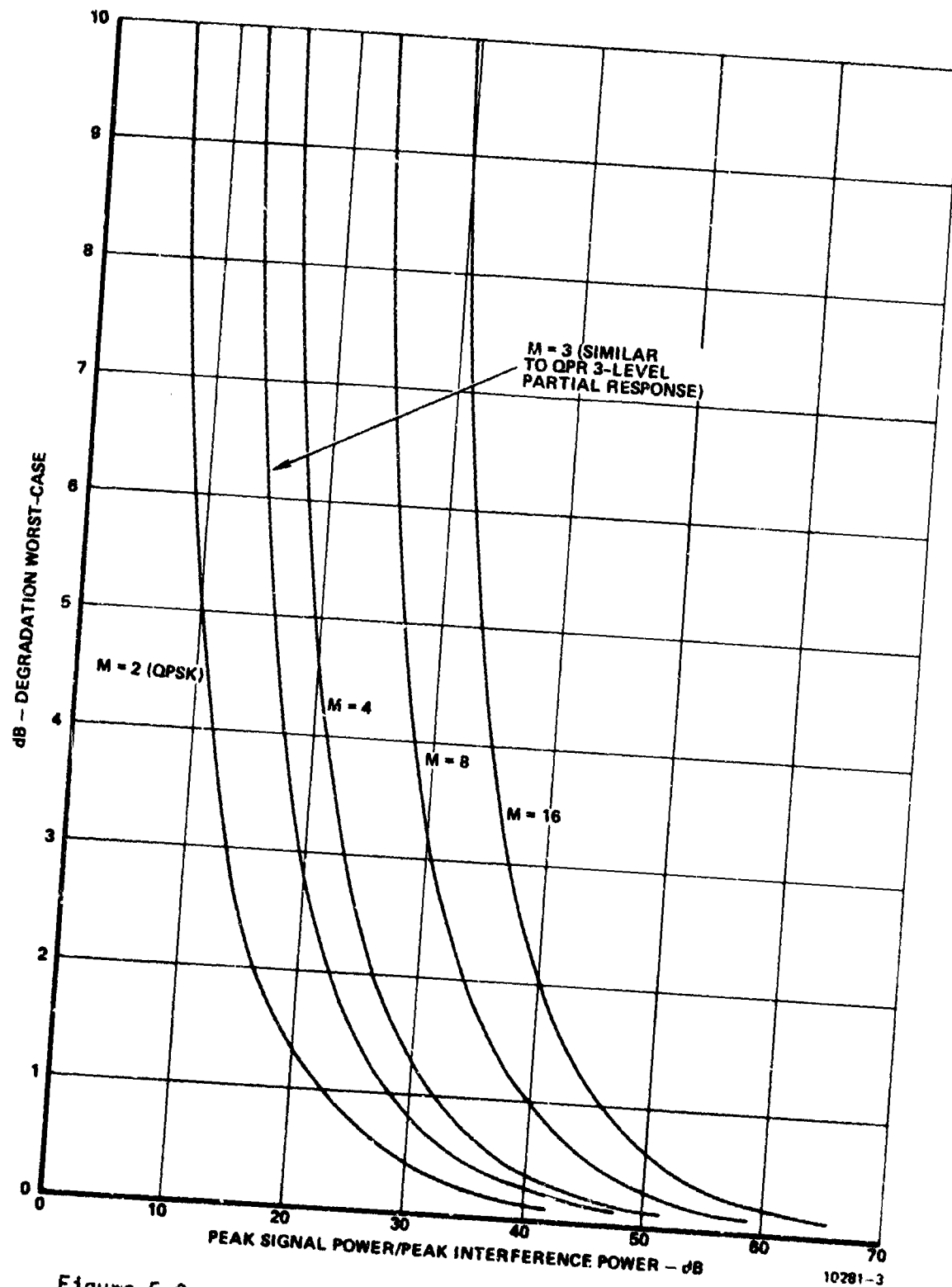


Figure 5-2. Worst-Case Degradation for M-ary PAM on Quadrature Carriers Versus Interference

6. PERFORMANCE OF PRACTICAL DIGITAL COMMUNICATION SYSTEMS

6.1 Introduction

The performance of the ideally bandlimited uncoded digital systems of Section 4. are theoretically interesting as references against which to compare the performance of more practical systems. The capacity available with the ideal systems are simply unavailable with more practical systems, however. The ideally bandlimited filters used in the ideal systems are, of course, unavailable.

A practical system also must use a realistic power amplifier having various practically-encountered imperfections, such as nonlinearity. On the other hand, the ideal system performances are derived under the implicit assumption of perfect linearity throughout the transmitter-receiver signal path.

The introduction of more realistic filters in the signal path, having various degrees of amplitude and group delay distortion, forces the practical system designer to reckon with the attendant problem of providing for equalization to avoid severe performance degradation.

Thus, in the practical digital system, the designer must account for both nonlinear and linear distortions which are always present before realistic performance predictions and comparisons can be made. This section considers most of the important practical constraints that are encountered in real systems. These include: 1) The effect of nonideal sharp cutoff spectral shaping filters; 2) The effect of additional linear distortion created by realistic filters; 3) The effect of signaling with a peak power limited amplifier; 4) The relative efficiency between preamplifier filtering and postamplifier filtering; 5) The effect of practical nonlinearities encountered with real amplifiers on system performance; 6) Presentation of a technique for adapting to realistic amplifier nonlinearities in order to render the amplifier

linear for the purpose of supporting highly bandwidth efficient digital data transmission; and, finally 7) The effect on performance of practical imperfections in an implementation of a bandwidth efficient modem including a baseband equalizer for counteracting linear distortion caused by realistic filter characteristics.

6.2 Systems Using Square Root Nyquist Shaping Filters

In this section we examine the general system of Figure 2-5 of Section 2. for the specified case of no intersymbol interference at the receiver, i.e., for $f(D) = 1$. In this case, the samples fed to the sample processor are replicas of the transmitted samples, but perturbed by a Gaussian noise sample of variance $= N_0/2$. This system is shown in Figure 6.2-1. The optimum sample processor in this case is a memoryless device since there is no correlation between input samples. The sample processor takes the form of a threshold device with thresholds midway between transmitted levels.

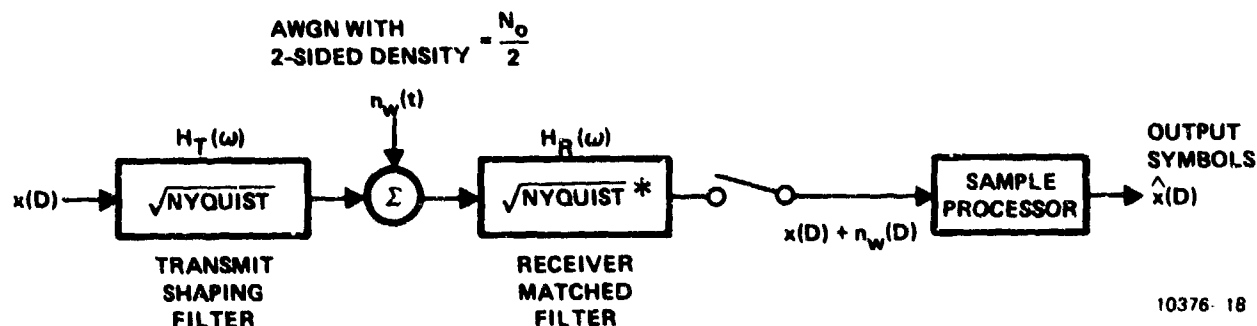


Figure 6.2-1. Systems With Square Root Nyquist Shaping Filters

The performance in terms of E_b/N_0 required for given symbol error rate is known for many types of digital signalling schemes of the type shown in Figure 6.2-1. The M-QAM and M-PSK schemes discussed in Section 4. are examples for which performance is known. In Section 4. the ideal systems considered were a special case of Figure 6.2-1

where the square root Nyquist filters were ideal sharp cutoff filters. Here, we wish to describe the capacity versus performance curves when the square root Nyquist filters are of a particular form which is not ideal sharp cutoff.

The particular form of square root Nyquist transmit shaping filter examined here is the square root of the so-called raised-cosine filter ⁵, i.e.,

$$H_T(\omega) = \begin{cases} T^{1/2} (2\pi)^{-1/2} & , 0 < \omega < \frac{\pi}{T} (1-\alpha) \\ \left| \frac{T}{2} - \frac{T}{2} \sin \left[\frac{T}{2\alpha} \left(\omega - \frac{\pi}{T} \right) \right] \right|^{1/2} (2\pi)^{-1/2} & , \frac{\pi}{T} (1-\alpha) \leq \omega \leq \frac{\pi}{T} (1+\alpha) \end{cases} \quad (6.2-1)$$

where T = symbol time

α = Filter parameter designating excess bandwidth over Nyquist bandwidth.

The spectrum of the signal is given by

$$S(\omega) = |H_T(\omega)|^2 \quad (6.2-2)$$

and consequently the spectrum has the raised-cosine shape shown in Figure 6.2-2 for several values of rolloff parameter, α . As shown, these filters all produce spectra which are down 3 dB at the Nyquist band edge at $fT = 0.5$. The spectra are also of finite bandwidth - decreasing to zero for frequencies greater than $0.5(1/T)(1+\alpha)$. The ideal sharp cutoff filter is shown as the limiting case of $\alpha = 0$, in which case the spectrum is constant out to the Nyquist band edge.

The spectra of Figure 6.2-2 have all been normalized to produce unit total power in the radiated signal, i.e.,

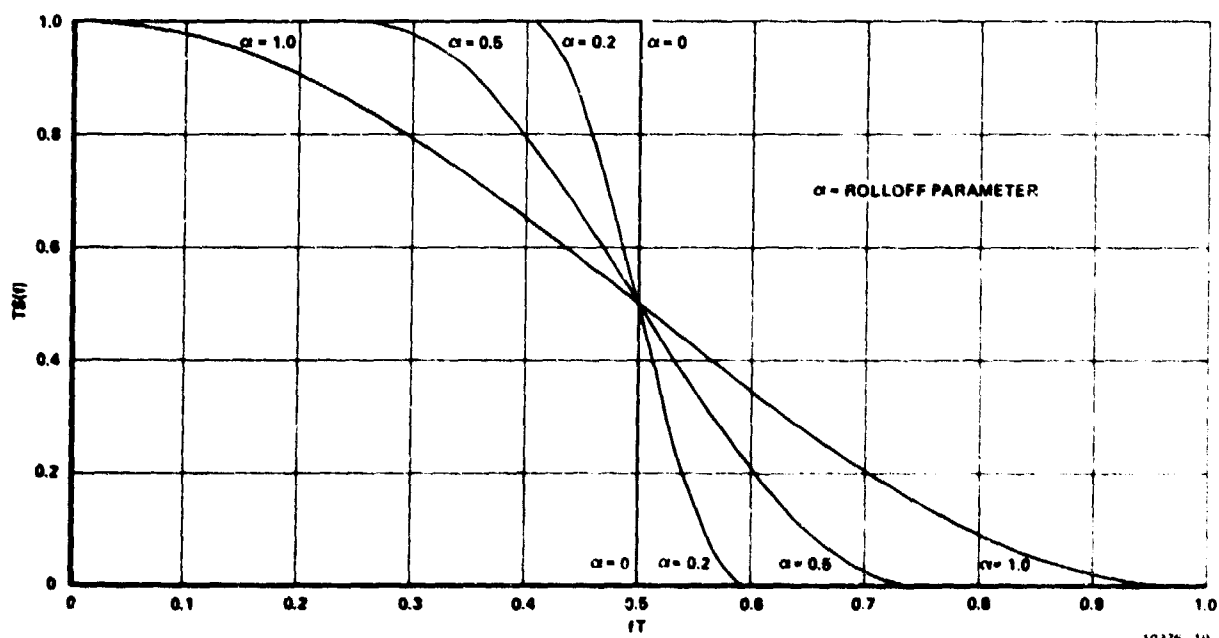


Figure 6.2-2. Spectra With Square Root Raised Cosine Filters

$$\int_{-\infty}^{+\infty} S(\omega) df = 1. \quad (6.2-3)$$

The spectra are plotted on a dB scale in Figures 6.2-3, 6.2-4, and 6.2-5 for $\alpha = 0.2, 0.5, \text{ and } 1.0$ respectively. Also shown on the spectral plots are the most restrictive FCC 19311 masks, for authorized bandwidth of 3.5 MHz, within which each spectrum will fit. The masks are obtained by the technique described in Paragraph 3.2. The time-bandwidth product, $B_a T$, is given on each curve that dictates the minimum authorized RF bandwidth allowable under FCC 19311 as β times the symbol rate, i.e.,

$$B_a T = \beta \quad (6.2-4)$$

where β = constant depending on rolloff parameter, α .
 B_a = minimum FCC 19311 authorized RF bandwidth.
 T = Symbol time.

The maximum number of symbols/sec/Hz, S , is given by:

$$S = \frac{1}{B_a T} \quad (6.2-5)$$

S is plotted versus the rolloff parameter α in Figure 6.2-6. To determine capacity, C , in bits/sec/Hz, multiply S by number of bits carried per RF symbol, i.e.,

$$C = BS \quad (6.2-6)$$

where C = capacity in bits/sec/Hz
 B = bits carried by each RF symbol
 S = capacity in symbols/sec/Hz.

Since the E_b/N_0 performance is the same as ideal systems and the capacity is determined from Equation (6.2-6) and S from Figure 6.2-6, one can plot the capacity versus E_b/N_0 curves of Figure 6.2-7

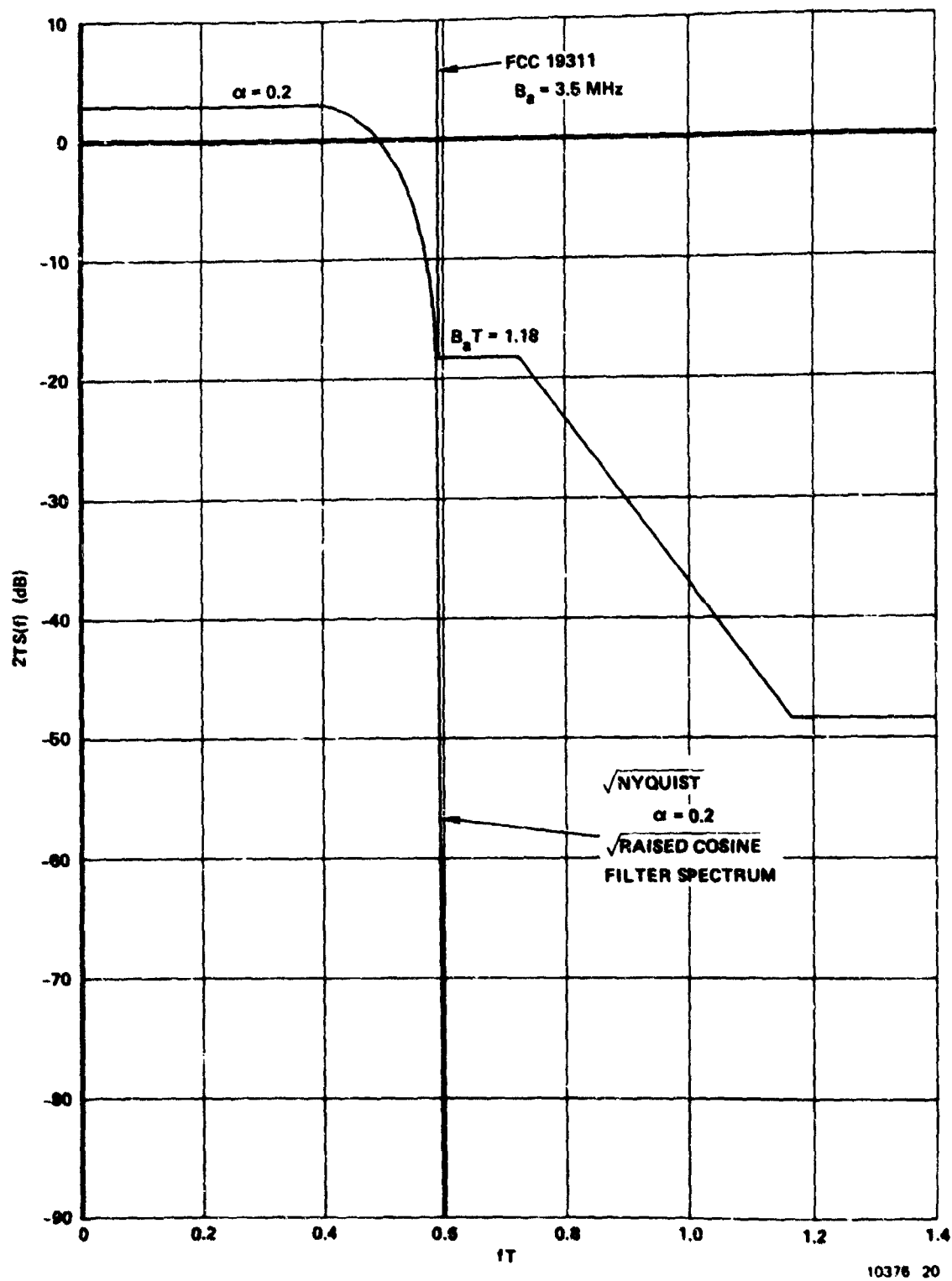
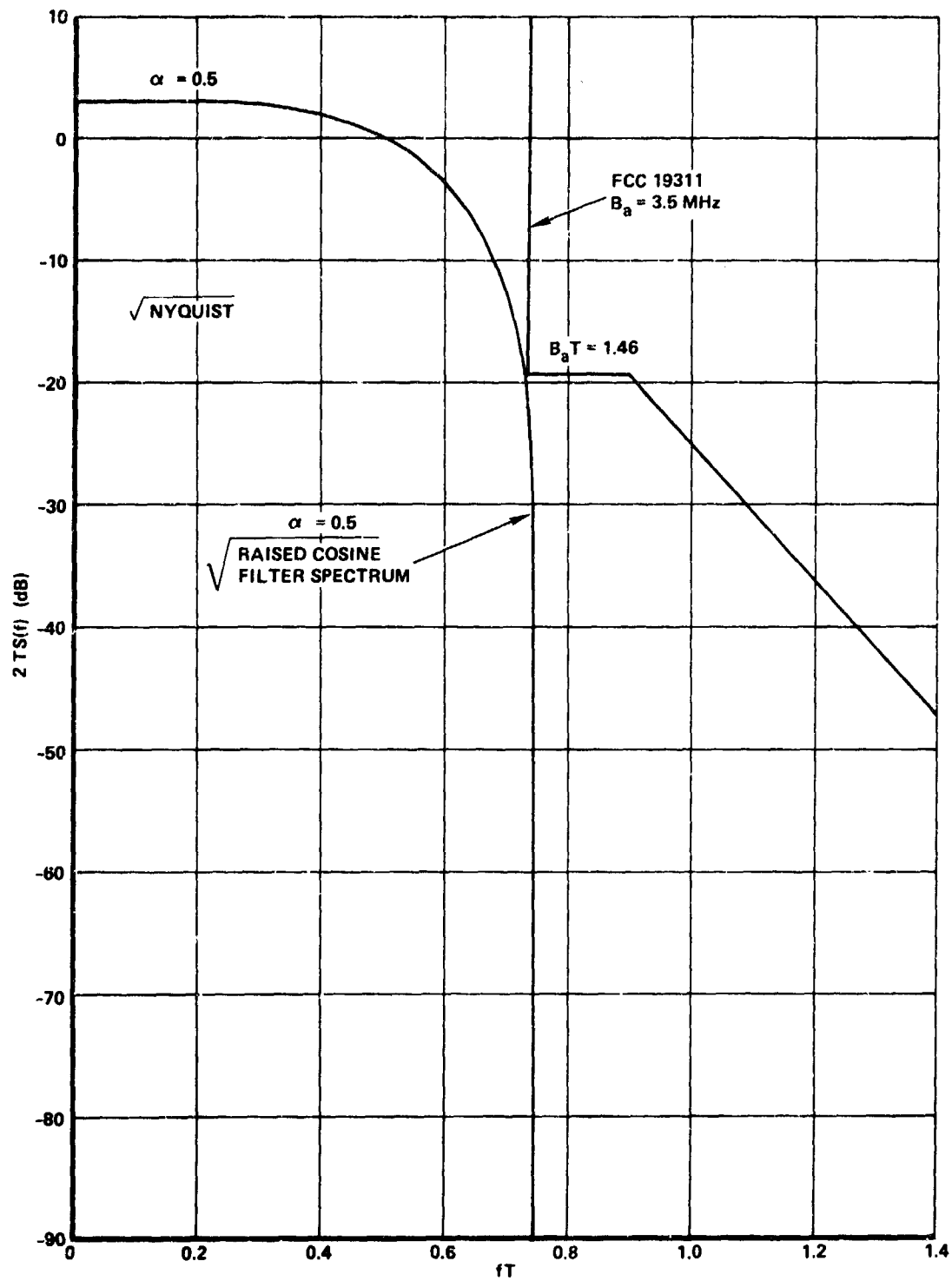


Figure 6.2-3. Spectrum for $\alpha = 0.2$ Square Root Raised Cosine Filter



10376-21

Figure 6.2-4. Spectrum for $\alpha = 0.5$ Square Root Nyquist Shaping Filter

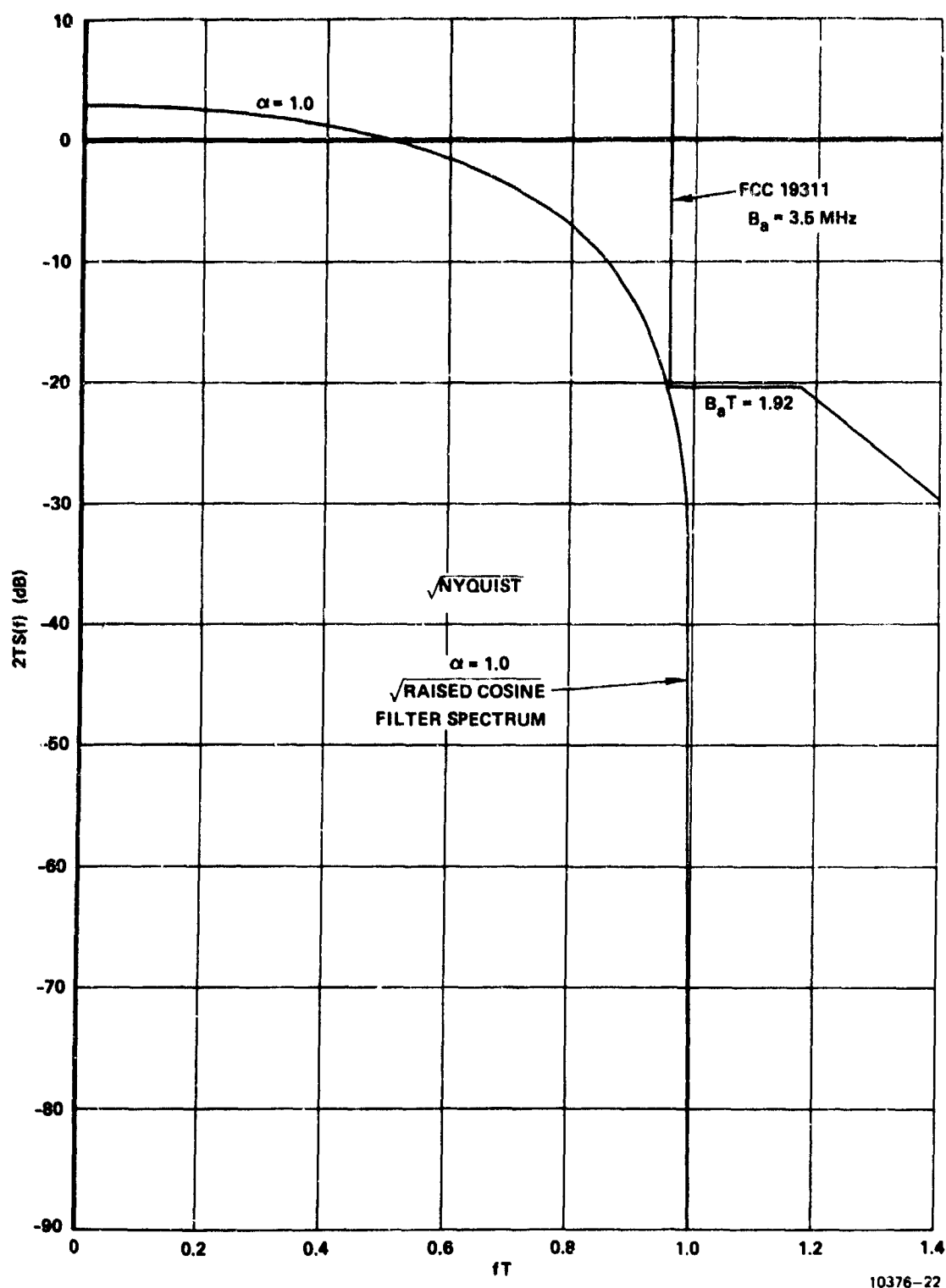


Figure 6.2-5. Spectrum for $\alpha = 1.0$ Square Root Raised Cosine Filter

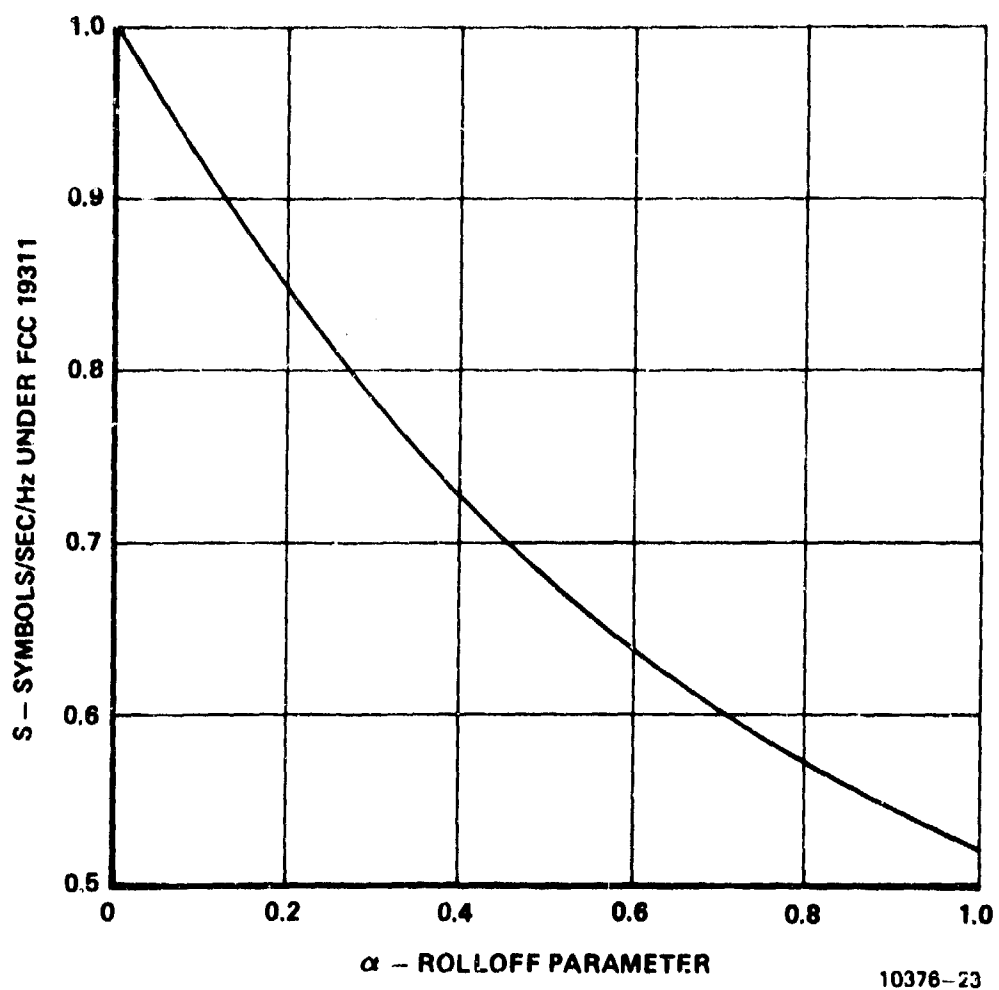


Figure 6.2-6. Symbols/Sec/Hz For Square Root Raised Cosine Shaping Filters

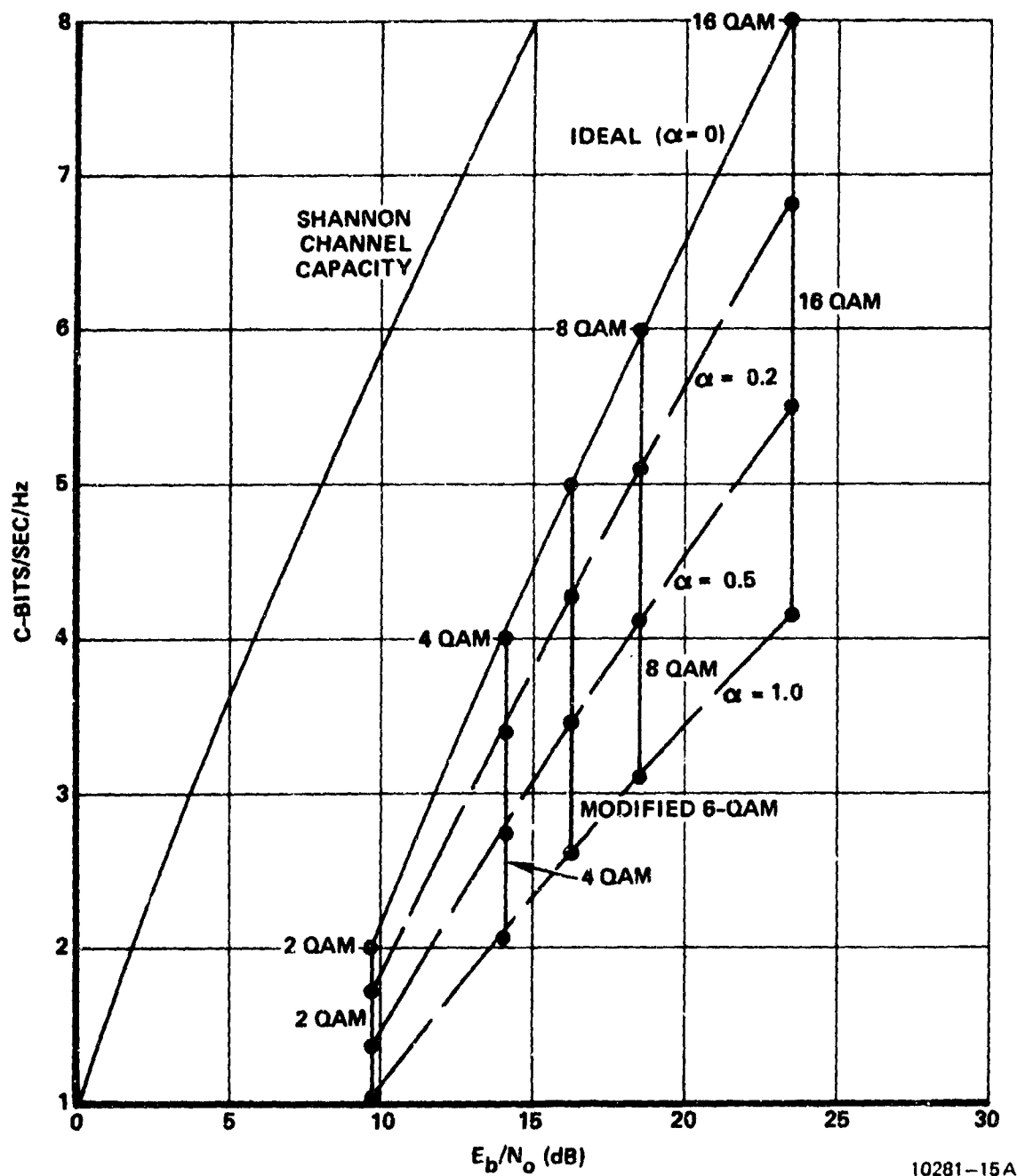


Figure 6.2-7. Capacity Versus Performance With M-QAM Signaling for Square Root Raised Cosine Shaping Filters, α = Rolloff Parameter, $P(E) = 10^{-5}$

for M-QAM transmission and Figure 6.2-8 for M-PSK transmission. One notes from these plots that allowance of realistic filter rolloffs causes significant capacity loss relative to ideal, $\alpha = 0$, sharp cutoff filters. For example, $\alpha = 0.5$ rolloff produces capacity which is only 68 percent of ideal capacity.

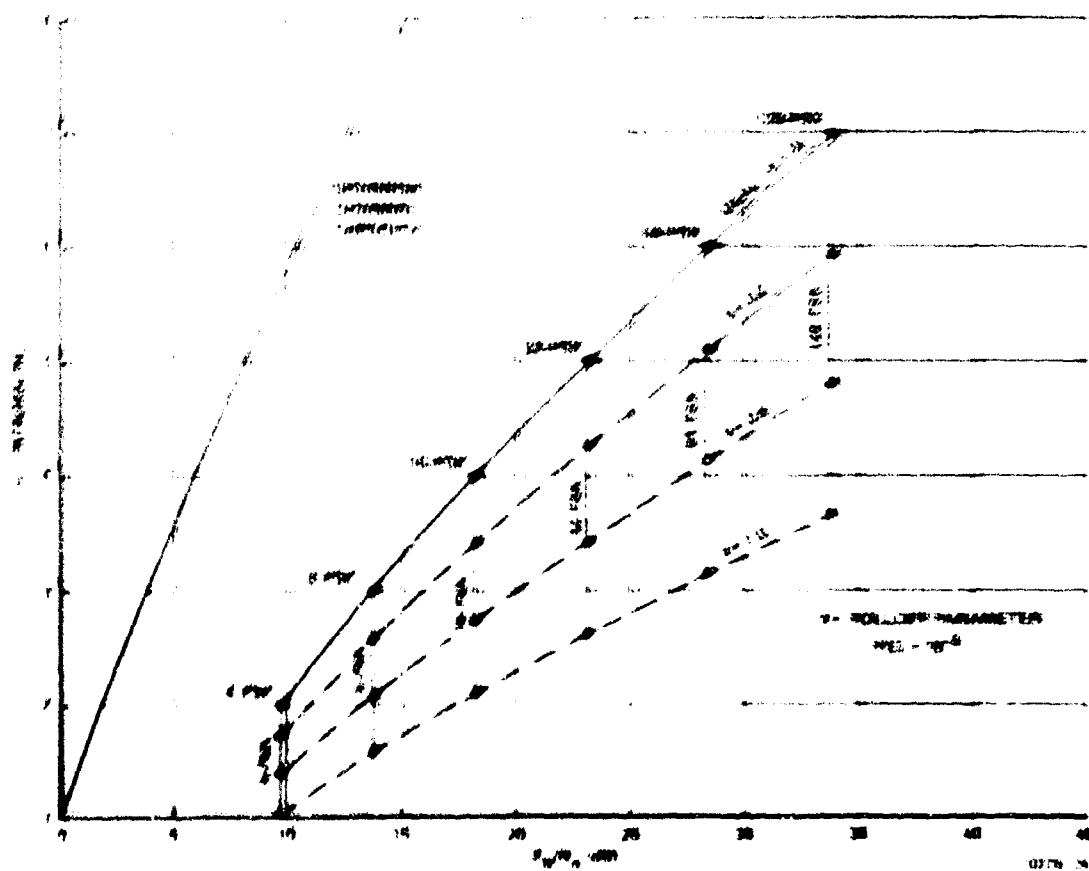


Figure A 2-8. Capacity Versus Performance with M-PSK Signaling for Square Root Raised Cosine Shaping Filters

6.3

Partial Response in Conjunction with Square Root Nyquist Filters

In Section 2. it has been shown that a general shaping filter is always representable as a combination of a partial response filter (transversal filter) specified by the polynomial, $f(D)$ and a square root Nyquist filter. Further, in Paragraph 2.2.5, the optimum finite degree polynomial, $f(D)$, for maximizing percent power in a specified band was shown to be the eigenvector of a matrix depending on the square root Nyquist filter. (See Equation (2.2-37) of Paragraph 2.2.5.) In this section we find the optimum $f(D)$ partial responses to use with square root Nyquist filters of the raised cosine variety. The spectrum produced by these square root Nyquist filters is

$$N(\omega) = \begin{cases} T/2\pi & , \quad 0 < |\omega| < \frac{\pi}{T} (1-\alpha) \\ \frac{T}{2\pi} \left\{ \frac{1}{2} - \frac{1}{2} \sin \left[\frac{T}{2\alpha} \left(\omega - \frac{\pi}{T} \right) \right] \right\} & , \quad \frac{\pi}{T} (1-\alpha) \leq |\omega| \leq \frac{\pi}{T} (1+\alpha) \end{cases} \quad (6.3-1)$$

where α = Rolloff parameter for the filter

T = Symbol time

As shown in Equation (2.2-37) of Paragraph 2.2.5, the matrix, $\{m_{ik}\}$ for which we need the eigenvectors to locate optimum $f(D)$'s is defined by elements

$$m_{ik} = \int_{-\omega_B}^{+\omega_B} e^{j(i-k)\omega T} N(\omega) d\omega \quad (6.3-2)$$

where ω_B = band within which power is to be maximized.

Since the $N(\omega)$ defined by Equation (6.3-1) is an even function of ω , Equation (6.3-2) can be written:

$$m_{ik} = 2 \int_0^{\omega_B} \cos [(i-k)\omega T] N(\omega) d\omega \quad (6.3-3)$$

If $\omega_B \leq \frac{\pi}{T}$ ($1 - \alpha$) then (6.3-3) is

$$m_{ik} = 2 \int_0^{\omega_B} \frac{T}{2\pi} \cos [(i-k)\omega T] d\omega$$

or

$$m_{ik} = \frac{1}{\pi} \int_0^{\omega_B T} \cos [(i-k)\theta] d\theta \text{ for } \omega_B T \leq \pi(1-\alpha)$$

or

$$m_{ik} = \frac{\omega_B T}{\pi} \text{Sinc} [(i-k) \omega_B T], \text{ for } \omega_B T \leq \pi(1-\alpha) \quad (6.3-4)$$

For an ideal sharp cutoff filter, Equation (6.3-4) defines the matrix used to determine optimum partial response for any $\omega_B T$ product out to Nyquist band edge, $\omega_B T = \pi$. It is interesting to note that when $\alpha = 0$ and $\omega_B T = \pi$ = Nyquist band edge, that the matrix defined by Equation (6.3-4) is the identity matrix. An arbitrary vector is an eigenvector of the identity matrix with eigenvalue = 1 which indicates that an arbitrary partial response places 100 percent of the power in the ideal sharp cutoff bandwidth - as it should. Further, it is also interesting to note that in the ideal sharp cutoff filter, $\alpha = 0$ case, the matrix for finding the optimal length 2 partial response for maximizing power in a band $\omega_B < \frac{\pi}{T}$, is given by the 2 x 2 matrix:

$$M = \begin{bmatrix} a & b \\ b & a \end{bmatrix} \quad (6.3-5)$$

where $a = \omega_B T / \pi$
 $b = (\omega_B T / \pi) \text{Sinc}(\omega_B T)$

Since $\omega_B T < \pi$, both a and b are positive numbers and the eigenvector with maximum eigenvalue is

$$\vec{f} = (0.707, 0.707) \quad (6.3-6)$$

The maximum eigenvalue, λ_m , is

$$\lambda_m = \frac{\omega_B T}{\pi} (1 + \text{Sinc}(\omega_B T)) \quad (6.3-7)$$

Equation (6.3-6) indicates that duobinary is the optimum length 2 partial response to maximize power in any band less than the ideal cutoff filter's bandwidth and the corresponding maximal fractional power in band is given by λ_m of Equation (6.3-7).

The matrix, M , is defined by Equation (6.3-4) whenever $\omega_B T \leq \pi(1-\alpha)$. We still must determine the elements, m_{ik} , for $\omega_B T > \pi(1-\alpha)$ in the general case. Using Equations (6.3-3) and (6.3-1) for this case, we obtain

$$m_{ik} = \begin{cases} \frac{\pi}{T} (1-\alpha) & \text{for } \omega_B T \leq \pi(1-\alpha) \\ 2 \int_0^{\frac{\omega_B T}{2\pi}} \frac{T}{2\pi} \cos[(i-k)\omega T] d\omega & \text{for } \frac{\pi}{T} (1-\alpha) < \omega_B T < \frac{\pi}{T} (1+\alpha) \\ + 2 \int_{\frac{\omega_B T}{2\pi}}^{\frac{\pi}{T} (1+\alpha)} \left[\frac{1}{2} - \frac{1}{2} \sin\left[\frac{T}{2\alpha}(\omega - \frac{\pi}{T})\right] \right] \cos[(i-k)\omega T] d\omega & \text{for } \omega_B T > \frac{\pi}{T} (1+\alpha) \end{cases} \quad (6.3-8)$$

The first integral is the same as that which led to Equation (6.3-4) except evaluated for the special case $\omega_B T = \pi(1 - \alpha)$. Therefore, we can write Equation (6.3-8) as

$$m_{ik} = (1 - \alpha) \text{Sinc} [(i-k)\pi (1 - \alpha)] \\ + 2 \int_{\frac{\pi}{T}(1 - \alpha)}^{\omega_B} \frac{T}{2\pi} \left| \frac{1}{2} - \frac{1}{2} \text{Sinc} \left[\frac{T}{2\alpha} (\omega - \frac{\pi}{T}) \right] \right| \cos [(i-k) \omega T] d\omega. \quad (6.3-9)$$

Evaluating the remaining integral in Equation (6.3-9), one obtains

$$m_{ik} = \frac{(1 - \alpha)}{2} \text{Sinc} [(i-k)(1 - \alpha)\pi] + \frac{\omega_B T}{2\pi} \text{Sinc} [(i-k) \omega_B T] \\ + \frac{1}{4\pi} \frac{\left| \cos \left[(i-k - \frac{1}{2\alpha}) \omega_B T - \frac{\pi}{2\alpha} \right] + \sin [(i-k)(1 - \alpha)\pi] \right|}{i-k - 1/2\alpha} \\ - \frac{1}{4\pi} \frac{\left| \cos \left[(1 - k - \frac{1}{2\alpha}) \omega_B T - \frac{\pi}{2\alpha} \right] + \sin [(1-k)(1 - \alpha)\pi] \right|}{1-k - 1/2\alpha} \quad (6.3-10)$$

$$\text{for } \pi(1 - \alpha) < \omega_B T < \pi(1 + \alpha)$$

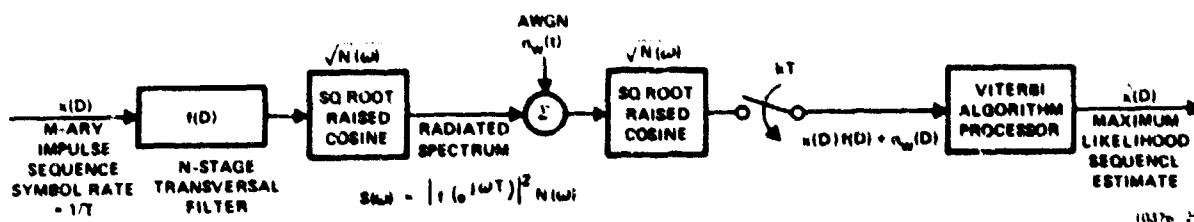
Thus, between Equations (6.3-4) and (6.3-10) we have defined the matrix necessary to locate the partial response of any length which will maximize percent power in any band, ω_B , for the square root raised cosine filters with general rolloff parameter, α .

During the course of this study, a computer program was written to determine the matrix, $|m_{ik}|$, and find its eigenvectors and eigenvalues. As shown in Paragraph 2.2.5, the eigenvector with maximum eigenvalue defines the tap gains of the optimal partial response

transversal filter and the corresponding eigenvalue is the fraction of total power in-band. We present some of the results found for these optimal partial responses in the following section.

6.3.1 Some Optimal Partial Response Results

In this section we display some of the optimal partial response results. These partial responses were found by the method just outlined in the previous section for the square root Nyquist filters of the raised cosine variety. As we shall see, these partial response schemes generally place nulls on and/or inside the Nyquist band edge and consequently do not lend themselves to Nyquist equalization because of the severe noise enhancement incurred for such cases. Such schemes do, however, lend themselves to Viterbi algorithm demodulation without severe performance penalties and we show results using these sample processors at the receiver. To be clear, let us remind the reader that the scheme investigated is as shown in Figure 6.3.1. The polynomial $f(D)$ of various lengths (degrees) has been chosen by the techniques of the previous section to maximize the percent power in the radiated spectrum, $S(\omega)$, contained within some selected bandwidth.



6.3.1. Partial Response Signaling System

6.3.1.1 Optimal Length Two Partial Response

The case of the 2×2 matrix $|m_{ik}|$, defined by the elements of Equation (6.3-4) or (6.3-10) has been found to have all positive elements for all α and ω_B . In this case the optimal Length 2 partial response is duobinary, i.e.,

$$f(D) = (1/\sqrt{2}) + (1/\sqrt{2})D \quad (6.3.1.1-1)$$

opt 2

The radiated spectrum in this case is given by

$$S(\omega) = |f(e^{j\omega T})|^2 N(\omega) \quad (6.3.1.1-2)$$

where $N(\omega)$ given by Equation (6.3-1)
 $f(D)$ given by Equation (6.3.1.1-1)

Evaluating Equation (6.3.1.1-2) for the duobinary case, we obtain

$$S(\omega) = 2 \cos^2(\omega T/2) N(\omega) \quad (6.3.1.1-3)$$

The spectra produced per Equation (6.3.1.1-3) for α 's of 0, 0.2, 0.5, and 1.0 are shown in Figures 6.3.1.1-1 through 6.3.1.1-4 respectively. Also shown on each spectrum is the FCC 19311 spectral mask for 3.5 MHz authorized bandwidth, and the spectrum for the square root raised cosine filter without the duobinary partial response. Note that not until $\alpha \leq 0.2$ does any improved spectral economy result relative to just using the square root cosine filter without partial response. In the $\alpha = 1$ case, the spectrum with duobinary partial response is actually slightly wider than with no partial response.

The performance of the duobinary partial response channel when M-ary impulses are used in the system of Figure 6.3.1 has been determined using our computer program. The results obtained are shown in Figure

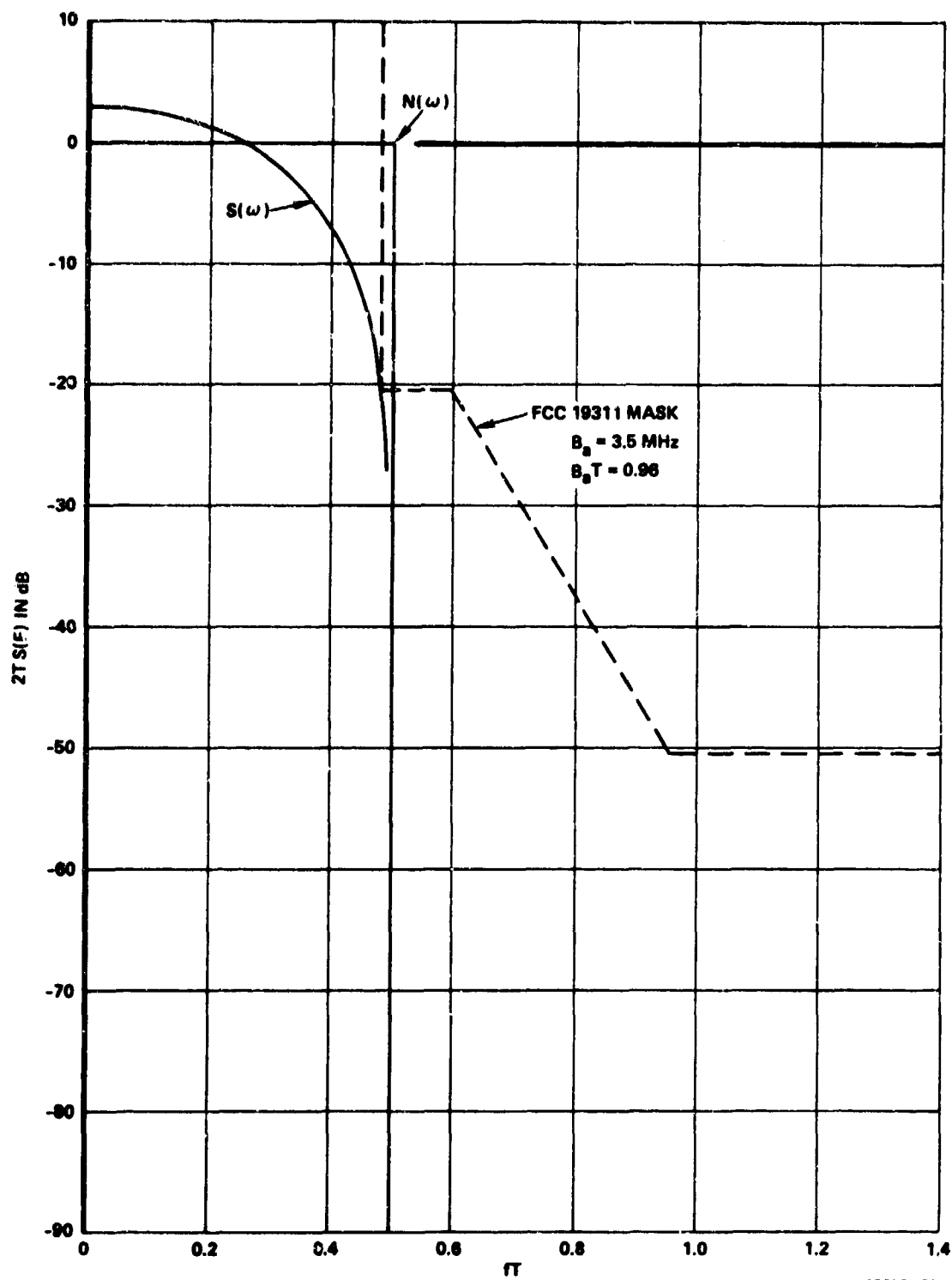


Figure 6.3.1.1-1. Duobinary Partial Response With $\alpha = 0$ Filter

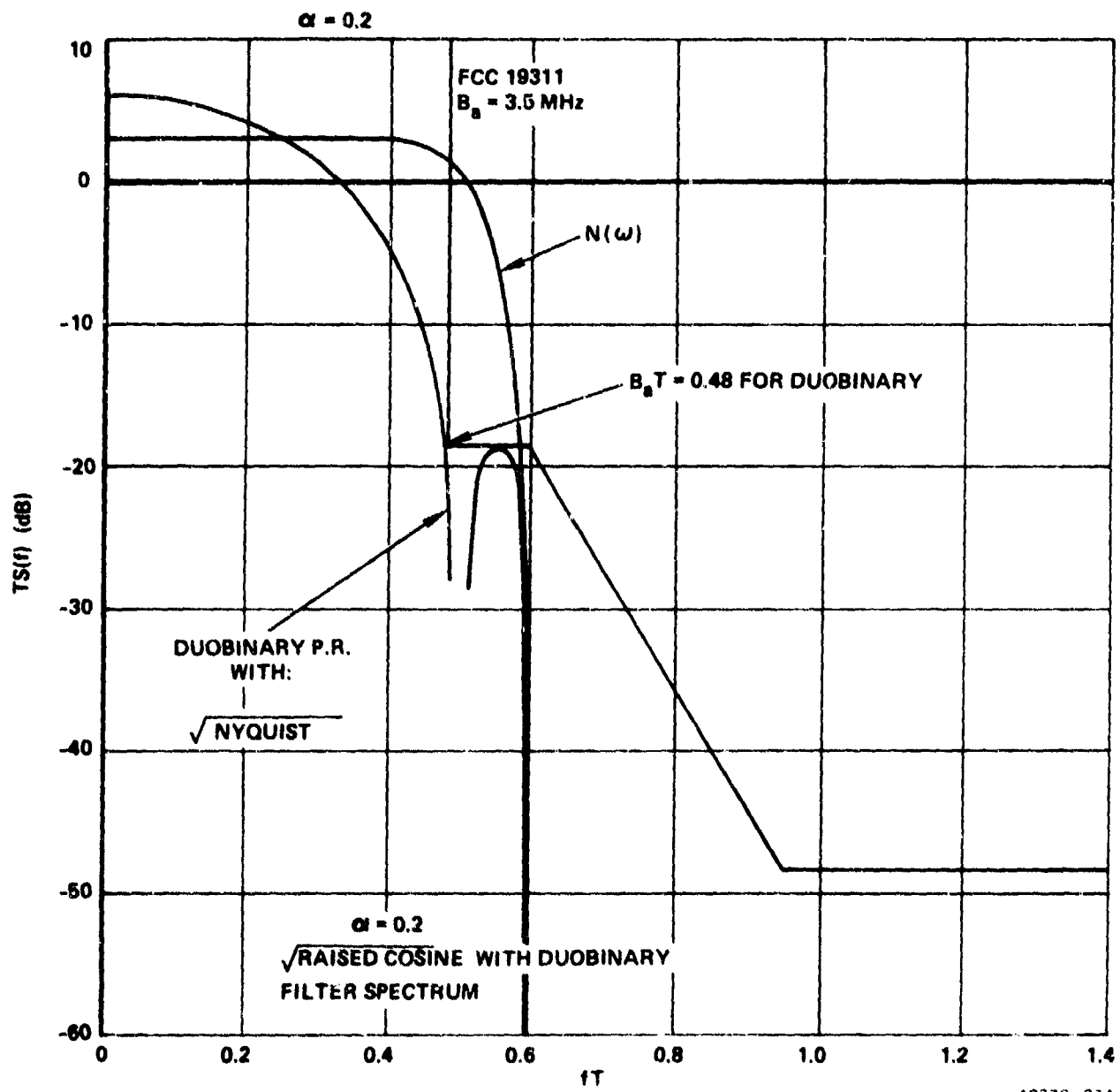


Figure 6.3.1.1-2. Duobinary Partial Response With $\alpha = 0.2$

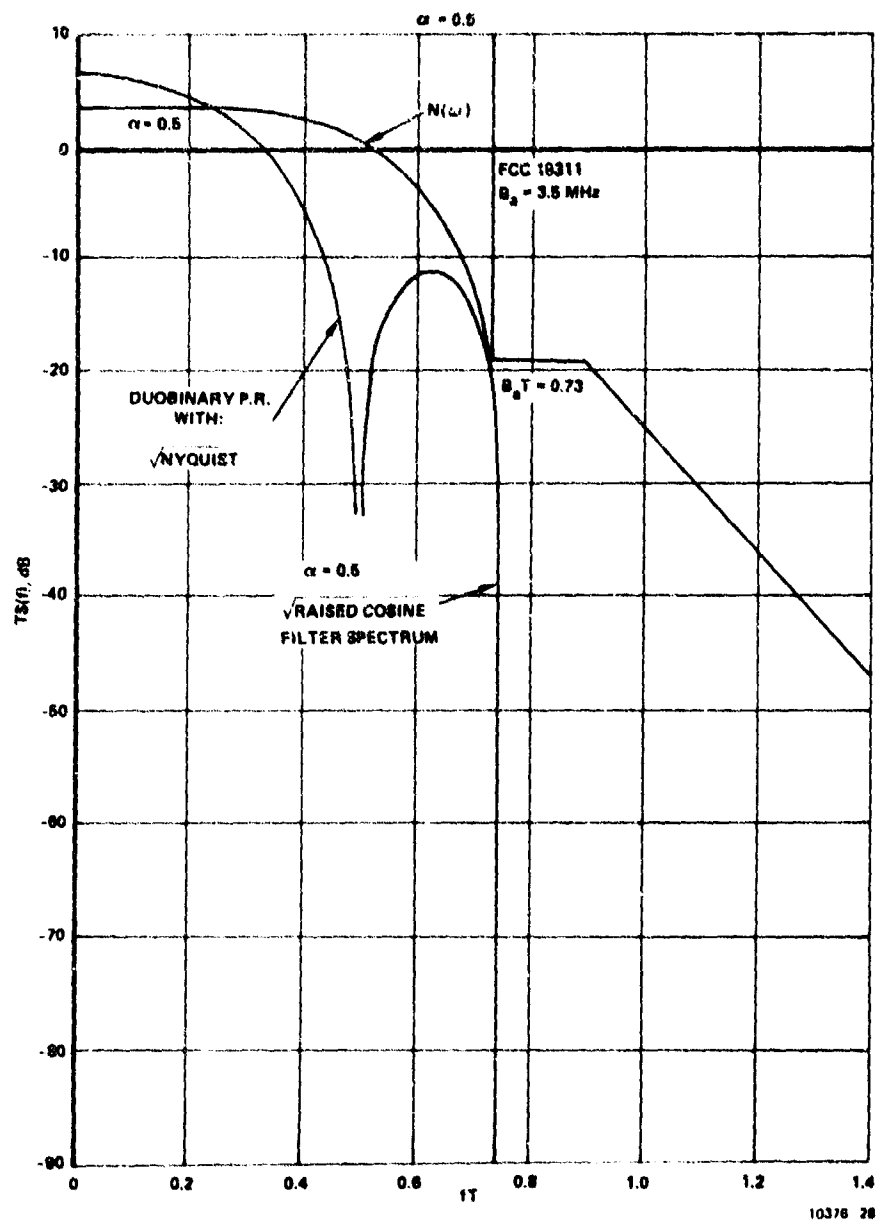


Figure 6.3.1.1-3. Duobinary Partial Response With $\alpha = 0.5$

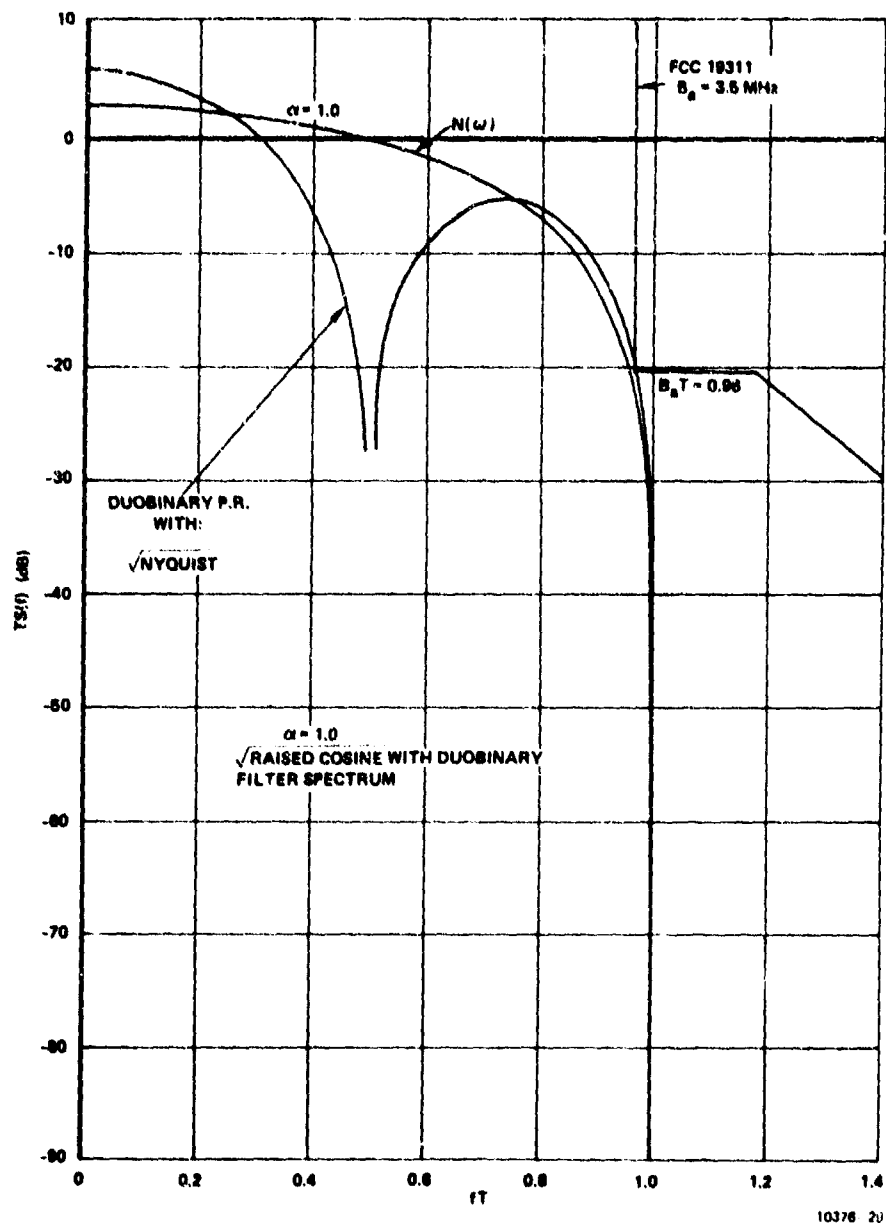


Figure 6.3.1.1-4. Duobinary Partial Response With $\alpha = 1.0$

6.3.1.1-5 for M ranging from two through 16. The symbol error rate versus E_b/N_0 performance with these schemes does not depend on the rolloff parameter α of the particular filter used at the transmitter in Figure 6.3.1. The spectral efficiency does, however, depend upon α .

From the spectral plots of Figures 6.3.1.1-1 through 6.3.1.1-4, we plot the symbols/s/Hz capacity under FCC 19311 spectral criterion versus the transmit filter rolloff parameter α as shown in Figure 6.3.1.1-6. There is a discontinuity around $\alpha = 0.2$ because at $\alpha = 0.2$, the spectral side lobe just becomes low enough to clear the 50 dB mask corner. At lower α , the mask is dictated by the main lobe and at higher α , the mask is dictated by the side lobe.

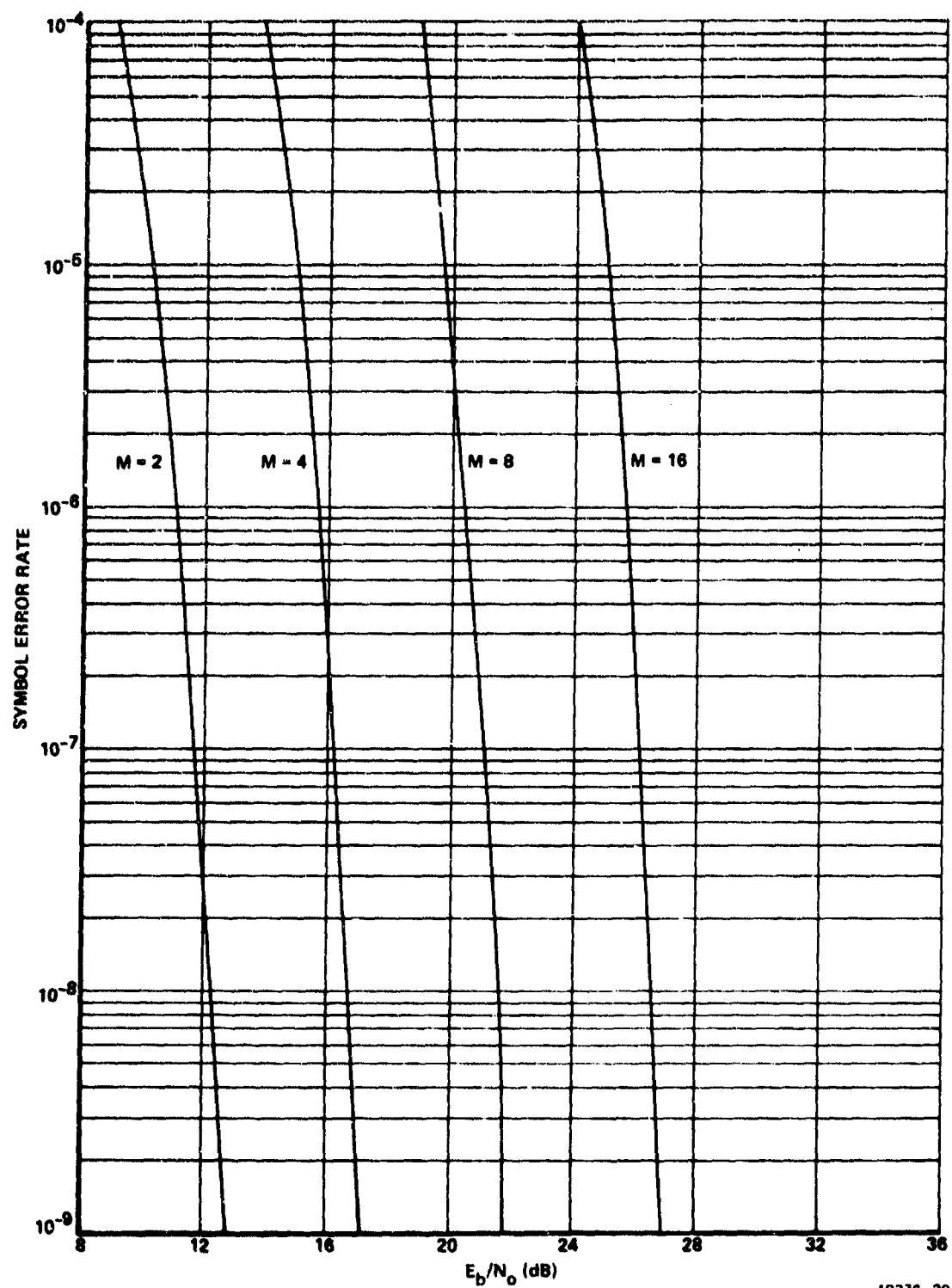
One obtains Capacity, C , in bits/s/Hz by multiplying S plotted in Figure 6.3.1.1-6 by B , the number of bits carried per RF symbol, i.e.,

$$C = BS \quad (6.3.1.1-4)$$

Assuming that the scheme of Figure 6.3.1 is used on two quadrature carriers, the number of bits per RF symbol is

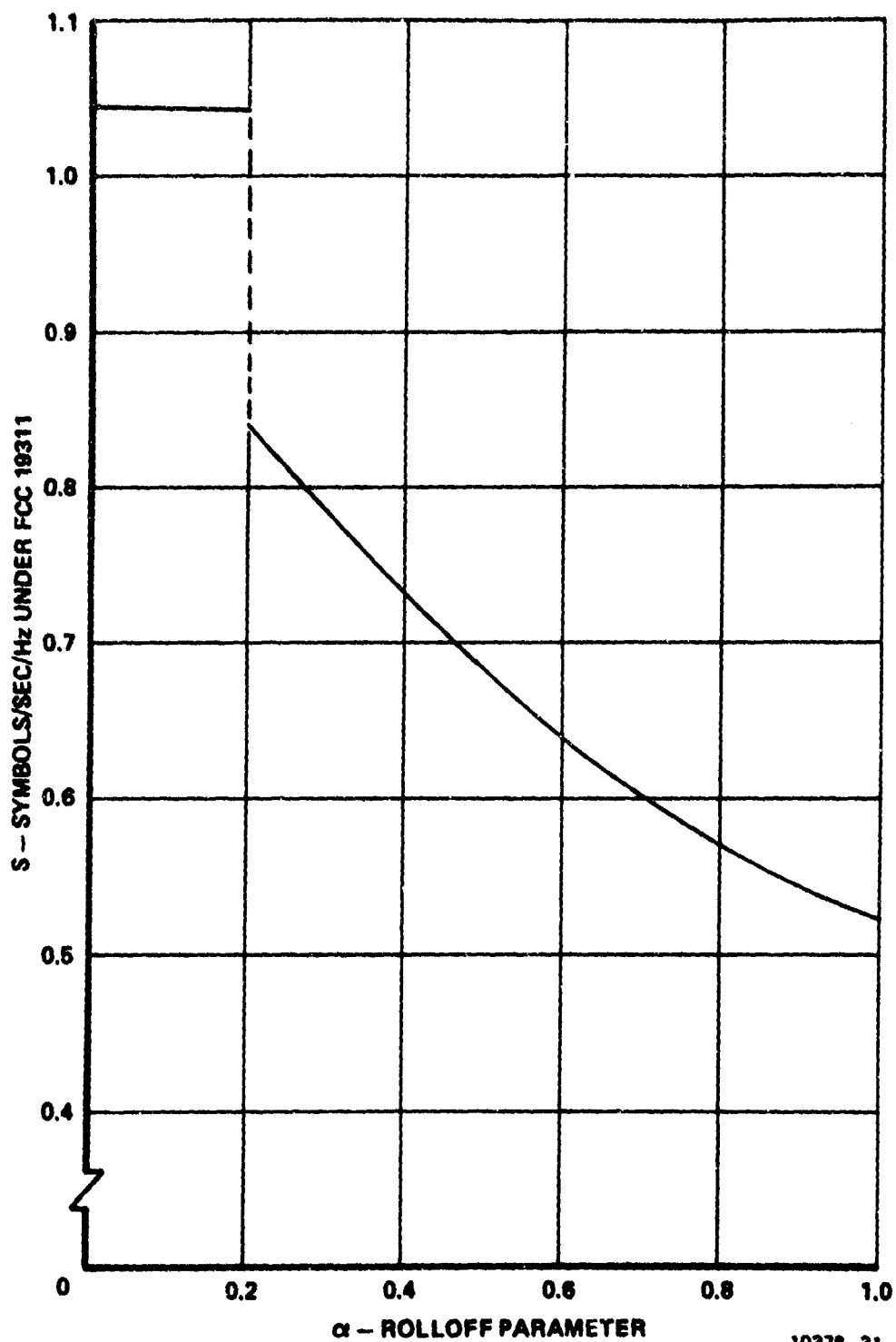
$$B = 2 \log_2 M \quad (6.3.1.1-5)$$

Using the data of Figures 6.3.1.1-5 and 6.3.1.1-6 along with Equations (6.3.1.1-4) and (6.3.1.1-5), one can plot the capacity, C , versus required E_b/N_0 for 10^{-5} error rate as shown in Figure 6.3.1.1-7. Also shown in Figure 6.3.1.1-7 is the curve for ideal M-QAM using $\alpha = 0$ filter with no partial response. The duobinary partial response shaping filter with $\alpha \leq 0.2$ comes very close to the ideal M-QAM curve. Before becoming overly impressed by the performance of the duobinary partial response schemes, however, one should consider the comparison shown in Figure 6.3.1.1-8, of this duobinary scheme with the case of using no partial response for $\alpha = 0.2$. The curve for no partial response is taken from Figure 6.2-7 of Paragraph 6.2. In the region of 3 and 4 bits/s/Hz,



10376-30

Figure 6.3.1.1-5. Performance of M-ary Signaling Through Duobinary Transmit Filter for Viterbi Algorithm Demodulation



10376-31

Figure 6.3.1.1-6. Symbols/s/Hz for Duobinary Partial Response Through Square Root Cosine Filter with Rolloff Parameter, α

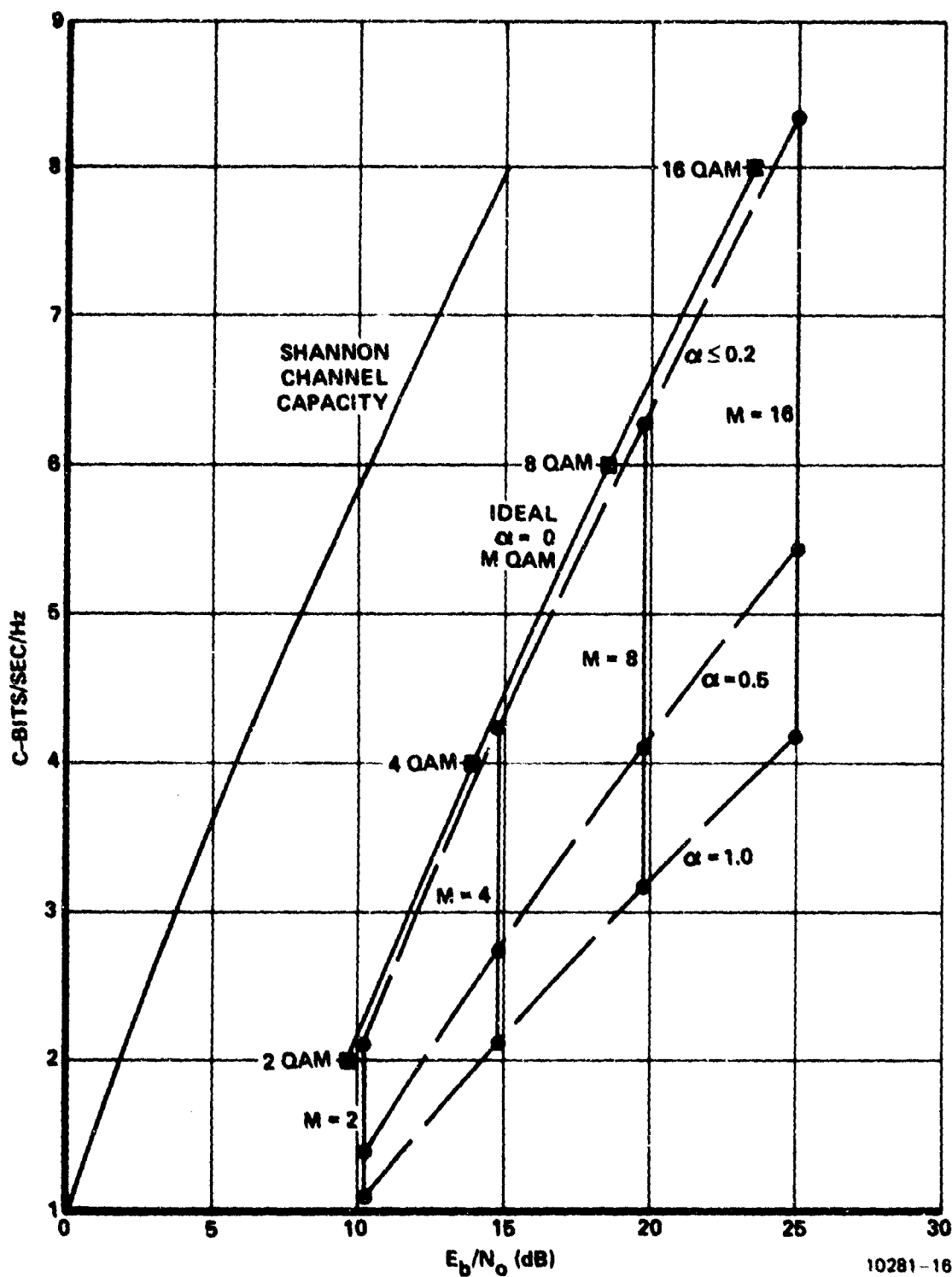


Figure 6.3.1.1-7. Capacity Versus Performance of Duo M-ary Partial Response Shaping with Viterbi Algorithm
Receiver $P(E) = 10^{-5}$

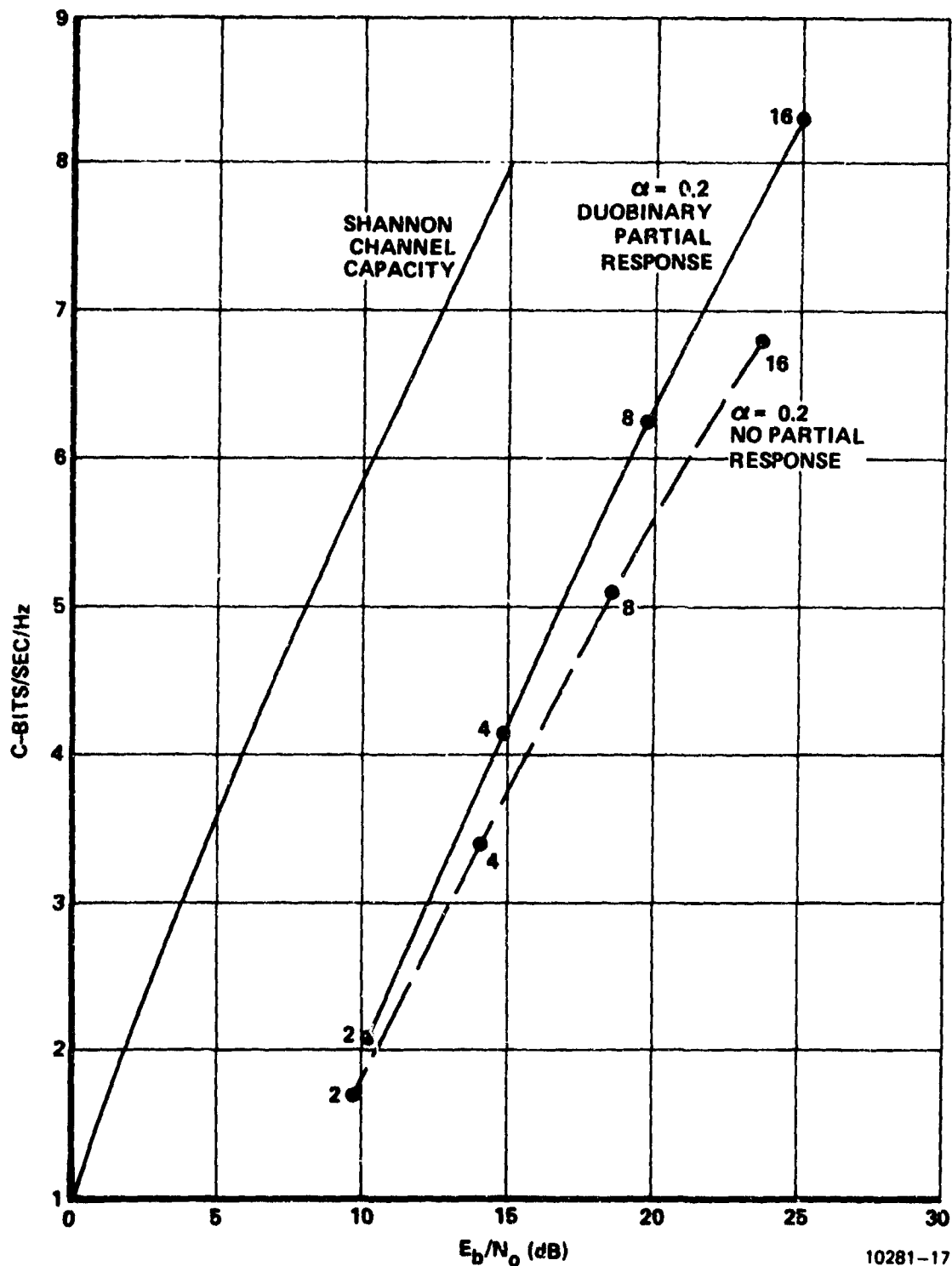


Figure 6.3.1.1-8. Comparison of Systems Using No Partial Response and Duobinary Partial Response for $\alpha = 0.2$

the two curves are within 1 dB of each other. Thus, one could simply use no partial response with the $\alpha = 0.2$ filter and a simple slicer receiver and come within 1 dB of the performance available with duobinary partial response using a more complex Viterbi algorithm processor.

Before leaving this discussion of the optimal spectral concentration length 2 partial response (which is duobinary) it is interesting to note that since the performance curve of Figure 6.3.1.1-7 for $\alpha = 0.2$ is so close to ideal band-limited M-QAM performance, the use of partial response of greater length than 2 may not be justified. Since the Viterbi algorithm complexity increases exponentially with the length of the partial response, one should keep the length as small as possible. The use of longer partial response may, however, allow the use of a gentler rolloff square root cosine filter which is desirable from implementation viewpoints.

6.3.1.2 Near-Optimal Length Three Partial Response

The search for the optimal spectrum concentration length 2 partial response of the preceding section was simplified in that duobinary was optimum for all α rolloff parameters and all specified bandwidths within which power was to be concentrated. For partial responses of lengths greater than two, no such universally optimum partial response can be found. For lengths three and greater, the optimal partial response in general depends upon the filter rolloff and the bandwidth within which power is to be maximized. Therefore, to simplify matters, we restricted our search for the optimal length 3 partial response to the case of $\alpha = 0.5$ rolloff parameter for the square root raised cosine filter.

Figures 6.3.1.2-1 through 6.3.1.2-4 show the resultant spectra for time bandwidth (BT) products of 0.3, 0.4, 0.5, and 0.6 respectively. (A BT product of 0.3, for example, means that the bandwidth within which power is maximally concentrated is chosen to be ± 0.3 times the symbol

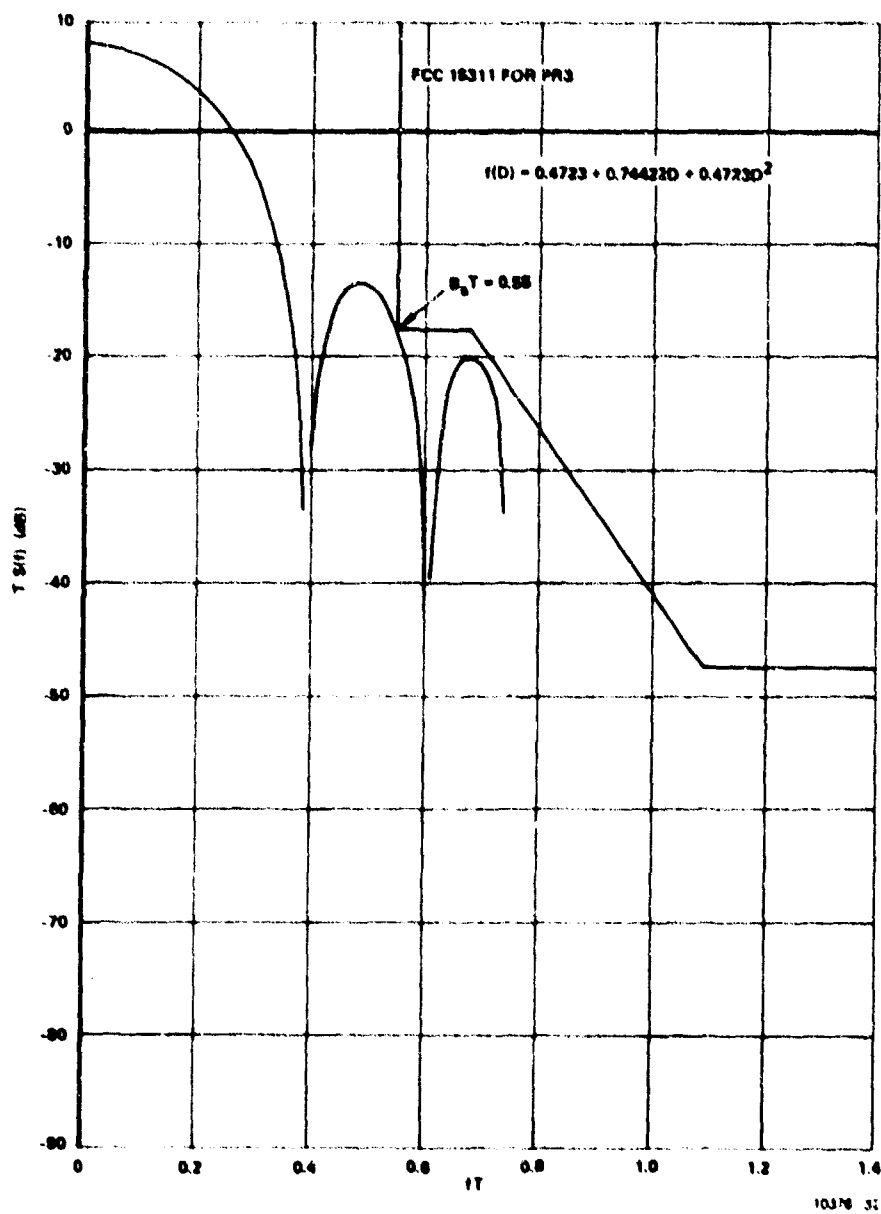


Figure 6.3.1.2-1. $f(D) = 0.4723 + 0.74422D + 0.4723D^2$ PR 3, $\alpha = 0.5$,
 $BT = 0.3$

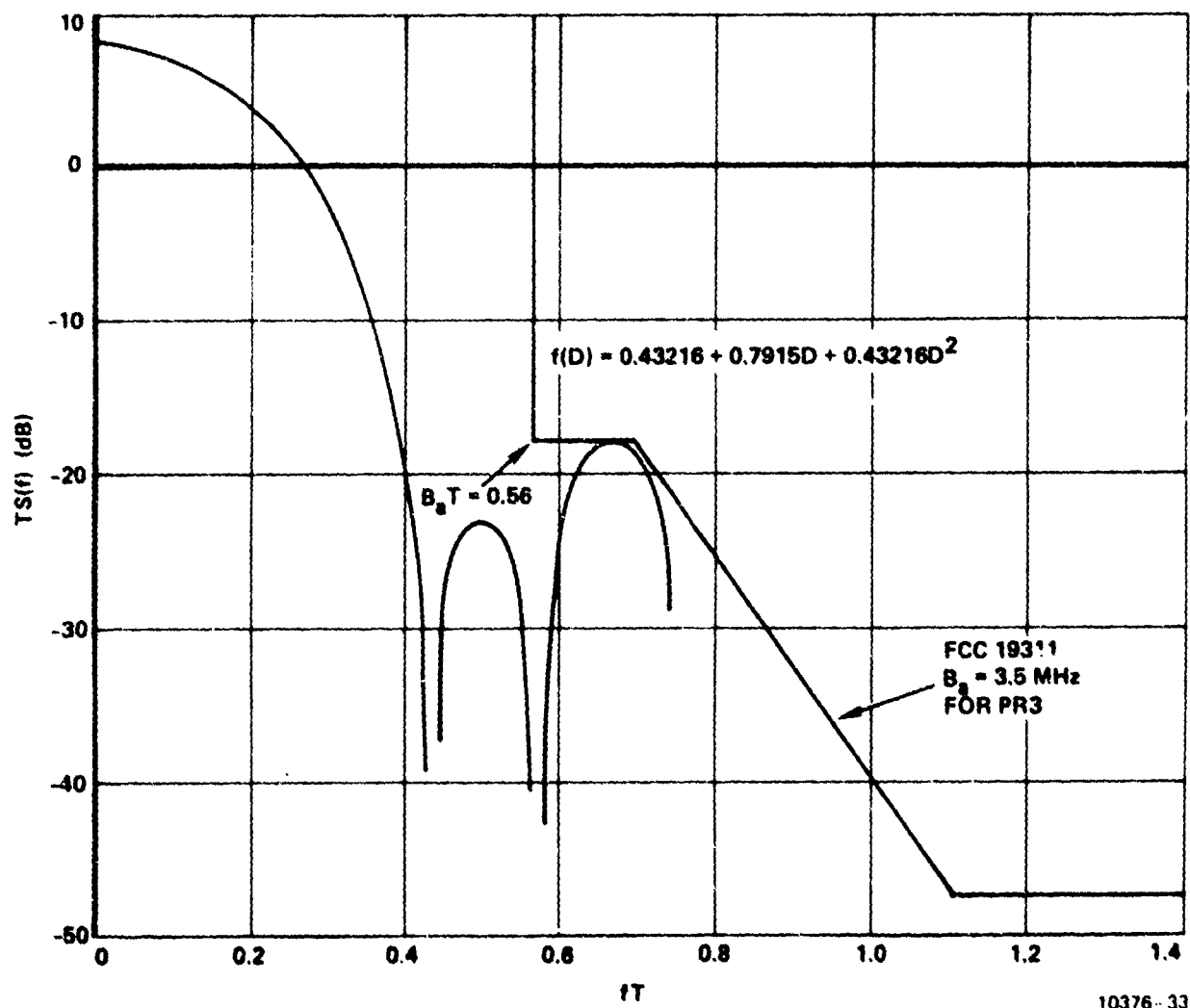
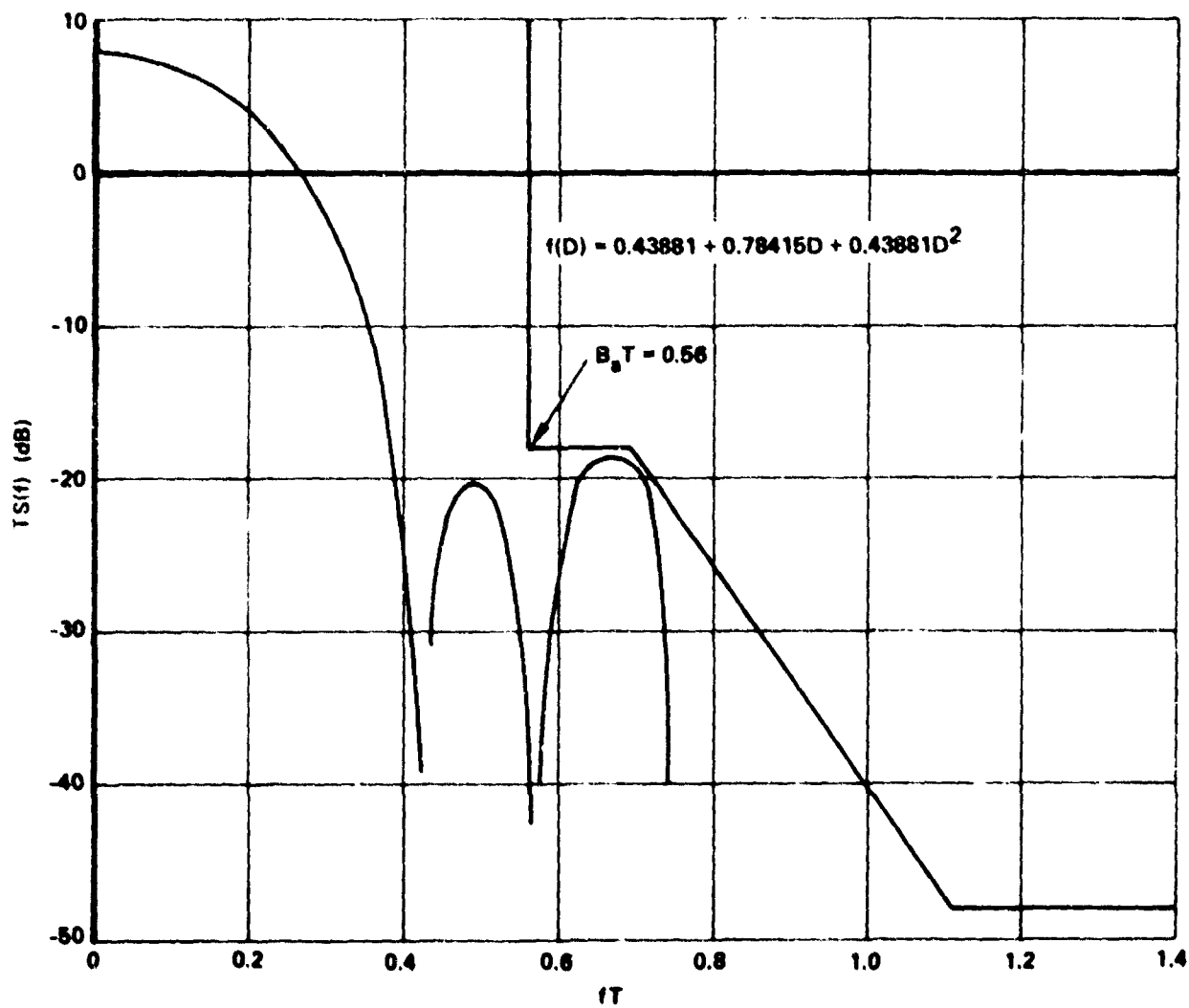


Figure 6.3.1.2-2. $f(D) = 0.43216 + 0.7915D + 0.43216D^2$
 PR 3, $\alpha = 0.5$, $BT = 0.4$



10376 34

Figure 6.3.1.2-3. Optimum Length 3 Partial Response for
 $BT = 0.5$ for $\alpha = 0.5$ $\sqrt{\text{Raised Cosine Filter}}$

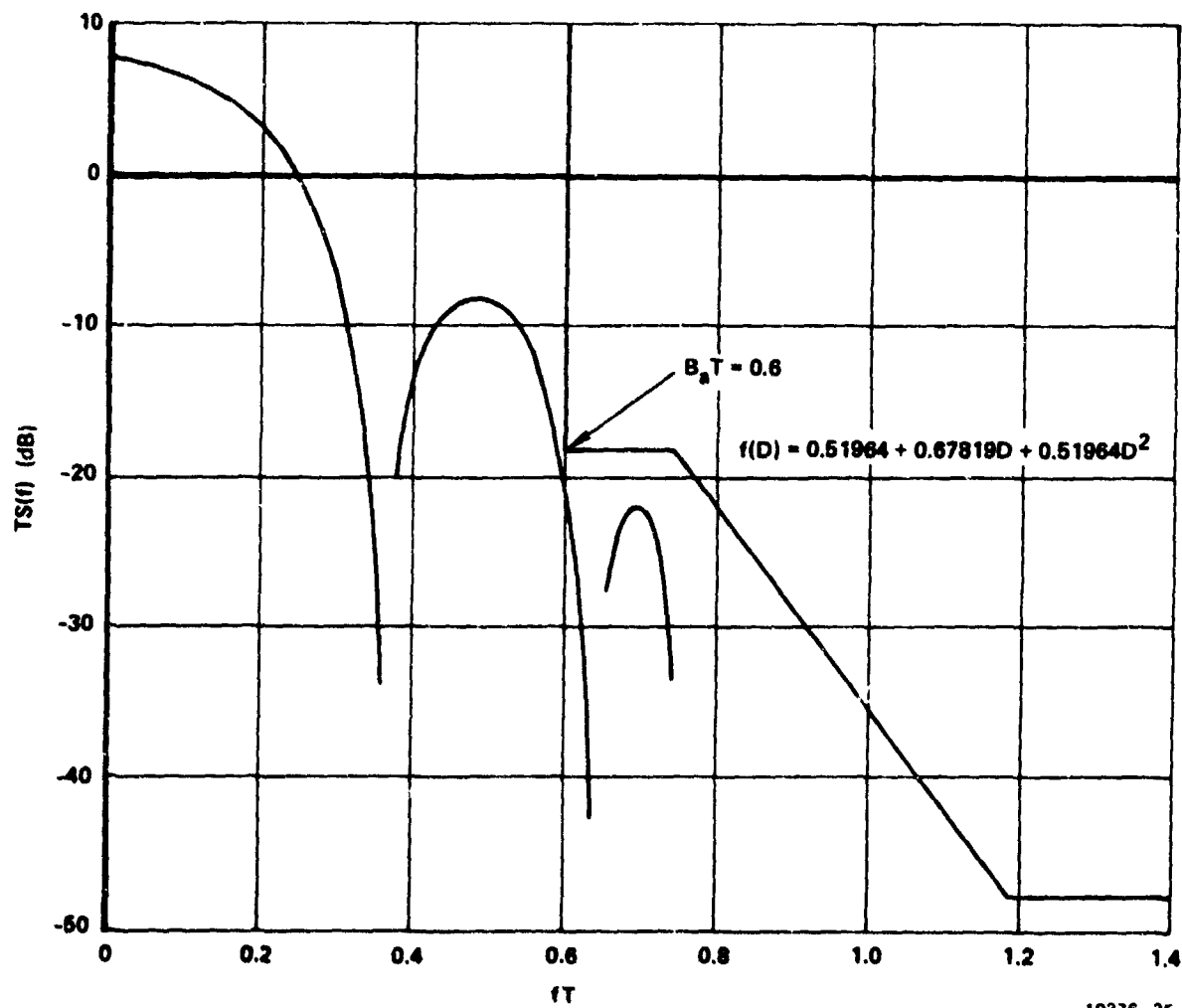


Figure 6.3.1.2-4. Optimum Length 3 Partial Response for
 $BT = 0.6$ for $\alpha = 0.5$ Raised Cosine Filter

rate.) Shown on each curve is the corresponding partial response specified by the $f(D)$ polynomial. Also shown is the corresponding FCC 19311 spectral mask. For $BT = 0.3$, the smallest FCC 19311 RF bandwidth that can be achieved is 1.1 times the symbol rate. The associated partial response polynomial is given by

$$f(D) = 0.4723 + 0.74422D + 0.4723D^2 \quad (6.3.1.2-1)$$

Using the partial response polynomial of Equation (6.3.1.2-1) in our computer program for computing the performance of M-ary PAM through a specified partial response channel with Viterbi demodulation resulted in the performance curves of Figure 6.3.1.2-5 for $M = 2, 4, 8$, and 16.

For the spectrum of Figure 6.3.1.2-1, the RF authorized bandwidths, B_a , and symbol time, T , are related by

$$B_a T = 1.1 \quad (6.3.1.2-2)$$

and consequently symbols/s/Hz, S , is given by

$$S = 1/B_a T$$

$$S = 0.91 \quad (6.3.1.2-3)$$

Assuming M-ary signaling through the partial response of Equation (6.3.1.2-1) carried on each of two quadrature carriers, the capacity in bits/s/Hz is given by

$$C = 2S \log_2 M$$

$$C = 1.82 \log_2 M \quad (6.3.1.2-4)$$

Using the capacity of Equation (6.3.1.2-4) and the performance E_b/N_0 at symbol error rate of 10^{-5} from Figure 6.3.1.2-5, we obtain the capacity versus performance of Figure 6.3.1.2-6.

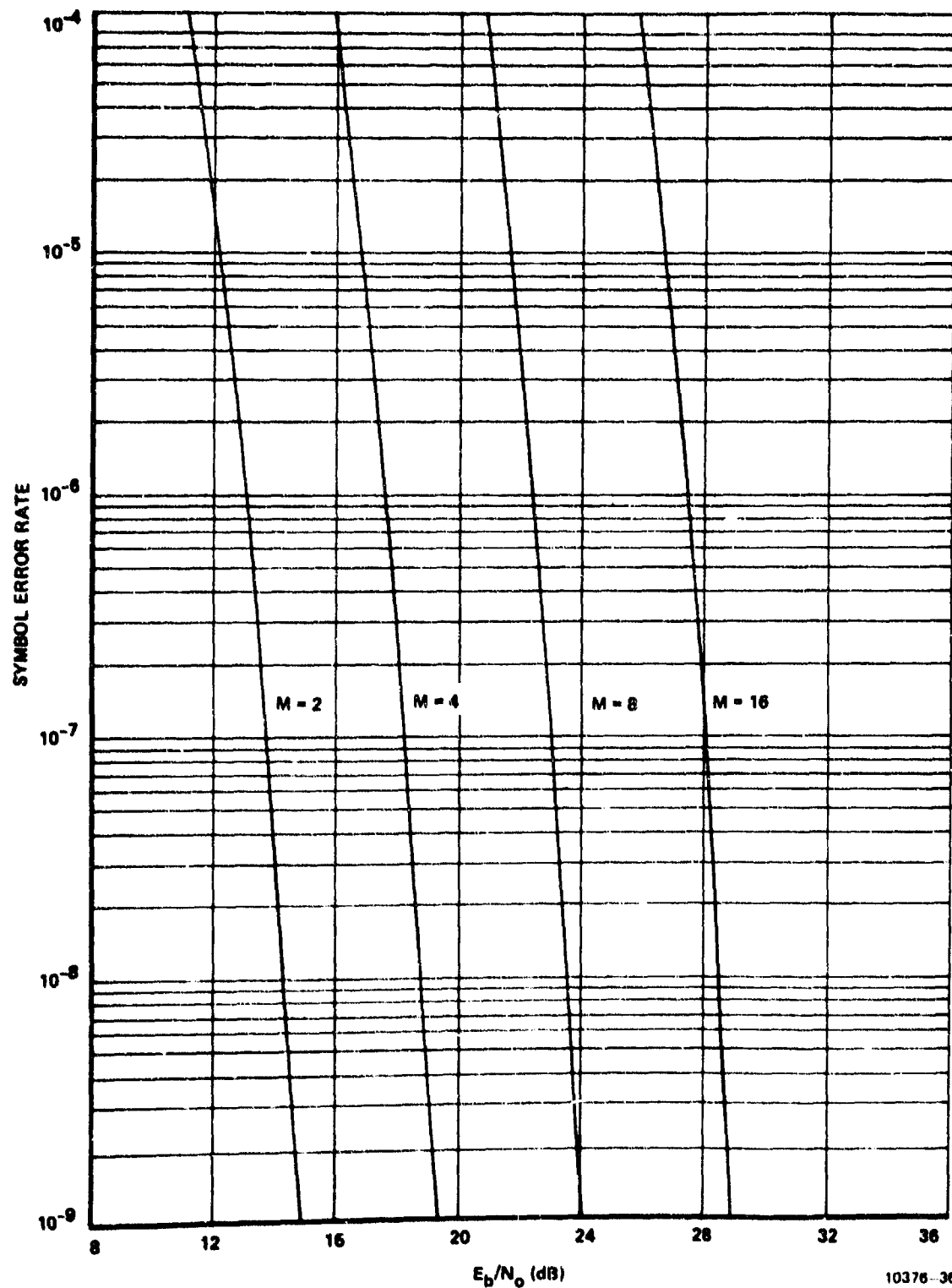


Figure 6.3.1.2-5. Performance of M-ary Signaling Through
 Partial Response $f(D) = 0.4723 + 0.74422 D + 0.4723 D^2$
 With Viterbi Algorithm Demodulation

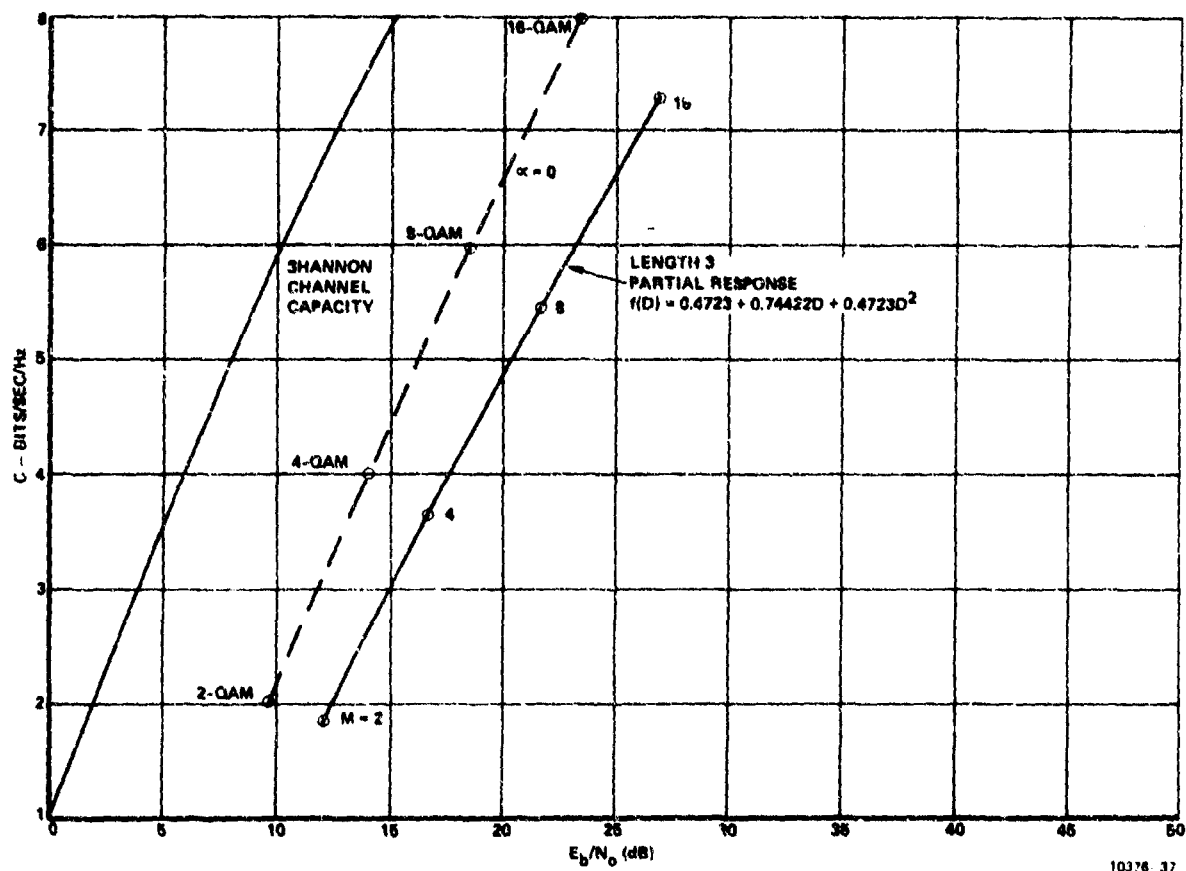


Figure 6.3.1.2-6. Capacity Versus Performance for Optimal Length 3 Partial Response Through $\alpha = 0.5$ Square Root Raised Cosine Shaping Filter, Viterbi Demodulation

Also shown for comparison in Figure 6.3.1.2-6 is the performance for $\alpha = 0$ (ideal sharp cutoff filter) M-QAM schemes using no partial response.

It is informative to plot together all the results we now have for length 1 (no partial response), length 2, and length 3 optimal spectrum concentration partial responses for the system of Figure 6.3.1 when the square root Nyquist filter is an $\alpha = 0.5$ rolloff square root raised cosine filter. This has been done in Figure 6.3.1.2-7. As shown, the case of no partial response (PR1) does quite well - being better than duobinary (PR2) and only slightly bettered by the length 3 partial response at high capacity. With PR1, the Viterbi processor becomes a simple M-ary slicer whereas the PR3 performance is obtained with an M^2 state Viterbi processor. Thus we conclude that especially in the 3 to 4 bits/s/Hz region, the use of partial response is not worth the additional receiver complexity. One can do almost as well by just using the $\alpha = 0.5$ filter to shape the spectrum of M-ary impulses and using a simple slicer receiver.

6.4 Performance of Systems Using Prolate Spheroid Pulse Shaping Filters

The truncated prolate spheroidal functions^{25,26} (see Appendix 2) represent the finite time duration impulse response filters which maximize the percent power in a selected bandwidth. Here we envision the use of these filters in the digital transmission scheme shown in Figure 6.4-1. The shaping filter pulse is presumed to be of duration, T_p , which is μ times the symbol time, T , i.e.,

$$T_p = \mu T \quad (6.4-1)$$

where T_p = Impulse response duration

T = Symbol time

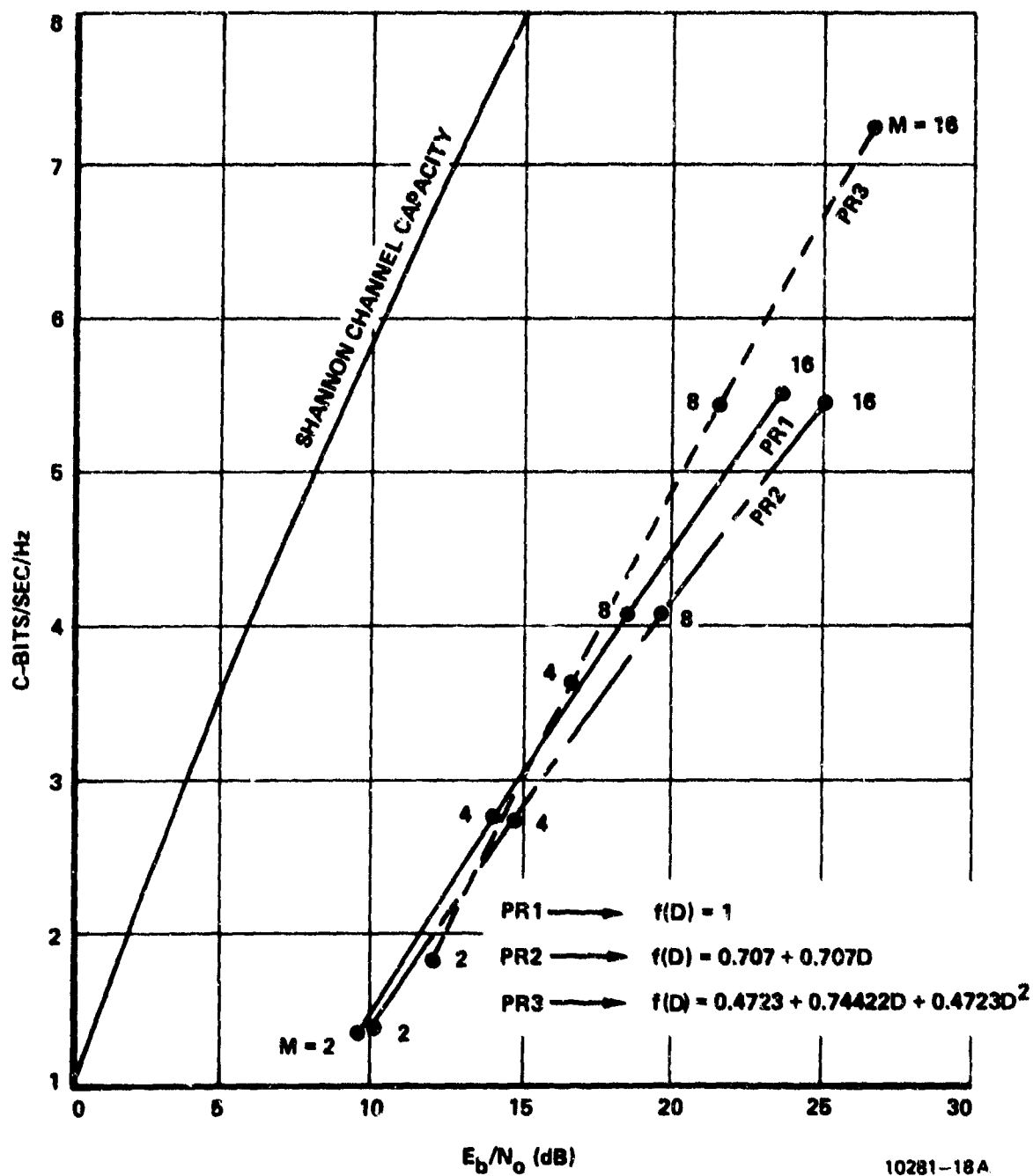


Figure 6.3.1.2-7. Capacity Versus Performance for Optimum Partial Responses Used With $\alpha = 0.5$ Rolloff Square Root Cosine Filter Viterbi Demodulation, $P(E) = 10^{-5}$

μ = Number of symbols covered by pulse

When μ is greater than unity, intersymbol interference exists and it can be analytically described by the techniques discussed in Section 2.

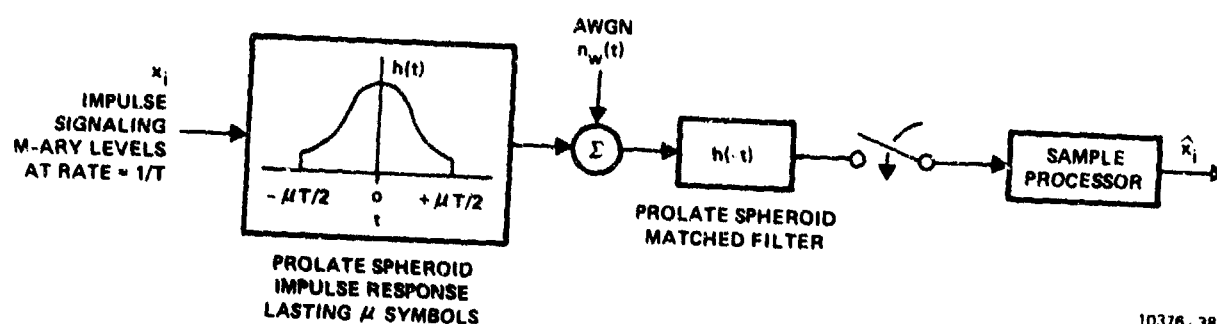
As shown in Appendix 2, the particular prolate spheroid function required in the system of Figure 6.4-1 depends upon the time-bandwidth product, c , where

$$c = B_m T_p \quad (6.4-2)$$

where B_m = Low pass bandwidth within which the power is to be maximized,

T_p = Duration of the pulse

Figures 6.4-2 and 6.4-3 show the spectra resulting from the use of the prolate spheroid functions for time-bandwidth products of 1.9 and 2.2 respectively. The out-of-band power [$B = 1.9 (1/T)$] for Figure 6.4-2 is down -40 dB relative to total power, and for Figure 6.4-3, out-of-band power is down -50 dB. Also shown on these spectral plots are the



10376-38

Figure 6.4-1. Digital System with Prolate Spheroid Shaping Filters

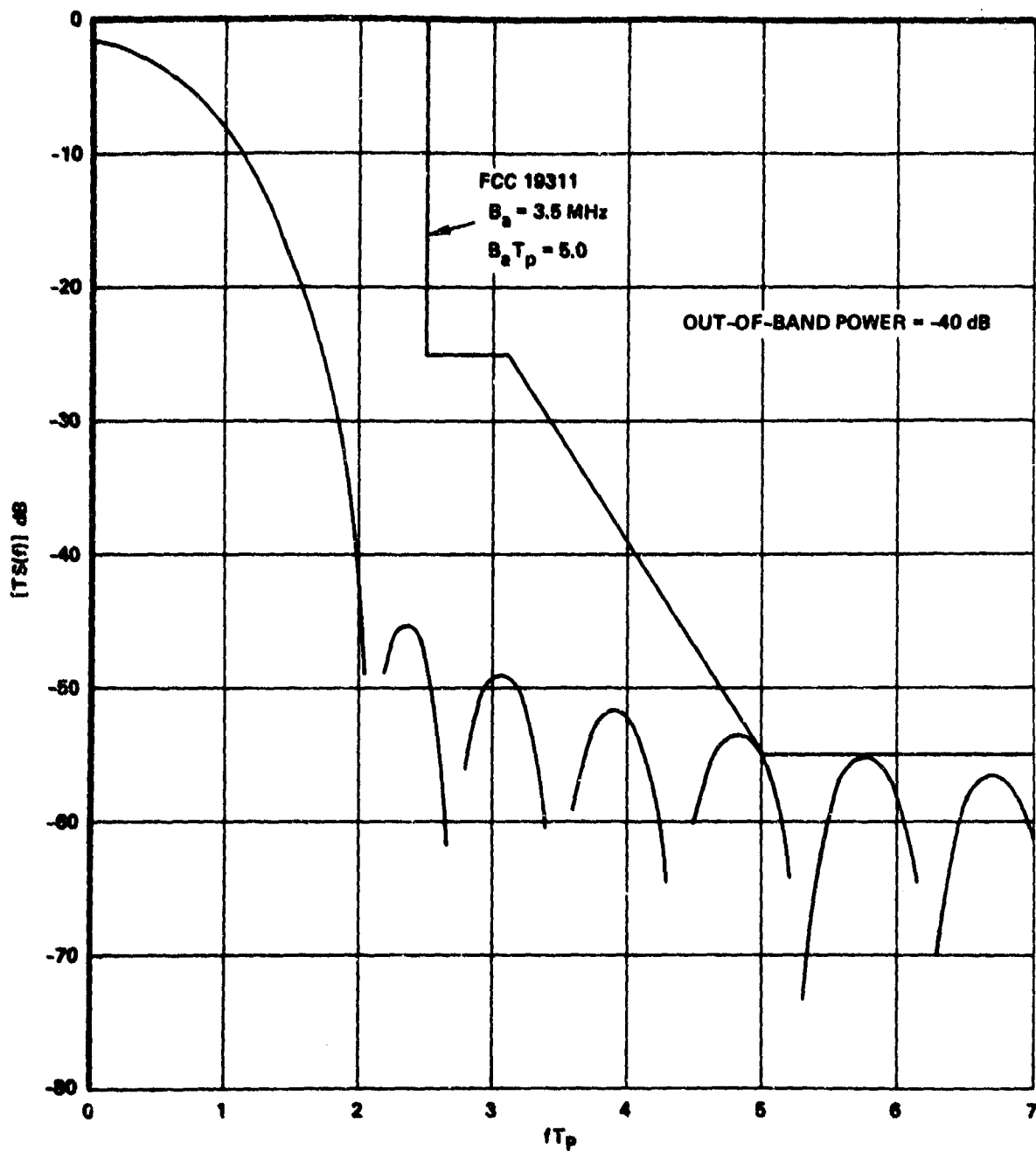


Figure 6.4-2. Prolate Spheroid Spectrum for $BT_p = 1.9$
Out-of Band Power = -40 dB

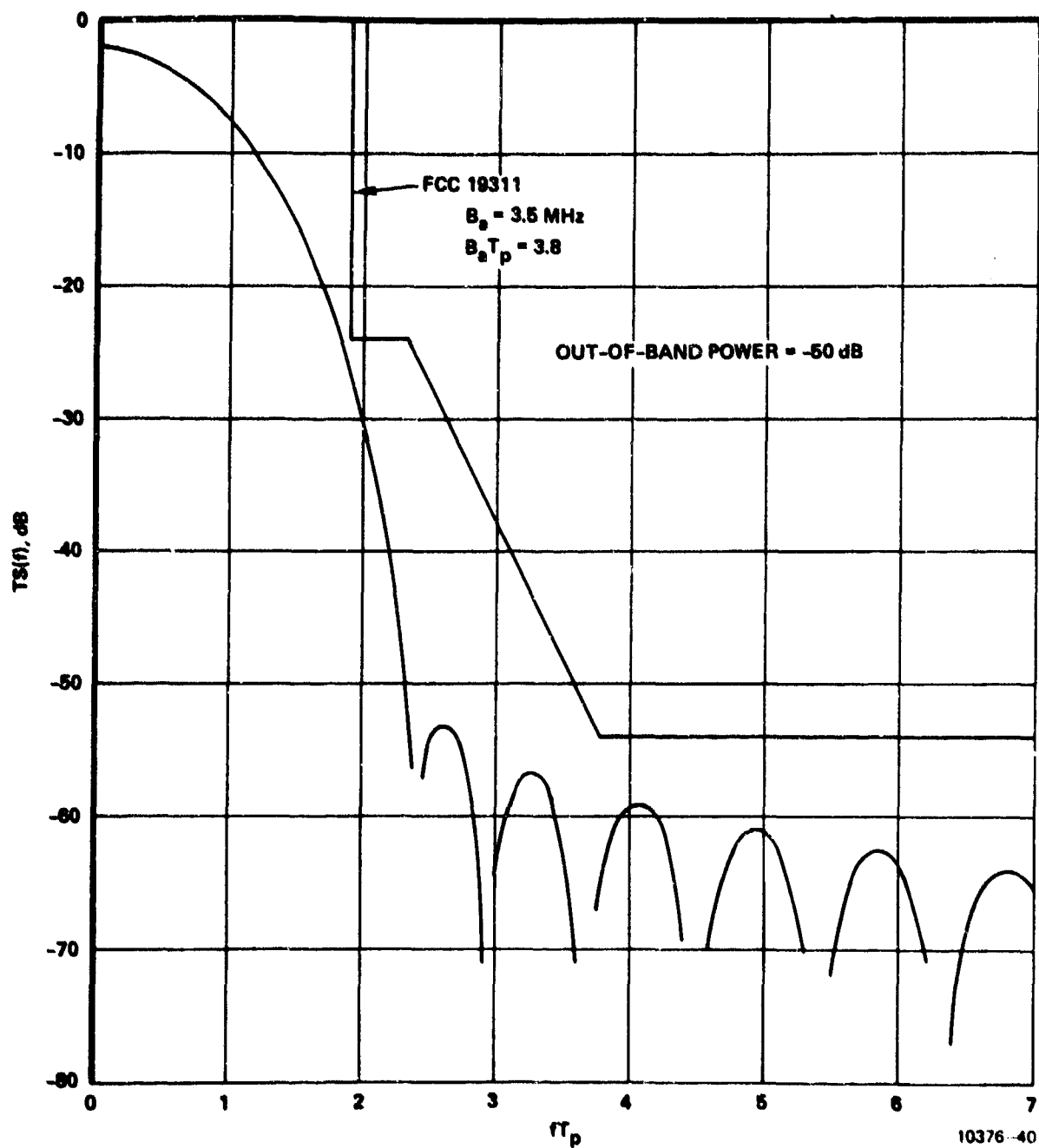


Figure 6.4-3. Prolate Spheroid Spectrum for $B_m T_p = 2.2$
 Out-of-Band Power = -50 dB

FCC 19311 spectral masks that these spectra can meet for an assumed 3.5 MHz authorized bandwidth. Also indicated is the necessary FCC 19311 authorized RF bandwidth - pulse duration product, $B_a T_p$.

Note in Figure 6.4-2 that the required FCC 19311 bandwidth is dictated by the low level spectrum side lobes, whereas in Figure 6.4-3 the main lobe of the spectrum dictates the FCC 19311 bandwidth. It was found throughout this study that spectra having out-of-band power down approximately -50 dB were necessary to keep side lobes under the 4 kHz power -80 dB mask floor. This seems reasonable when one considers that 4 kHz of bandwidth at the peak of the main lobe typically contains power down approximately 30 dB relative to total power for the authorized bandwidths of interest (3.5-20 MHz) and thus to get under the -80 dB floor, the power in 4 kHz centered on the side lobes must be down an additional 50 dB.

In the capacity versus performance results presented in the following sections, we have used the prolate spheroid shaping filter having the spectrum shown in Figure 6.4-3 which meets an FCC 19311 mask dictated by the main lobe. The impulse response for this shaping filter is shown in Figure 6.4-4.

6.4.1 Discrete Characterization of the Prolate Spheroid Shaping Filter

As shown in Section 2., an important element required for characterizing the performance of any shaping filter is the $f(D)$ polynomial of Equation (2-4). As shown in Section 2. it is necessary to obtain the shaping filter pulse autocorrelation function defined in Equation (2-1). The autocorrelation function of the prolate spheroid function shown in Figure 6.4-4 was found to have the shape shown in Figure 6.4.1. As shown in Figure 6.4.1, the pulse autocorrelation function for the specific filter is time limited to $|t| < T_p$. The polynomial, $R(D)$, defined in Equation (2-4) is found by sampling the autocorrelation function at the symbol rate. The polynomial $R(D)$ is then factored to yield

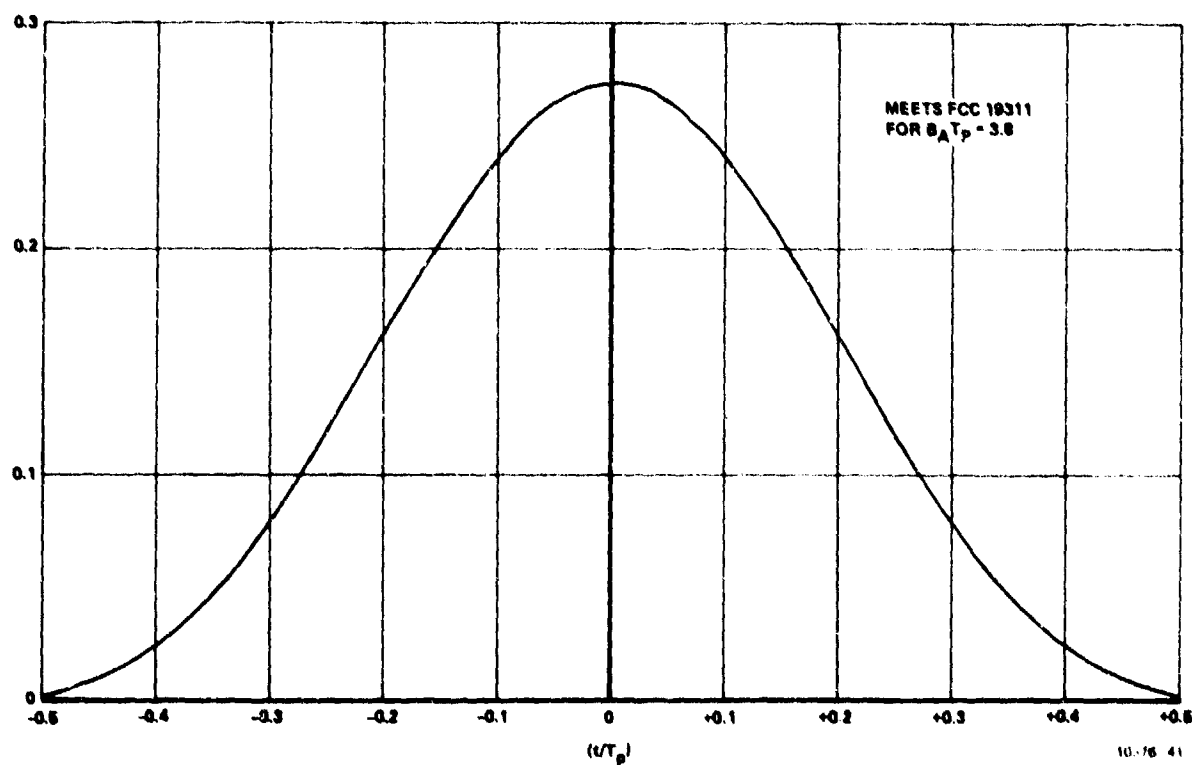
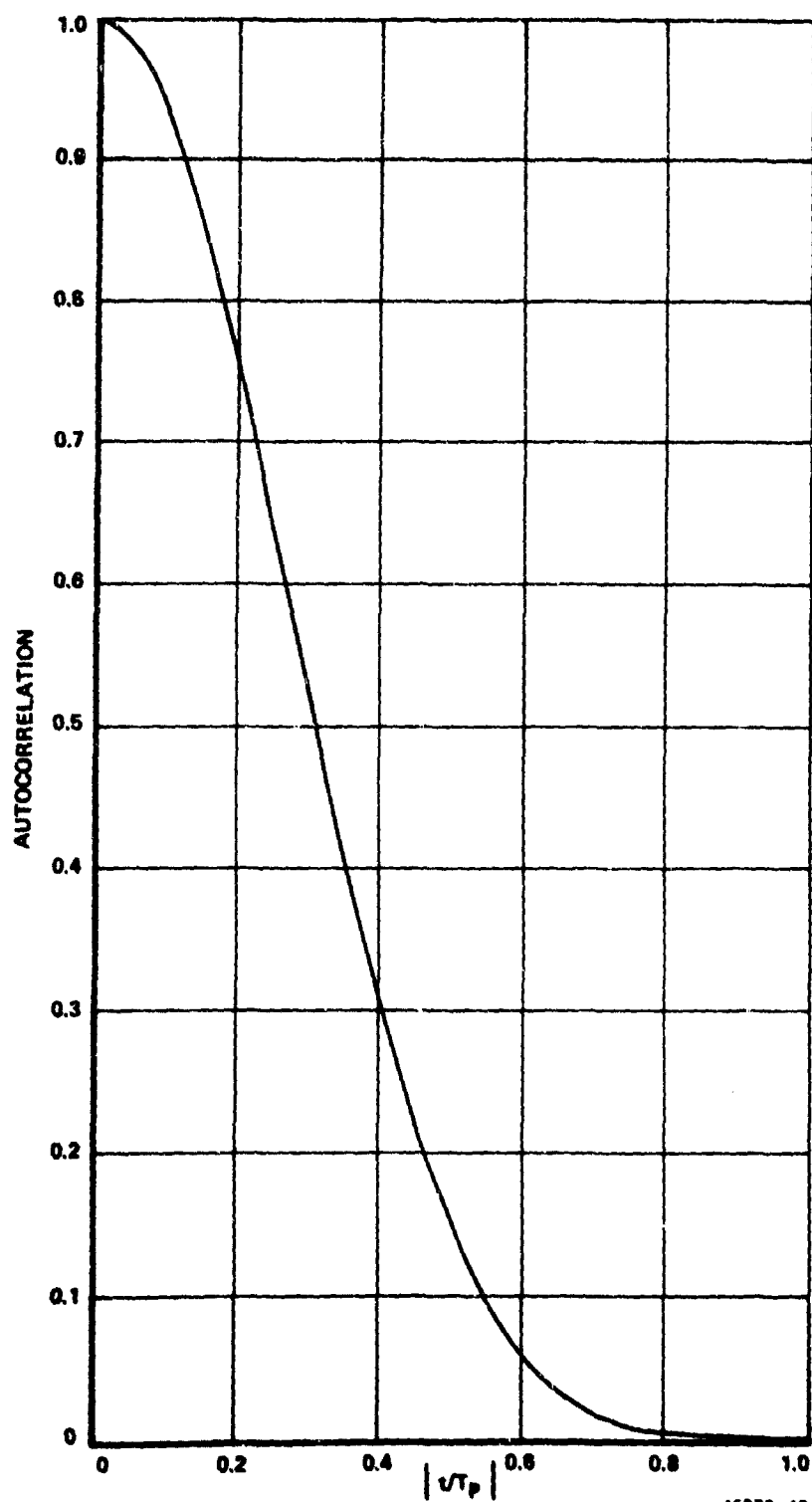


Figure 6.4-4. -50 dB Spectral Occupancy
Prolate Spheroid Pulse Shape



16376-42

Figure 6.4.1. Pulse Autocorrelation Function
for Prolate Spheroid -50 dB Pulse

$$R(D) = f(D)f(D^{-1}) \quad (6.4.1-1)$$

from which $f(D)$ is defined. Using the techniques outlined in Paragraph 2.2.6, knowing $f(D)$, the performance for perfectly equalized receivers and Viterbi Algorithm receivers can be ascertained.

The $R(D)$ and corresponding $f(D)$ polynomials obtained for the pulse autocorrelation in Figure 6.4.1 are given in Table 6.4.1 for various μ = number of symbols spanned by the shaping pulse as defined in Equation 6.4-1. Also given are the roots of the $f(D)$ polynomial which are necessary for computing the performance of perfectly equalized receivers as shown in Paragraph 2.2.6.

Table 6.4.1. $R(D)$, $f(D)$, and Roots of $f(D)$ for System Using Prolate Spheroid μ Symbols Long

COEF μ	$R(D), f(D)$							$ \beta $ ROOTS OF $f(D)$
	D^{-3}	D^{-2}	D^{-1}	D^0	D^1	D^2	D^3	
2			0.15	1 1	0.15 0.15354			-8.513
3		0.0265	0.44	1 1	0.44 0.55822	0.0265 0.034788		-2.054 -13.991
4	0.007	0.15	0.632	1 1	0.632 1.08504	0.15 0.32515	0.007 0.015983	1.948 + j 0.09393 1.948 - j 0.09393 -16.44728

10375-43

6.4.2 Capacity of the Prolate Spheroid Pulse Shape under FCC Docket 19311

In this section, the capacity in symbols/s/Hz under FCC 19311 spectral criterion is presented for the prolate spheroid shaping filter having the spectrum of Figure 6.4-3. As shown on Figure 6.4-3, the RF

authorized bandwidth B_a and the pulse duration, T_p , are related by the expression

$$B_a T_p = 3.8, \quad (6.4.2-1)$$

From Equations (6.4-1) and (6.4.2-1) for the prolate spheroid function covering μ symbol times, T , we have

$$\mu B_a T = 3.8 \quad (6.4.2-2)$$

Since the number of symbols/s/Hz, S , is given by

$$S = \frac{1}{B_a T} \quad (6.4.2-3)$$

We have from Equations (6.4.2-2) and (6.4.2-3)

$$S = \frac{\mu}{3.8}, \quad (6.4.2-4)$$

for the prolate spheroid shape shown in Figure 6.4-4. S versus μ is plotted in Figure 6.4.2.

To obtain the capacity, C , in bits/s/Hz under FCC 15311, one multiplies S by B , the number of bits per RF symbol, i.e.,

$$C = BS \quad (6.4.2-5)$$

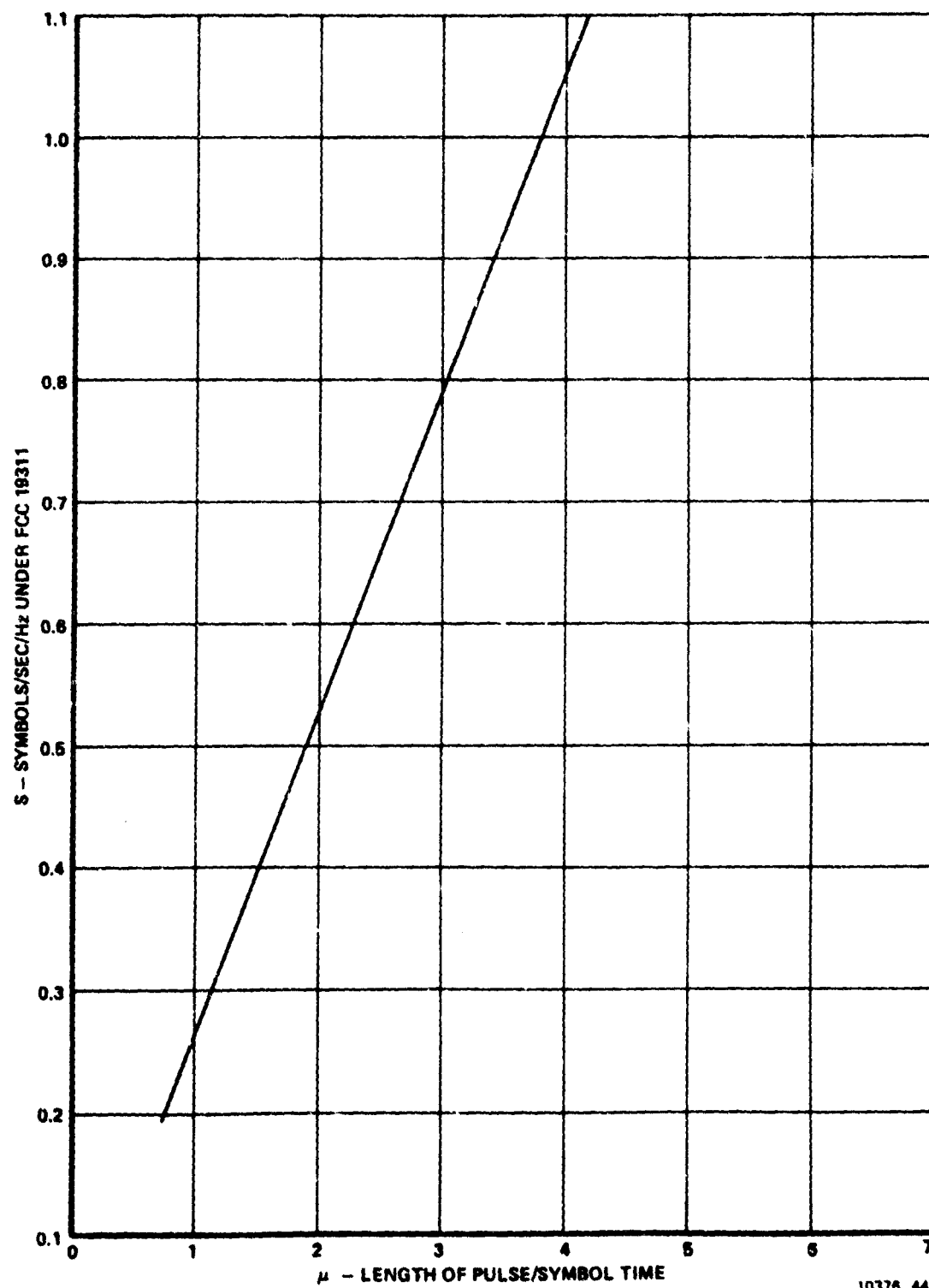
where

C = Capacity in bits/s/Hz

B = Number bits carried by each RF symbol

S = Capacity in symbols/s/Hz

The data displayed in Figure 6.4.2 is used in the next two sections to provide the capacity element in plots of capacity versus performance for several digital transmission schemes.



10376 44

Figure 6.4.2. Capacity in Symbols/s/Hz for
-50 dB Prolate Spheroid Function

6.4.3 Performance of the Prolate Spheroid Shaping Filter Scheme With Perfect Nyquist Equalization at Receiver

In this section we display the computed degradation in dB relative to one-shot (Nyquist) channel performance of digital receivers of the form shown in Figure 6.4-1 where the shaping filter impulse response is the prolate spheroid function shown in Figure 6.4-4 and the sample processor is a perfect equalizer ($g(D) = 1$) which totally removes intersymbol interference followed by a memoryless threshold decision device appropriate for the generally multilevel input impulses.

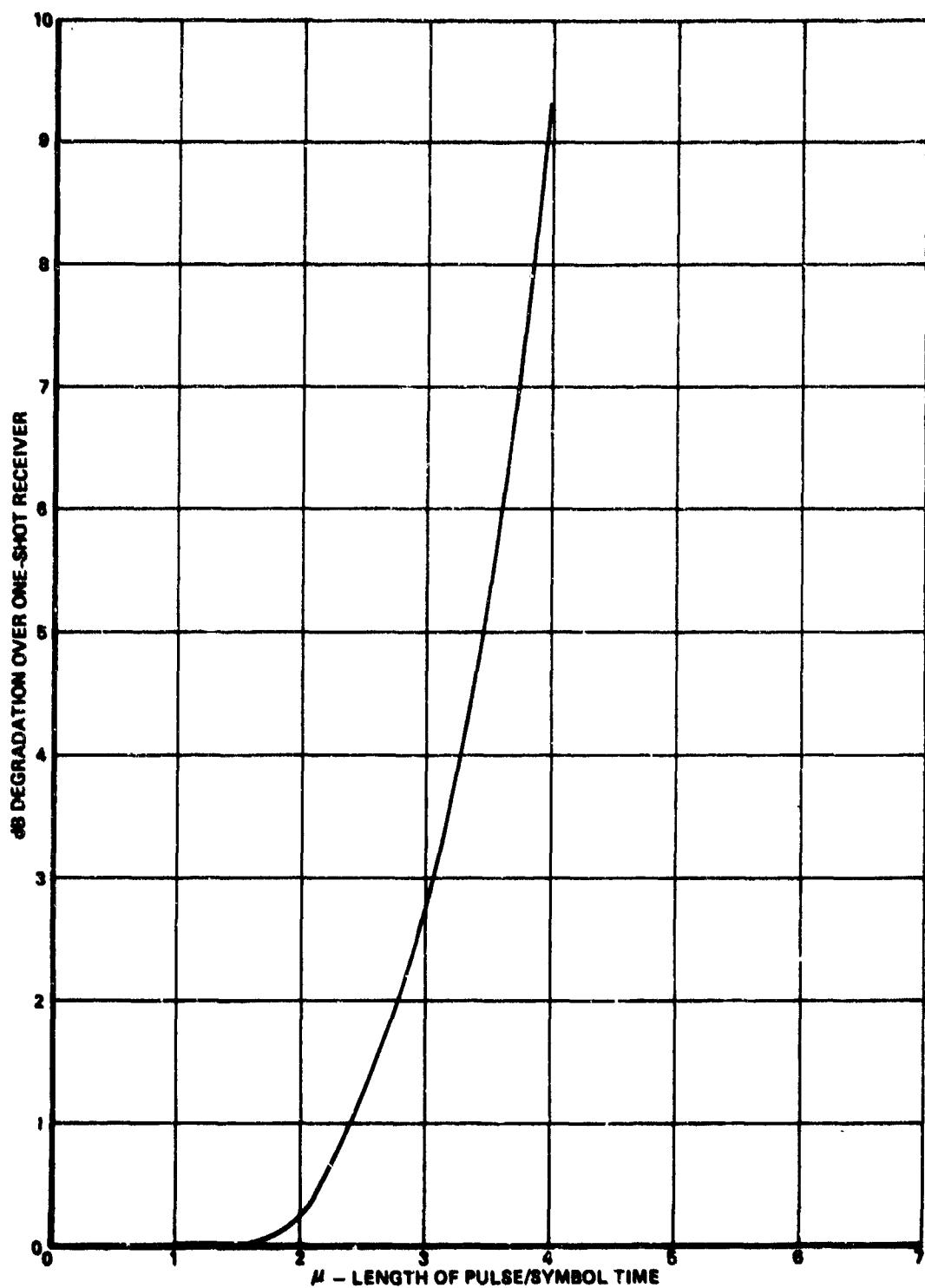
The degradation relative to one-shot (Nyquist) receiver of the equalized receiver was found in Paragraph 2.2.6.1.2, Equation (2.2.6-19), to be given by (for $g(D) = 1$):

$$D_T \text{ (dB)} = 10 \text{ Log}_{10} \left\{ \left| \left| \frac{1}{f(D)} \right| \right|^2 \cdot \left| \left| f(D) \right| \right|^2 \right\}. \quad (6.4.3-1)$$

For the prolate spheroidal function of interest here, the polynomial $f(D)$ for several μ 's is given in Table 6.4.1 preceding.

When one evaluates the degradation given by Equation (6.4.3-1) for the $f(D)$'s given in Table 6.4.1 by the techniques described in Paragraph 2.2.6.1 one obtains the degradation versus μ curve of Figure 6.4.3-1. Eliminating the parameter μ between the curves of Figures 6.4.2 and 6.4.3-1, the curve of symbols/s/Hz versus degradation shown in Figure 6.4.3-2 is obtained. The parameter μ varies as one traverses this curve and several values of μ are noted in Figure 6.4.3-2.

With M-QAM signaling through baseband filters having the prolate spheroid function impulse response, the linear equalized matched filter receiver produces the capacity versus E_b/N_0 for symbol error rate $= 10^{-5}$ shown in Figure 6.4.3-3. This curve has been obtained by multiplying S in Figure 6.4.3-2 by the number of bits carried per RF symbol to obtain C in bits/s/Hz and degrading ideal one-shot performance



10378-45

Figure 6.4.3-1. Degradation Versus μ for Prolate Spheroid Shaping Filter With Perfect Nyquist Equalization at Receiver

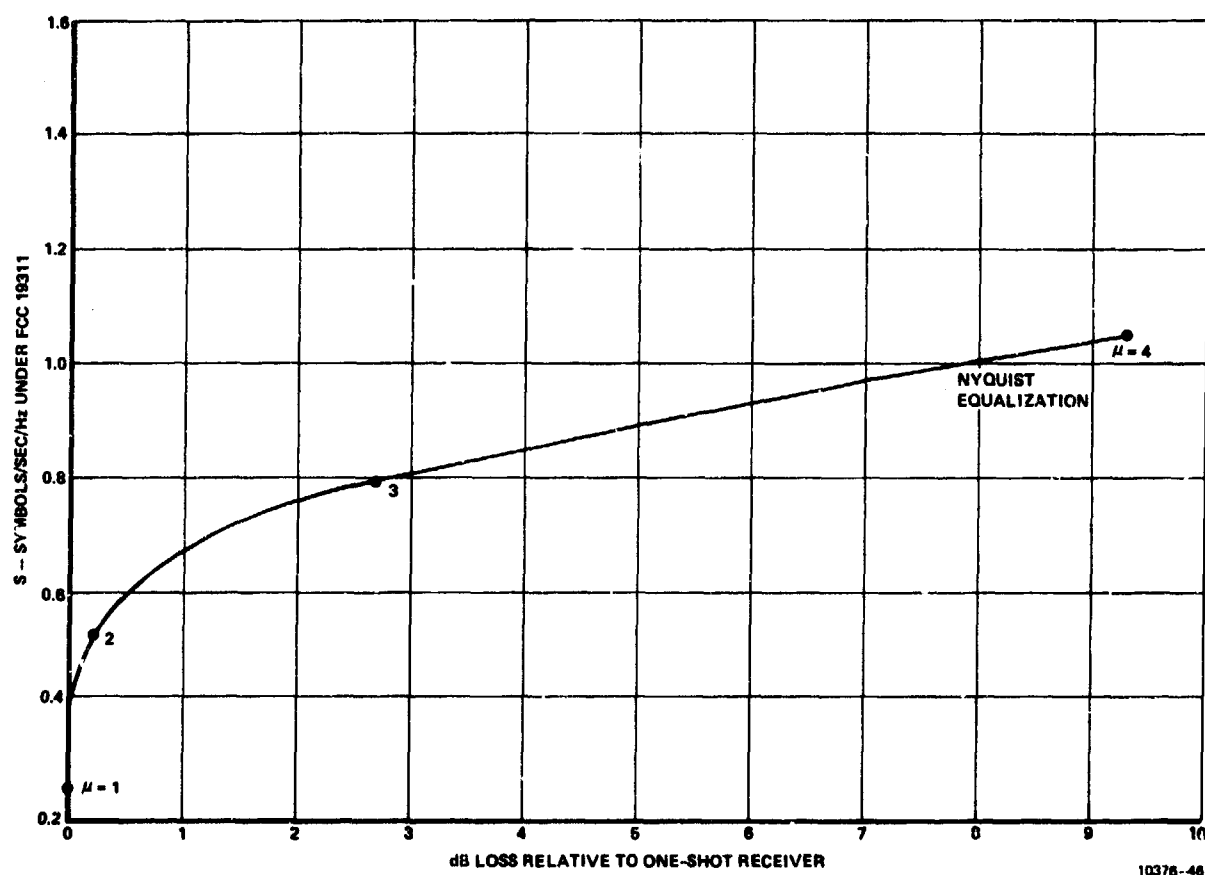


Figure 6.4.3-2. Combinations of Symbols/s/ Hz and Degradation for Prolate Spheroid Shaping Filter with Perfect Receiver Equalization

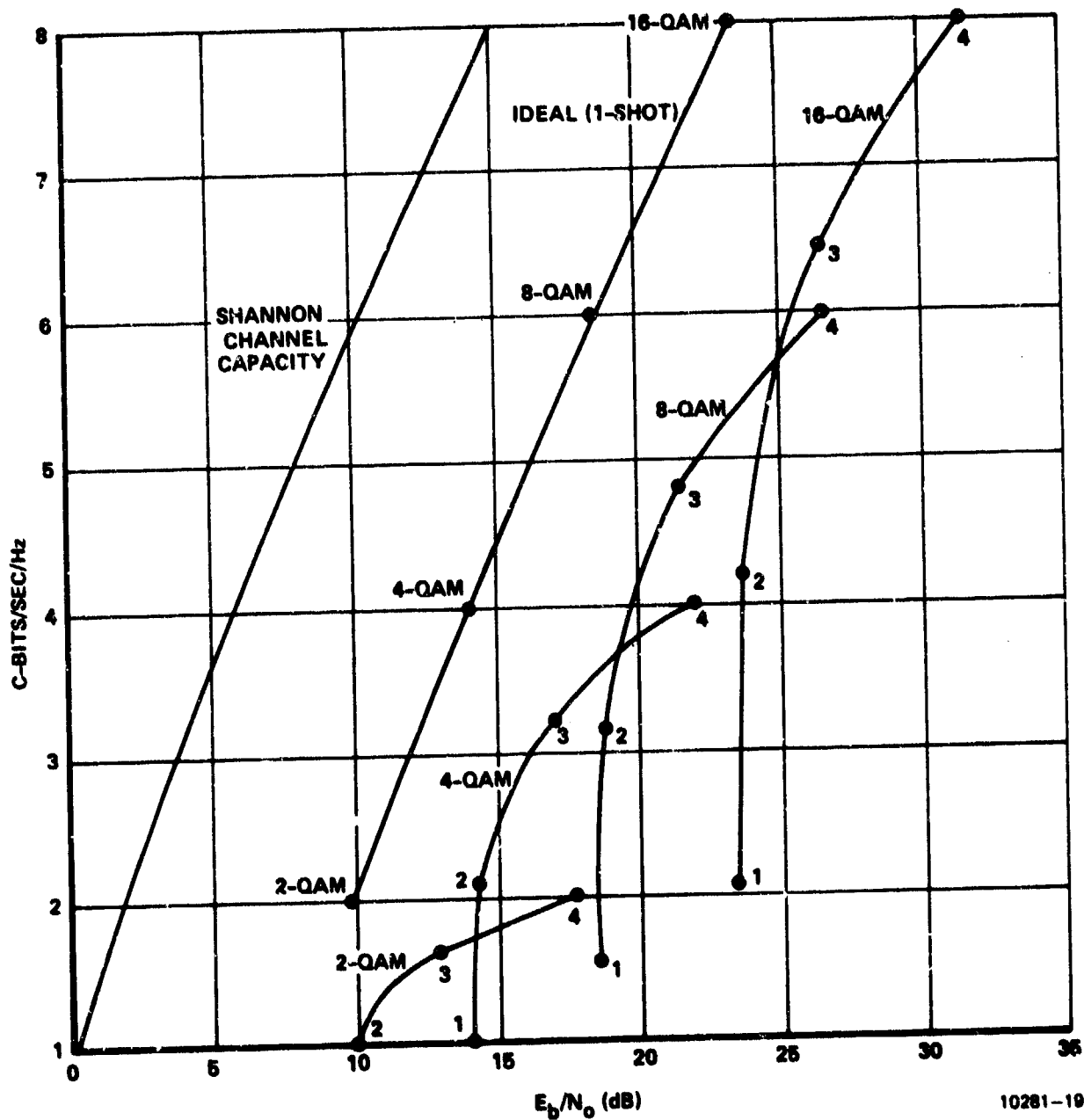


Figure 6.4.3-3. Capacity Versus Performance of Nyquist Equalized Prolate Spheroid Pulse Shape for M-QAM Signaling $P(E) = 10^{-5}$

by the corresponding number of dB from Figure 6.4.3-2. When the same procedure is applied to M-PSK systems, the capacity versus performance curve of Figure 6.4.3-4 results.

6.4.4 Performance of Prolate Spheroid Shaping Filter with Viterbi Algorithm Receiver

In this section we present the performance of the system shown in Figure 6.4-1 for the shaping filter pulse of Figure 6.4-4 when the sample processor is a Viterbi algorithm processor. As briefly discussed in Paragraph 2.2.6.2, the performance of such a processor is determined by the polynomial, $f(D)$, in the discrete characterization. The polynomial $f(D)$ for various values of μ is given in Table 6.4.1 for the shaping filter pulse considered here. The $f(D)$ polynomials of Table 6.4.1 were used in our computer program to determine the probability of symbol error for a Viterbi algorithm processor. The curve of M-QAM probability of symbol error versus E_b/N_0 obtained in the cases $\mu = 2, 3$ and 4 are shown in Figures 6.4.4-1, 6.4.4-2, and 6.4.4-3 respectively.

Using the capacity data of Figure 6.4.2 along with the E_b/N_0 required for 10^{-5} error rate from Figures 6.4.4-1, 6.4.4-2, and 6.4.4-3, one can plot the capacity versus E_b/N_0 curves of Figure 6.4.4-4, for the Viterbi Algorithm receiver for the Prolate Spheroid Shaped M-QAM transmission schemes. Also shown in Figure 6.4.4-4, is the performance of ideal M-QAM schemes from Paragraph 4.3. As shown in Figure 6.4.4-4 the Viterbi algorithm processor can do quite well compared to the ideal band-limited M-QAM case. This good performance comes, however, at the expense of a $M^{(\mu-1)}$ state M-ary Viterbi demodulator for each of the quadrature QAM channels.

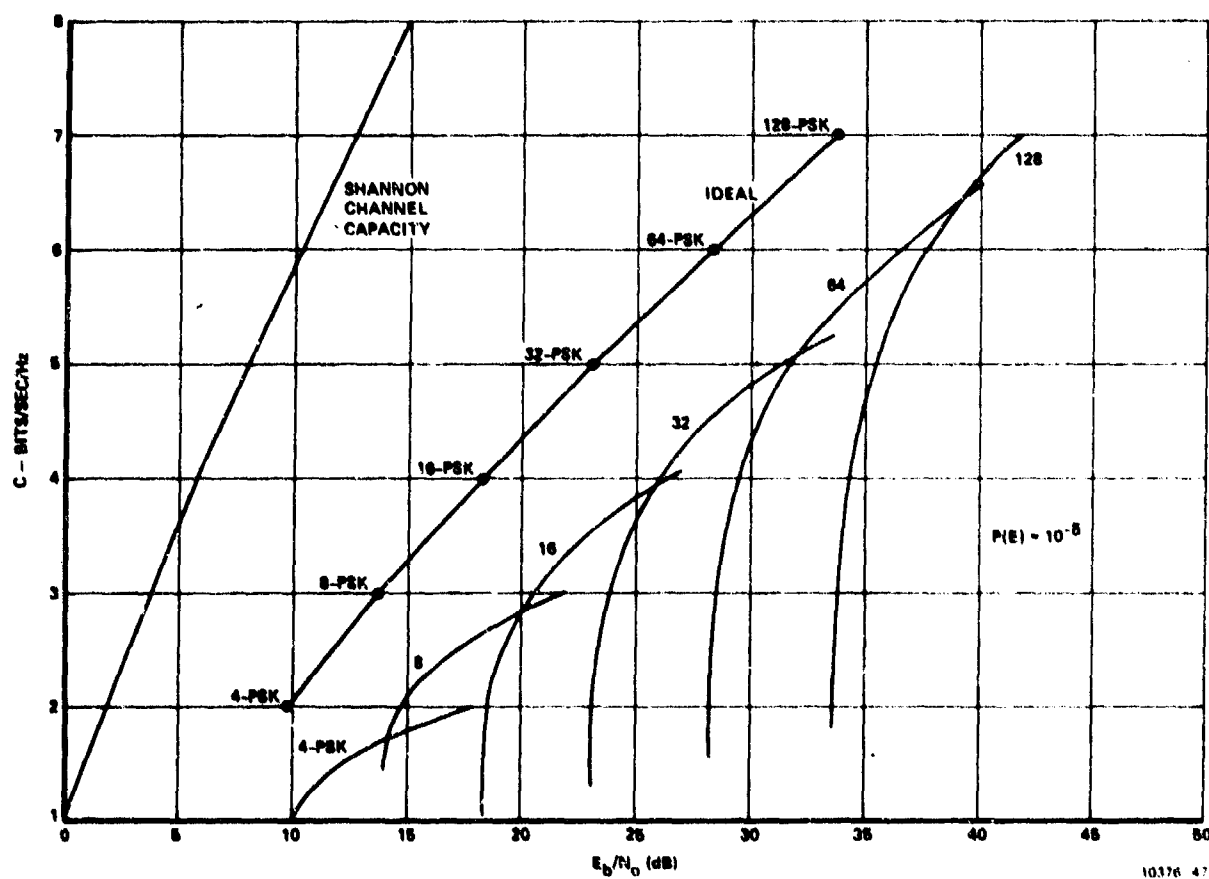


Figure 6.4.3-4. Capacity Versus Performance of Nyquist Equalized Prolate Spheroid Pulse Shape for M-PSK Signaling $P(E) = 10^{-5}$

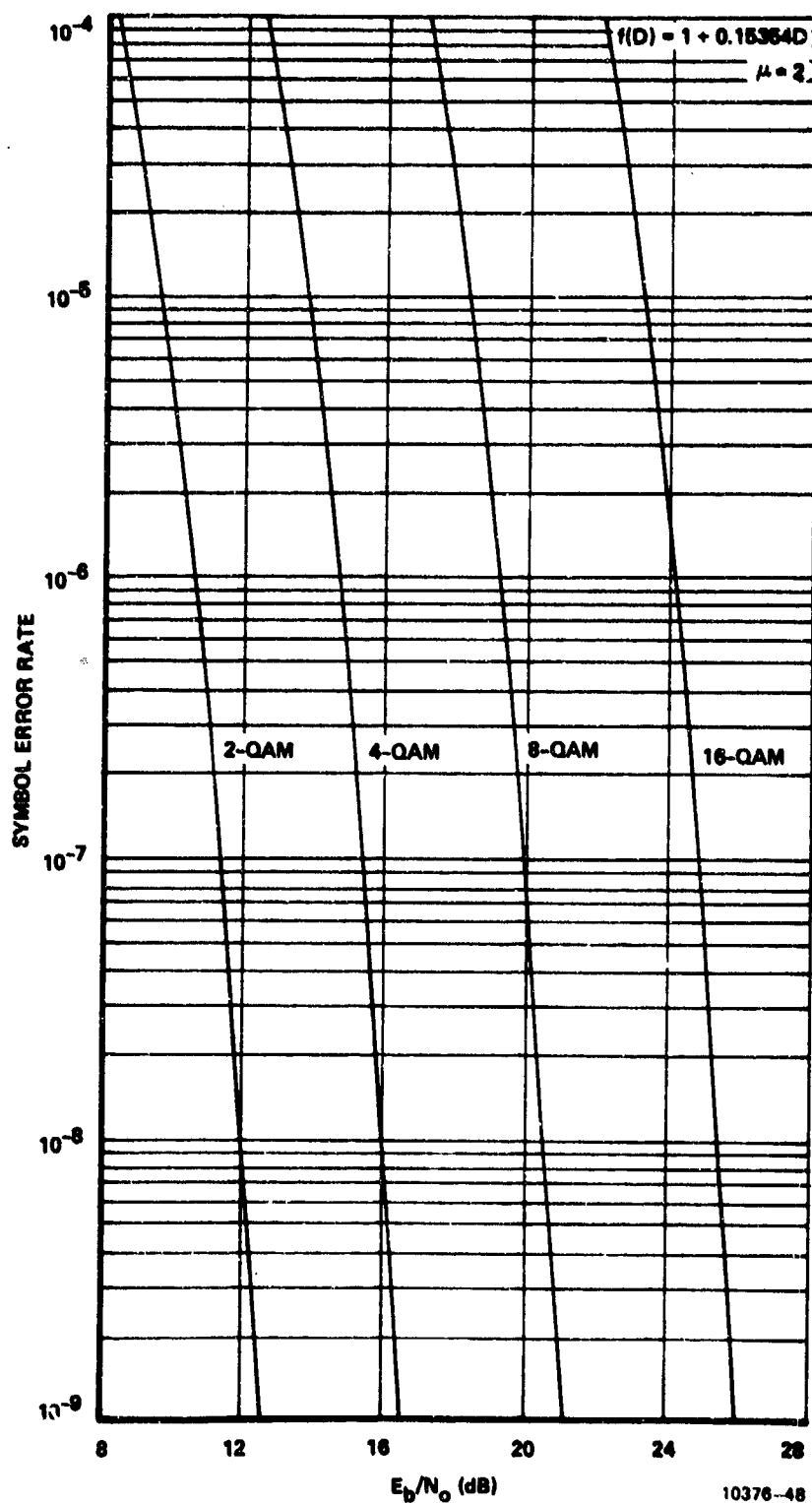
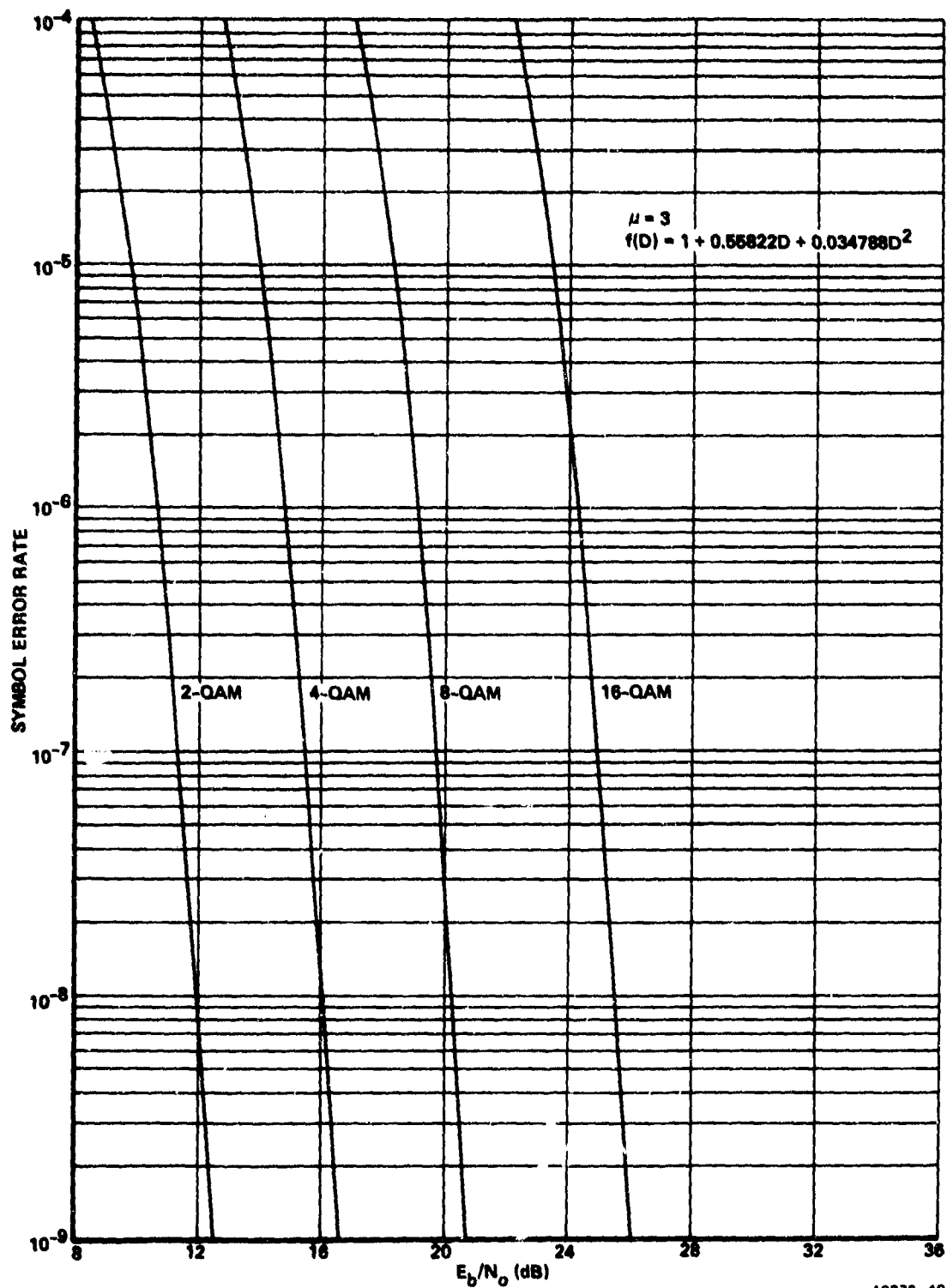


Figure 6.4.4-1. Viterbi Algorithm Performance for Prolate Spheroid Pulse Shaped M-QAM



10376-49

Figure 6.4.4-2. Viterbi Algorithm Performance for Prolate Spheroid Pulse Shaped M-QAM

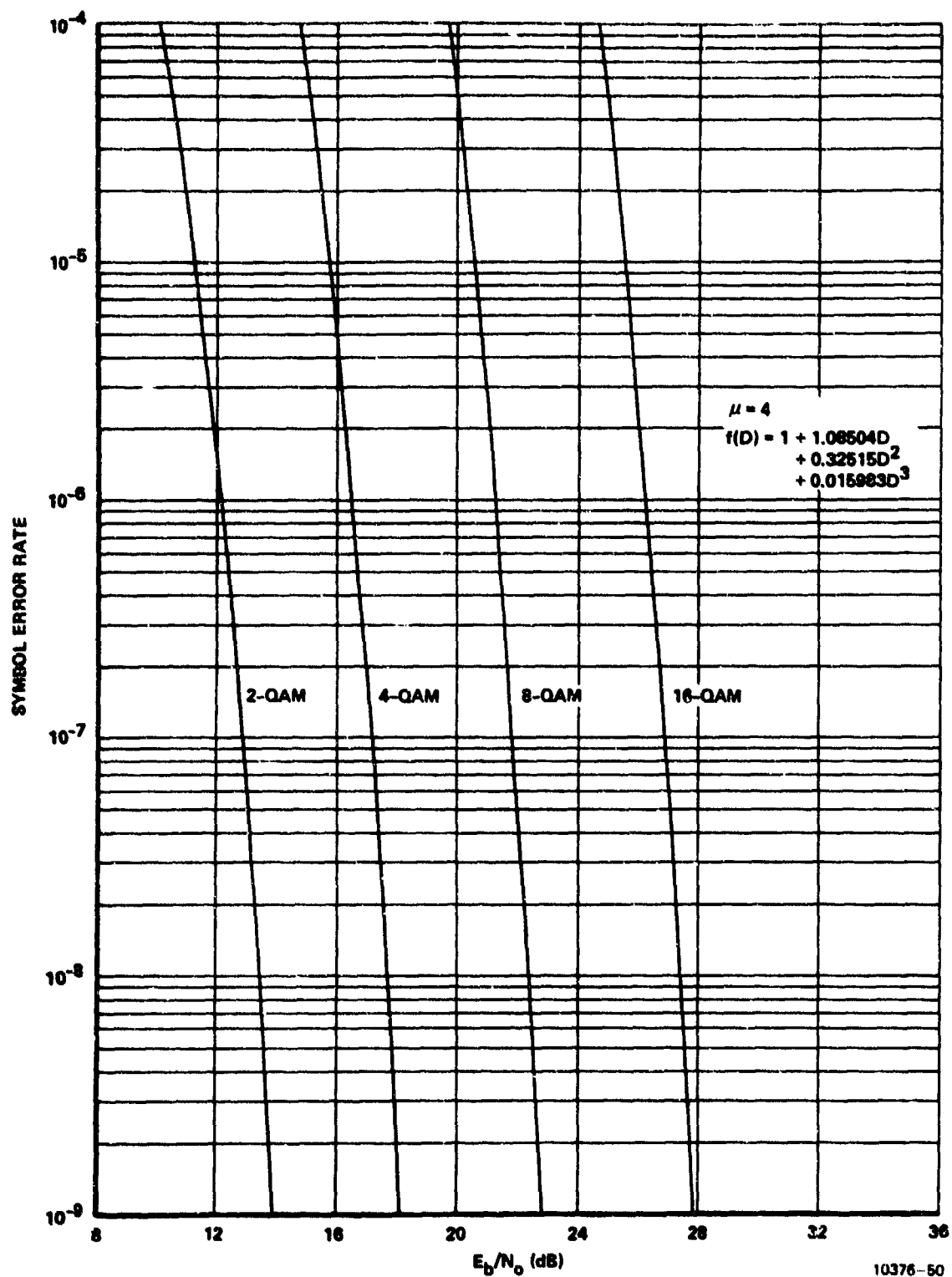


Figure 6.4.4-3. Viterbi Algorithm Performance for Prolate Spheroid Pulse Shaped M-QAM

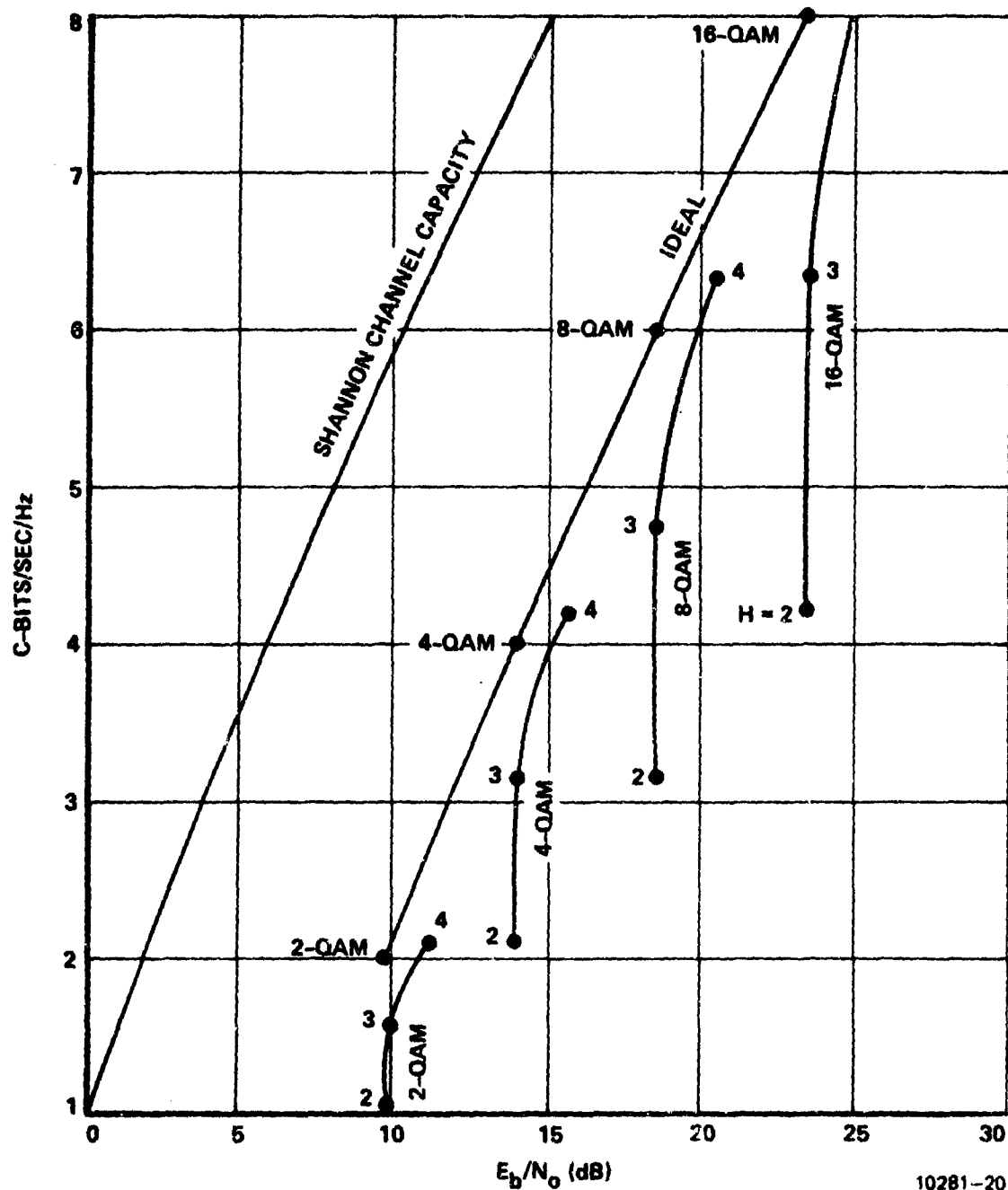


Figure 6.4.4-4. Capacity Versus Performance for Viterbi Algorithm Processor for Prolate Spheroid Pulse Shaped M-QAM $P(E) = 10^{-5}$

6.5 Performance of Transmitter-Filtered and Receiver-Equalized Systems

6.5.1 Introduction

In this section, the performance of the digital transmission system of Figure 6.5.1 will be examined. This system uses multilevel

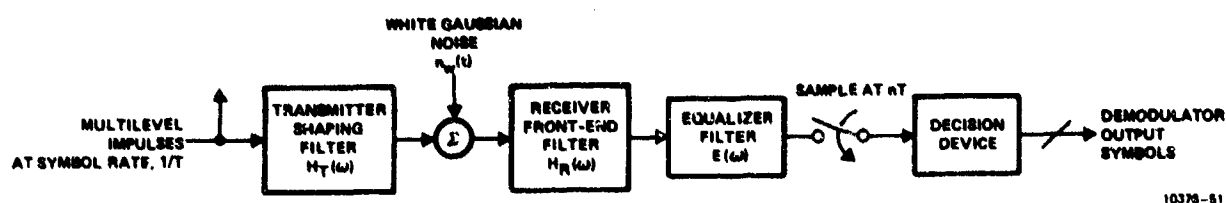


Figure 6.5.1. Digital System With Transmit Shaping Filter and Receiver Equalization

impulses into a shaping filter, $H_T(\omega)$, at the transmitter. The purpose of $H_T(\omega)$ in our case is to shape the transmitted spectrum for meeting the requirements of FCC 19311. At the receiver, a front-end filter $H_R(\omega)$ is included to limit out-of-band noise. Following this filter is an equalizer filter, $E(\omega)$, used to force the overall filtering action represented by

$$H(\omega) = H_T(\omega) H_R(\omega) E(\omega) \quad (6.5.1-1)$$

to display a desired partial response. Two types of equalization considered in this work included Nyquist and duobinary partial response. A computer program was written to determine the dB degradation of the system shown in Figure 6.5.1 over the one-shot receiver performance. The one-shot performance is that obtained by a scheme which uses only a

receiver filter matched to the transmitter filter. One impulse of a set of possible impulses is communicated and the one-shot receiver optimally decides which of the set was sent. In this one-shot problem, the effects of intersymbol interference are nonexistent since there is but one impulse ever conveyed. As such, the one-shot receiver makes the best possible use of the transmitter pulse energy and there are no intersymbol effects to degrade performance. The E_b/N_0 for a given error rate for the one-shot receiver is the same as the ideal systems of Section 4 in the M-QAM and M-PSK cases. The best the equalized receiver of Figure 6.5.1 can ever possibly perform is identical to the one-shot receiver, since there is generally always some performance penalty incurred (usually through noise enhancement) at the receiver for the removal of intersymbol interference.

In the following paragraphs we present results obtained for the system shown in Figure 6.5.1.

6.5.2 Equalization Results for Impulse Signalling Through Butterworth Baseband Filters

Results were obtained for the system of Figure 6.5.1 for five- and eight-pole Butterworth shaping filters. Performance for systems with both Nyquist and Duobinary channel equalization were obtained.

Figure 6.5.2-1 shows the spectra obtainable with the Butterworth shaping filters and the corresponding FCC 19311 spectral masks for the five-pole and eight-pole case. The authorized bandwidth assumed for plotting the masks was 3.5 MHz. As shown, the five-pole Butterworth filter requires an authorized RF bandwidth of 3.5 times the filter low pass 3 dB bandwidth, and the eight-pole filter requires 2.8 times the 3 dB low pass bandwidth.

The degradation relative to one-shot receiver performance for Nyquist equalization of five-pole Butterworth filters is shown in Figure

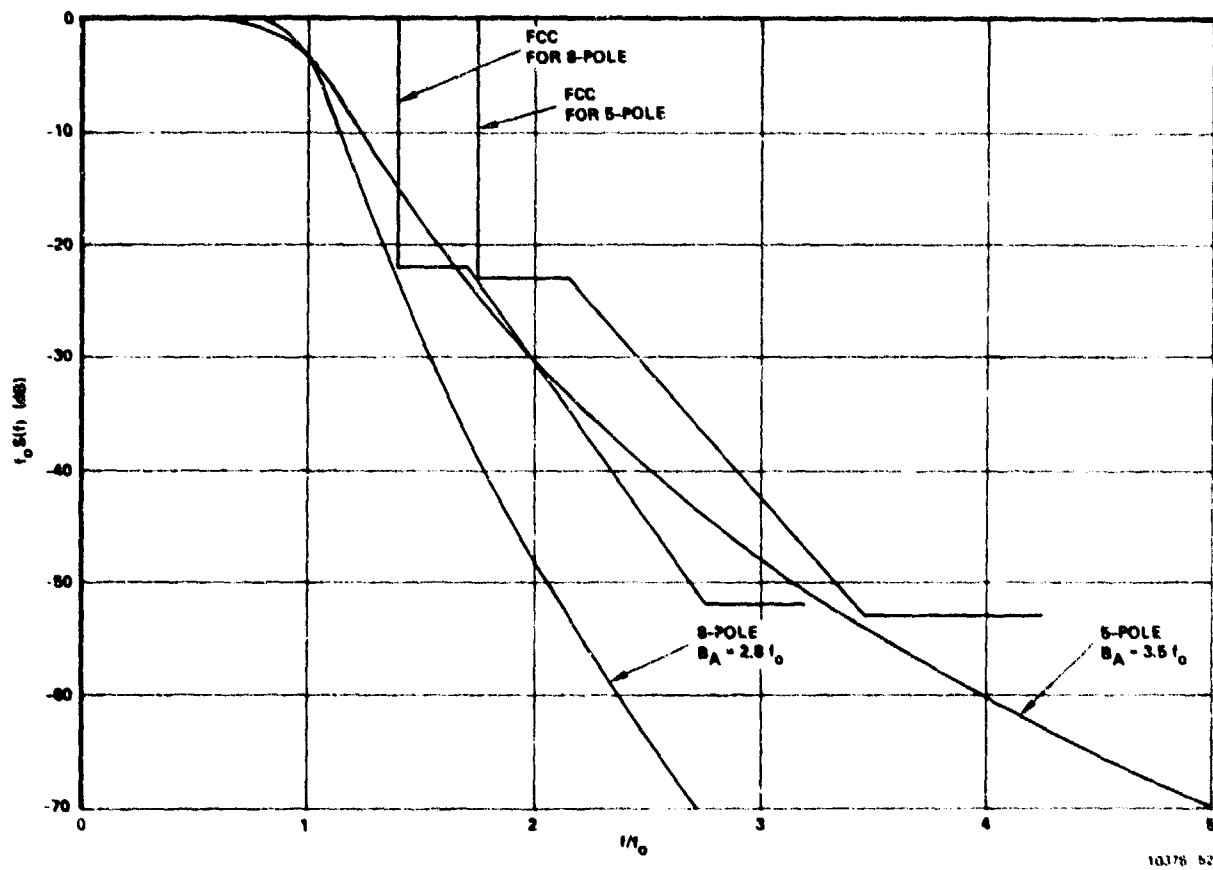


Figure 6.5.2-1. Butterworth Spectra $f_0 = 3$ dB BW

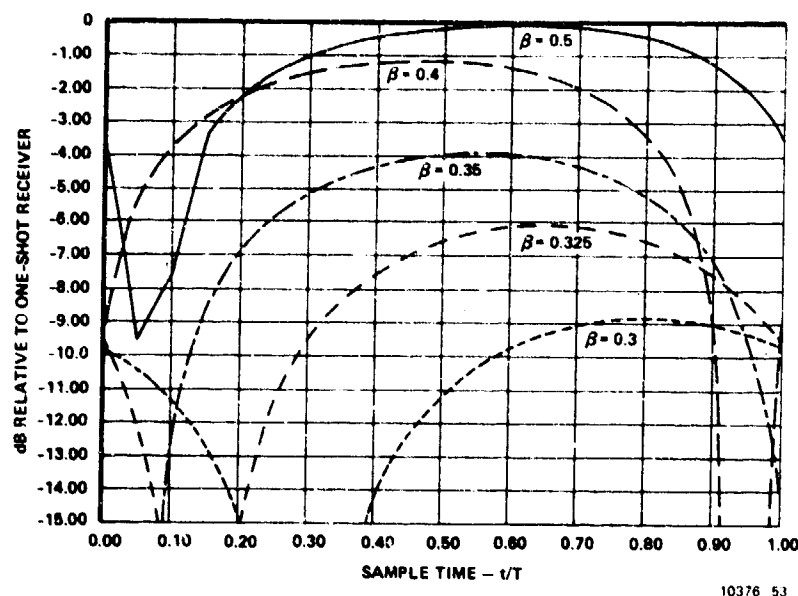


Figure 6.5.2-2. Five-Pole Butterworth Transmit and Receiver Filters
 3 dB BW = β x Symbol Rate
 Performance With Ideal Nyquist Equalization

6.5.2-2. Identical transmitter and receiver filters were assumed in generating this data. The parameter β is the ratio of filter 3 dB low-pass bandwidth to symbol rate. The degradation is displayed, for a given β , versus the relative symbol timing location at the receiver. One notes that for $\beta = 0.5$, virtually no degradation occurs with the equalized receiver structure. If the filter 3 dB bandwidth is lowered below the Nyquist rate (one-half symbol rate) degradation begins to occur because of a requirement for the equalizer to provide significant frequency response boost at the Nyquist rate to maintain zero intersymbol interference. Because of this frequency response boost, the effect of channel noise is increased.

Figure 6.5.2-3 shows the results obtained for duobinary partial response equalization for the five-pole Butterworth filters. Here, the best choice of filter bandwidth occurs around $\beta = 0.4$ and the degradation is about 2.2 dB. The best duobinary can do is 2.1 dB (see Lucky, Salz and Weldon⁵) relative to one-shot receiver, so this represents near-optimal duobinary performance for the filter-equalizer approach.

In Figure 6.5.2-4 the degradation incurred in Figures 6.5.2-2 and 6.5.2-3 at the best sampling times has been plotted to show the loss

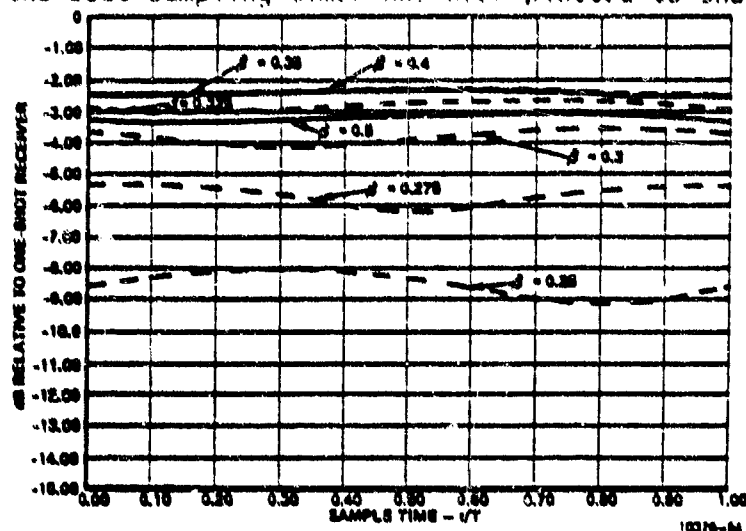


Figure 6.5.2-3. Five-Pole Butterworth Transmit and Receiver Filters
3 dB BW = $\beta \times$ Symbol Rate Ideal Equalization to Duobinary

relative to one-shot receiver performance versus the five-pole Butterworth filter, 3 dB bandwidth. From Figure 6.5.2-4, one concludes that if the 3 dB bandwidth of the shaping filter is greater than 0.375 symbol rate, Nyquist equalization results in the least degradation and if less than 0.375 symbol rate, duobinary equalization is better.

A similar set of data was gathered for the eight-pole Butterworth filter case and these results are shown in Figures 6.5.2-5, 6.5.2-6, and 6.5.2-7. As shown in Figure 6.5.2-7, the changeover from Nyquist to duobinary should be made in this case at a filter bandwidth of less than 0.41 times symbol rate.

Figures 6.5.2-4 and 6.5.2-7 provide the performance element required in a trade-off of various schemes for meeting the goals of this study. Another required element is the FCC 19311 spectral efficiency for these schemes. Figure 6.5.2-1 will provide the spectral efficiency measure. As shown in Figure 6.5.2-1, the required FCC 19311 authorized

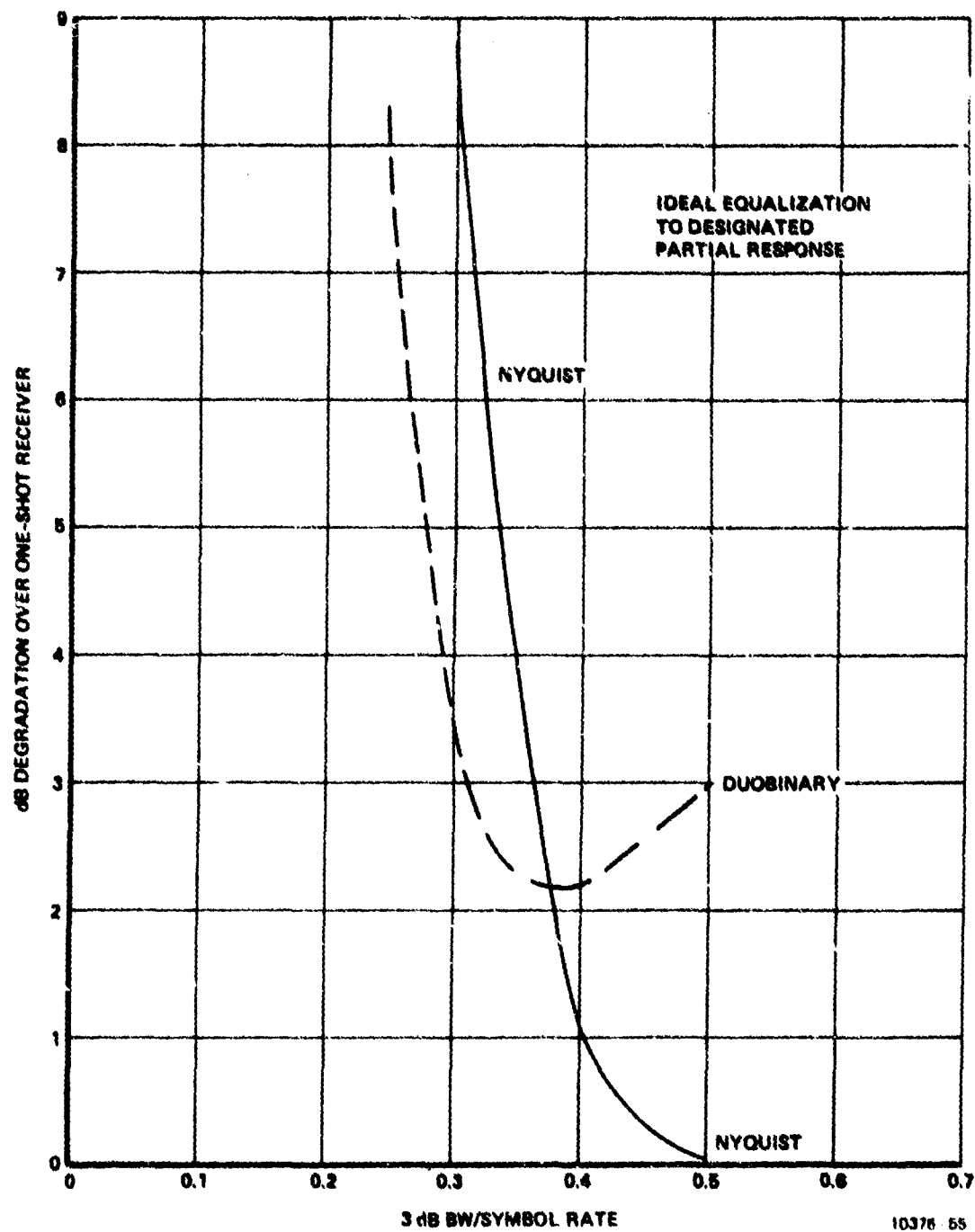


Figure 6.5.2-4. Degradation for Five-Pole Butterworth Transmit and Receiver Filters

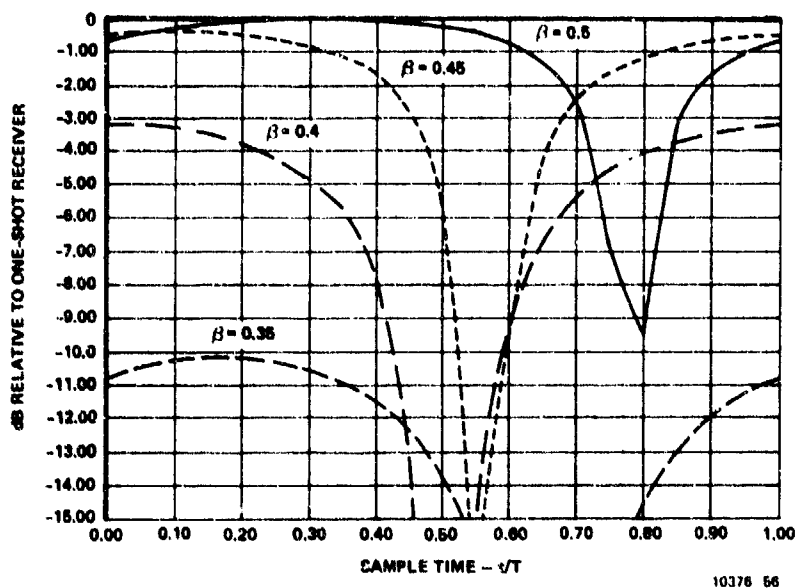


Figure 6.5.2-5. Eight-Pole Butterworth Transmit and Receive Filters 3 dB BW = β x Symbol Rate
Ideal Nyquist Equalization

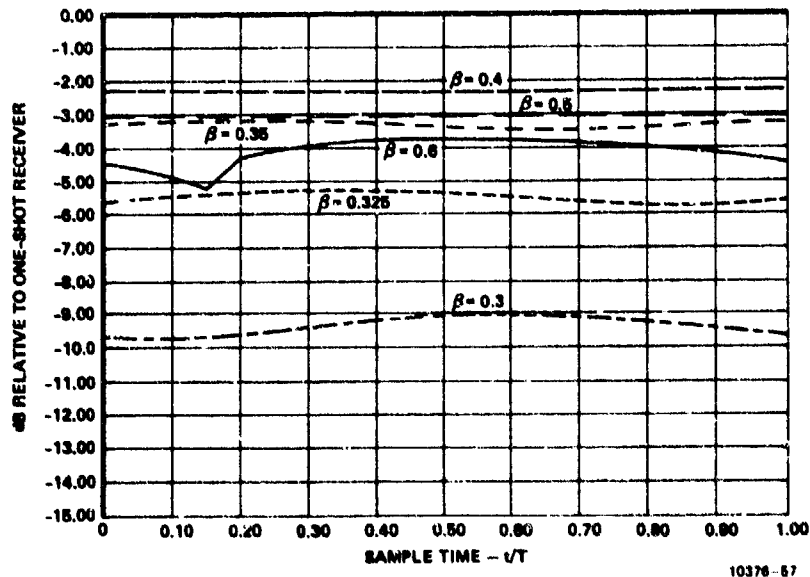


Figure 6.5.2-6. Eight-Pole Butterworth Transmit and Receive Filters 3 dB BW = β x Symbol Rate
Ideal Duobinary Equalization

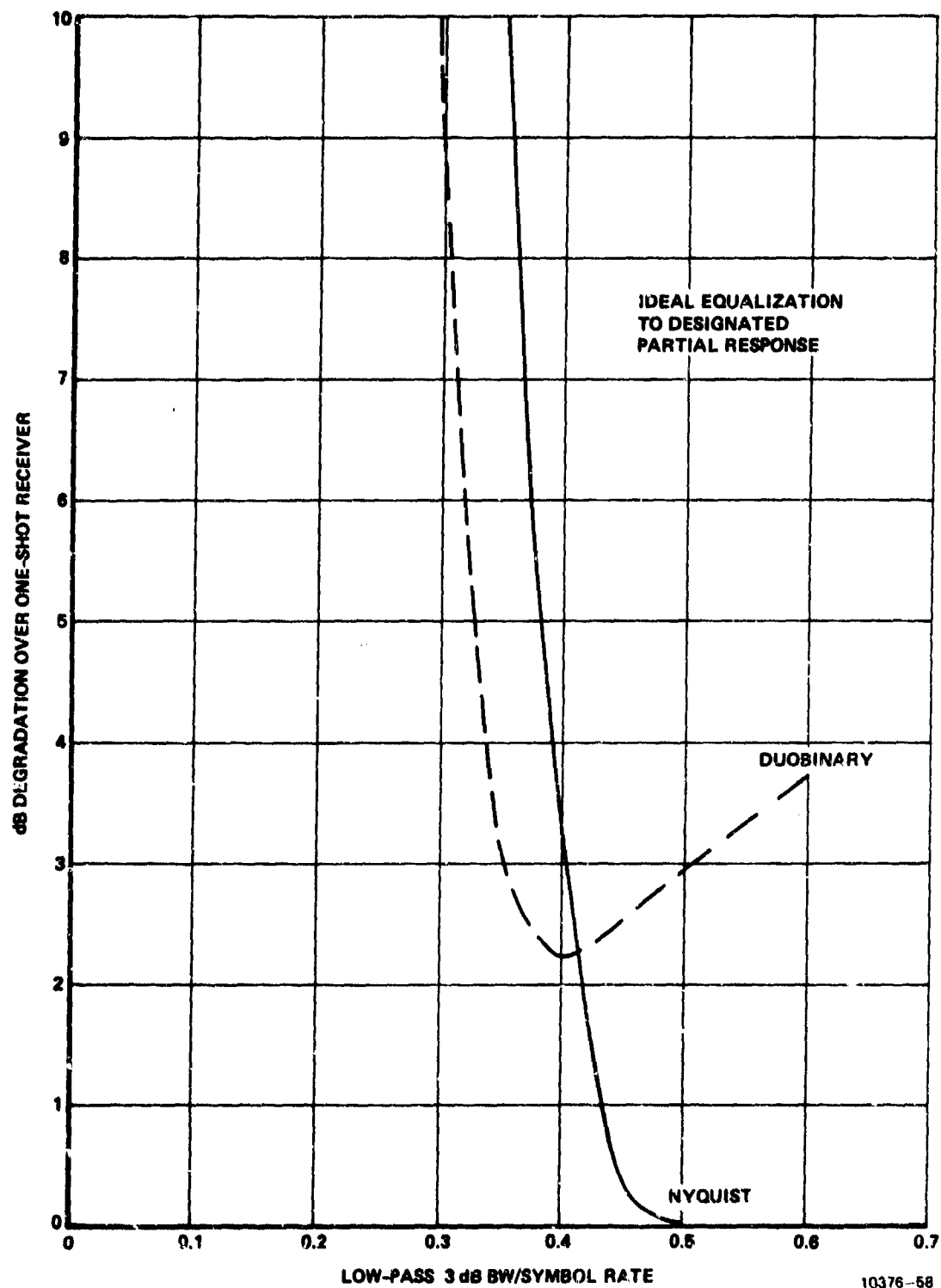


Figure 6.5.2-7. Eight-Pole Butterworth Transmit and Receive Filters Ideal Equalization to Designated Partial Response

RF bandwidth is some multiple, say α , of the low-pass filter 3 dB bandwidth, i.e.,

$$B_a = \alpha f_o \quad (6.5.2-1)$$

where

B_a = FCC 19311 authorized bandwidth

f_o = Filter 3 dB bandwidth (low-pass)

Further, we have been using the parameter β to relate the low pass 3 dB filter bandwidth to the symbol rate, i.e.,

$$f_o = \beta(1/T) \quad (6.5.2-2)$$

where

T = Symbol time

f_o = Low pass filter 3 dB bandwidth

From Equations (6.5.2-1) and (6.5.2-2) we have

$$B_a = \alpha\beta(1/T) \quad (6.5.2-3)$$

The number of symbols/s/Hz of authorized bandwidth is given by

$$S \triangleq \frac{(1/T)}{B_a}$$

$$S = \frac{1}{\alpha\beta} \text{ symbols/s/Hz} \quad (6.5.2-4)$$

As shown in Figure 6.5.2-1, $\alpha = 3.5$ for the five-pole filter and $\alpha = 2.8$ for the eight-pole filter. Equation (6.5.2-4) has been used to plot Figure 6.5.2-8 for the five- and eight-pole Butterworth filters.

The curve of S in symbols/s/Hz shown in Figure 6.5.2-8 can be converted to capacity in bits/s/Hz simply by multiplying S by the number of bits conveyed per RF symbol for the selected modulation schemes, i.e.,

$$C = BS \quad (6.5.2-5)$$

where

C = Capacity in bits/s/Hz under FCC 19311

B = Bits/RF symbol

S = Symbols/s/Hz under FCC 19311

The performance (i.e., E_b/N_0 for a designated error rate) is obtained by taking the E_b/N_0 required for the designated error rate for an ideal system (one-shot receiver performance) and adding the degradation displayed in Figure 6.5.2-4 or 6.5.2-7.

The obtaining of a pair of C and E_b/N_0 for plotting on a capacity versus E_b/N_0 curve is rendered easier if we eliminate the parameter β between Figures 6.5.2-7 and 6.5.2-8 by making the parameter implicit, i.e., choose a value for β and determine S and degradation from Figures 6.5.2-4 and 6.5.2-8 for example and plot S versus degradation. This has been done in Figures 6.5.2-9 and 6.5.2-10 for the five-pole and eight-pole Butterworth filters, respectively. From Figure 6.5.2-9, we note that for Nyquist equalization of five-pole Butterworth shaping filters, the least degradation (≈ 0 dB) occurs at around 0.57 symbols/s/Hz of authorized bandwidth. For duobinary equalization, the minimum degradation (2.2 dB) occurs at approximately 0.75 symbols/s/Hz of

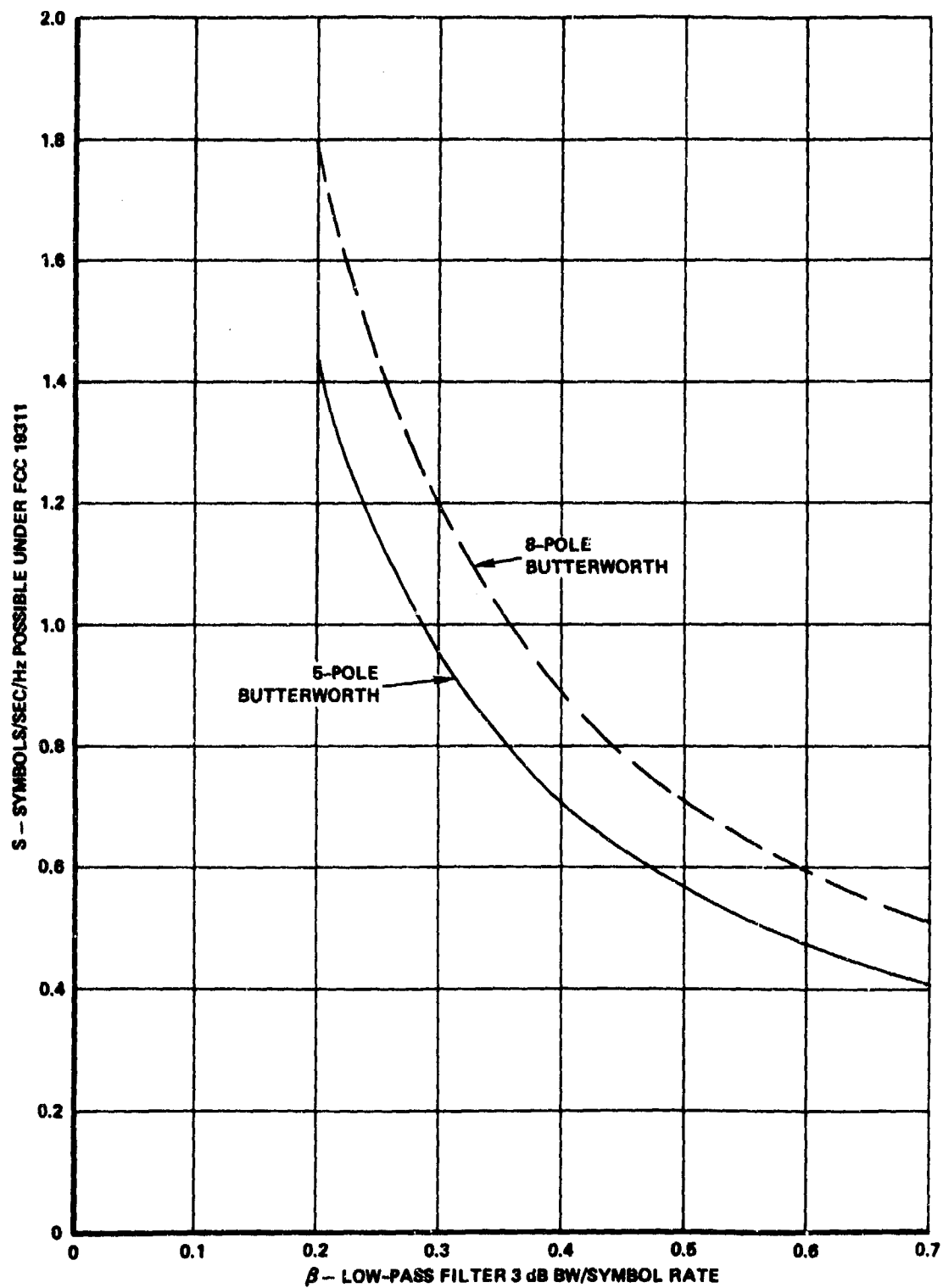


Figure 6.5.2-8. Symbols/s/Hz Under FCC 19311 for Butterworth Spectra Versus Filter Bandwidth

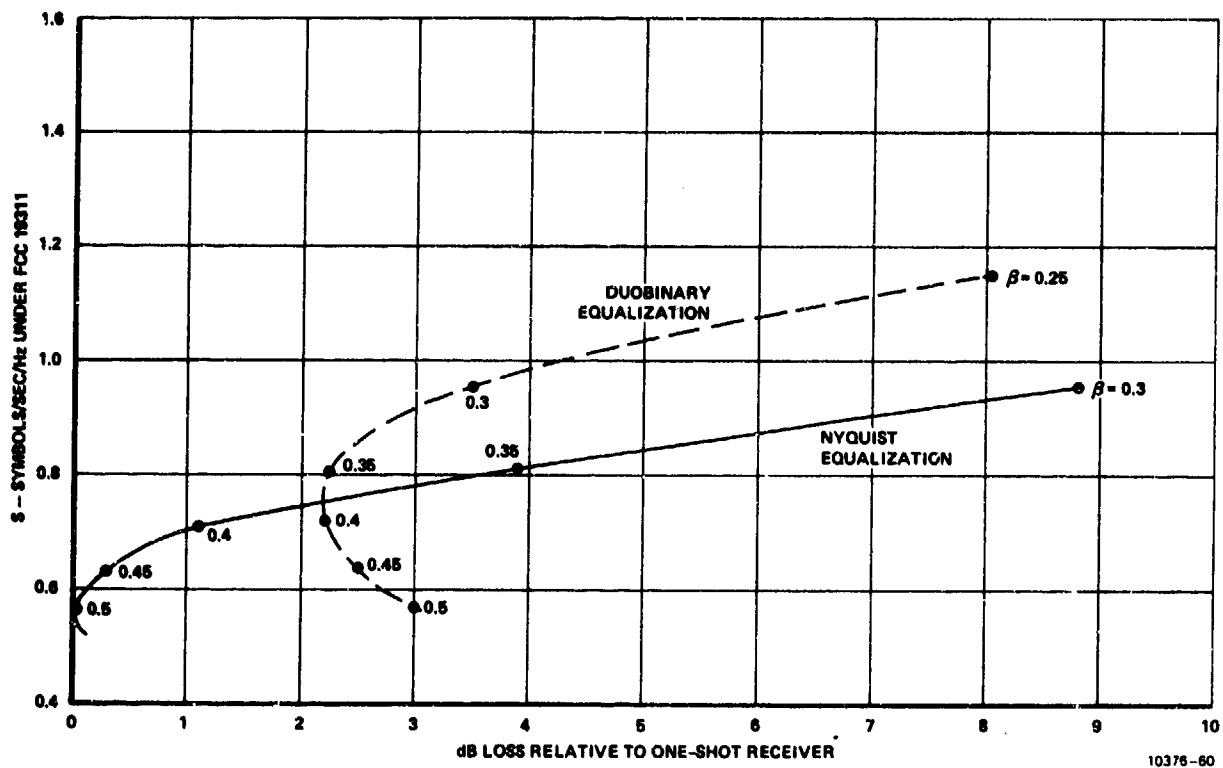


Figure 6.5.2-9. Combinations of Symbols/s/Hz and Degradation for Equalized Five-Pole Butterworth Filters

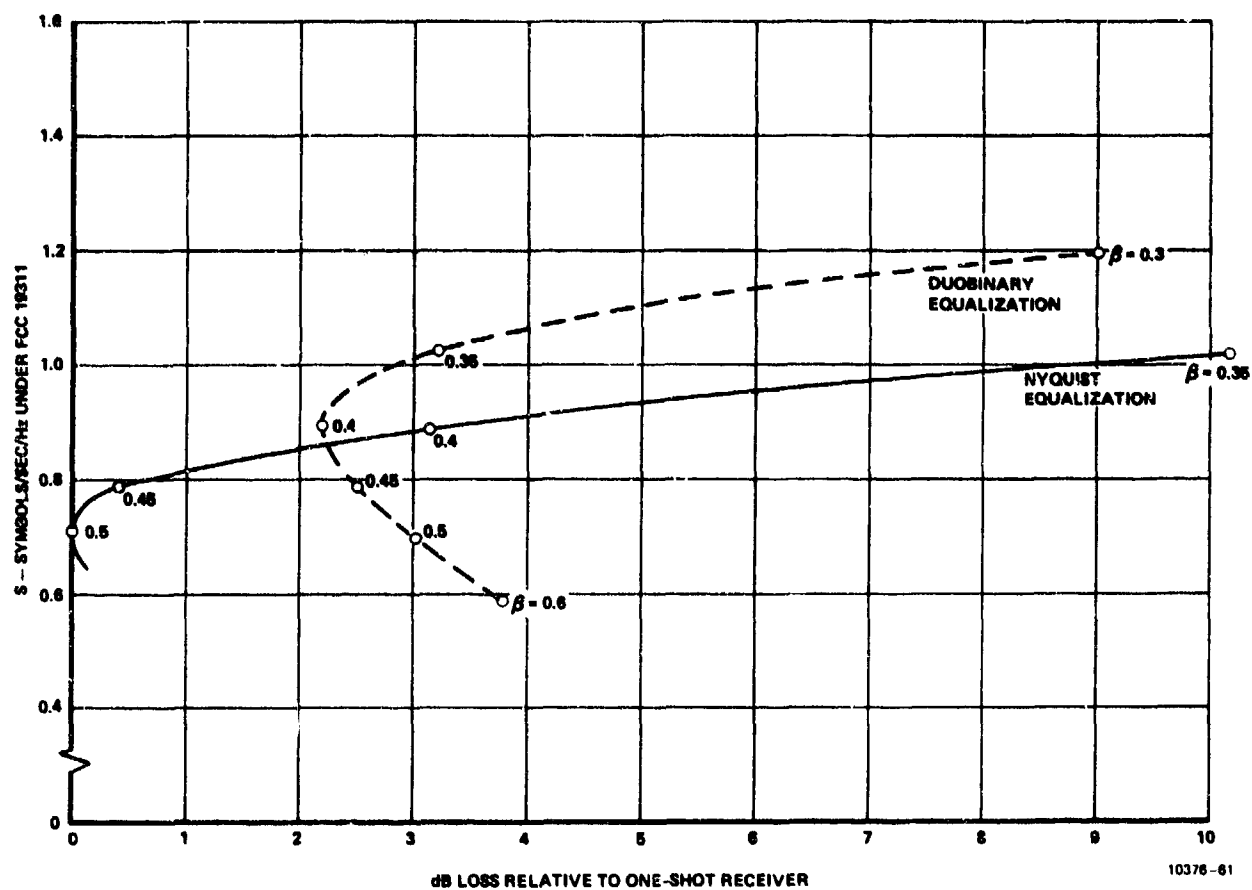


Figure 6.5.2-10. Combinations of Symbols/s/Hz and Degradation for Equalized Eight-Pole Butterworth Filters

authorized bandwidth. From Figure 6.5.2-10 the minimal degradation values of symbol rate for eight-pole Butterworth filters are 0.7 symbols/s/Hz for Nyquist equalization and 0.9 symbols/s/Hz for duobinary equalization.

6.5.2.1 M-QAM Results

The data of Figure 6.5.2-9 and the ideal performance (one-shot receiver performance) from Section 4 for M-QAM systems at 10^{-5} error rate have been used to plot the capacity under FCC 19311 versus performance curves shown in Figure 6.5.2.1-1 for equalized five-pole Butterworth shaping filters. We note that at 3 and 4 bits/s/Hz capacities, there is not a clear choice between Nyquist and duobinary equalization. (The advantage of 4-QAM with duobinary equalization in the region between 3 and 4 bits/s/Hz can be reduced by employing Nyquist equalized M-QAM for $4 < M < 8$ in this region. For example, the modified 6-QAM scheme of Paragraph 4.2.1 can be used.) However, above approximately 4.5 bits/s/Hz, a superiority of duobinary equalized M-QAM schemes begins to emerge.

Similar data are obtained for the eight-pole Butterworth filters from Figure 6.5.2-10 in conjunction with the ideal performance data of Section 4 and this data has been plotted in Figure 6.5.2.1-2.

The data presented in Figures 6.5.2.1-1 and 6.5.2.1-2 show the combinations of capacity (in bits/s/Hz) under the FCC 19311 spectral criterion versus the average E_b/N_0 (signal-to-noise ratio in a bandwidth equal to bit rate) required to provide 10^{-5} error rate. The curves are useful to show the capacity regions of greatest usefulness for each of the equalized M-QAM schemes. The curves show that generally as the capacity is increased there comes a point where choosing greater M is advantageous in terms of required E_b/N_0 . For example, around 3 bits/s/Hz 4-QAM is useful but at 4 to 4.5 bits/s/Hz, 8-QAM is a better choice.

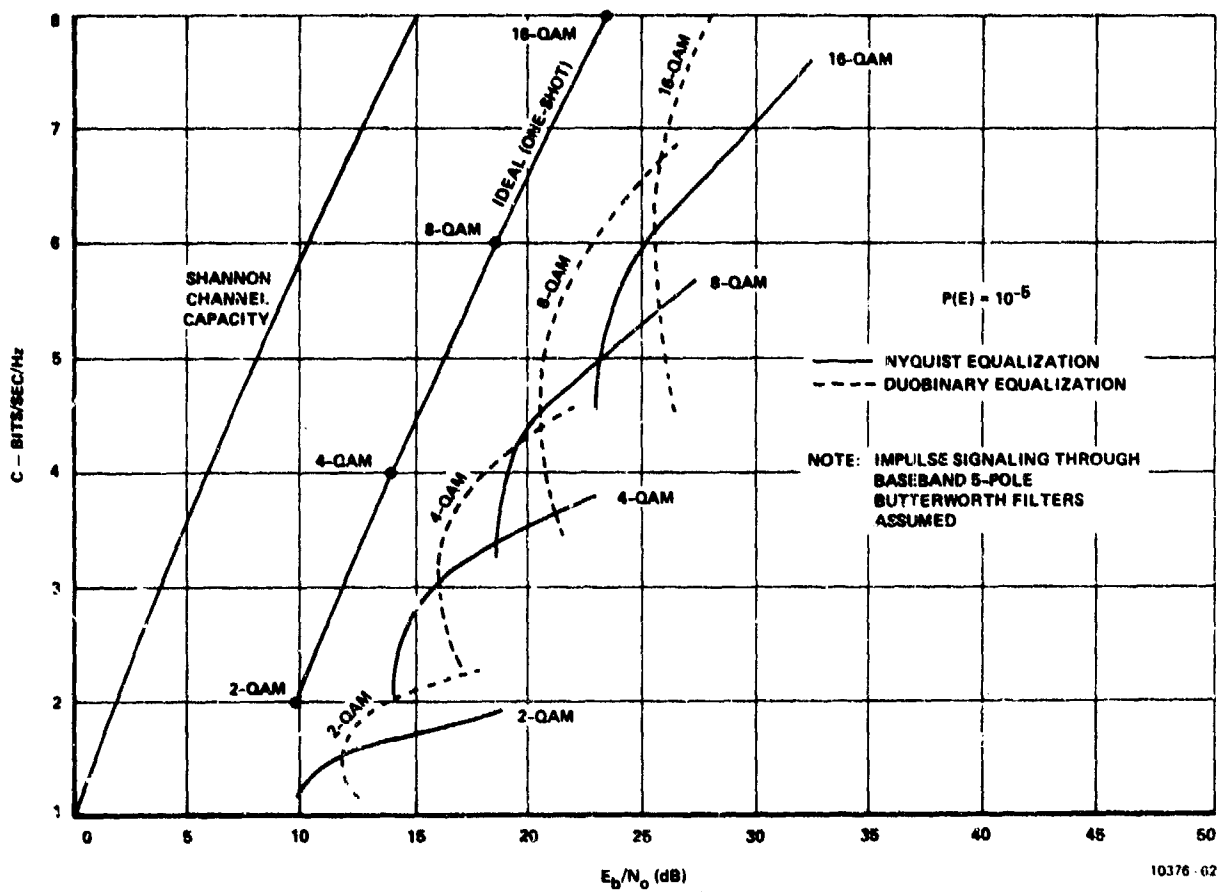


Figure 6.5.2.1-1. Capacity Versus Performance of Equalized Five-Pole Butterworth Filters for M-QAM Signaling $P(E) = 10^{-5}$

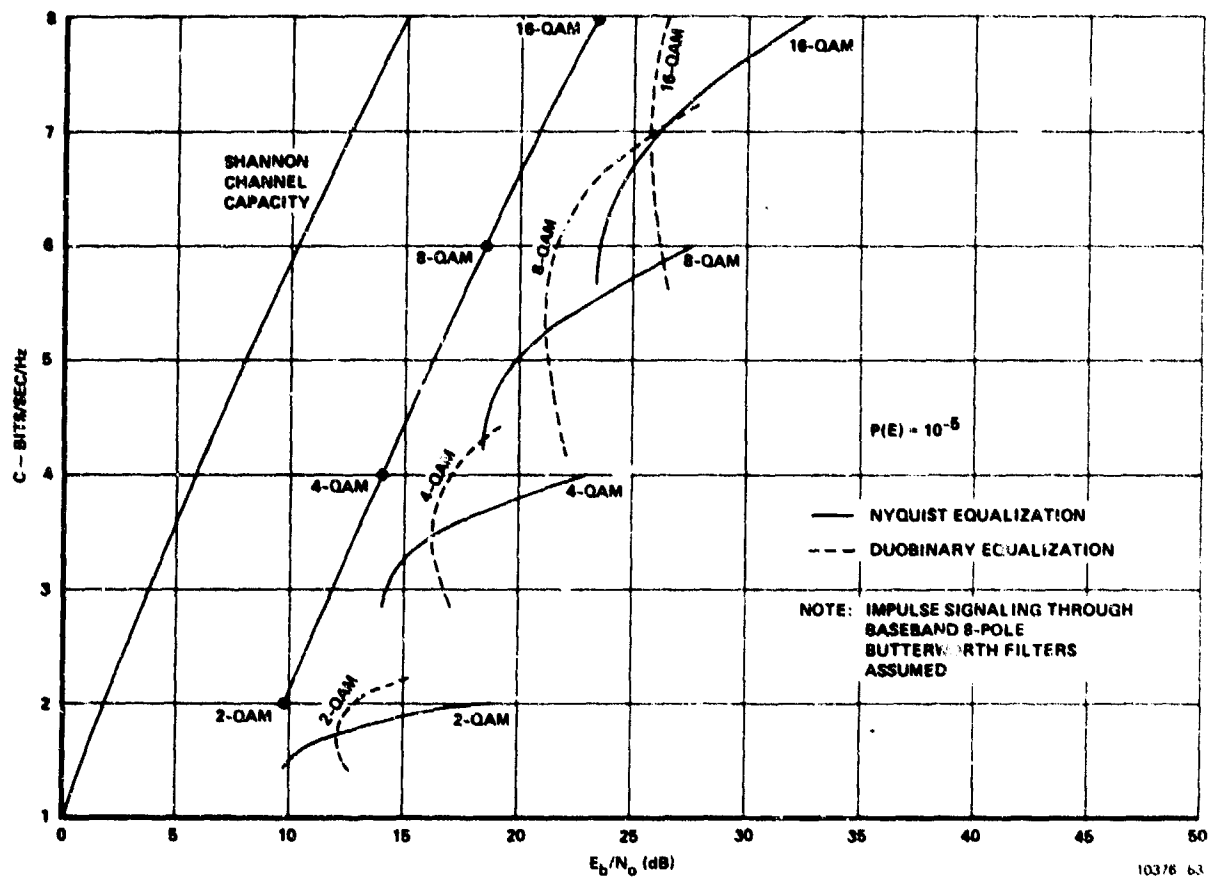


Figure 6.5.2.1-2. Capacity Versus Performance of Equalized Eight-Pole Butterworth Filters for M-QAM Signaling $P(E) = 10^{-5}$

6.5.2.2 M-PSK Results

The data presented in Figures 6.5.2-9 and 6.5.2-10 for the degradation of Nyquist equalized receivers is used to produce the capacity versus E_b/N_0 for M-PSK schemes of the type described in Section 4. Here the use of baseband impulse pairs in a single design as shown in Figure 4-2a of Section 4 is assumed and Butterworth baseband shaping filters are used. At the receiver each quadrature channel is equalized to overall Nyquist response and the received equalized quadrature signals are fed to the decision device as shown in Figure 4-1 of Section 4. The capacity versus E_b/N_0 one obtains for this system is shown in Figure 6.5.2.2-1 for five-pole Butterworth filters and in Figure 6.5.2.2-2 for eight-pole Butterworth filters. Also plotted on this curve is the performance for the ideal M-PSK schemes presented in Paragraph 4.1 for comparison.

Comparing Figures 6.5.2.1-1 and 6.5.2.1-2 for M-QAM systems with Figures 6.5.2.2-1 and 6.5.2.2-2 for M-PSK systems, one notes the superiority of the QAM schemes over PSK schemes in the nonideal band-limited and equalized case just as in the ideal band-limited case of Section 4.

6.5.3 Filtered and Equalized Square-Pulse Signaling

In addition to determining the equalized receiver performance for the case of impulses into the baseband filter as shown in the previous section (Figure 6.5.1), we have also determined the performance for the system shown in Figure 6.5.3. Here the inputs to the shaping filter are square pulses. As shown in Figure 6.5.3, this transmission scheme fits into the same framework as Figure 6.5.1 with impulse signalling, if we include in the transmitter an aperture filter with impulse response as shown in Figure 6.5.3. The aperture filter has frequency response given by

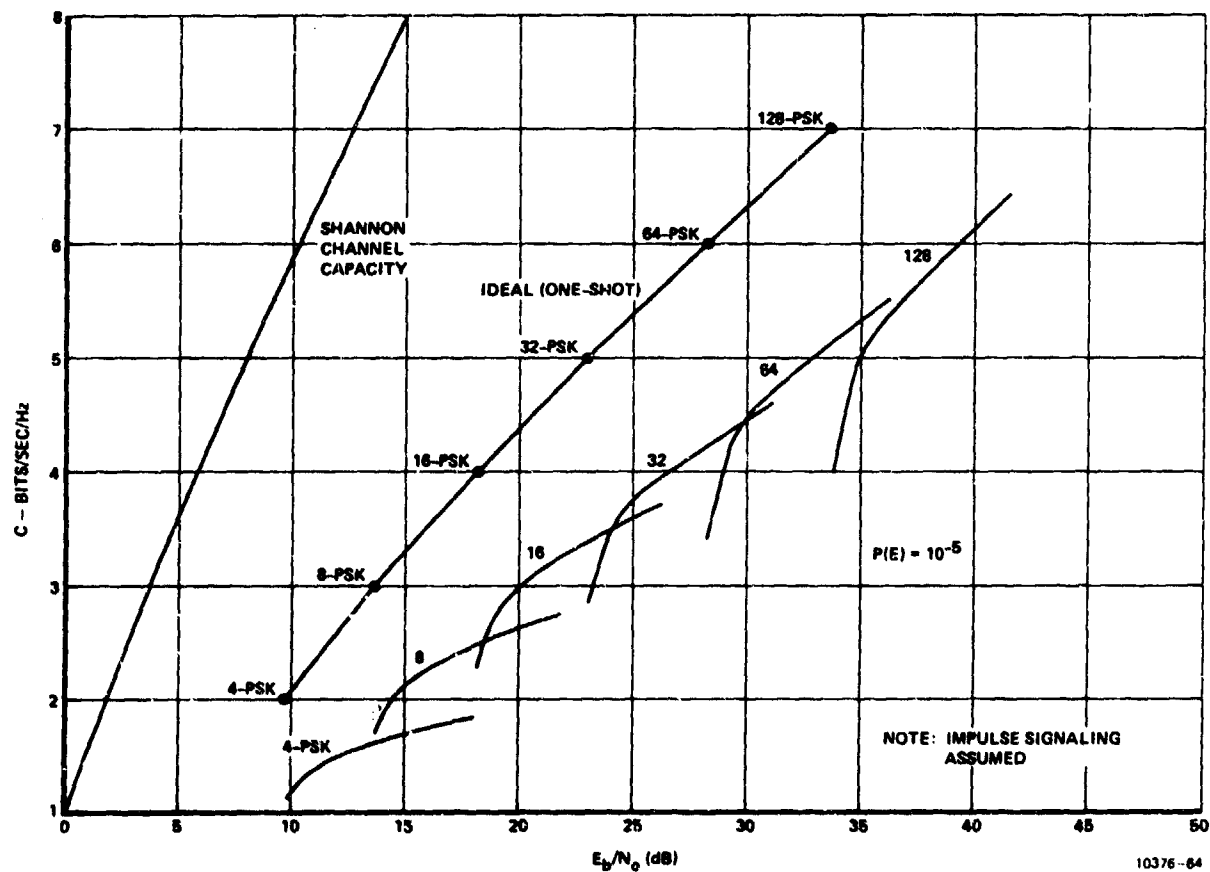


Figure 6.5.2.2-1. Capacity Versus Performance of Nyquist Equalized Five-Pole Butterworth Filters for M-PSK Signaling $P(E) = 10^{-5}$

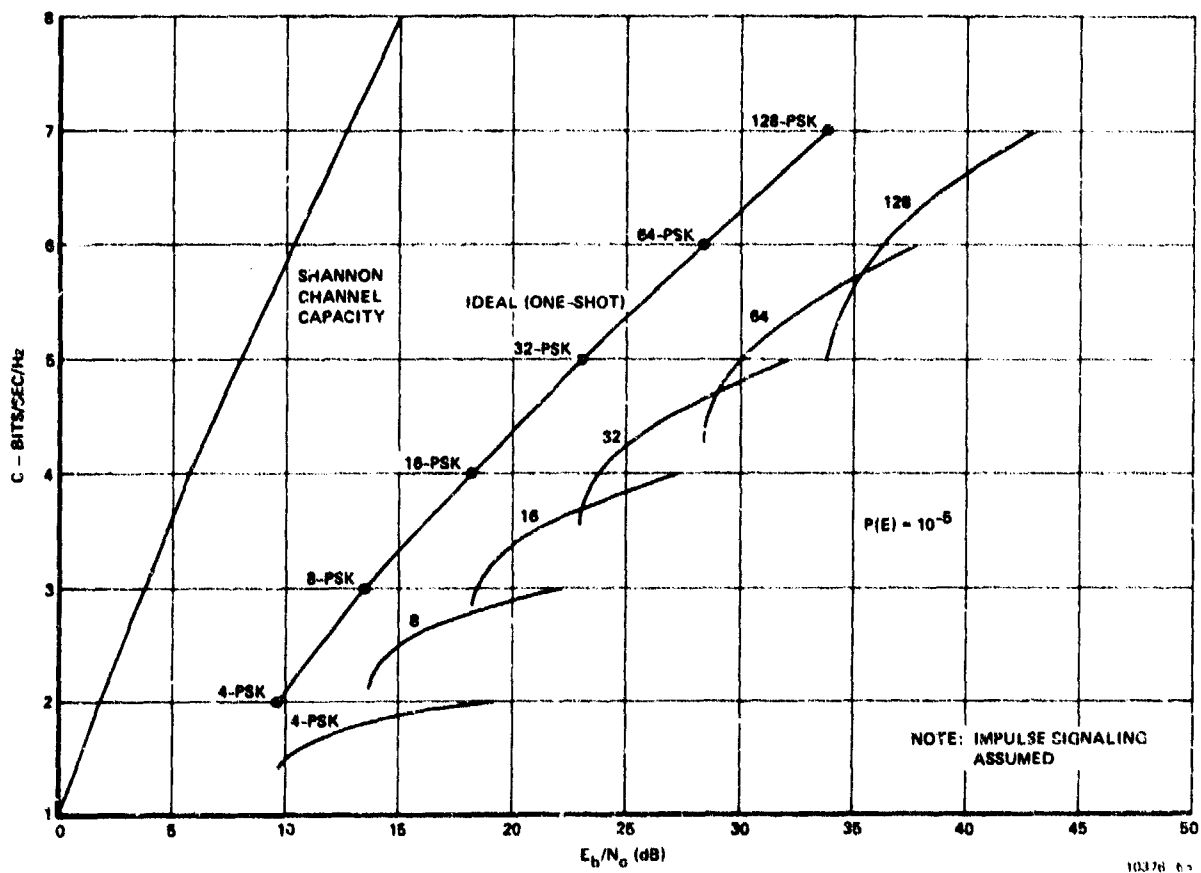


Figure 6.5.2.2-2. Capacity Versus Performance of Nyquist Equalized Eight-Pole Butterworth Filters for M-PSK Signaling $P(E) = 10^{-5}$

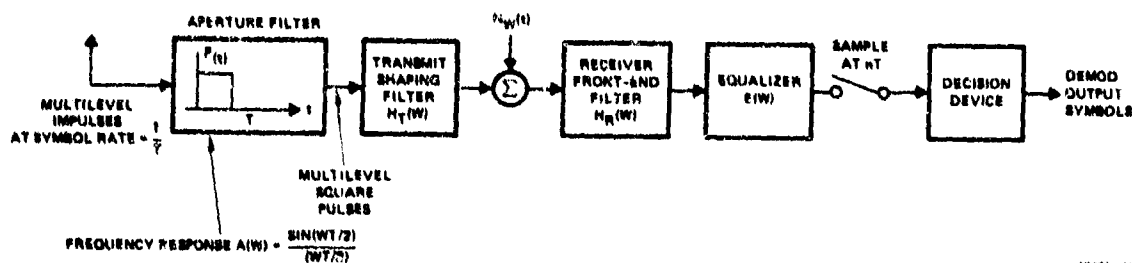


Figure 6.5.3. Digital Transmission With Square Pulse Signalling Shaping Filter and Equalized Receiver

$$A(\omega) = [\sin(\omega T/2)] / (\omega T/2) \quad (6.5.3-1)$$

and $A(\omega)$ can be included in $H_T(\omega)$ and the problem is identical to the system shown in Figure 6.5.1 previously.

In this section we present the performance of systems of the type shown in Figure 6.5.3 for $H_T(\omega) = H_R(\omega) =$ five-pole Butterworth response and where the equalizer, $E(\omega)$ is chosen such that the overall filtering effect, $H(\omega)$, given by

$$H(\omega) = A(\omega)H_T(\omega)H_R(\omega)E(\omega) \quad (6.5.3-2)$$

is such that either Nyquist or duobinary response results.

6.5.3.1 Spectrum Results

The transmitted signal spectrum, $S(\omega)$, for the system shown in Figure 6.5.3 is obviously

$$S(\omega) = |A(\omega)H_T(\omega)|^2 \quad (6.5.3.1-1)$$

the spectra for various values of β where

$$\beta = f_0 T$$

f_0 = Low pass 3 dB filter bandwidth (6.5.3.1-2)

T = Symbol time

are shown in Figures 6.5.3.1-1 through 6.5.3.1-5. Also shown on each of these figures is the most restrictive FCC 19311 spectral mask within which each of the spectra will fit. Also noted is the required RF authorized bandwidth as a multiple of symbol rate in each case, i.e.,

$$B_a = \alpha (1/T) \quad (6.5.3.1-3)$$

where

B_a = Required FCC 19311 authorized bandwidth

From Equation (6.5.3.1-3), one sees that the symbols/s/Hz supported by the filtered square pulse scheme of Figure 6.5.3 is given by

$$S = \frac{1/T}{B_a} = 1/\alpha \quad (6.5.3.1-4)$$

= Symbols/s/Hz under FCC 19311.

From Equation (6.5.3.1-4) and the values of α given in Figures 6.5.3.1-1 through 6.5.3.1-5, one obtains the plot of S versus low pass filter bandwidth given in Figure 6.5.3.1-6. Just as in the previous section, the number of bits/s/Hz capacity, C , for a particular modulation is given by

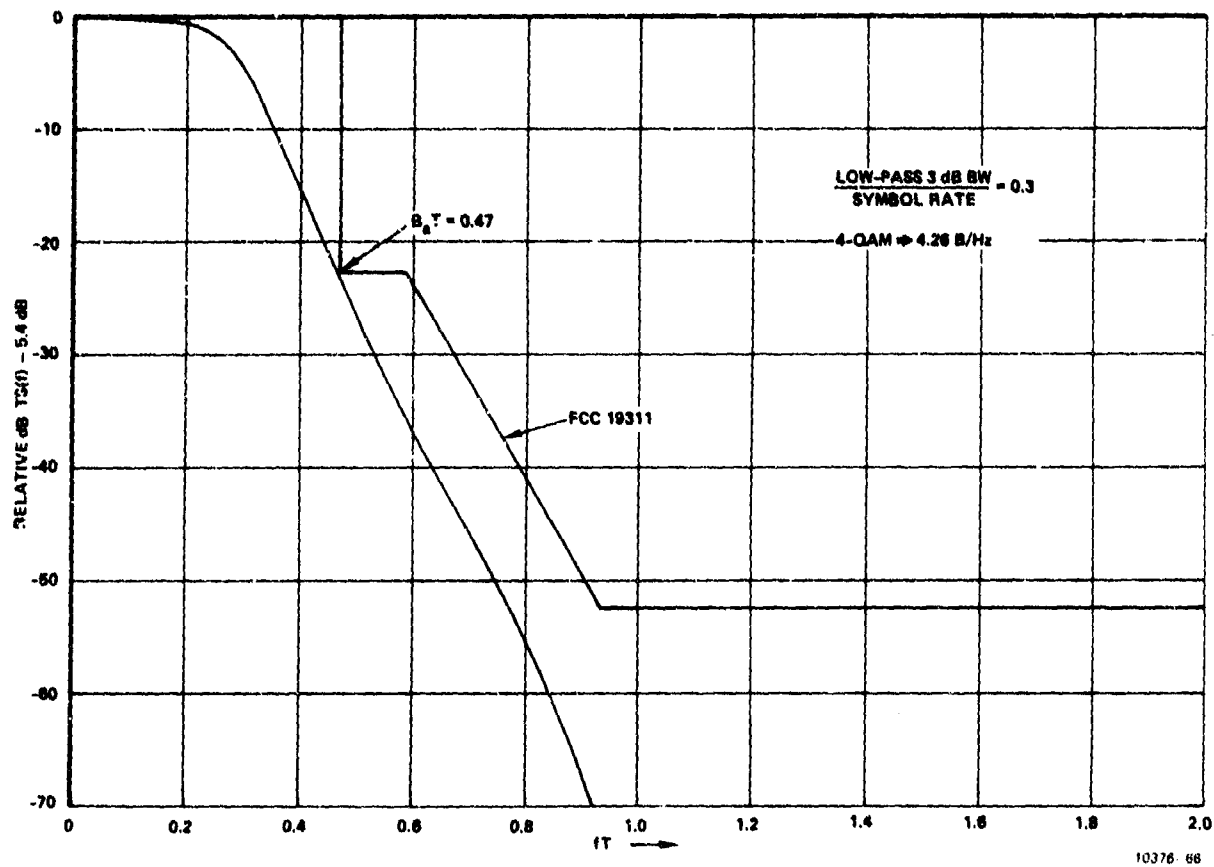


Figure 6.5.3.1-1. $\beta = 0.3$ Five-Pole Butterworth Filter on PAM

$$\frac{\text{Low-pass 3 dB BW}}{\text{Symbol Rate}} = 0.3$$

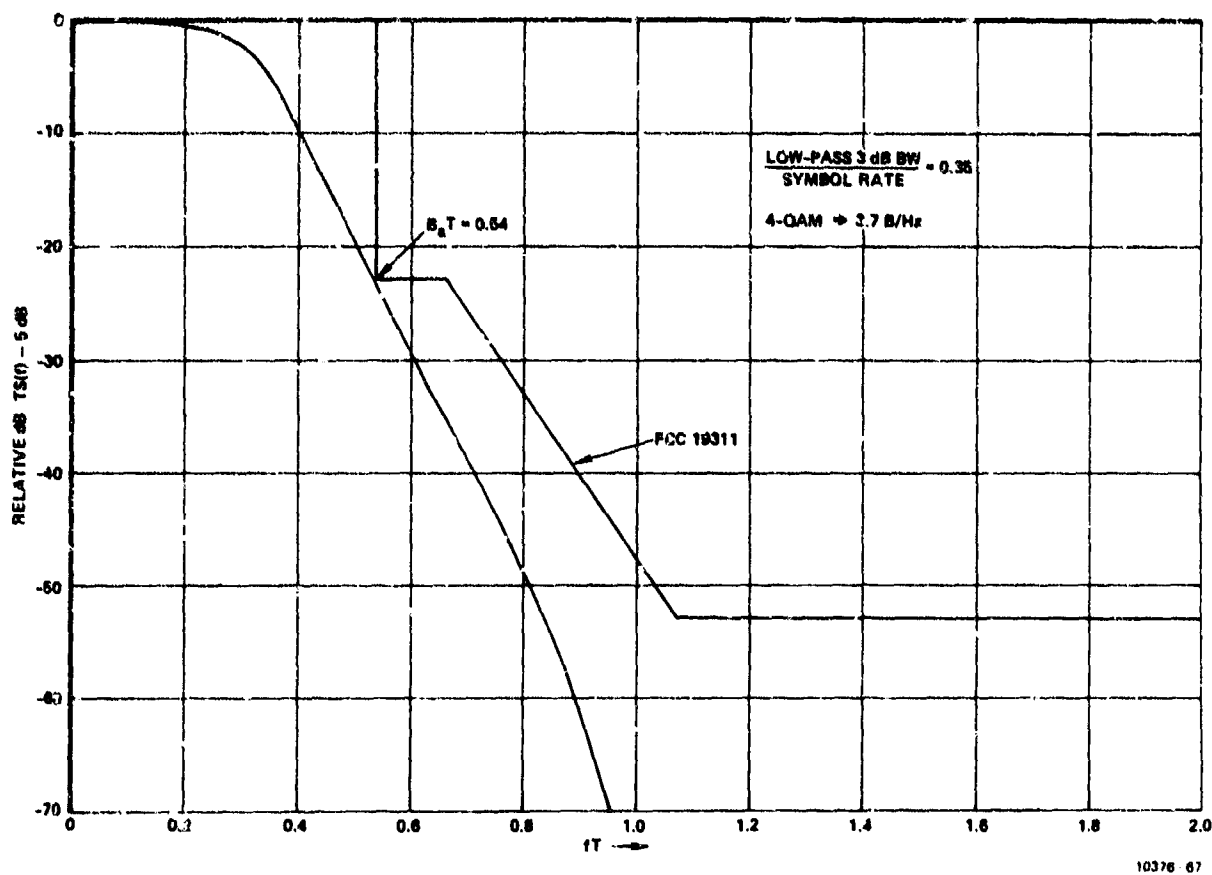


Figure 6.5.3.1-2. $\beta = 0.35$ Five-Pole Butterworth Filter on PAM

$$\frac{\text{Low-Pass 3 dB BW}}{\text{Symbol Rate}} = 0.35$$

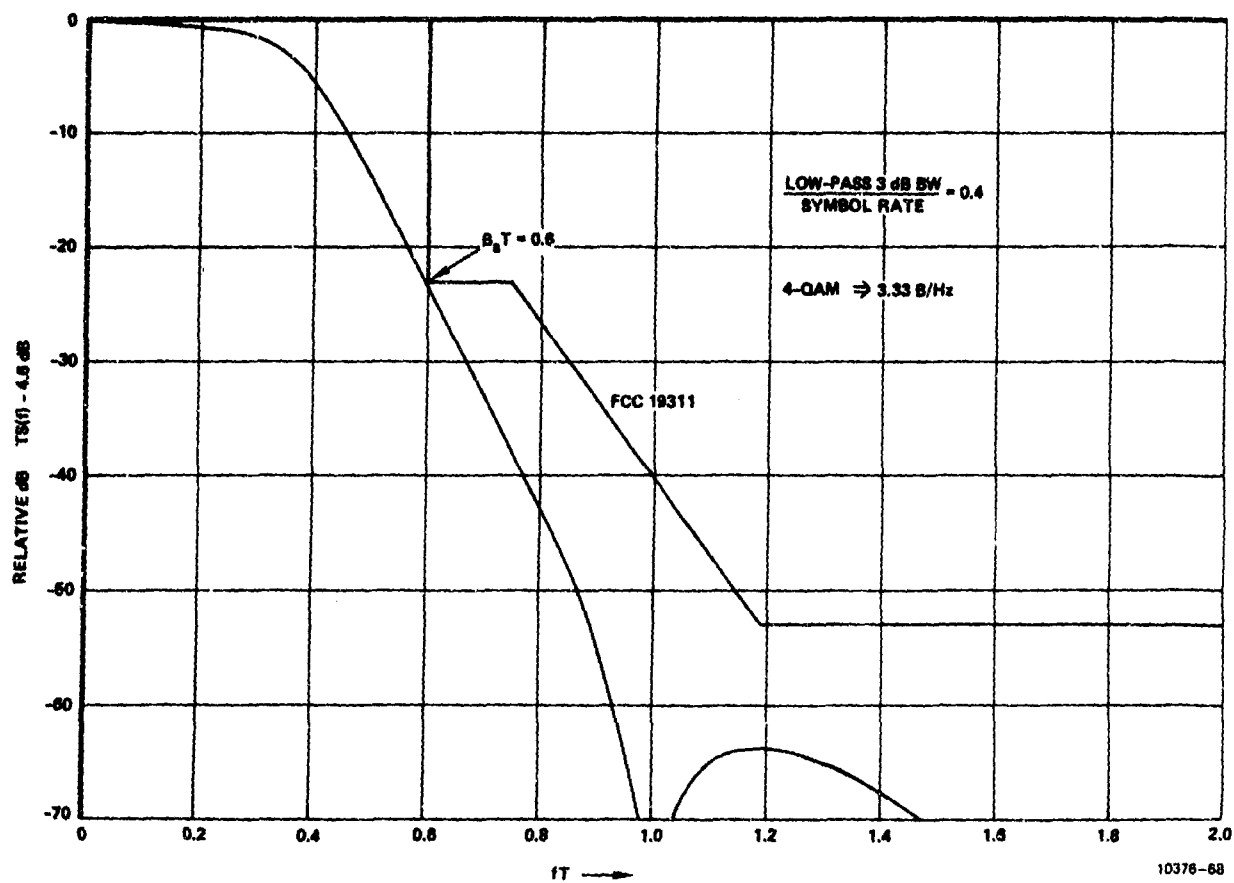


Figure 6.5.3.1-3. $\beta = 0.14$ Five-Pole Butterworth Filter on PAM

$$\frac{\text{Low-pass 3 dB BW}}{\text{Symbol Rate}} = 0.4$$

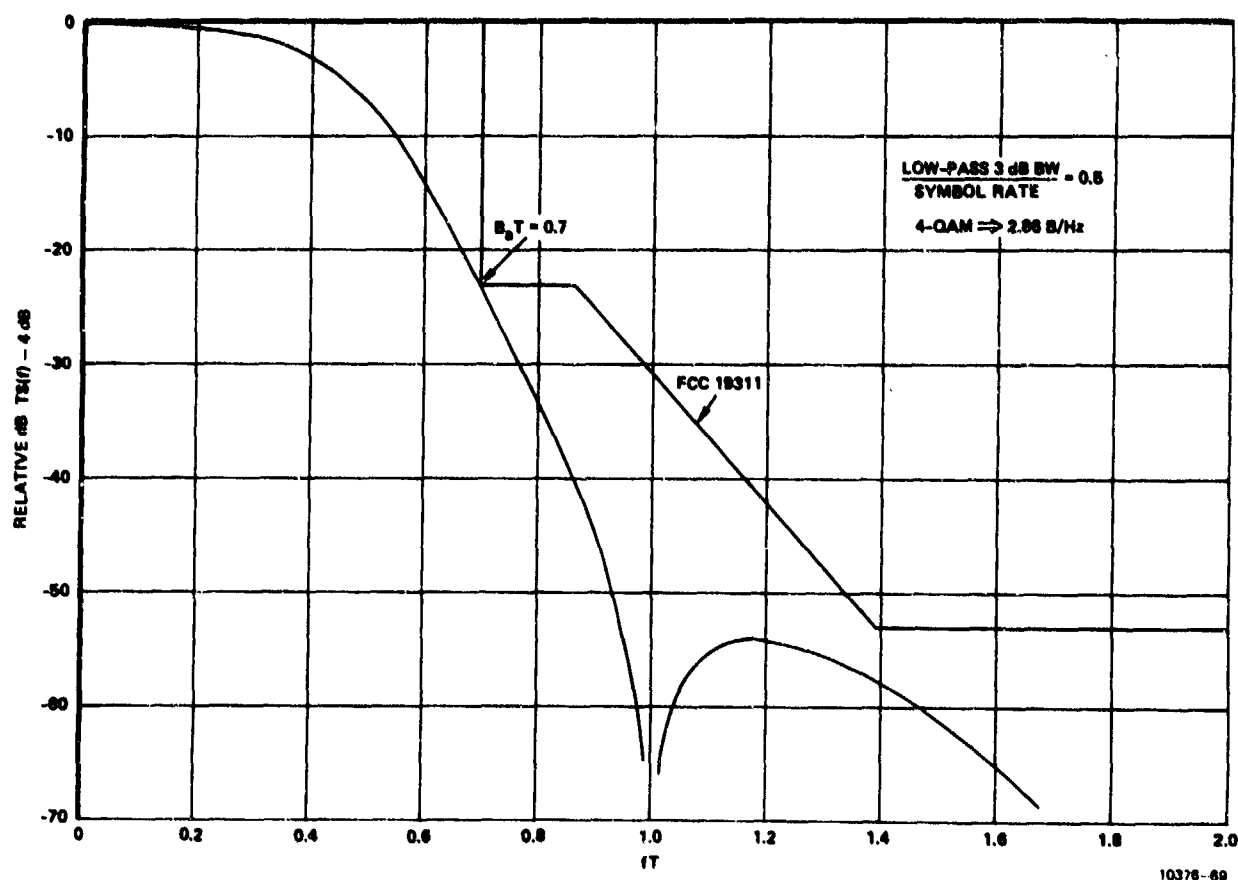


Figure 6.5.3.1-4. $\beta = 0.5$ Five-Pole Butterworth Filter on PAM

$$\frac{\text{Low-Pass 3 dB BW}}{\text{Symbol Rate}} = 0.5$$

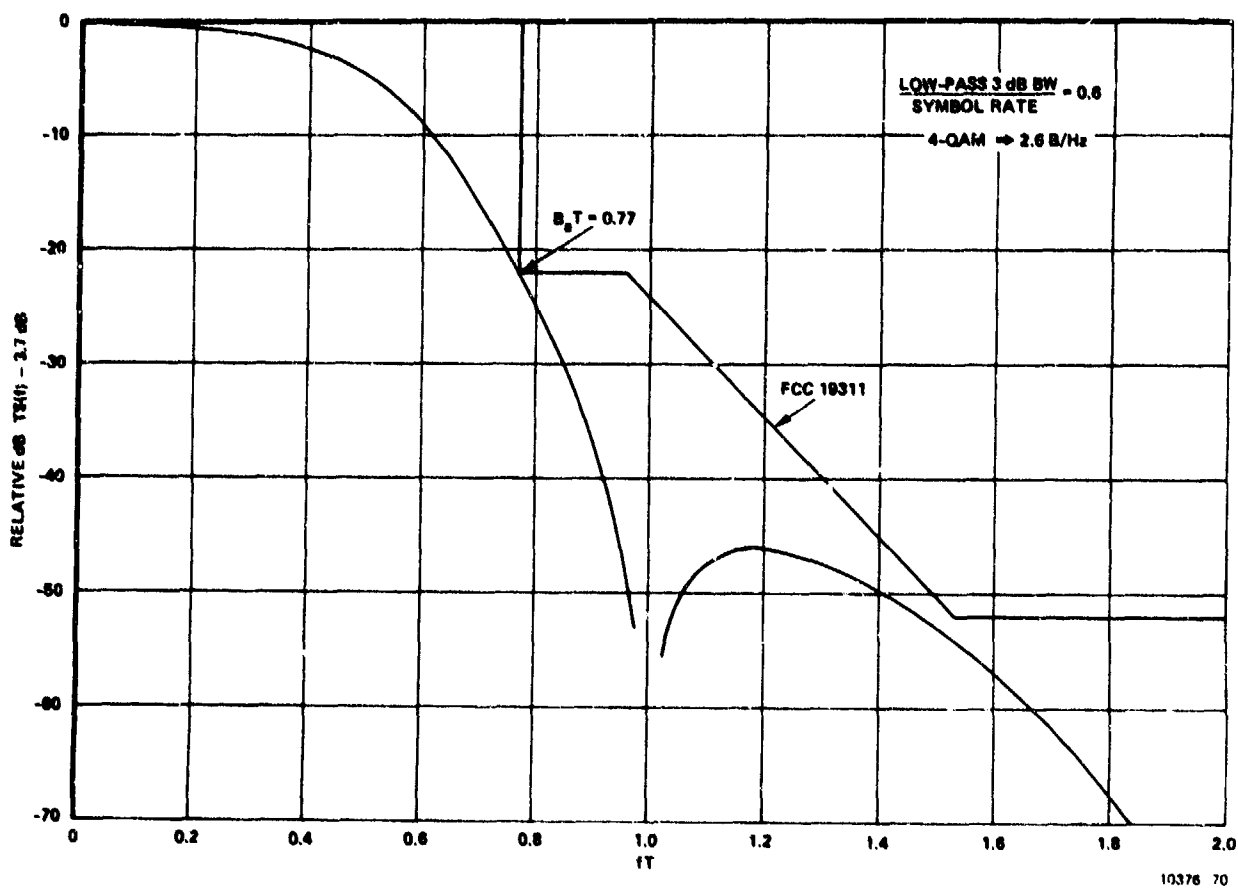
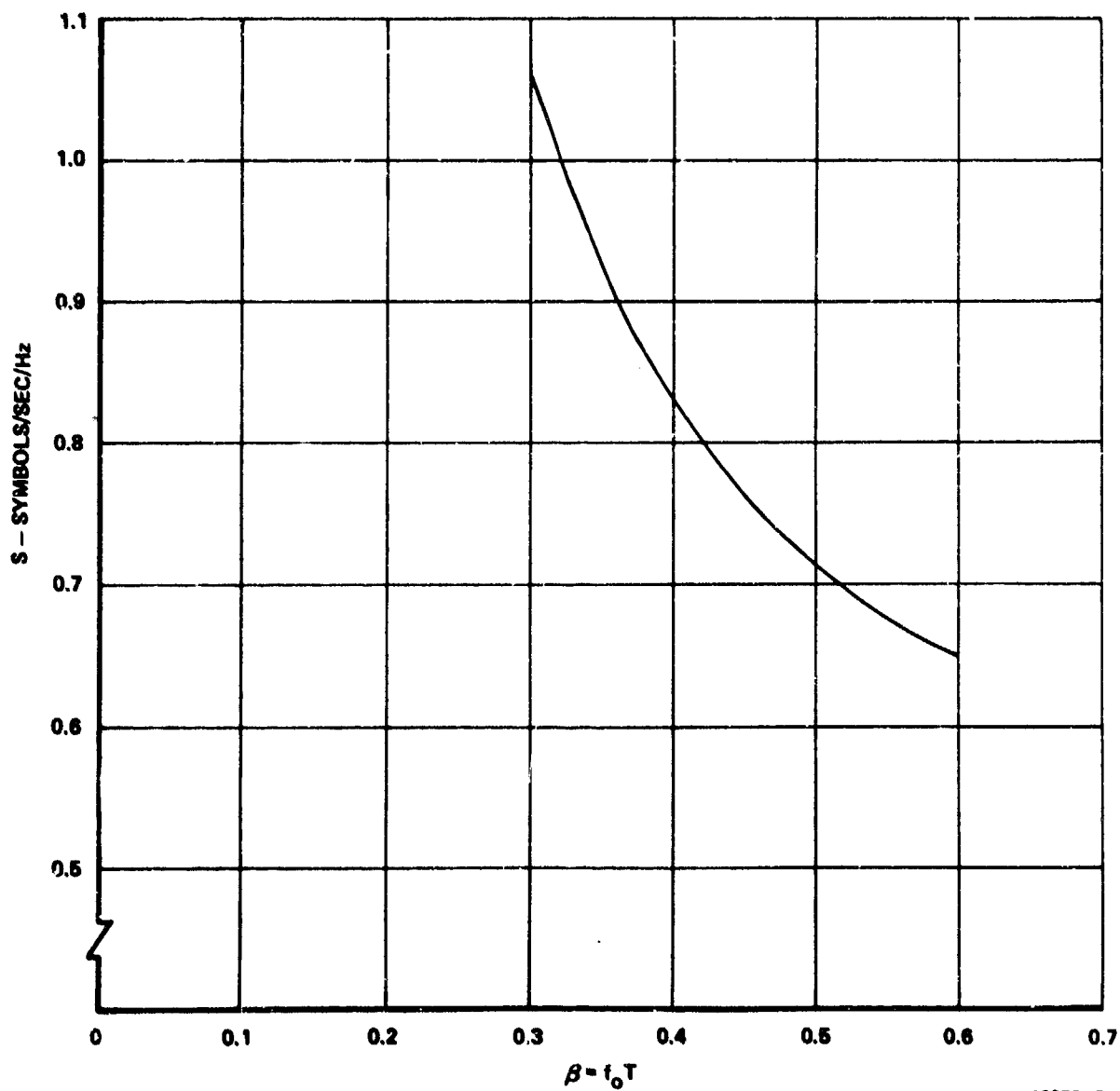


Figure 6.5.3.1-5. $\beta = 0.6$ Five-Pole Butterworth Filter on PAM

$$\frac{\text{Low-pass 3 dB BW}}{\text{Symbol Rate}} = 0.6$$



10376--71

Figure 6.5.3.1-6. Symbols/s/Hz Possible Under FCC 19311
for Square Pulse Signalling Through Five-Pole Butterworth Filter

$$C = BS$$

(6.5.3.1-5)

where

C = Capacity in bits/s/Hz under FCC 19311

B = Number of bits carried per RF symbol

S = Symbols/s/Hz under FCC 19311

The data of Figure 6.5.3.1-6 is used later along with performance loss associated with the equalizer scheme of Figure 6.5.3 to generate capacity versus E_b/N_0 curves.

6.5.3.2 Performance Results

In this section, the performance loss (relative to one-shot receiver performance) of the equalized system of Figure 6.5.3 is present. This data was generated by a computer program.

The results obtained with the computer program are displayed in Figure 6.5.3.2 where the dB of performance loss relative to one-shot receiver performance is plotted versus the five-pole Butterworth transmit and receive (identical) filters' low-pass 3 dB bandwidth. The performance loss is plotted for both Nyquist and duobinary-type partial response equalization. This plot shows that it is advantageous to Nyquist equalize for filter bandwidths above 0.41 times symbol rate and duobinary equalize for filter bandwidths below 0.41 symbol rate.

6.5.3.3 General Capacity Curve

Just as in the previous work for impulse signalling, the parameter β is eliminated between Figures 6.5.3.1-6 and 6.5.3.2 to produce the plot of symbols/s/Hz capacity versus dB performance loss shown in Figure 6.5.3.3-1. Here again, the parameter β (ratio of

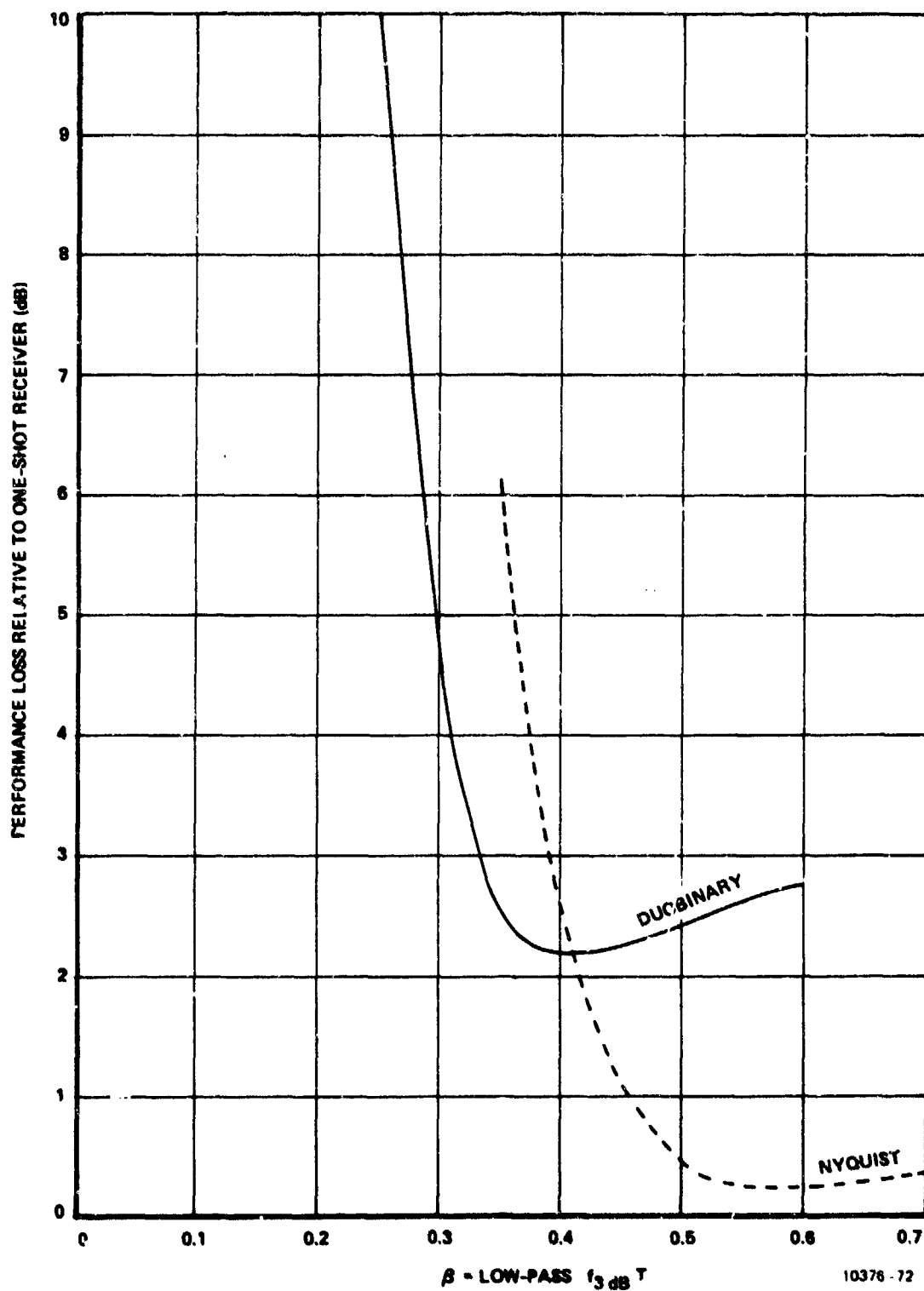
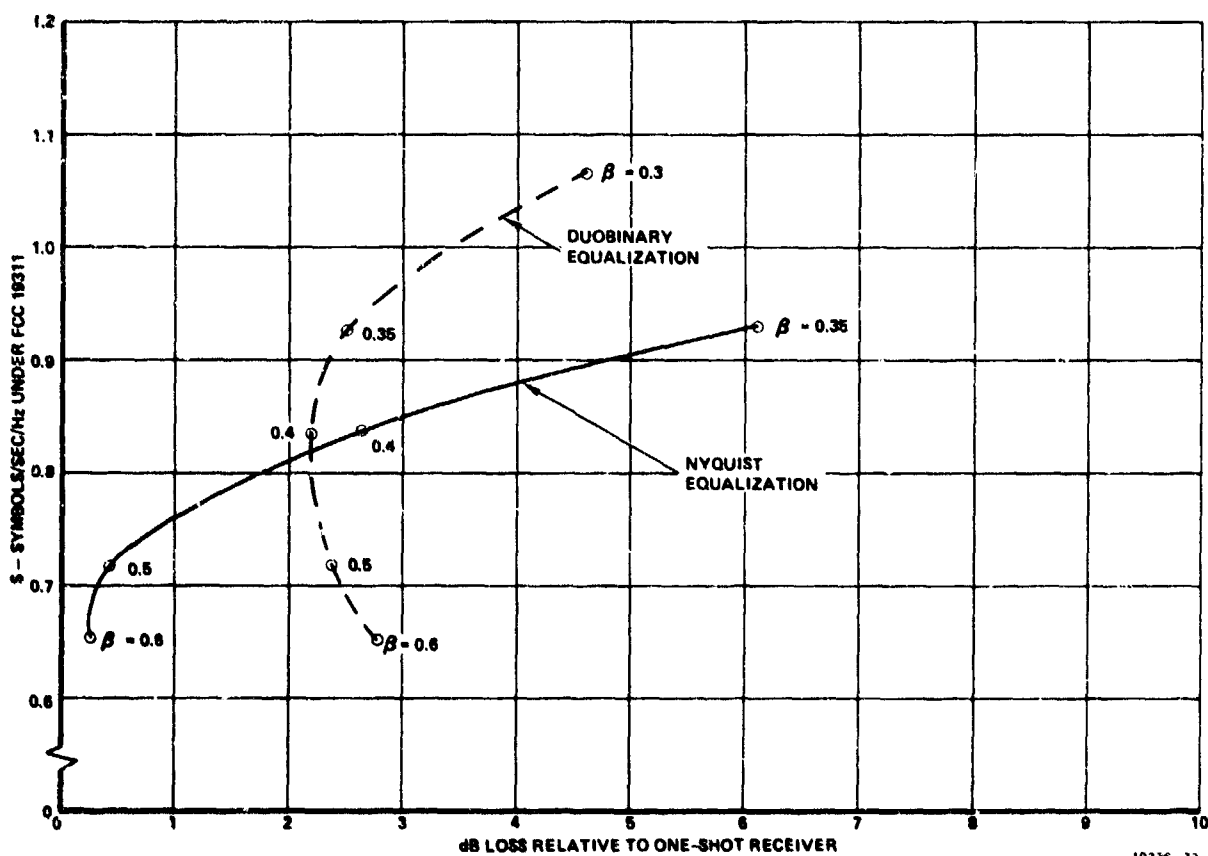


Figure 6.5.3.2. Five-Pole Butterworth Filters
on PAM With Receiver Equalization



10376 73

Figure 6.5.3.3-1. Combinations of Symbols/s/Hz and Performance for Square Pulse Signalling Through Five-Pole Butterworth Filters With Receive Equalization

low-pass filter 3 dB bandwidth to symbol rate) is an implicit parameter on the curves and several values of β are noted in Figure 6.5.3.3-1.

The data of Figure 6.5.3.3-1 has been used along with the ideal performance of M-QAM from Section 4 to produce the capacity versus E_b/N_0 for various five-pole Butterworth filtered square pulse M-QAM signalling/receiver equalized systems shown in Figure 6.5.3.3-2.

The same type of capacity versus E_b/N_0 curves have been produced for square pulse M-PSK modulation schemes from the data of Figure 6.5.3.3-1 and ideal performance from Section 4. These M-PSK curves are shown in Figure 6.5.3.3-3.

The capacity curves are used later in trade-offs among the candidate schemes.

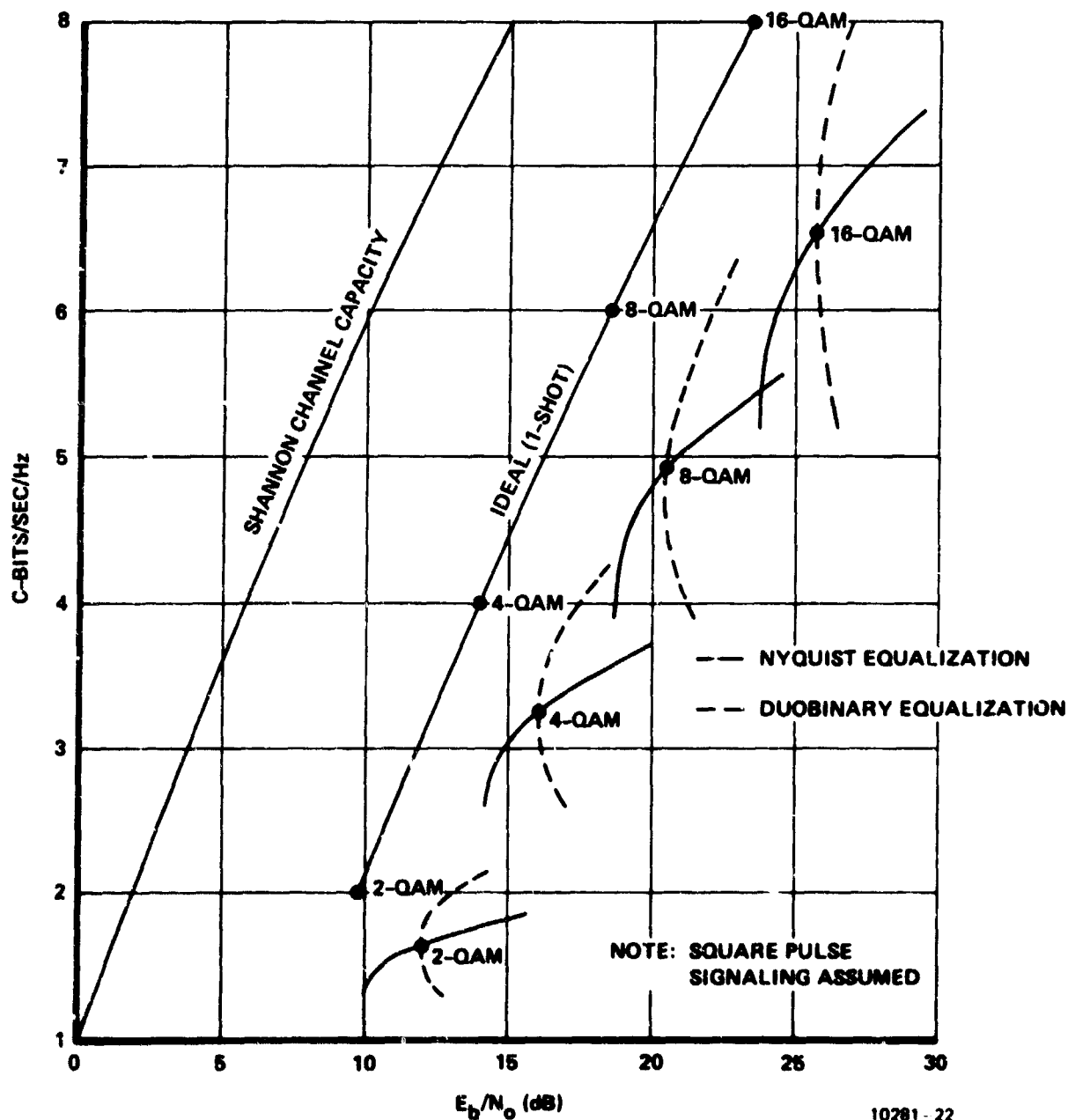


Figure 6.5.3.3-2. Capacity Versus Performance of Equalized Five-Pole Butterworth Filters for M-QAM Signalling $P(E) = 10^{-5}$

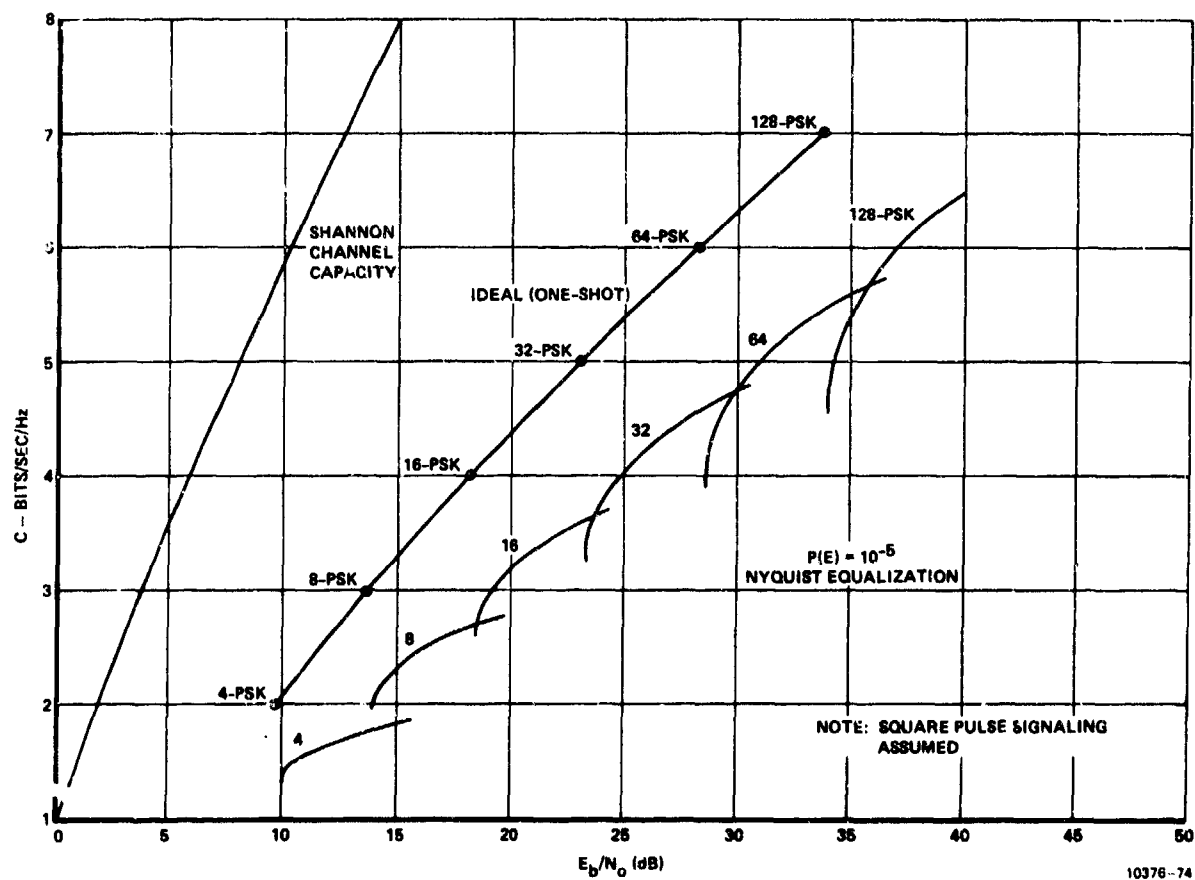


Figure 6.5.3.3-3. Capacity Versus Performance of Equalized Five-Pole Butterworth Filters for M-PSK Signalling $P(E) = 10^{-5}$

6.6

Comparing Digital Transmission Schemes When the Power Amplifier Is Peak Power Limited

Figure 6.6 shows a general digital transmission scheme of the type commonly used for the line-of-sight microwave channel. We leave out

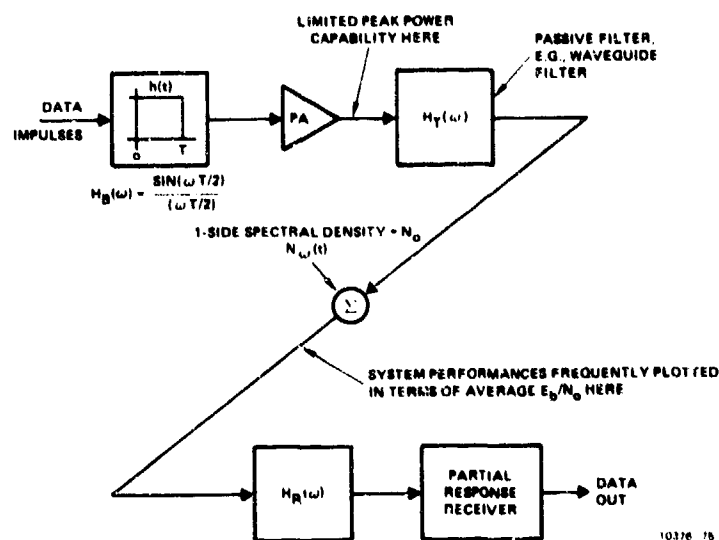


Figure 6.6. General Digital Transmission Scheme

the analytically nonessential upconversion and downconversion components necessary in the actual RF system. Also, we consider that the data impulses applied to the pulse-stretching (aperture) filter are complex quantities to handle the quadrature modulations usually employed (e.g., M-PSK, M-QAM or QASK signal formats). The power amplifier is usually a microwave amplifier such as a TWT with limited peak power capability. We shall in fact be concerned here with the comparison of various modulation schemes under a peak energy constraint at the output of the power amplifier. It is felt that this should be the basis upon which modulation schemes are chosen for the LOS microwave channel, and not in terms of the frequently used average E_b/N_0 at the receive filter input. When the peak amplifier power requirement is minimized over the set of modulation schemes under consideration, one guarantees he has

chosen the scheme which makes best use of a given peak power capability in the microwave amplifier. Generally, no particular advantage should be attributed to a modulation scheme in the LOS situation if it requires smaller average radiated power but the same peak power as some other scheme under consideration. In prime supply power limited situations such as occurs with satellites, this is not the case, and there is merit in average power comparisons. Generally though, the LOS situation is not prime power limited.

As shown in Figure 6.6 the power amplified signal is filtered by a transmit filter, $H_T(\omega)$, which, for the purposes of meeting FCC Docket 15311 requirements, is usually a passive waveguide filter. A consequence of this filter being restricted to a passive filter is that the maximum gain at any frequency must be less than unity, i.e., the filter cannot amplify at any frequency in its passband.

The signal from the transmit filter is transmitted over the channel, where it is perturbed by additive white Gaussian noise of one-sided spectral density, N_0 . At the receiver, the signal is filtered by receiver filter, $H_R(\omega)$, and passed to a (generally) partial response receiver where the data impulses are demodulated by one of many techniques.

The pulse stretching (aperture) filter at the transmitter is included in Figure 6.6 since square pulse signaling is usually employed in most of the modulation schemes. The frequency response of this filter is given by

$$H_B(\omega) = \frac{\sin(\omega T/2)}{(\omega T/2)} \quad (6.6-1)$$

Where T = Symbol Time

The overall filtering action occurring in the system of Figure 6.6 is given by

$$H_O(\omega) = \frac{H_T(\omega) H_R(\omega) \sin(\omega T/2)}{(\omega T/2)} \quad (6.6-2)$$

$H_0(\omega)$ is usually chosen to correspond to some form of Nyquist or partial resonce signalling, i.e.,

$$\sum_{k=-\infty}^{+\infty} H_0\left(\omega + \frac{k2\pi}{T}\right) = X(\omega), \quad |\omega| < \pi/T \quad (6.6-3)$$

For example, in duobinary

$$\text{Duobinary: } X(\omega) = \cos(\omega T/2), \quad |\omega| < \pi/T$$

and for Nyquist signaling

$$X(\omega) = 1, \quad |\omega| < \pi/T$$

This overall shaping is obtained in many different ways of splitting the overall filter between the transmitter and receiver. We shall later consider some specific cases.

In what follows we assume that the transmitter filter $H_T(\omega)$ is of the following form

$$H_T(\omega) = \frac{H'_T(\omega) (\omega T/2)}{\sin(\omega T/2)} \quad (6.6-4)$$

i.e., $H_T(\omega)$ includes compensation for $H_B(\omega)$, the $\sin X/X$ rolloff implied by square pulse signaling.

The spectrum out of the power amplifier is given by

$$S_A(f) = \sigma_d^2 T \frac{\sin^2(\omega T/2)}{(\omega T/2)^2} \quad (6.6-5)$$

Where $S_A(f)$ = Power Amplifier Output Spectrum

σ_d^2 = Mean Square Data Impulse

The average power output from the power amplifier is given by

$$\begin{aligned}
 P_A &= \int_{-\infty}^{+\infty} S_A(f) df = \frac{1}{2\pi} \int_{-\infty}^{+\infty} \sigma_d^2 T \frac{\sin^2(\omega T/2)}{(\omega T/2)^2} d\omega \\
 &= \frac{\sigma_d^2}{\pi} \int_{-\infty}^{+\infty} \frac{\sin^2(\theta)}{\theta^2} d\theta \\
 P_A &= \sigma_d^2 \quad (6.6-6)
 \end{aligned}$$

The average power out of the transmit filter is given by P_F where

$$\begin{aligned}
 P_F &= \int_{-\infty}^{+\infty} S_A(f) |H_T(f)|^2 df \\
 P_F &= \sigma_d^2 T \int_{-\infty}^{+\infty} |H_T'(fT)|^2 df \quad (6.6-7)
 \end{aligned}$$

The average power loss in passing through the waveguide filter $H_T(\omega)$ is thus given by

$$\frac{P_F}{P_A} = \int_{-\infty}^{+\infty} |H_T'(fT)|^2 d(fT) \quad (6.6-8)$$

If we label the peak power out of the amplifier as P_p then the ratio of average filter output power to peak amplifier output is given by the ratio P_F/P_p which is:

$$\frac{P_F}{P_p} = \frac{P_F}{P_A} \cdot \frac{P_A}{P_p} \quad (6.6-9)$$

From (6.6-8) and (6.6-9) we have

$$\frac{P_F}{P_p} = \frac{P_A}{P_p} \int_{-\infty}^{+\infty} |H_T'(fT)|^2 d(fT) \quad (6.6-10)$$

The ratio P_A/P_P in Equation (6.6-10) is the ratio of average-to-peak energy in the data impulses. Equation (6.6-10) gives the amount of dB degradation to apply to a curve of performance in terms of average signal-to-noise ratio at the receiver filter input (or E_b/N_0 at the receiver) in order to obtain a curve of performance in a peak power amplifier limited situation such as the LOS link.

The term in Equation (6.6-10) given by P_A/P_P is average-to-peak power loss inherent in the particular choice of data impulses. The loss given by the integral in (6.6-10) will be called the spectral truncation loss, S_T , since it is the loss in average power incurred in passing the sinc^2 spectrum through the transmit filter, $H_T(\omega)$. S_T is given by

$$S_T = \frac{\int_{-\infty}^{+\infty} S_A(f) |H_T(f)|^2 df}{\int_{-\infty}^{+\infty} S_A(f) df} \quad (6.6-11)$$

$$S_T = \int_{-\infty}^{+\infty} \frac{\sin^2(\pi fT)}{(\pi fT)^2} |H_T(fT)|^2 d(fT) \quad (6.6-12)$$

or

$$S_T = \int_{-\infty}^{+\infty} |H_T'(fT)|^2 d(fT) \quad (6.6-13)$$

which is the integral in Equation (6.6-10).
where $S_T \triangleq$ Spectral Truncation power loss.

There is an additional power loss that technically should be included in trade-offs amongst various modulation schemes requiring different $H_T(\omega)$. That is the minimum passband insertion loss of the waveguide filter, A_m . Thus the overall correction to an average received signal-to-noise ratio performance curve is

$$\frac{P_F}{P_P} = A_m \left(\frac{P_A}{P_P} \right) (S_T) \quad (6.6-14)$$

where

$$\begin{aligned} \frac{P_F}{P_P} &= \text{Average received S/N/Peak Amplifier Output S/N,} \\ A_m &= \text{Minimum waveguide filter passband insertion loss.} \\ \frac{P_A}{P_P} &= \text{Average-to-Peak power ratio for signal before transmit} \end{aligned}$$

filter, and S_T = Spectral Truncation power loss.

6.6.1. Specific Cases - Power Amplifier Peak-Limited Performance

With the results of the previous section we now make performance comparisons amongst primary candidate modulation schemes for a peak power limited amplifier case such as the LOS microwave link.

6.6.1.1 Nyquist Signaling

With Nyquist signaling, the transmit filter, $H_T(\omega)$, and receiver filter, $H_R(\omega)$, are frequently chosen to yield overall raised-cosine filtering, i.e., in the system of Figure 6.6,

$$H_T(\omega)H_R(\omega) \frac{\sin(\omega T/2)}{(\omega T/2)} = H_0(\omega) \quad (6.6.1.1-1a)$$

$$\text{where } H_0(\omega) = 1, \quad 0 < |f| < \frac{1}{2T} (1 - a) \quad (6.6.1.1-1b)$$

$$= \frac{1}{2} - \frac{1}{2} \sin \left| \frac{\pi}{a} (fT - .5) \right|, \quad \frac{1}{2T} (1 - a) < |f| < \frac{1}{2T} (1 + a)$$

= Raised Cosine Shaping (Nyquist Channel)

If the optimal split of the overall filter given in Equation (6.6.1.1-1), equally between transmitter and receiver is made, we see that

$$H_T(\omega) = \frac{\sqrt{H_0(\omega)} \omega T/2}{\sin(\omega T/2)} \quad (6.6.1.1-2)$$

and

$$H_R(\omega) = \sqrt{H_0(\omega)} \quad (6.6.1.1-3)$$

in Figure 6.6. This makes the total transmit filtering, including the pulse stretching filter, $H_B(\omega)$ in Figure 6.6, be

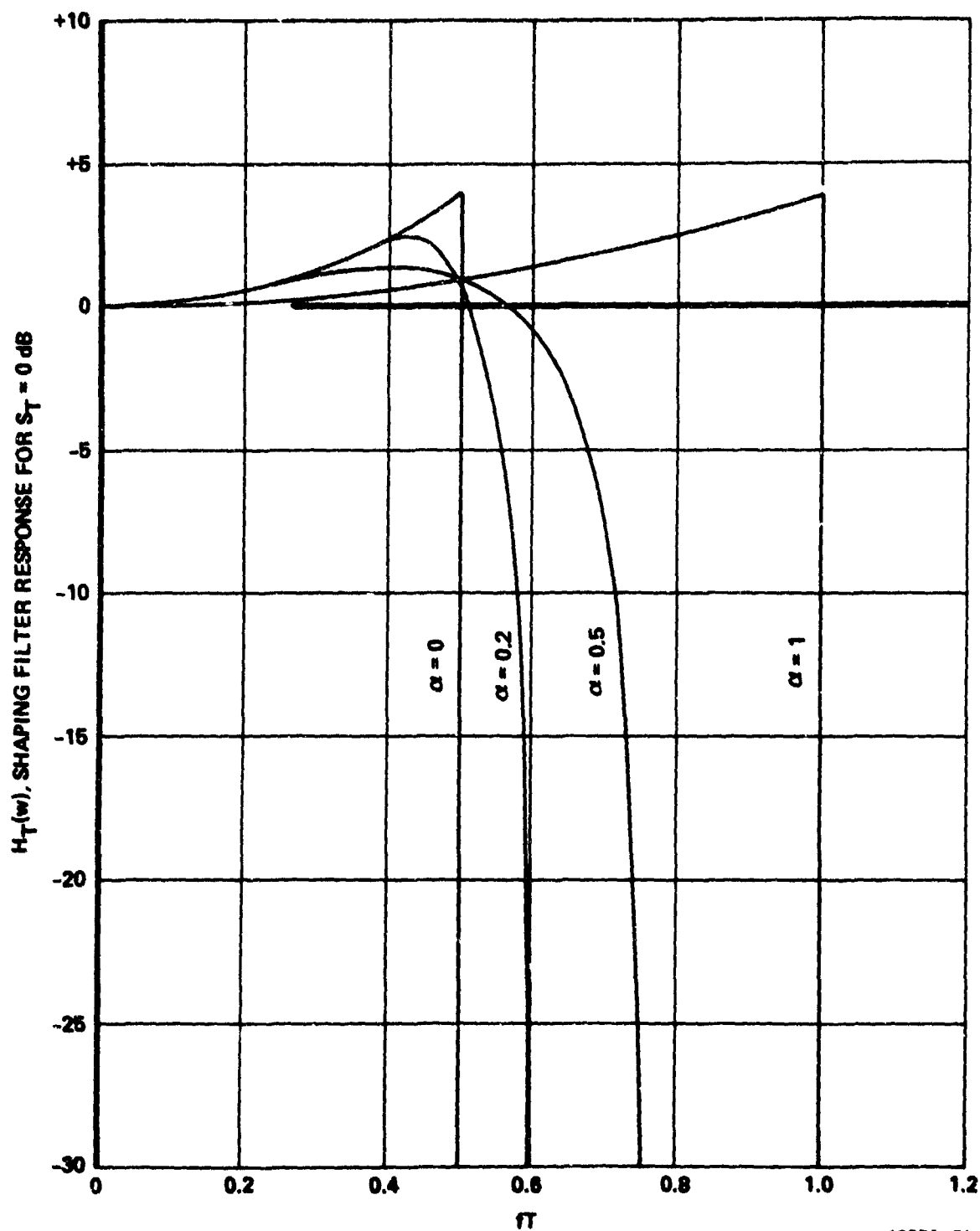
$$H_T(\omega)H_B(\omega) = \sqrt{H_0(\omega)} \quad (6.6.1.1-4)$$

Figure 6.6.1.1 shows the transmit filtering function given by Equation (6.6.1.1-2) for $H_0(\omega)$ corresponding to various rolloff factors, α . One can verify that the use of the filters shown in Table 6.6.1.1 would result in no spectral truncation loss by substituting $H_T(\omega)$ given by (6.6.1.1-2) and (6.6.1.1-1) into Equation (6.6-12) for the truncation loss, S_T . The problem with the use of the filters given in Equation (6.6.1.1-2) and shown in Figure 6.6.1.1 is that they are not passive filters - as the waveguide filter $H_T(\omega)$ must be - since they have gain at frequencies in their passbands. In the real system, then, we can obtain at least an approximation to the filters shown in Figure 6.6.1.1, but the peak gain over the passband must be less than 0 dB. Thus, the spectral truncation loss with passive waveguide filtering is given by the peak gain in the passband shown in Figure 6.6.1.1. Thus, Table 6.6.1.1 shows the spectral truncation loss associated with using passive transmit filtering for various α .

Table 6.6.1.1 thus gives the loss in average power output relative to average filter input for the system in Figure 6.6 for this case of equal filter division Nyquist signaling. This table does not include dB of insertion loss of the actual waveguide filter at peak of the passband response, i.e., we have assumed 0 dB insertion loss at the peak.

We have already plotted the performance/capacity for systems using this shaping filter response for equal transmit-receiver filtering in Paragraph 6.2. The plots of capacity under FCC 19311 were made versus average received E_b/N_0 . We now make the same plots here in terms of peak amplifier output E_b/N_0 .

To do so we simply add the dB degradation given by Equation (6.6-14) for these schemes. We assume that the passband insertion loss A_m of the waveguide filter is 0 dB in these plots.



10376-76

Figure 6.6.1.1. Transfer Functions for Square Root Raised Cosine Filters Compensated for $\text{SIN}(\pi fT)/\pi fT$ Roll-off

Table 6.6.1.1. Spectral Truncation Power Loss when Equal Transmit Receive Raised-Cosine Nyquist Signaling is used.

	α			
	0	.2	.5	1.0
S_T , dB	4.0	2.5	1.5	4.0

$H_T(\omega)$, Passive Filter

6.6.1.1.1 M-QAM, Nyquist Shaping

For M-QAM the ratio of peak-to-average energy is given by

$$\frac{P_P}{P_A} = \frac{3(M-1)}{M+1} \quad (6.6.1.1.1-1)$$

Using Equation (6.6.1.1.1-1) and the S_T given in Table 6.6.1.1 along with the curves given in Figure 6.2.7 of Paragraph 6.2, we obtain the capacity versus peak amplifier E_b/N_0 plot shown in Figure

6.6.1.1.1-1. We note that from the loci of constant M shown by the dotted lines in Figure 6.6.1.1.1-1 that minimum peak E_b/N_0 is required for $\alpha \approx 0.5$ for a given M-ary signaling. If peak E_b/N_0 required is to be minimized independent of capacity, then $\alpha = .5$ represents a near-optimum solution.

We point out that all the performances shown in Figure 6.6.1.1.1-1 are not necessarily practical since as α decreases the transmit filters become too sharply bandlimited to be realizable in a waveguide design. Reasonable values for α range between 0.2 and 0.5.

The performance of the modified 6-QAM signal design (see Paragraph 4.2.1) is also plotted on Figure 6.6.1.1.1-1. The performance for the modified 6-QAM signal lies about 1 dB inside the lines connecting the performances of standard M-QAM schemes for a given α . The reason for this is the approximate 1 dB lower peak-to-average power ratio for modified 6-QAM than normal 6-QAM. This 1 dB improvement comes from eliminating the 4 peak corner signals in the normal 6-QAM format as explained in Paragraph 4.2.1.

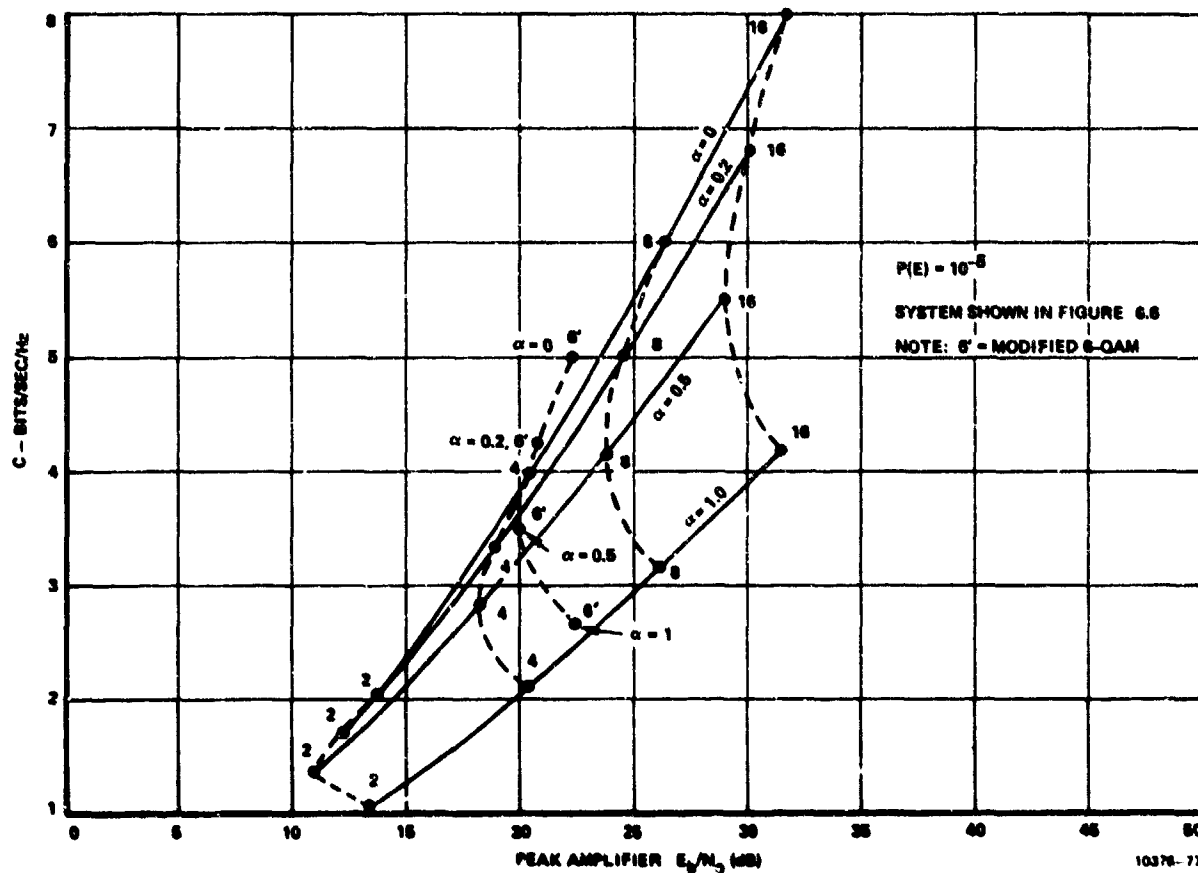


Figure 6.6.1.1.1-1. Amplifier Peak-Limited M-QAM Nyquist Signaling Performance Equal Transmit-Receive Filtering

Figure 6.6.1.1.1-2 shows the performance for $\alpha = 0, 0.2$, and 0.5 raised cosine filters used with M-QAM signaling. For 10^{-5} symbol error rate, modified 6-QAM format requires around 21 dB peak E_b/N_0 and provides 4.25 bits/sec/Hz operation for $\alpha = 0.2$ filters.

6.6.1.2 Duobinary Partial Response Shaping

Here we examine the performance of the system shown in Figure 6.6 when the overall partial response is duobinary, i.e.,

$$H_T(\omega)H_R(\omega) \frac{\omega T/2}{\sin(\omega T/2)} = \cos(\pi f T), |f| < \frac{1}{2T}$$

$$= 0, \text{ otherwise}$$

We will examine two different cases. Case 1 will have the full duobinary shaping at the transmitter, i.e.,

$$\text{Case 1: } H_T(f) = \frac{\cos(\pi f T) \pi f T}{\sin(\pi f T)}, |f| < 1/2T \quad (6.6.1.2-1)$$

$$H_R(f) = 1, |f| < \frac{1}{2T}$$

Case 2 will divide the duobinary shaping equally between transmitter and receiver, i.e.,

$$\text{Case 2: } H_T(f) = \frac{\sqrt{\cos(\pi f T)}}{\sin(\pi f T)} (\pi f T), |f| < 1/2T$$

$$H_R(f) = \sqrt{\cos(\pi f T)}, |f| < 1/2T \quad (6.6.1.2-2)$$

6.6.1.2.1 Case 1: Duobinary-All Partial Response Filter at Transmitter

We now find the spectral truncation loss for the $H_T(f)$ given in Equation (6.6.1.2-1). The transmit filter response is shown in Figure 6.6.1.2.1-1. The filter is passive as required for a waveguide filter. The spectral truncation power loss is given by Equation (6.6-12) as

$$S_T = \int_{-0.5}^{+0.5} \cos^2(\pi f T) d(fT)$$

$$= \frac{1}{\pi} \int_{-\pi/2}^{+\pi/2} \cos^2 \theta d\theta$$

$$S_T = 1/2$$

$$\text{or } S_T, \text{ dB} = -3 \text{ dB}$$

$$(6.6.1.2.1-1)$$

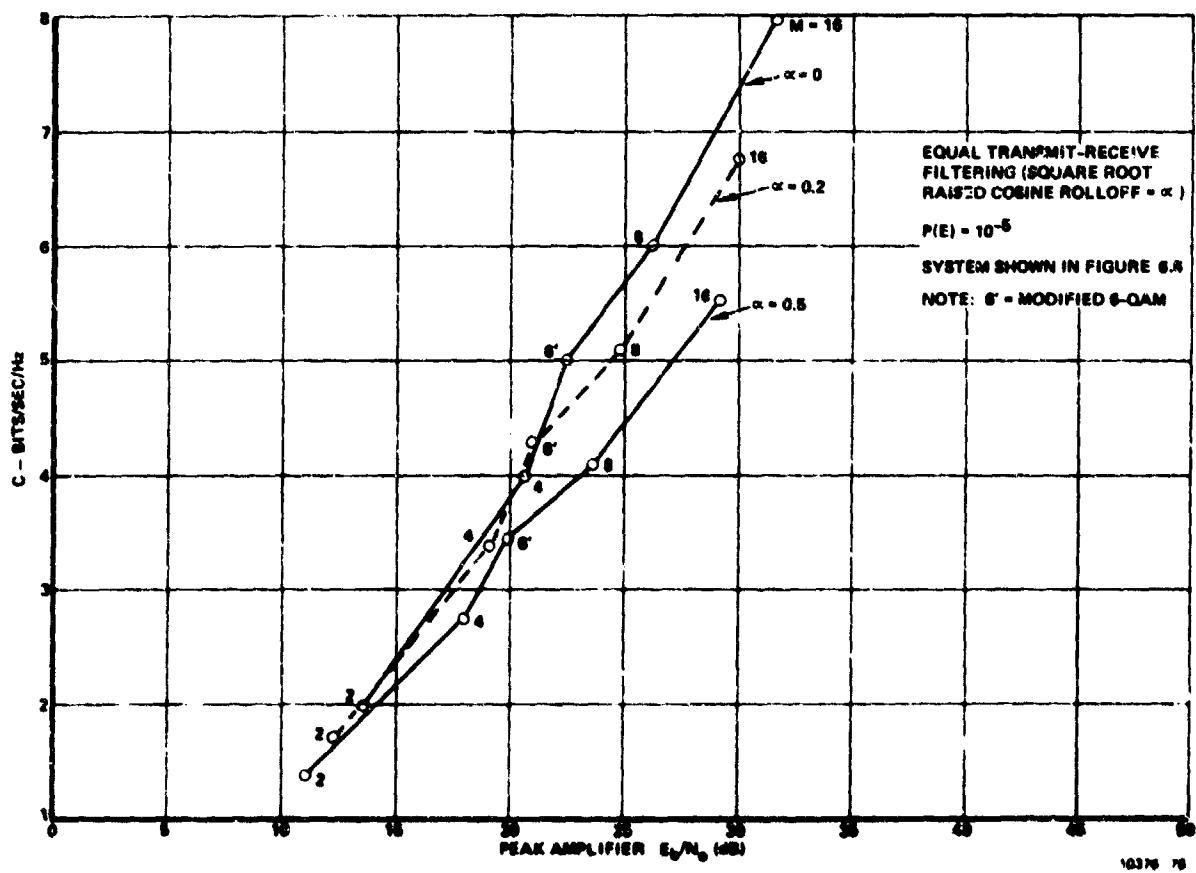
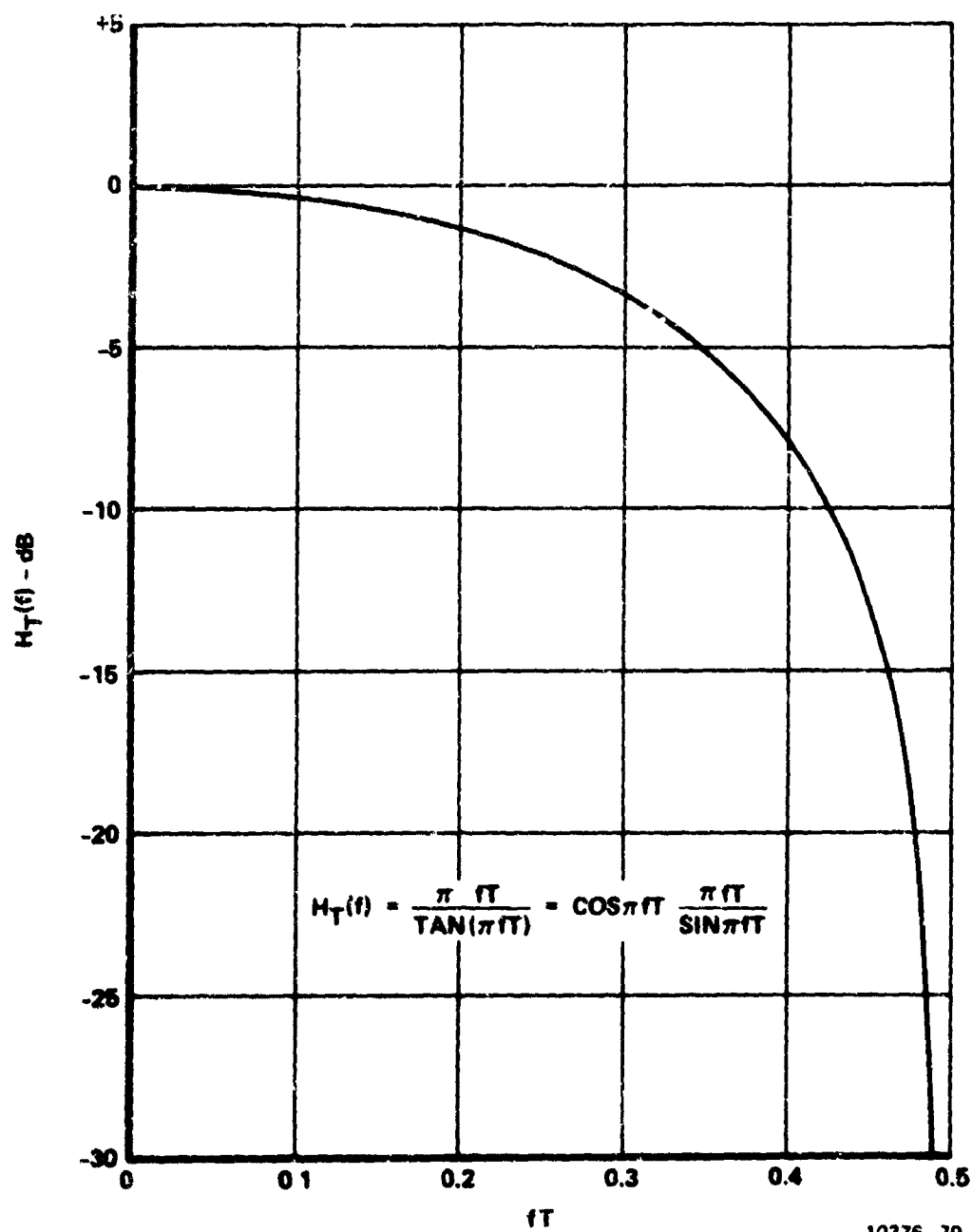


Figure 6.6.1.1.1-2. Amplifier Peak-Limited M-QAM Nyquist Signaling Performance



10376-79

Figure 6.6.1.2.1-1. Full Duobinary Transmit Filter with $\text{Sin}(\pi fT) / \pi fT$ Compensation

After applying the 3 dB spectral truncation loss and the peak-to-average ratio of M-QAM signaling to previously presented curves of Paragraph 6.3 for average signal-to-noise performance, one obtains the curves of Figure 6.6.1.2.1-2 for performance under peak amplifier power limit.

6.6.1.2.2 Case 2: Duobinary Partial Response with Equal Division of Filtering

The transmit filter, $H_T(f)$, from Equation (6.6.1.2-2) in this case is shown in Figure 6.6.1.2.2-1. The filter is again passive (≤ 0 dB response at all frequencies). The spectral truncation power loss from Equation (6.6-12) is given by

$$S_T = \int_{-0.5}^{+0.5} \cos(\pi fT) d(fT) \quad (6.6.1.2.2-1)$$

$$= \frac{1}{\pi} \int_{-\pi/2}^{+\pi/2} \cos \theta d \theta$$

$$S_T = \frac{2}{\pi}$$

Thus S_T , dB is

$$S_T, \text{ dB} = -2 \text{ dB} \quad (6.6.1.2.2-2)$$

Figure 6.6.1.2.2-2 shows the peak amplifier power limited performance for equal split duobinary filtering performance for M-QAM. Precoding is used at the transmitter and a simple slicer receiver is used.

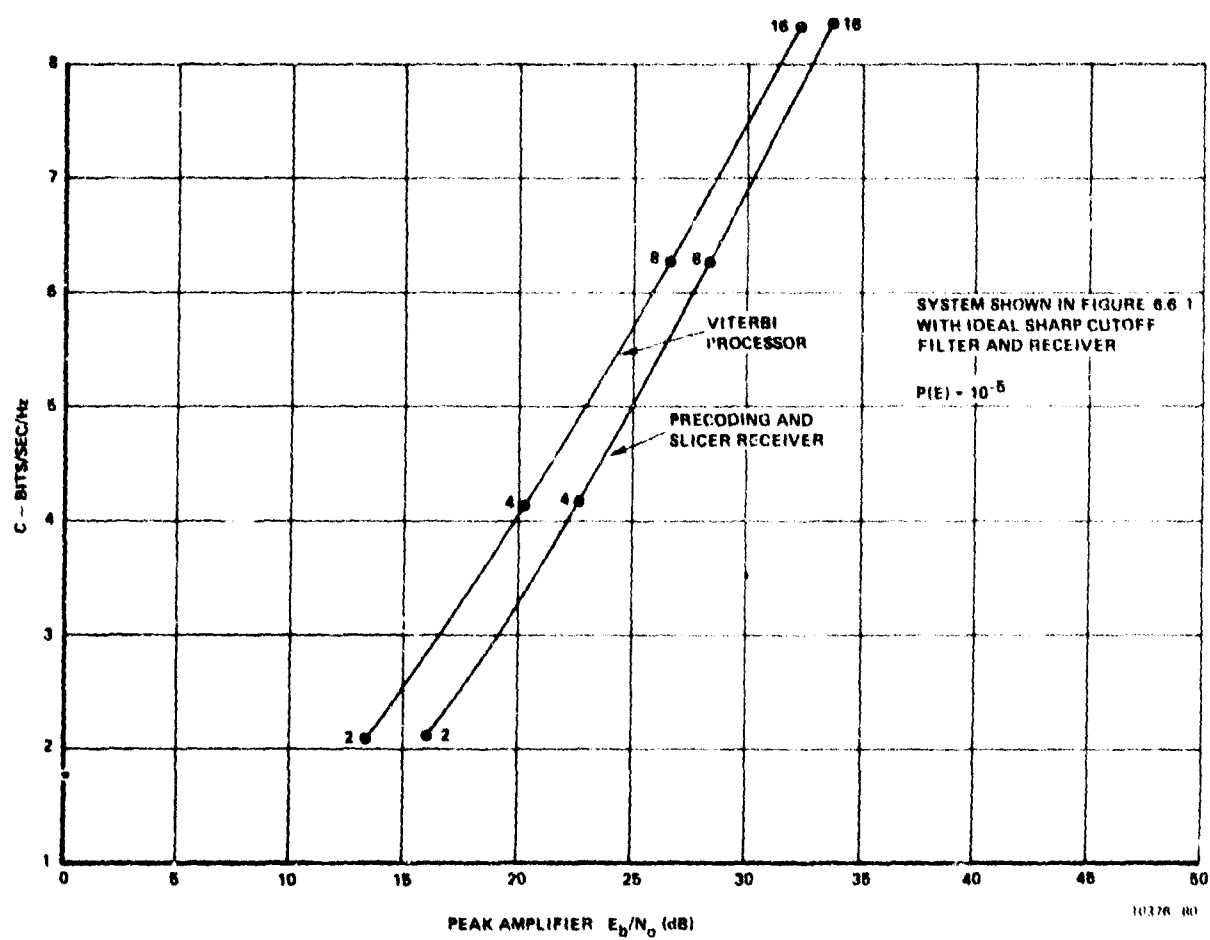


Figure 6.6.1.2.1-2. Amplifier Peak Limited M-QAM With Duobinary Partial Response Shaping Filter All at Transmitter

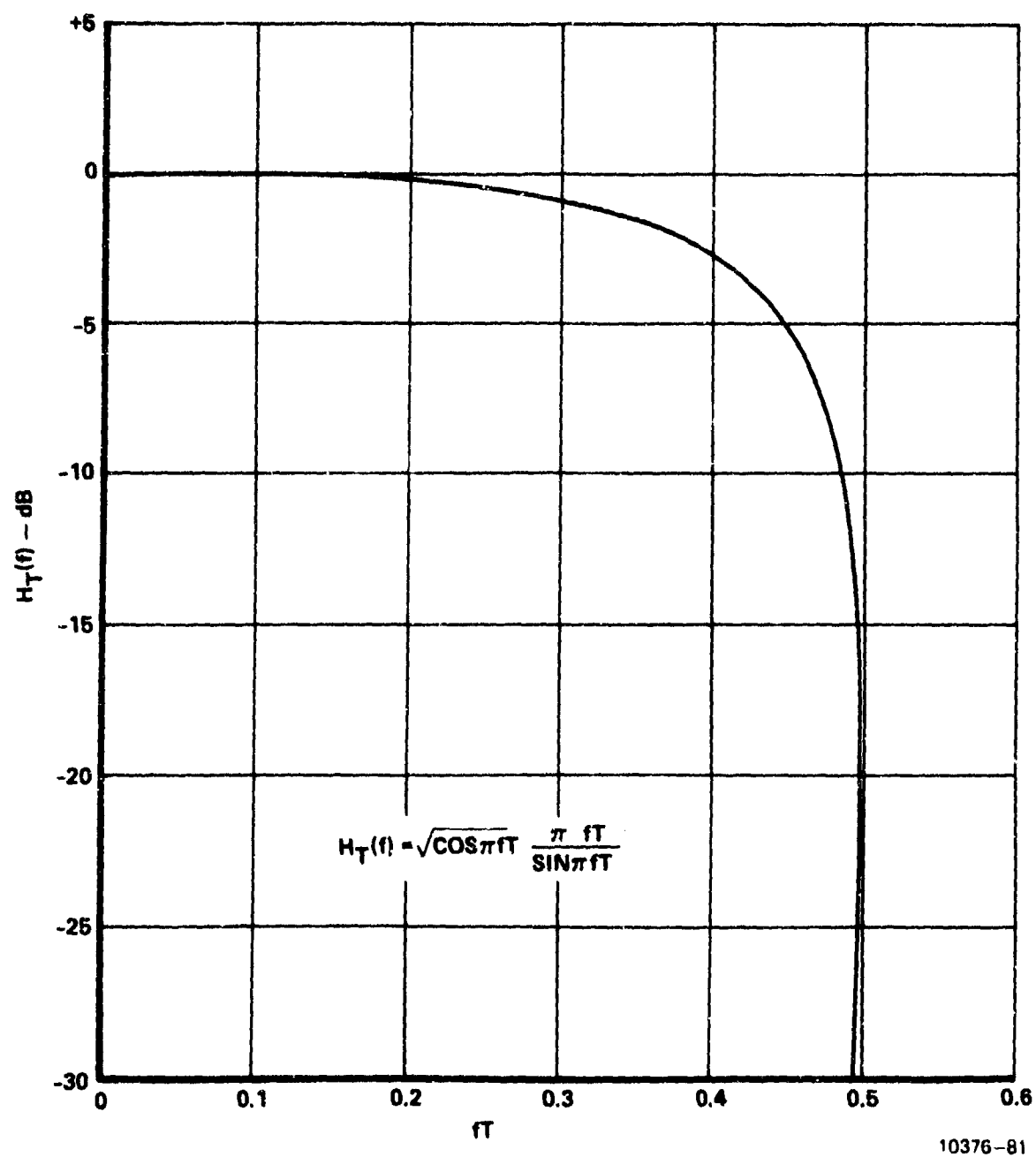


Figure 6.6.1.2.2-1. Transfer Function of Transmit Filter for Equal Division of Duobinary Signaling

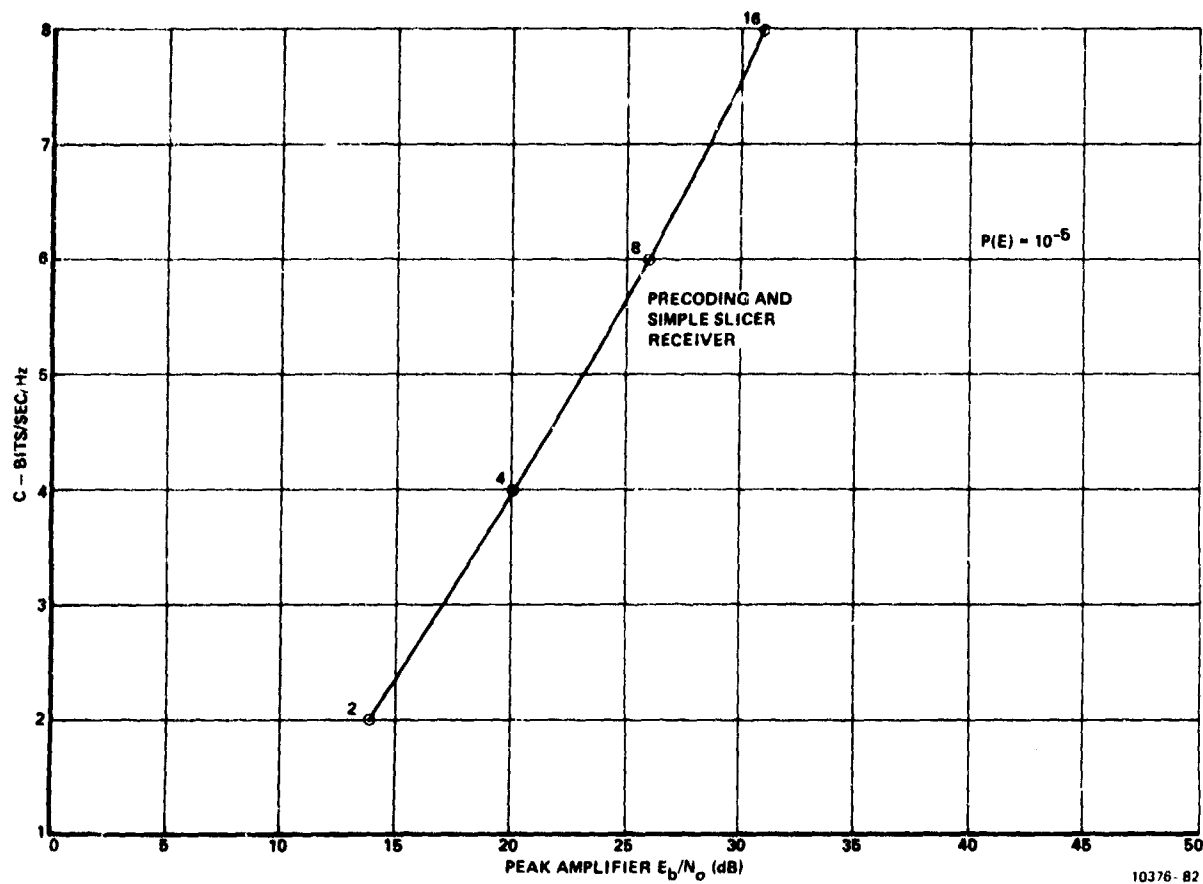


Figure 6.6.1.2.2-2. Amplifier Peak Limited M-QAM With Duobinary Partial Response Shaping Filter Equally Divided Between Transmitter and Receiver

6.6.1.3 Peak Amplifier Power Limited M-QAM Signaling With 5-Pole Butterworth Transmit Waveguide Filter

The results of the preceding Paragraph 6.6.1 are for idealized transmit filters, perfectly equalized for the $\sin x/x$ rolloff created by square pulse signaling. Such filters are not easily realized in a waveguide design. Here we turn to a determination of peak-limited performance for the system of Figure 6.6 when the transmit filter, $H_T(\omega)$, is a more realizable 5-pole Butterworth design. As in Paragraph 6.5.3, we assume that the receiver filter $H_R(\omega)$ in Figure 6.6 consists of a 5-pole Butterworth filter equal in 3 dB bandwidth to the transmit filter, followed by an equalizer to yield either Nyquist or duo-M-ary partial response. The performance of such a system has been plotted in Figure 6.5.3.3-2 of Paragraph 6.5.3.3 in terms of capacity versus average E_b/N_0 at the receive filter input.

Obviously we need simply to apply the spectral truncation loss, S_T , for the 5-pole Butterworth filter along with the ratio of peak-to-average power at the amplifier output to convert the curves of Figure 6.5.3.3-2 to peak amplifier E_b/N_0 curves. That is, we must compute the correction, P_F/P_A , given in Equation (6.6-14) previously.

The spectral truncation power loss for the 5-pole Butterworth filter is given in Figure 6.6.1.3-1 versus the ratio of low-pass 3 dB bandwidth, f_{3dB} , to symbol rate, $1/T$. Applying this spectral truncation loss, along with the ratio of peak-to-average power for M-QAM pulses $\left[3 \frac{(M-1)}{(M+1)} \right]$, to the results of Paragraph 6.5.3.3, the curves of Figure 6.6.1.3-2 are produced.

Figure 6.6.1.3-2 shows the combinations of bits/s/Hz under FCC 19311 and peak amplifier E_b/N_0 required for a symbol error rate, $P(E)$, equal to 10^{-5} . From these curves we note that on a peak power basis the M-QAM schemes outperform the duo-M-ary equalized schemes in the 3 to 4.9 bits/s/Hz region of primary interest on this study. For example, at 4 bits/s/Hz, modified 6-QAM requires 21.5 dB peak

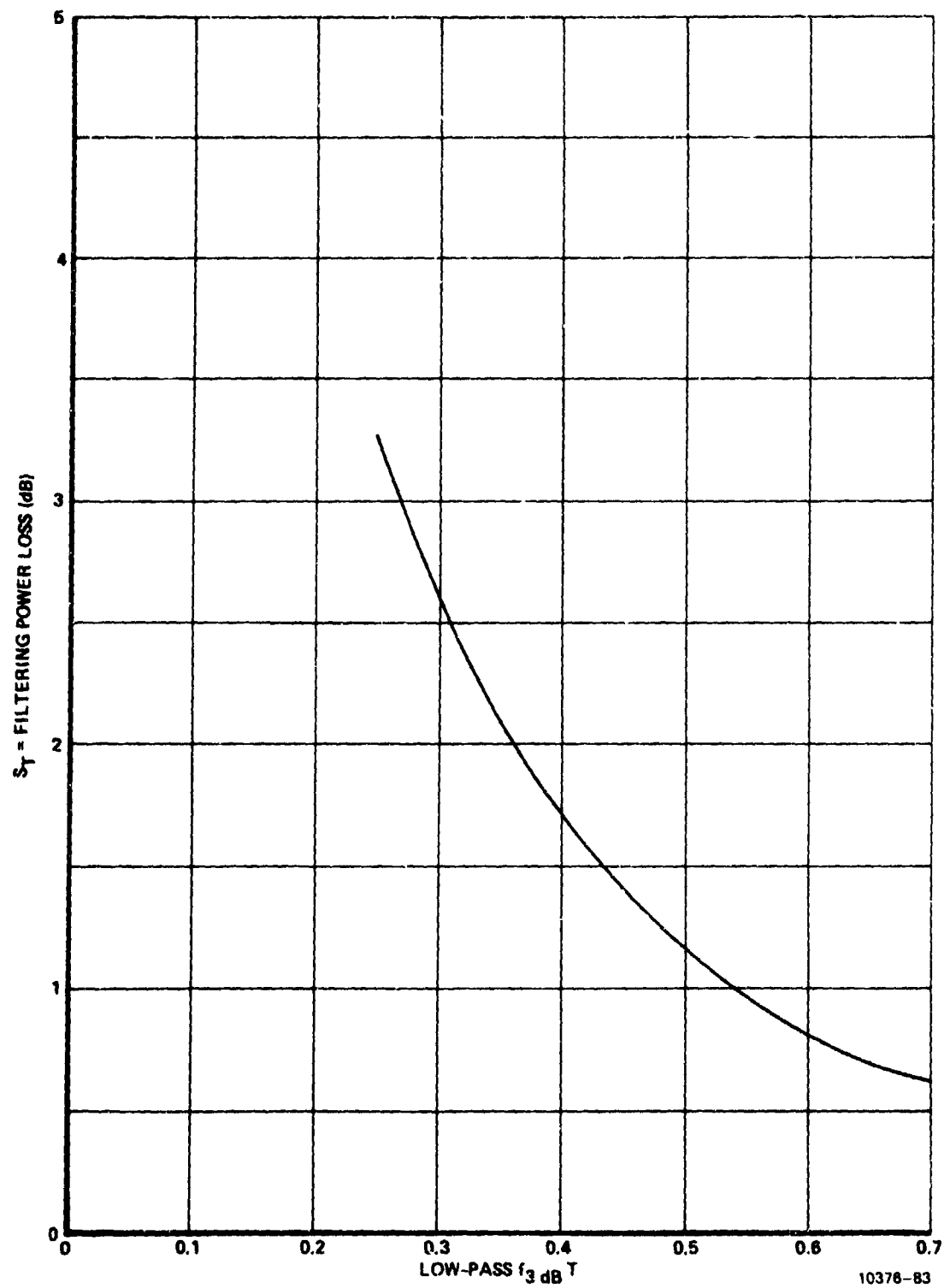


Figure 6.6.1.3-1. dB Power Loss Due to Filtering PAM
With 5-Pole Butterworth Filters

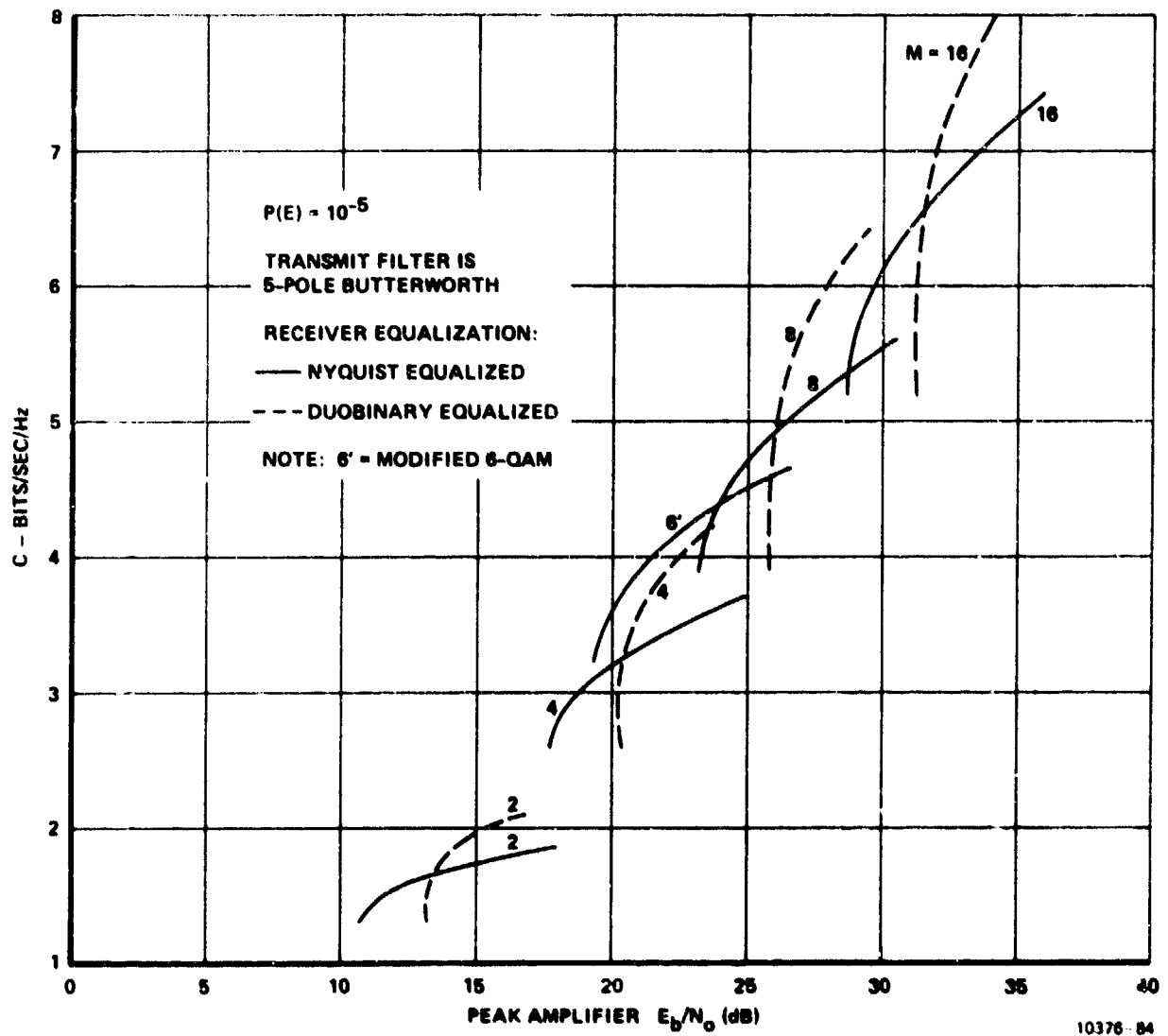


Figure 6.6.1.3-2. Peak Power Limited Filtered M-QAM With Receiver Equalization

E_b/N_0 for 10^{-5} , whereas duo-M-ary requires 22.6 dB peak E_b/N_0 . Above approximately 5 bits/s/Hz, a superiority of duo-M-ary equalization begins to emerge. These peak power curves should be compared with the average power curves of Figure 6.5.3.3-2 in Paragraph 6.5.3.3 where roughly the same type of behavior is noted.

It is concluded from the curves of Figure 6.6.1.3-2, that M-QAM signaling with Nyquist receiver equalization represents the more desirable technique in the capacity range between 3 to 5 bits/s/Hz. Therefore, we adopt this type signaling in preference to the duobinary equalized technique.

6.6.2 Trade-Offs of Primary Candidate Schemes on Basis of Peak Power

Figure 6.6.2-1 shows the peak power limited capacity versus peak power amplifier E_b/N_0 comparisons for the systems considered in the preceding two sections. The ideal spectral shaping (equal-division cosine rolloff for duobinary and equal-division raised cosine, $\alpha = 0.2$, for Nyquist signaling) performances are shown for comparison with the 5-pole Butterworth shaping filter-with-receiver-equalization performances.

We note that the systems using the 5-pole Butterworth shaping filter perform well relative to the more idealized raised cosine transmit shaping filters. Because of the greater realizability in a waveguide filter of the 5-pole Butterworth shaping filter design as compared to $\sin x/x$ compensated square root raised cosine design with $\alpha = 0.2$, the M-QAM modulation with a Butterworth waveguide filter is selected as the more desirable practical system.

We also note again in Figure 6.6.2-1 that, with the practical Butterworth waveguide design, Nyquist equalization at the receiver displays a performance advantage relative to duo-M-ary equalization in the 3 to 4.9 bits/s/Hz capacity region. The 4-, 6-, and 8-QAM schemes cover this range of capacity in a power efficient manner.

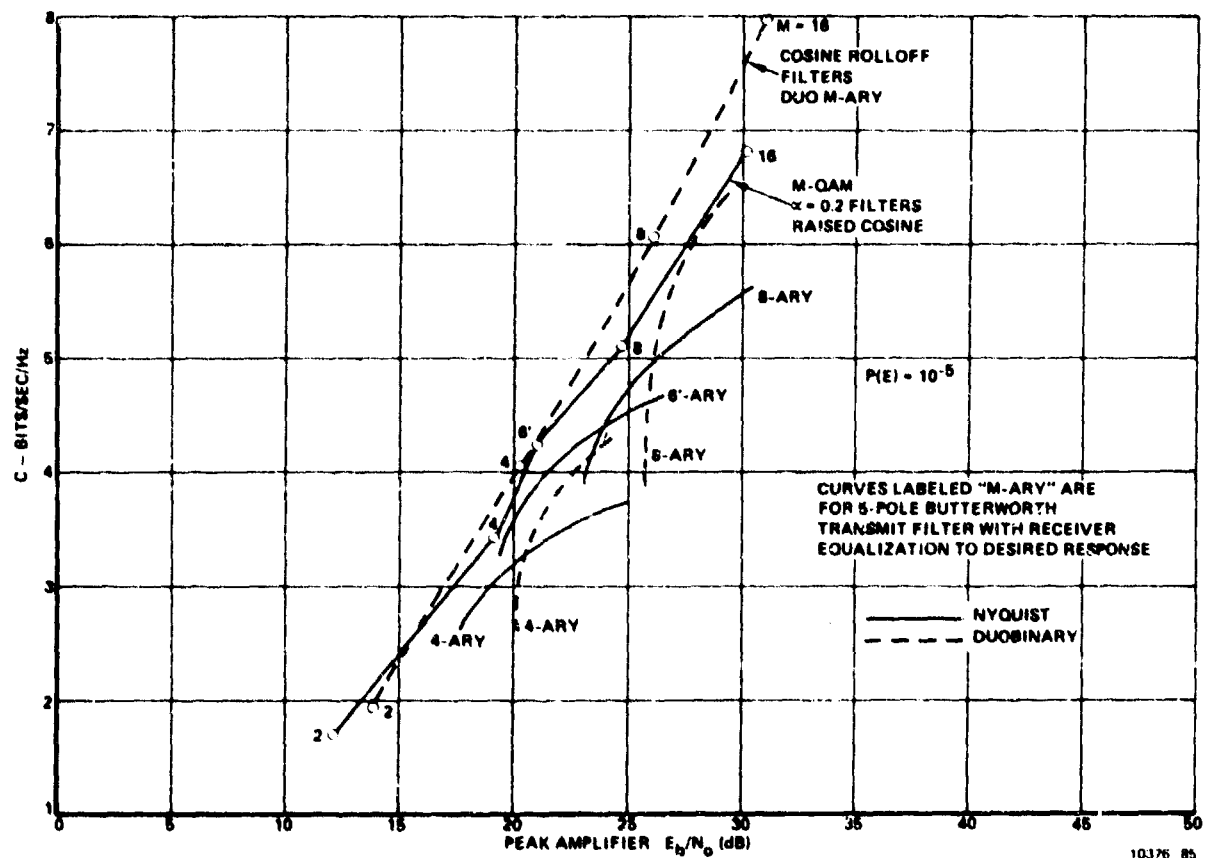


Figure 6.6.2-1. Comparison of Equalized Butterworth Performance With Cosine Rolloff (Duobinary) and Raised Cosine Rolloff (Nyquist) Performance

The M-QAM and duo-M-ary signaling schemes have been shown in previous sections to be the best candidate signaling techniques for the high spectral efficiency regions of capacity. On the basis of the peak power comparisons between these two primary practical candidate schemes displayed in Figure 6.6.2-1, we conclude that the M-QAM schemes offer the best performance in the 3 to 5 bits/s/Hz capacity region.

To fully understand just how good the Butterworth transmit waveguide filtered-receiver equalized performance is, we show the comparison in Figure 6.6.2-2. Here, the capacity in bits/s/Hz is plotted for the ideal sharp cutoff filtered M-QAM system versus peak amplifier E_b/N_0 . This performance is compared with the Butterworth filtered-and-equalized system performance. At 4 bits/s/Hz, the performance of the modified 6-ary filtered-and-equalized system is within 1 dB of the ideal sharp cutoff filter system. The ideal sharp cutoff filter curve is taken from the $\alpha = 0$ curve of Paragraph 6.6.1.1.1 on M-QAM, Nyquist shaping. This very favorable performance comparison at 4 bits/s/Hz comes in part from the fact that the $\alpha = 0$ sharp cutoff waveguide filter has 4 dB of spectral truncation loss whereas the modified 6-QAM signaling scheme has only 1.5 dB of spectral truncation power loss with the Butterworth waveguide filter.

6.6.2.1 Comments on the Peak Power Performance Trade-Offs

The peak power performance trade-offs just made in the previous sections concentrated on the most promising M-QAM and duo-M-ary signaling schemes. Some of the schemes investigated in earlier sections using Viterbi algorithm sample processors at the receiver offer better performance than the M-QAM schemes on the basis of average power comparisons. See, for example, the curves in Figure 6.4.4-4 for M-QAM with prolate spheroid pulse shapes for pulse duration greater than 1 baud time and Viterbi demodulation. One problem with these pulse shapes is that they are not readily realized other than with baseband pulse shaping - e.g., they are not readily-realized with waveguide RF shaping

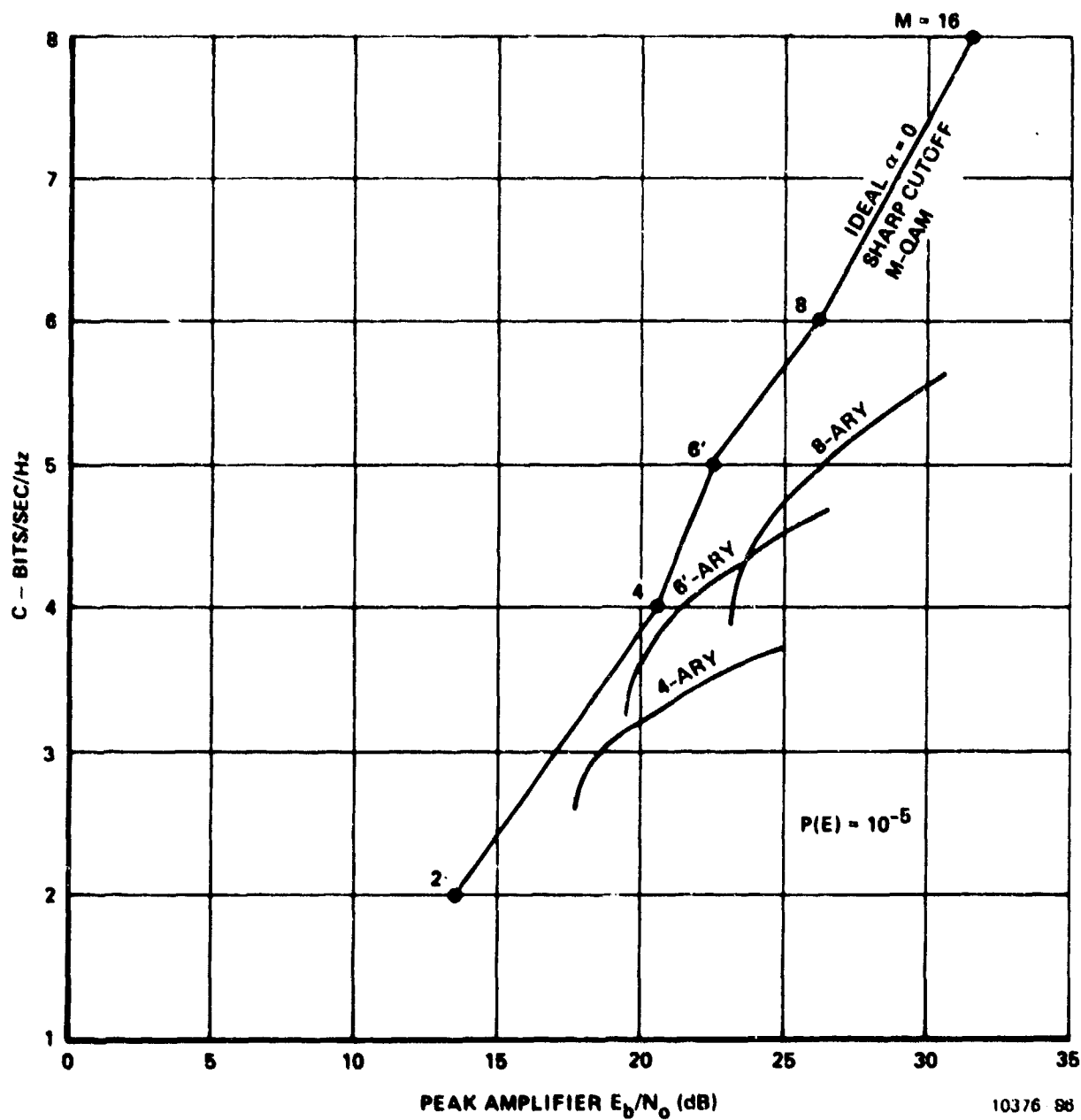


Figure 6.6.2-2. Peak Power Limited Comparison Between Ideal Sharp Cutoff M-QAM and 5-Pole Butterworth Filtered-and-Equalized M-QAM

filters. We show in later sections that because of typical amplifier nonlinearities, baseband spectral shaping is relatively ineffective at providing FCC Docket 19311 spectrum compliance since spectral side lobes are generated by the amplifier distortion. Generally, with baseband (or IF) filtering, the power amplifier has to be backed off excessively to obtain FCC Docket 19311 compliance. Another problem with the Viterbi algorithm processor schemes is the number of states (hence, complexity) required for implementation. For example, 4-QAM in conjunction with 4 baud time pulse shaping (which can be used to provide near optimal 4 bits/Hz capacity) requires the use of a 64 state Viterbi algorithm processor on each of the two quadrature channels at the receiver. For high bit rate operation, such processors can become quite complicated, requiring approximately 400 integrated circuit packages for each of the two processors at a 10 MHz symbol rate. At the present time, we feel that this additional complexity is not warranted in a practical modem.

What penalty have we paid for using the simpler equalized M-QAM demod scheme as opposed to the Viterbi algorithm? Figure 6.4.4-4 shows that the 4-QAM scheme, with prolate spheroid pulse shaping and Viterbi algorithm demodulation requires average $E_b/N_0 = 15.3$ dB for 10^{-5} symbol error rate at 4 bits/s/Hz. Figure 6.5.3.3-2, on the other hand, shows that the equalized modified 6-QAM scheme requires average $E_b/N_0 = 17.9$ dB at 4 bits/s/Hz for 10^{-5} error rate. Thus, solely on the basis of average received E_b/N_0 , the simpler equalized M-QAM scheme requires 2.6 dB more power than the more complicated Viterbi processor system. Some, perhaps even all, of this 2.6 dB average power advantage for the prolate spheroid spectral shaping, Viterbi algorithm receiver system will be lost in peak amplifier E_b/N_0 comparison. The reason for this is the amount of spectral truncation power loss incurred by using a waveguide filter with required narrow bandwidth to effect the length four prolate spheroid spectral shaping. Figure 6.4-3 shows the radiated spectrum for this prolate spheroidal shaping versus fT_p , where f is frequency from carrier and T_p = prolate spheroid pulse duration =

$4T_s$, where T_s = symbol time. The 3 dB bandwidth of a waveguide filter necessary to effect this spectral shaping can be seen to be around $0.36 \times$ symbol rate (from Figure 6.4-3, one-sided $fT_s = 4$ $fT_s = 0.7$ or $fT_s = 0.18$ one-sided 3 dB BW or 0.36 two-sided RF BW). Approximately 4 dB of spectral truncation power loss can be expected from this restrictive waveguide filter bandwidth when used in the system of Figure 6.6. The peak-to-average power ratio for 4-QAM pulses from the amplifier is 2.6 dB. Thus, the overall loss for the prolate spheroid pulse spectral shaping is approximately 6.6 dB. Thus, the peak amplifier E_b/N_0 for the prolate spheroid spectral shaping 4-QAM - 4 baud time pulse duration system with Viterbi algorithm receiver for 10^{-5} symbol error rate is given by:

$$\begin{aligned} \text{Peak } E_b/N_0 &= \text{average } E_b/N_0 + \text{Spectral Truncation Loss} \\ &\quad + \text{Peak-to-Average Ratio} \\ &= 15.3 + 4 + 2.6 \text{ dB} \\ \text{Peak } E_b/N_0 &= 21.9 \text{ dB for prolate spheroid} \end{aligned}$$

From Figure 6.6.2-2, the peak E_b/N_0 required by a Butterworth filter and equalized modified 6-QAM system at 4 bits/s/Hz is

$$\text{Peak } E_b/N_0 = 21.5 \text{ dB for modified 6-QAM.}$$

Therefore, we see that on the basis of a peak amplifier power requirement, the more complicated scheme using the prolate spheroid shaping actually requires greater peak amplifier power than the filtered and equalized 6-QAM scheme.

The spectral truncation power loss that weights heavily against the prolate spheroid spectral shaping in the above example is sometimes overlooked in comparisons among different modulation schemes for spectrally-efficient systems. We feel, however, that it is important and comparisons should be made on the basis of required peak amplifier power, since minimizing this requirement guarantees the greatest system margin given a specific amplifier.

The most desirable M-QAM modulation schemes isolated in the trade-offs are, of course, not constant envelope modulations. As such, they are susceptible to the nonlinearities of typical microwave power amplifiers - i.e., to AM/AM and AM/PM conversion.^{31,32} If considerable loss in system margin due to the amplifier backoff is to be avoided in the use of these variable amplitude schemes, the effects of AM/AM and AM/PM conversion must be counteracted. A means of doing so has been discovered on this study for the system of Figure 6.6. The technique discovered linearizes the microwave amplifier for the discrete digital signal space points for any square pulse quadrature amplitude modulation format, of which M-QAM is a prime example. The technique is continuously adaptive to track variations in radio and amplifier characteristics. The adaptive linearization virtually totally removes the effects of amplifier distortion so that the results we have shown (which tacitly assumed a linear amplifier) for square pulse M-QAM signaling through the power amplifier, followed by waveguide spectral shaping filter can be realistically achieved - even for peak drive levels into a TWT amplifier approaching saturation. This digital adaptive power amplifier linearization scheme represents one of our most important achievements on this study relative to linear modulation techniques for digital microwave. The linearization scheme is described in Paragraph 6.8.

6.6.3

The Relative Theoretical Efficiencies of Preamplifier and
Passive Postamplifier Spectral Shaping When the Amplifier is
Peak Power Limited

Figures 6.6.3a and 6.6.3b show the two possible techniques of pre- and post-amplifier filtering to obtain a given spectral shaping. As shown, ideally Nyquist band-limited signalling of data impulses having pk-avg energy ratio of σ_d^2 is to be employed, and the spectral shaping affected is equivalent to partial response with tap gain polynomial, $f(D)$. As explained in Section 2., any Nyquist band shaping filter whatsoever can be modeled as the series combination of the ideally band-limited filter (which is the only ideally band-limited square root Nyquist filter) and some partial response polynomial, $f(D)$. As shown in Paragraph 2.2.4, the preamplifier shaping filter will have frequency response given by $f(e^{j\omega T})$, and the peak-to-average pulse energy will be given by

$$\text{pk - avg (Preamp)} = \sigma_d^2 \frac{(\sum |f_i|)^2}{\sum f_i^2} \quad (6.6.3-1)$$

as shown in Paragraph 2.2.2, where f_i = tap gains of the equivalent $f(D)$. The amplifier is assumed to be peak power limited in that the peak sinc function pulse energy (produced by the ideally band-limited filter) must not exceed some specified value.

The system shown in Figure 6.6.3b obtains exactly the same spectral shaping as in Figure 6.6.3a except that here a passive postamplifier filter (such as a waveguide filter in microwave applications) is used to obtain the shaping. Obviously, the transfer function required of the postamplifier filter in order to produce the same spectrum as in the preamplifier filtered case is given by:

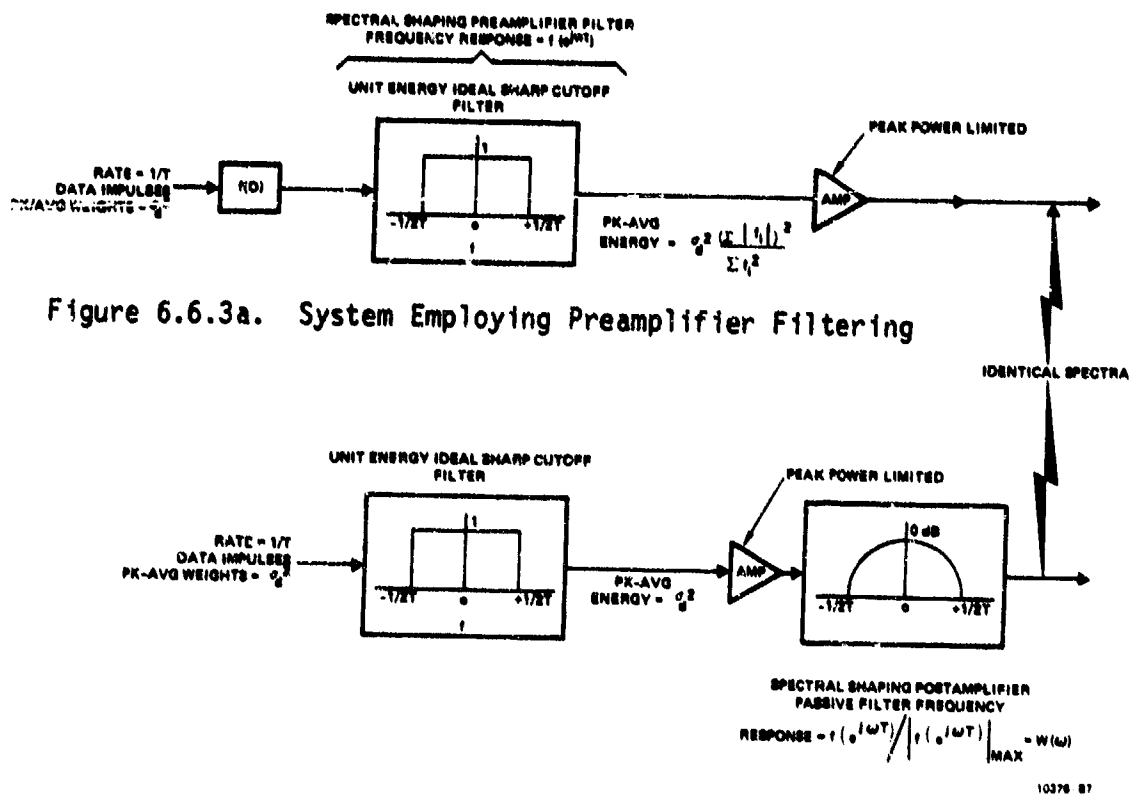


Figure 6.6.3b. System Employing Passive Postamplifier Filtering

$$W(\omega) = f(e^{j\omega T}) / \left| f(e^{j\omega T}) \right|_{\max} \quad (6.6.3-2)$$

where $\left| f(e^{j\omega T}) \right|_{\max}$ = Maximum response in the passband of $f(e^{j\omega T})$.

The normalizing denominator is required to comply with the constraint that the postamplifier filter be a passive device as with a waveguide filter in the microwave system case of interest. The input to the power amplifier has a pk-avg power ratio given by

$$\text{Pk-Avg (Postamp)} = \sigma_d^2 \quad (6.6.3-3)$$

i.e. the same pk-avg ratio as for the input data impulses. Comparing Equations 6.6.3-1 and 6.6.3-3, one observes that the preamplifier filtering system must be backed off in average power relative to the postamplifier filtering case to avoid exceeding the peak power capability specified for the power amplifier. The amount by which it must be backed off is given by the ratio of Equation 6.6.3-3 to Equation 6.6.3-1, i.e.:

$$\text{Backoff (Preamp)} = \frac{\sum_i^f 1}{\left(\sum_i |f_i| \right)^2} \quad (6.6.3-4)$$

The postamplifier filtered system would thus have a peak power utilization advantage given by Equation 6.6.3-4 over the preamplifier filtered system if it were not for the spectral truncation power loss incurred in passing the ideally band-limited spectrum through the postamplifier shaping filter, $W(\omega)$. In the postamplifier filtered case in Figure 6.6.3b, the average power at the input to the filter, $W(\omega)$, is given by

$$P_{in} = \int_{-1/2T}^{+1/2T} (1) df = 1/T \quad (6.6.3-5)$$

The average power at the output of the filter, on the other hand is,

$$P_{out} = \int_{-1/2T}^{+1/2T} (1) W(\omega) W^*(\omega) d\omega \quad (6.6.3-6)$$

Using Equation (6.6.3-2) in Equation (6.6.3-6), we obtain

$$P_{out} = \int_{-1/2T}^{+1/2T} f(e^{j\omega T}) f(e^{-j\omega T}) d\omega / |f(e^{j\omega T})|_{max}^2 \quad (6.6.3-7)$$

$$= \int_{-1/2T}^{+1/2T} \left[\sum_i f_i e^{-j i \omega T} \right] \left[\sum_k f_k e^{j k \omega T} \right] d\omega / |f(e^{j\omega T})|_{max}^2$$

$$= \sum_i \sum_k f_i f_k \int_{-1/2T}^{+1/2T} e^{j(k-i)\omega T} d\omega / |f(e^{j\omega T})|_{max}^2 \quad (6.6.3-8)$$

The integral in Equation (6.6.3-8) is zero for $k \neq i$ and is $1/T$ for $k = i$. Therefore:

$$P_{out} = \frac{1}{T} \sum_i f_i^2 / |f(e^{j\omega T})|_{max}^2 \quad (6.6.3-9)$$

Taking the ratio of Equation (6.6.3-5) to Equation (6.6.3-9), we obtain the spectral truncation power loss, S_T , in the postamplifier filtered case,

$$S_T = \frac{P_{in}}{P_{out}} = |f(e^{j\omega T})|_{max}^2 / \sum f_i^2 \quad (6.6.3-10)$$

It can be verified that

$$|f(e^{j\omega T})|_{max} = \left| \sum f_i e^{j\omega T} \right|_{max} \leq \sum |f_i| \quad (6.6.3-11)$$

Use of the inequality of Equation (6.6.3-11) in Equation (6.6.3-10) yields:

$$S_T \leq \frac{\sum f_i^2}{\left(\sum |f_i| \right)^2} \quad (6.6.3-12)$$

Comparing Equations (6.6.3-12) and (6.6.3-4), one concludes that the backoff required to accommodate the peaks caused by the preamplifier

shaping filter is exactly the same (when the equality of Equations (6.6.3-11) and (6.6.3-12) holds) as the spectral truncation power loss incurred by the use of passive postamplifier filtering. When the inequality does not hold, the postamplifier filtering approach has an advantage over the preamplifier filtering technique. Thus, the passive postamplifier filter (waveguide filtering) approach is always at least as good as the preamplifier filtering approach under a peak power constraint for the idealized systems shown in Figure 6.6.3. Although the filters employed in the systems of Figure 6.6.3 are rather idealized, it seems reasonable to expect similar conclusions when more practical filters are used. As a matter of fact, it can be proven that the same results hold for replacement of the ideal sharp cutoff filter with any square root Nyquist filter.

In the above comparison, the amplifier was assumed to be linear up to its peak power capability. Real amplifiers, of course, display nonlinear distortions in the forms of AM/AM and AM/PM conversion. The case against preamplifier filtering instead of postamplifier filtering may be made even stronger, perhaps, with real amplifiers, in that more amplitude levels are created (by the transversal filter, $f(D)$) in Figure 6.6.3a for transmission through the amplifier. This seems to imply that more stringent linearity specifications may have to be adhered to in the amplifier design than with postamplifier filtering.

In conclusion, the relative theoretical comparison made here between pre- and post-amplifier filtering, lends even more credence to our belief that the employment of waveguide filtering to perform the most significant spectral shaping represents the most efficient approach to obtaining FCC Docket 19311 compliance.

6.7 Performance of Preamplifier Filtered M-QAM in Conjunction With a Linear Amplifier

6.7.1 Introduction

The Ford Aerospace and Communications Corporation has developed³⁴ an experimental linear solid state 8 GHz microwave amplifier for Rome Air Development Center on Contract F30602-76-C-0271. This amplifier is taken as an example of an amplifier carefully designed to have good linearity for data transmission requirements. In later portions of this section, we show simulated performance results obtained for M-QAM signaling using baseband filtering with this power amplifier.

Figures 6.7-1 through 6.7-4 show measured performance characteristics of the Ford Experimental linear microwave amplifier. These curves are taken from the above-referenced technical report.³⁴ Figure 6.7-1 shows the measured two tone test third-order intermod distortion (IMD). At 35 dBm power output (3 watts), the third order IMD is around -30 dBc. If greater than 35 dBm in output power levels are used, the IMD rises rapidly. The plateau in IMD at around the -30 dBc level resulted from tuning and optimizing the amplifier for linear operation to delay the rapid rise that occurs as power output saturation is approached.

Figure 6.7-2 shows the power transfer or AM/AM conversion curve for the amplifier. Single signal saturation output power occurs at around 38.1 dBm or 6.45 watts. The two equal signal output power curve begins to compress at about a 3 dB lower average input power level than the single signal curve because of 3 dB higher peak-to-average power ratio for the two tone test. Thus, with the two tone test, when the average input power is 0 dBm, the peaks of the input signal go as high as +3 dBm. At this peak input power level, one can see that the single tone power output curve is in compression. Consequently, one should expect

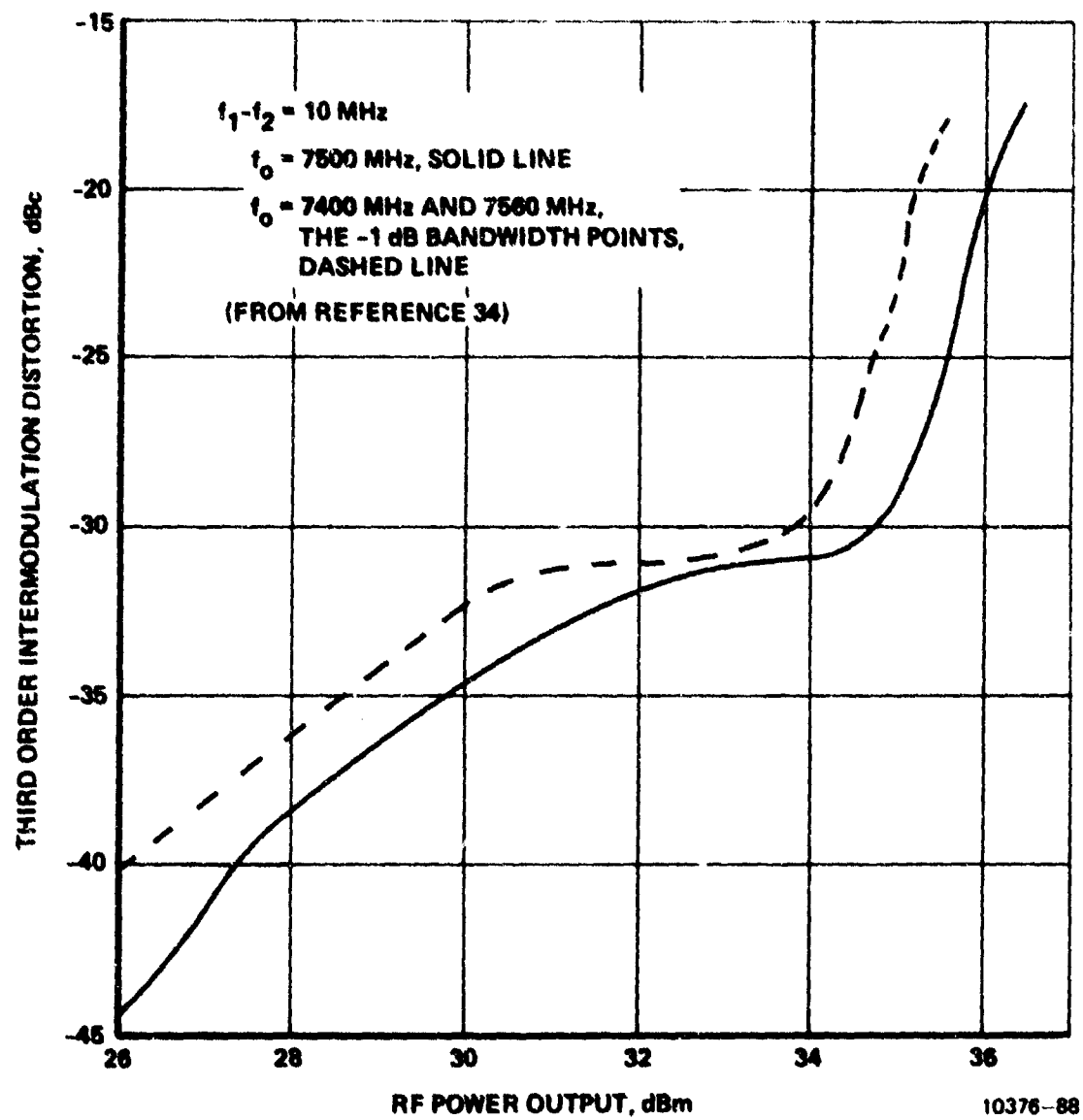


Figure 6.7-1. IMD Versus RF Power Output, Two Signal

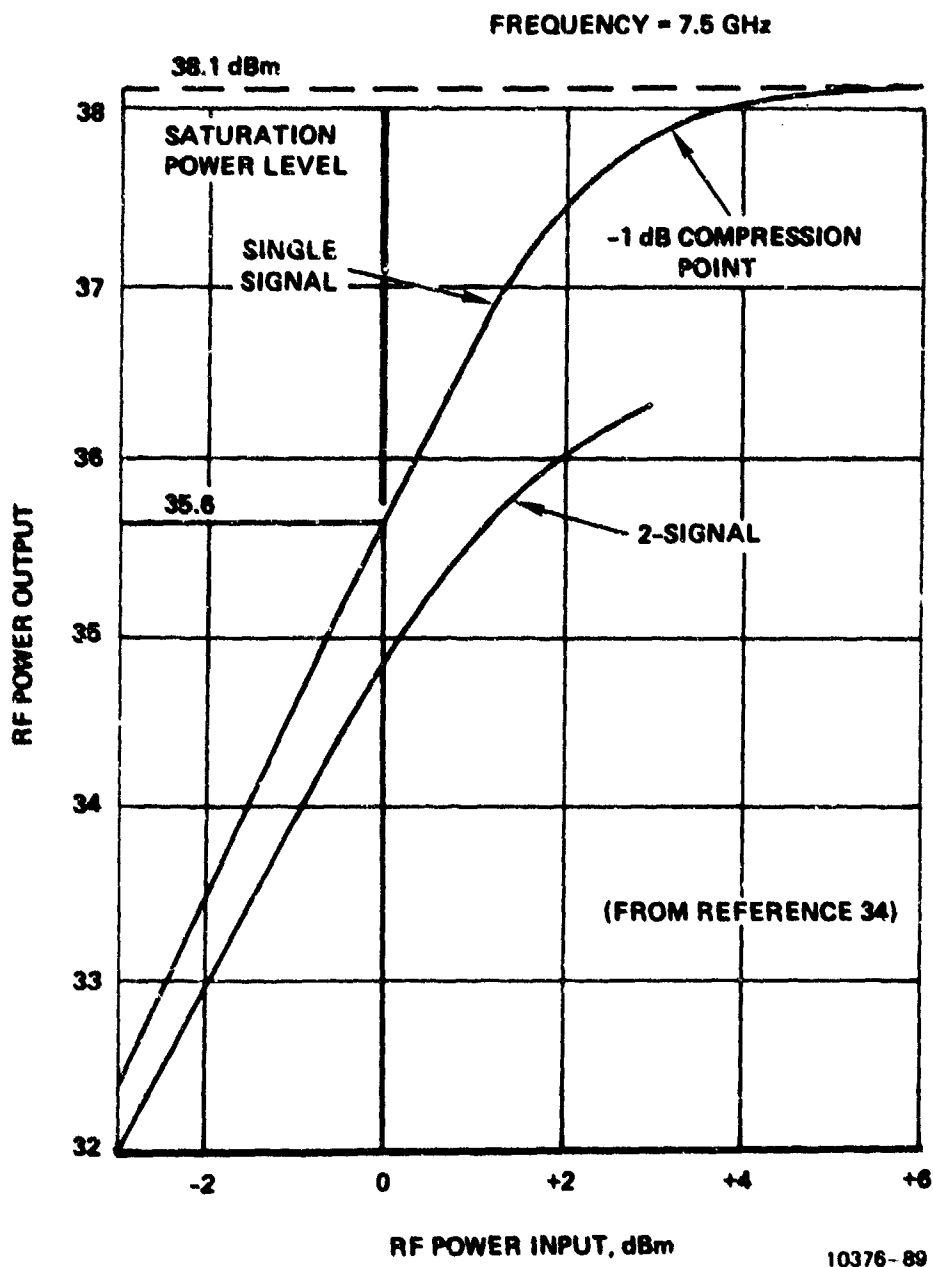


Figure 6.7-2. Power Transfer Curve (AM-AM)

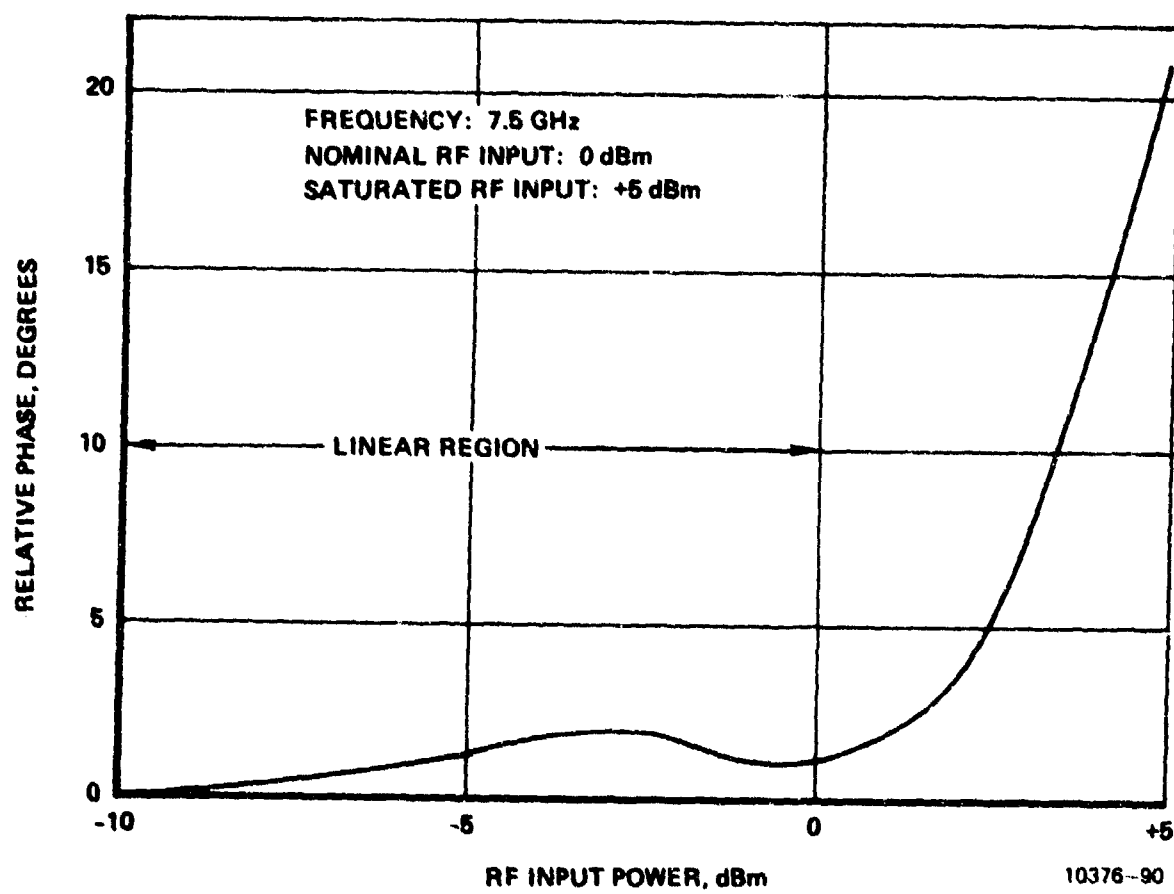
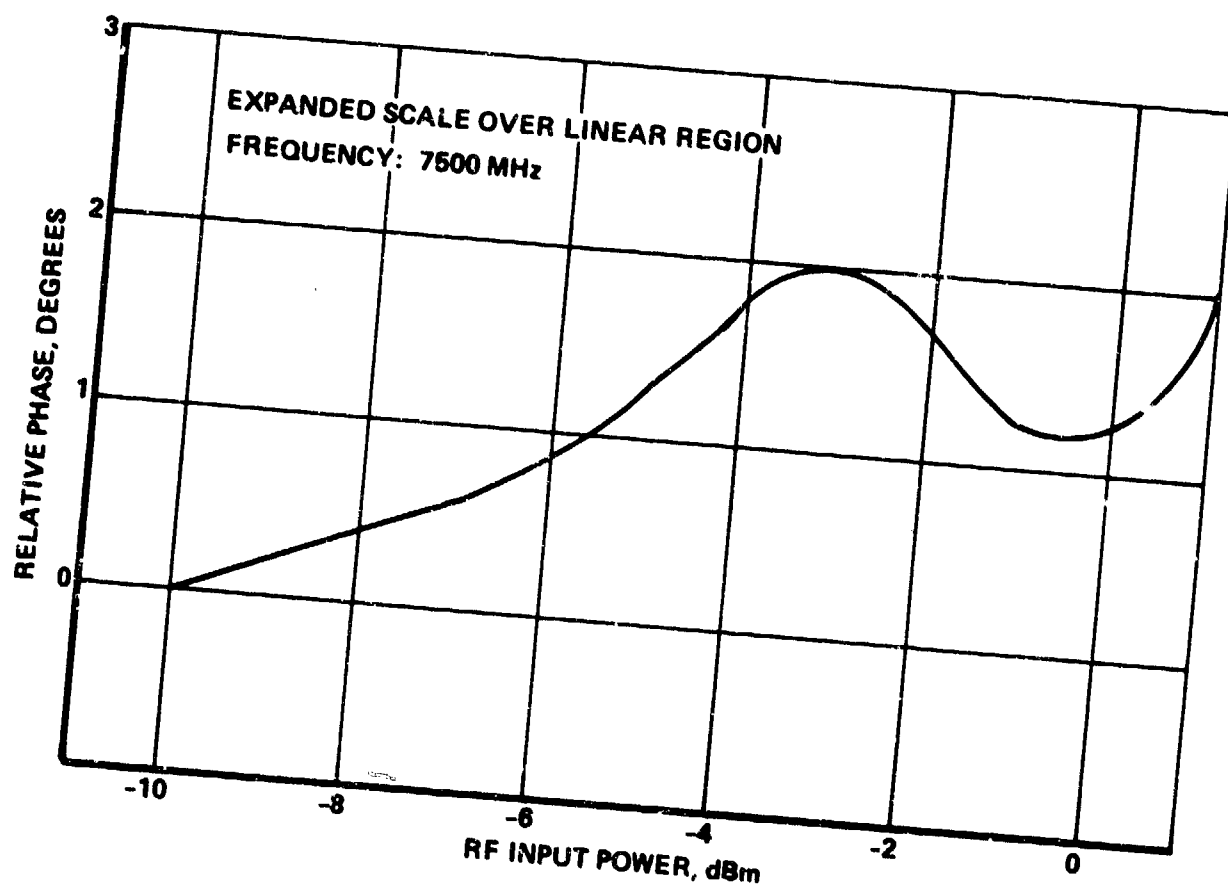


Figure 6.7-3. Relative Phase Versus RF Input Power



10376 -91

Figure 6.7-4. Relative Phase Versus RF Input Power

the two tone power curve to compress at the lower input drive level relative to single tone as shown in Figure 6.7-2. It is this peak distortion that causes the third-order IMD levels to increase drastically above about 34 dBm average output power in Figure 6.7-1 shown previously. This phenomenon highlights the fact that a "linear" amplifier is a peak power limited device in that the distortion rises dramatically as the input signal power peaks approach levels corresponding to single signal output power going into compression.

The distortion caused by output signal amplitude going into compression (deviation from a linear relation between input and output amplitude) is but one of the distortive effects relevant to evaluation of linear modulation techniques. In addition to the nonlinear relation between input and output amplitude, practical amplifiers also induce a phase shift on the output sinusoid relative to the input sinusoid that is a nonlinear function of the input signal amplitude. This is the well-known AM/PM conversion characteristic. Measurements of this phenomenon were made by Ford for the experimental microwave linear amplifier and the results are shown in Figures 6.7-3 and 6.7-4. Figure 6.7-4 is just an expanded scale plot of Figure 6.7-3 over the "linear" region (up to -0 dBm input power.) On these figures the relative phase shift of the output sinusoid from the amplifier is plotted versus the input power level.

Relative to the linear modulation techniques, the AM/PM conversion characteristics of the amplifier cause signal points at different discrete amplitude levels to undergo different amounts of phase rotation in passing through the amplifier. This phenomenon obviously causes performance degradation at the receiver since signal points in the quadrature signal space are then positioned incorrectly with respect to receiver slicing thresholds.

The AM/AM and AM/PM conversion characteristics discussed above not only cause performance degradation in terms of increased receiver signal/noise ratio requirements, but they also cause output signal spectral spreading relative to the spectrum of the filtered input signal.

The spectral spreading phenomenon is addressed in Paragraph 6.8.4.3. The performance degradation effect is addressed in the following paragraphs.

6.7.2 Performance Simulation Results for Filtered M-QAM Systems When Used with the Ford Linear Amplifier

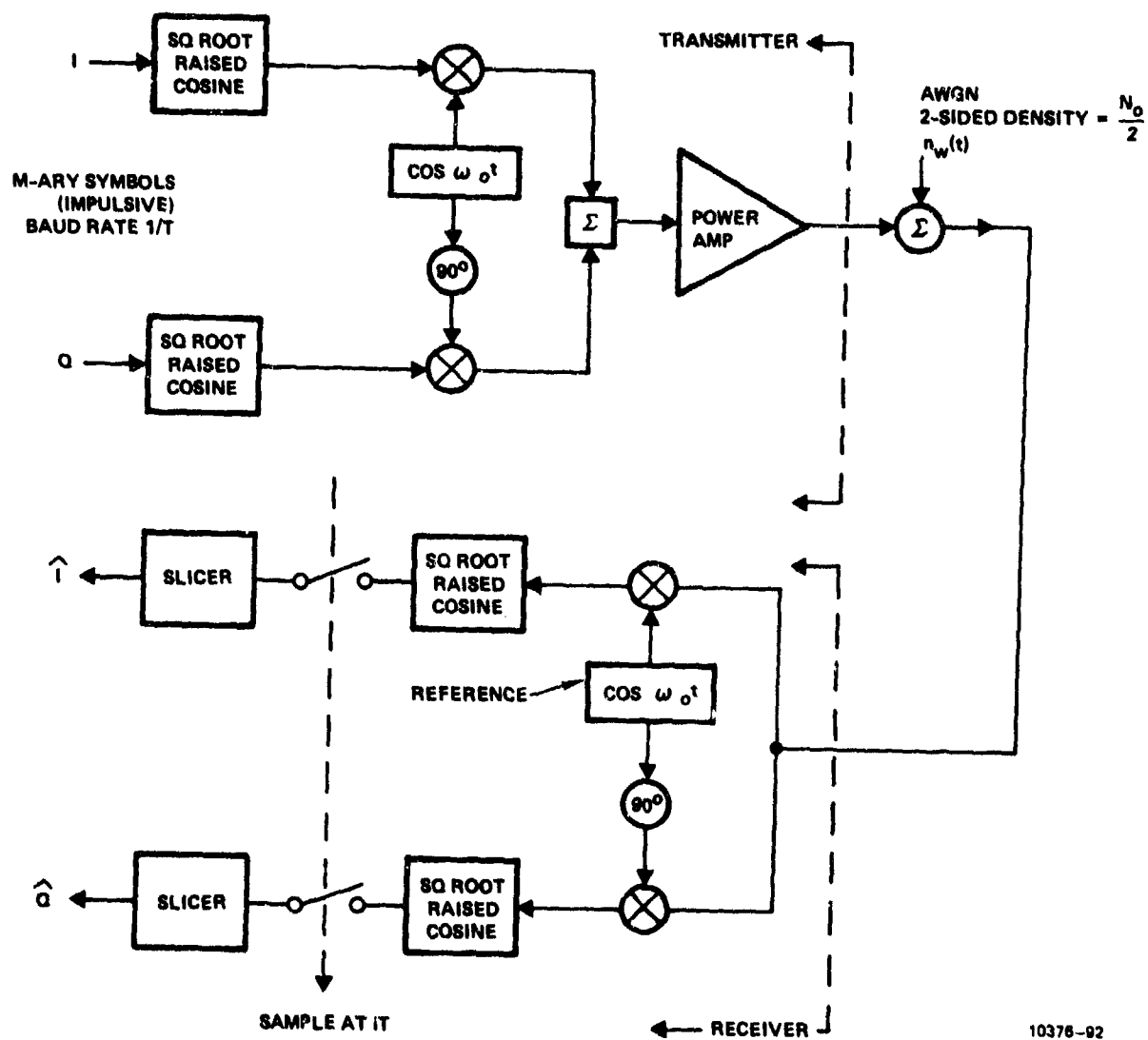
A computer program was written to evaluate the performance of filtered M-QAM systems used with the Ford linear amplifier for which the AM/AM and AM/PM characteristics were given in Figures 6.7-2 through 6.7-4 of the previous section.

The system modeled is shown in Figure 6.7.2-1. The square root raised cosine baseband filters shown at transmitter and receiver would combine to provide Nyquist signalling from baseband input to baseband output if the power amplifier were truly linear. With nonlinearity in the power amp, there will in general be distortion of the PAM eye pattern and degradation will be incurred. The question here was how much degradation is incurred for M-ary signalling on quadrature carriers with an amplifier having the distortion characteristics of the Ford power amplifier? The results shown in Figure 6.7.2-2 and 6.7.2-3 provide the answer for 4-ary PAM on each quadrature channel (4-QAM). Here, the symbol error rate is plotted versus E_p/N_0 where E_p is the peak energy in a transmitted symbol. The parameter on the curves is the backoff in dB of output power from the Ford amplifier. Reference point for 0 dB backoff corresponds to an output peak power of 35.6 dBm (input = 0 dBm) for this amplifier, which is 2.5 dB below saturation output power.

NOTE

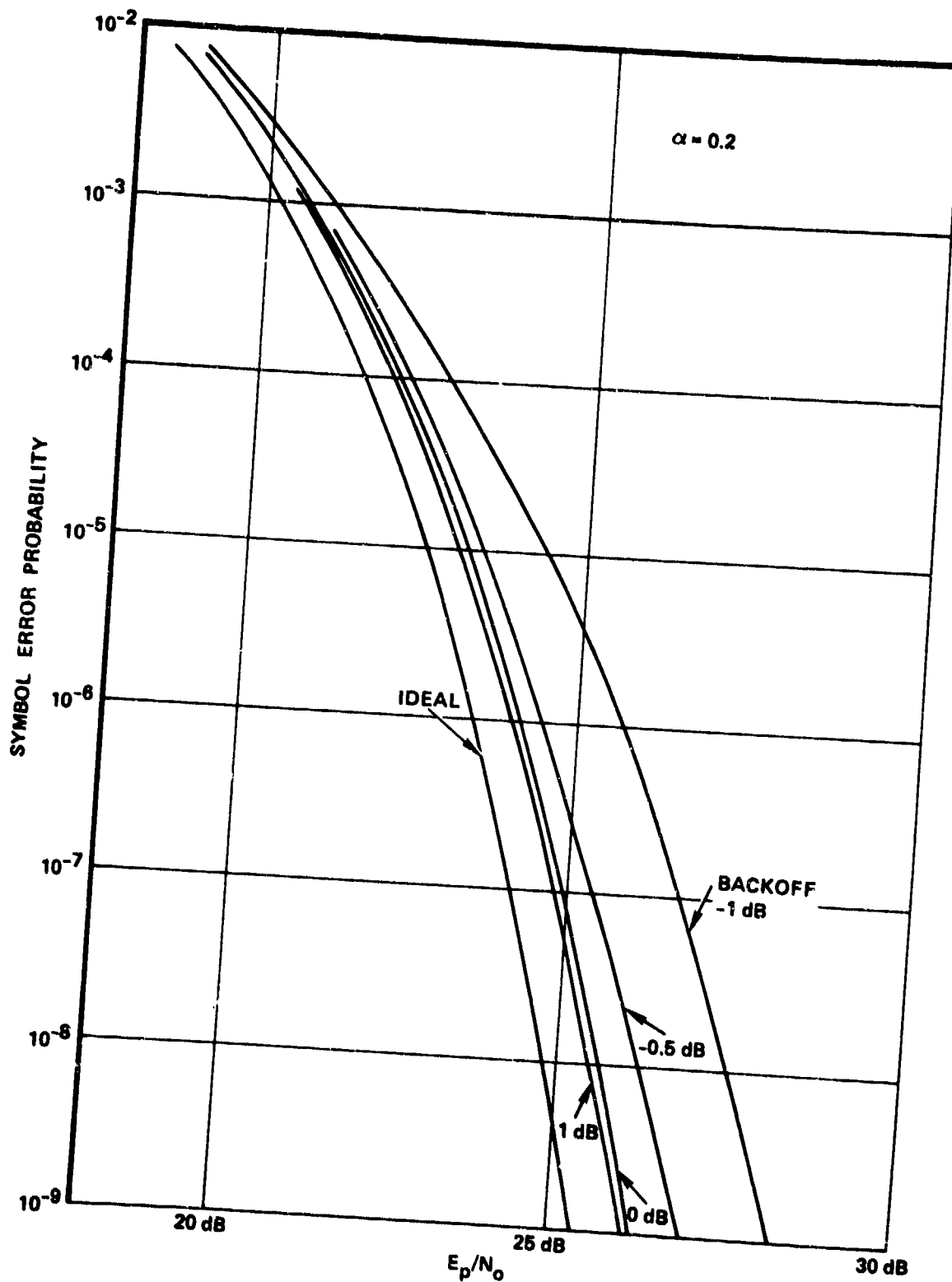
Positive dB backoff indicates reduction in output peak power from this reference level.

These curves show that the amplifier degrades the performance of 4-ary QAM by roughly 0.6 dB for reasonable backoff. There appears to be a plateau in performance as the output power is backed off. Apparently this is due to the plateau in intermod distortion at the -31 dB level noted in measurements on the Ford amplifier (see Figure 6.7-1, preceding section).



10376-92

Figure 6.7.2-1. Modelled System
6-129



10376-93

Figure 6.7.2-2. 4-ary QAM Ford Linear AMP

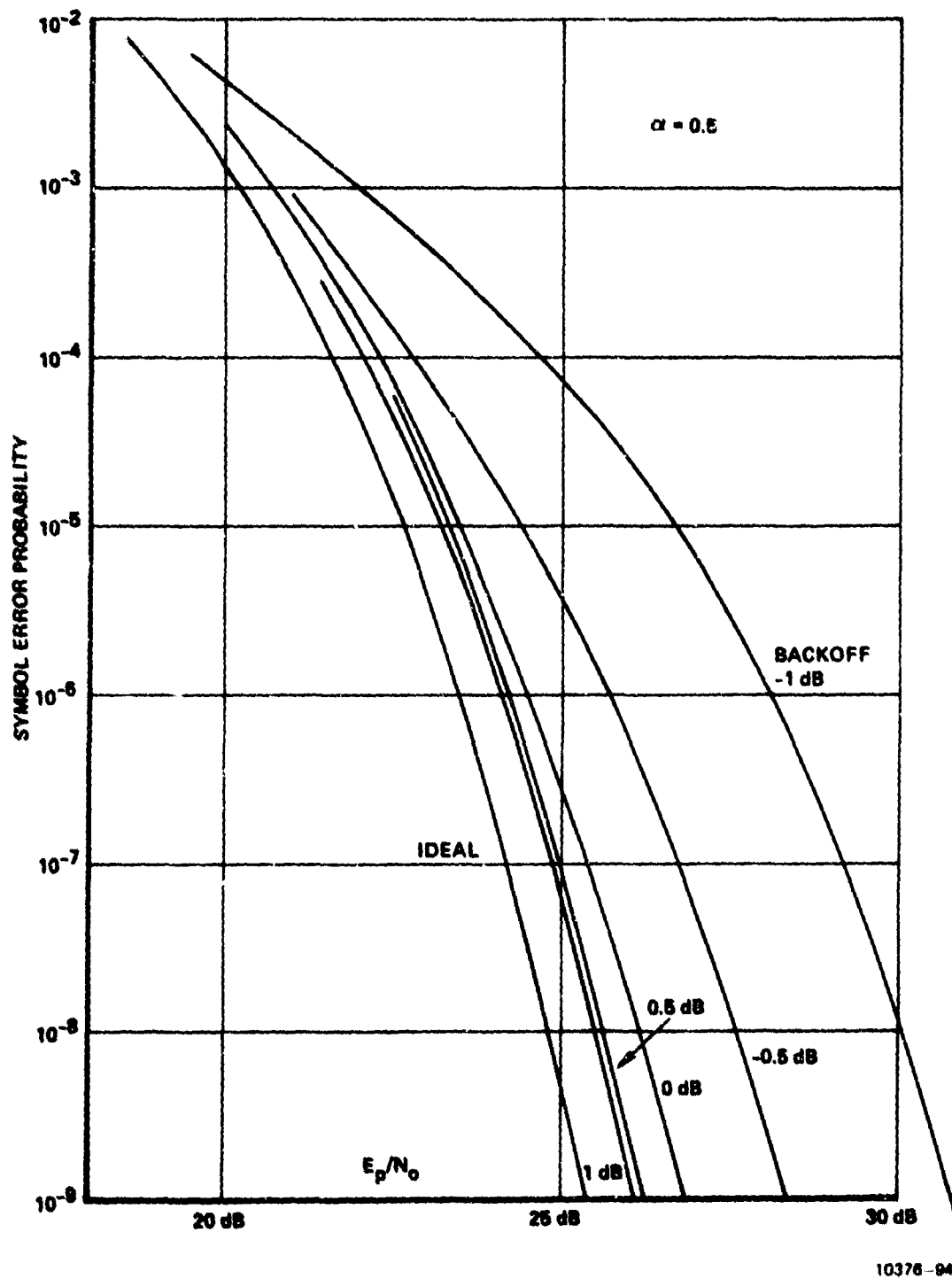


Figure 6.7.2-3. 4-ary Ford Linear AMP

The curves of Figures 6.7.2-2 and 6.7.2-3 do not convey the whole story from the system margin viewpoint in performance comparisons. That is, it is not necessarily desirable to closely approach the ideal performance curve if in order to do so the amplifier has to be backed off excessively. From the system margin viewpoint, it is better to use BE_p/N_0 as the performance measure, where B is amplifier backoff. This measure accounts for the dB loss due to amplifier backoff as well as the E_p/N_0 for a given error rate by appropriate choice of B. The data for doing this is plotted in Figures 6.7.2-4 and 6.7.2-5 for error rates 10^{-9} , 10^{-7} , and 10^{-5} . In all cases the optimum backoff point is within ± 0.5 dB of 0 dB backoff.

Figure 6.7.2-6 shows the behavior of BE_p/N_0 for constant 10^{-7} error rate versus backoff for a range of α rolloff factors from 0.2 to 1.0. As shown, the optimum backoff point increases as α increases - due primarily, it is believed, to the higher instantaneous peak-to-total pulse energy in the shaping filter pulses themselves as α increases.

For more than about 1 dB peak signal energy backoff, the curves for the various α merge, indicating essentially linear operation of the amplifier as far as 4-QAM signaling is concerned, with no difference in performance depending upon details of the Nyquist pulse shape.

For all the different α , Figure 6.7.2-6 shows that 0 dB backoff represents a near-optimum choice with the Ford linear amplifier. As mentioned previously, the reference for 0 dB backoff used here is actually 2.5 dB below saturated power output. 0 dB backoff means - in reference to Figure 6.7-2, showing the power transfer curve for the amplifier - that the peak pulse energy into the amplifier is at the 0 dBm level. The peak output power is at 35.6 dBm which is 2.5 dB below saturated power of 38.1 dBm.

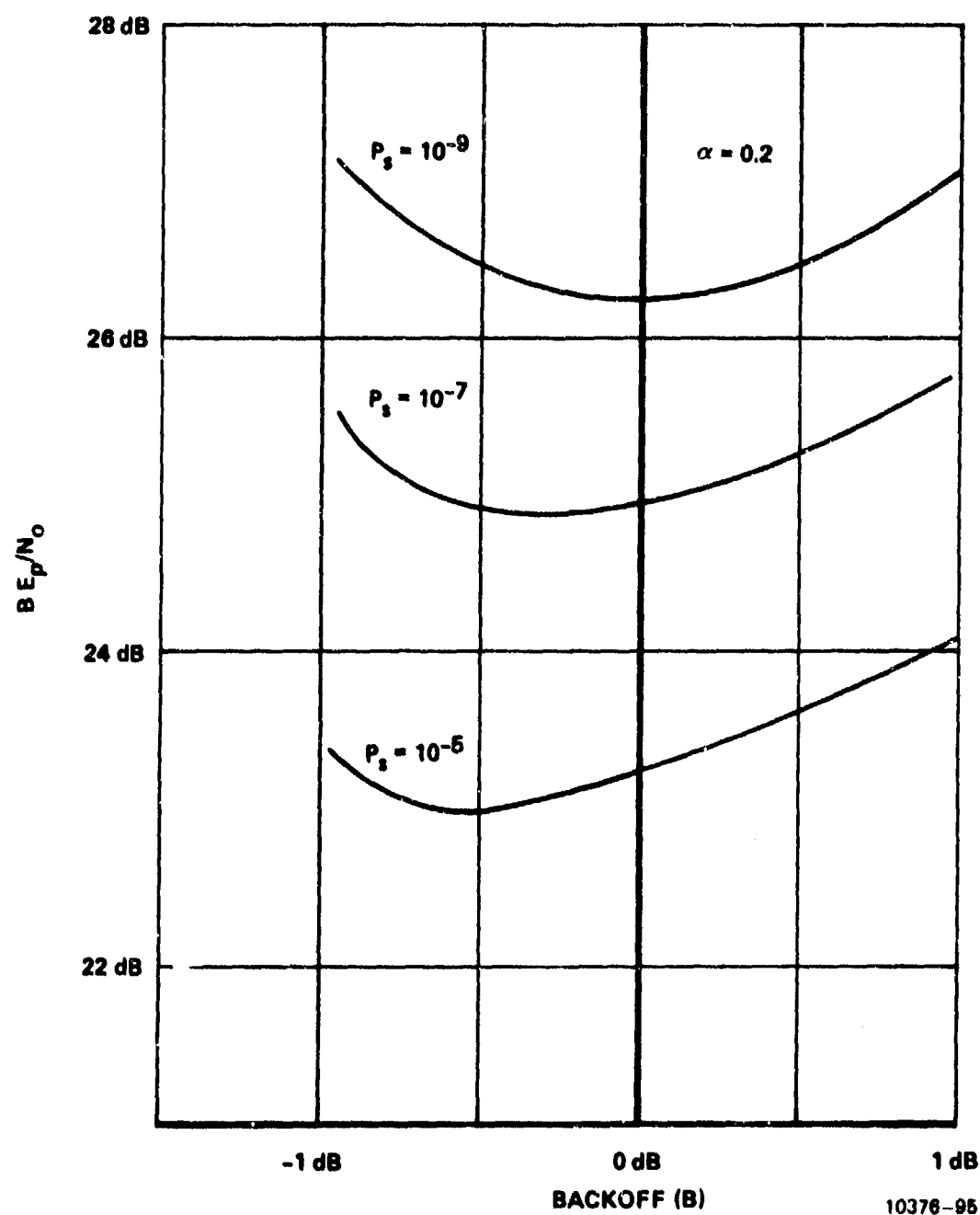


Figure 6.7.2-4. 4-ary QAM Ford Linear AMP

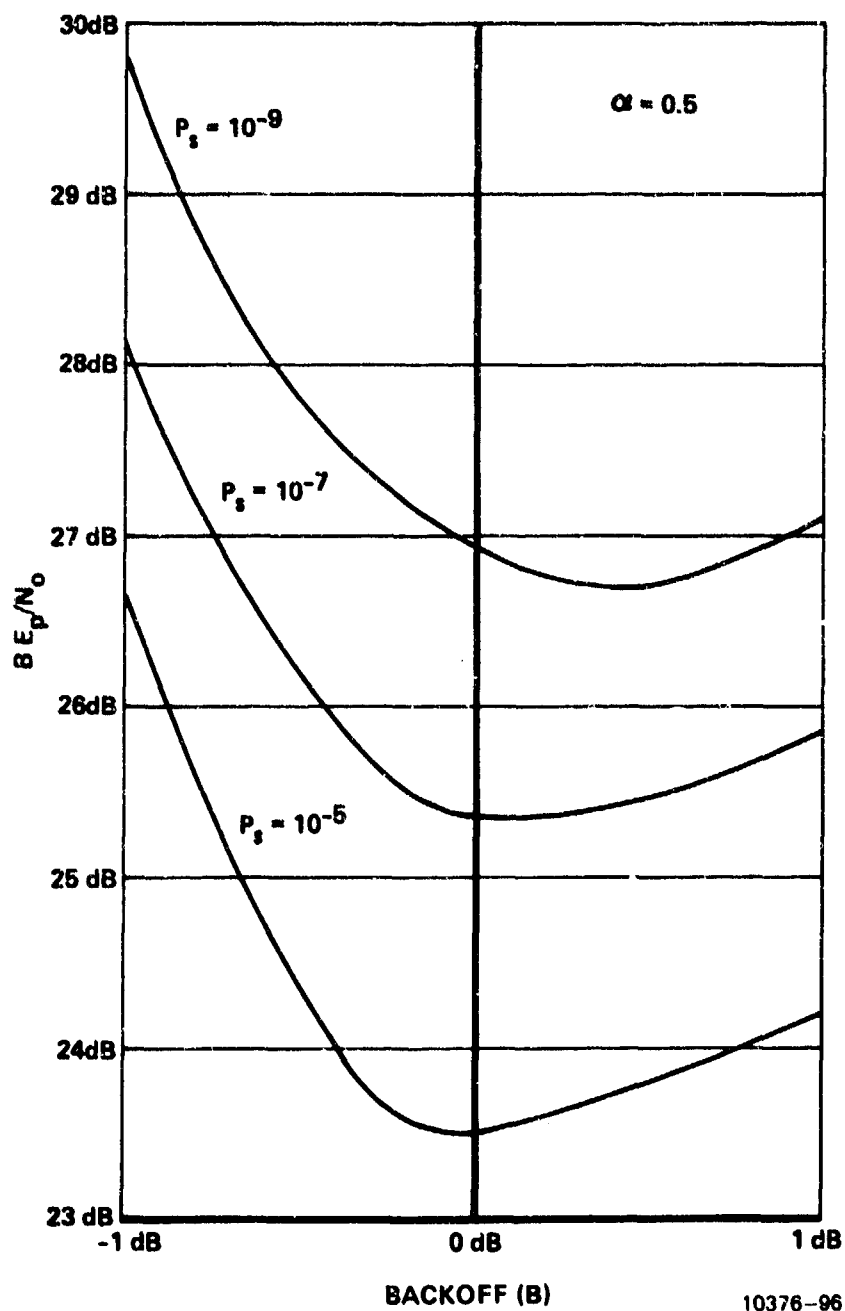


Figure 6.7.2-5. 4-ary QAM Ford Linear AMP

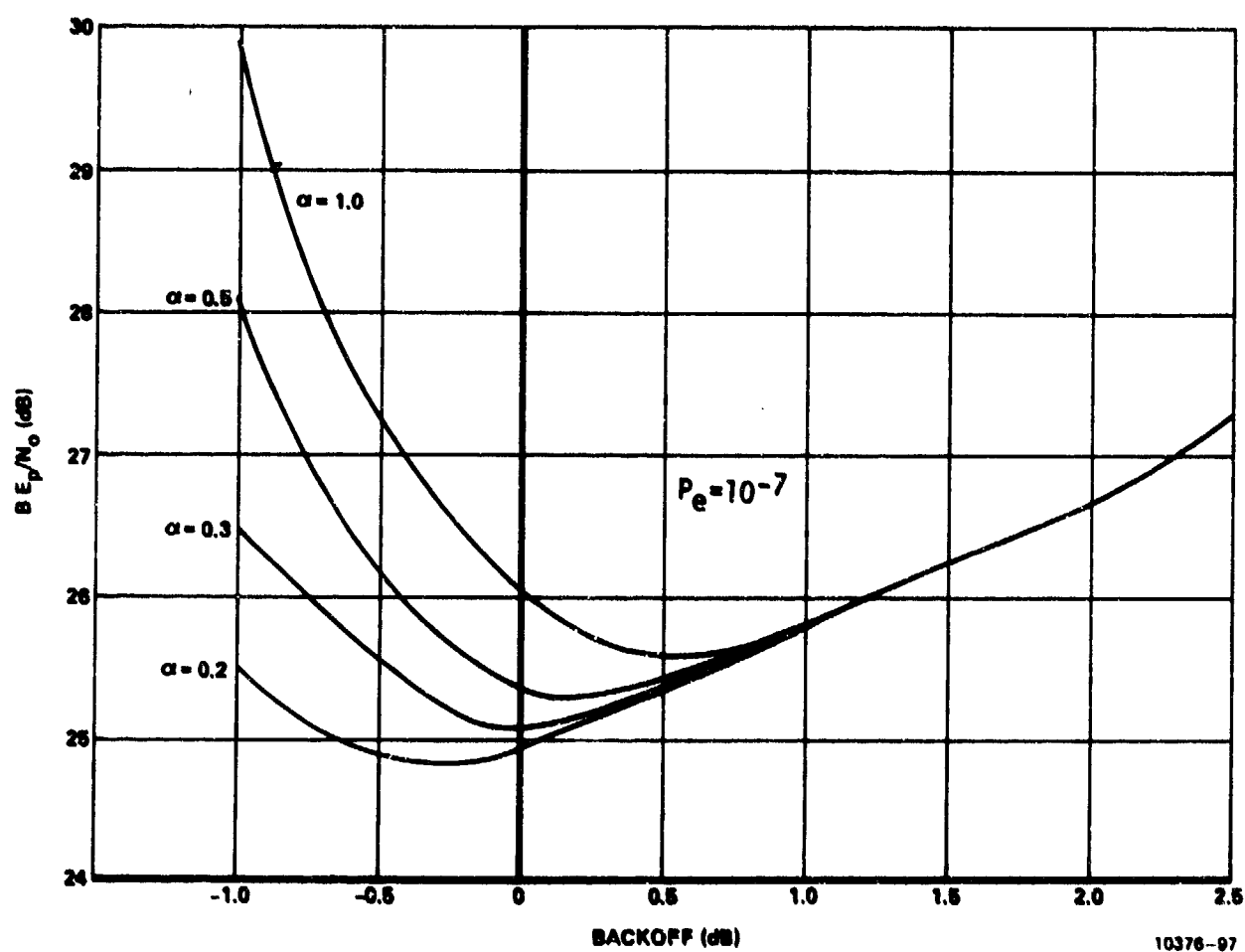


Figure 6.7.2-6. 4-ary QAM - Ford Linear AMP

Figures 6.7.2-7 through 6.7.2-9 show the results obtained using 8-QAM with the amplifier. The backoff parameter, B , employed in the figures represents backoff in peak output pulse power from the Ford amplifier. Reference point for 0 dB again corresponds to an output peak power of 35.6 dBm (input = 0 dBm) for this amplifier. This output power reference level is approximately 2.5 below single signal saturation which occurs at 38.1 dBm. Positive dB backoff again indicates reduction in output power.

Figure 6.7.2-7 shows the symbol error rate obtained versus E_p/N_0 where E_p is peak energy in a transmitted symbol. Backoff is 0 db. The filter with rolloff parameter $\alpha = 0.5$ is best. Evidently, the steeper rolloff filters with $\alpha = 0.2$ and 0.3 have impulse responses which last sufficiently long to cause severe distortion through the nonlinear amplifier in this 0 dB backoff case. The $\alpha = 1$ filter impulse response decays rapidly but the ratio of instantaneous peak to average pulse energy is higher and these peaks are apparently large enough to push the amplifiers into a severe distortion region, causing large degradation. The filter with $\alpha = 0.5$ evidently represents a good compromise between intersymbol interference due to duration of impulse response and distortion created by instantaneous peaks in the pulse shape. The $\alpha = 0.5$ filter provides operation which is 3 dB degraded relative to ideal at 10^{-7} error rate.

As a point of reference, we note here that the average signal-to-noise ratio (E_s/N_0) is 3.7 dB less than the quantity E_p/N_0 plotted in the figures. Also, average receiver E_b/N_0 is approximately 11.5 dB less than E_p/N_0 . For example, in Figure 6.7.2-7, the $\alpha = 0.5$ filter requires average E_b/N_0 for 10^{-9} error rate of $36.5 - 11.5 = 25$ dB E_b/N_0 .

Figure 6.7.2-8 shows the performance available for the various rolloff parameters with 1 dB of backoff from reference output peak power. As can be seen by comparing Figure 6.7.2-8 with Figure 6.7.2-7,

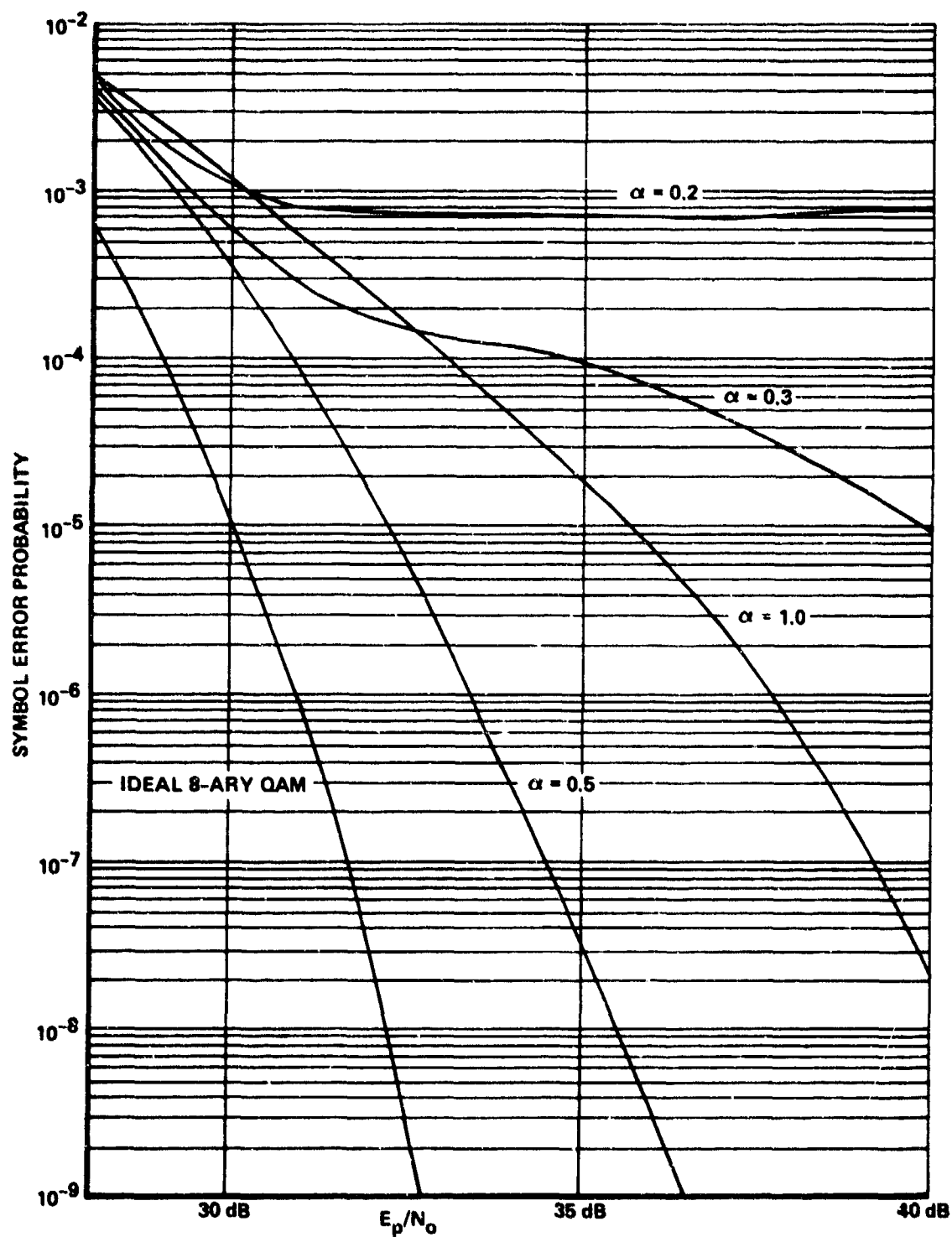


Figure 6.7.2-7. Ford Linear AMP 8-QAM 0 dB Backoff

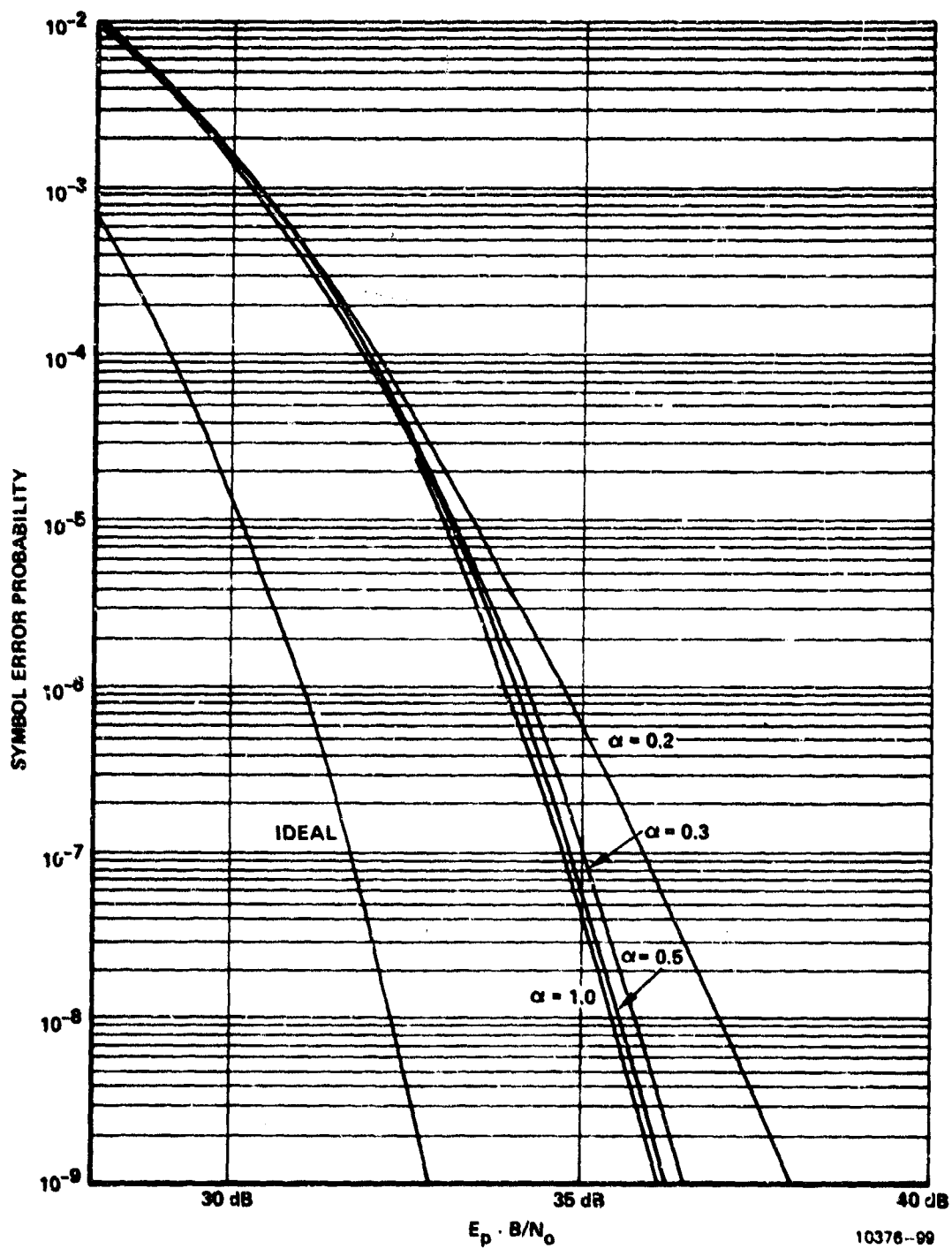
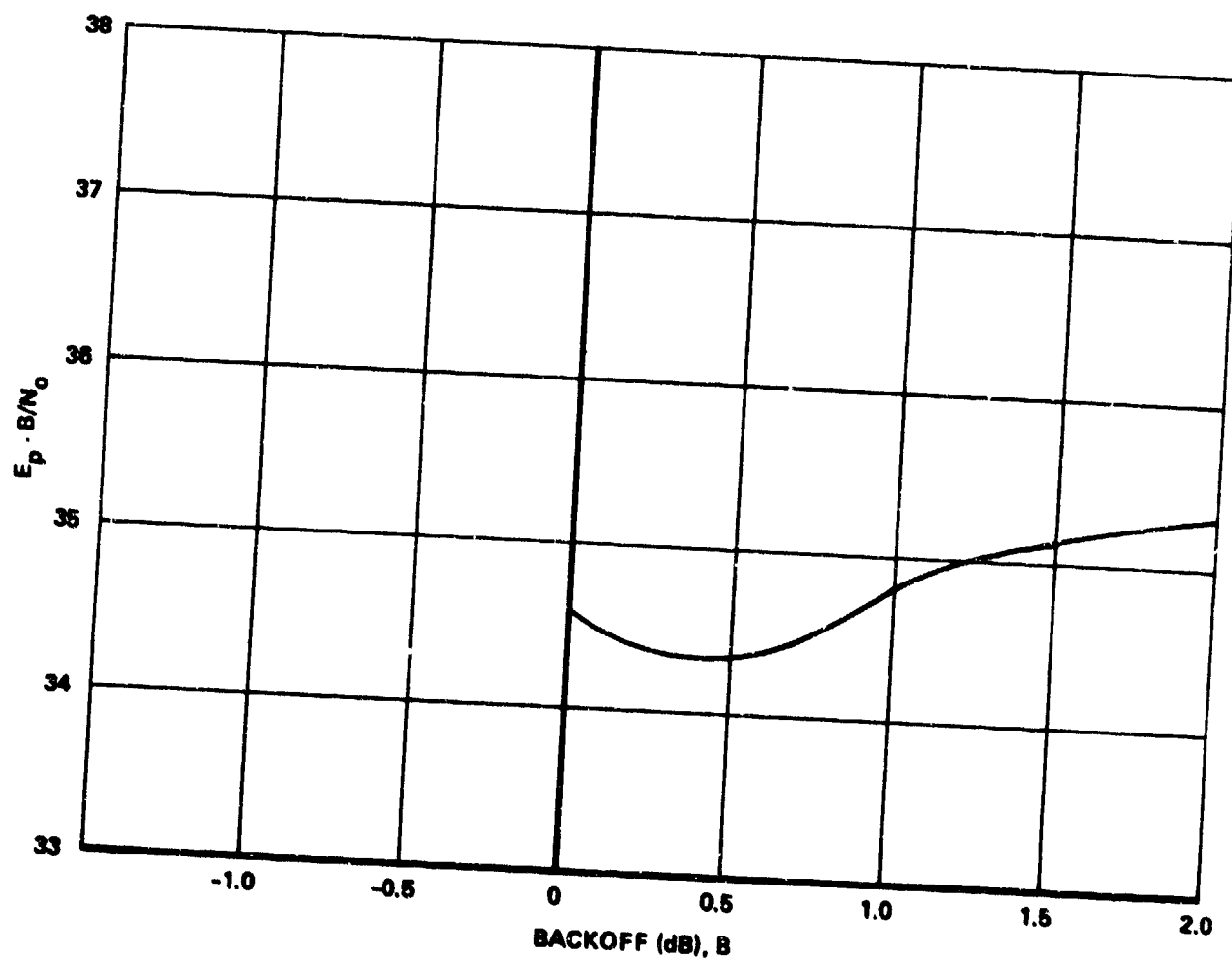


Figure 5.7.2-8. 8-QAM With Ford AMP 1 dB Backoff



10376-100

Figure 6.7.2-9. Power Versus Backoff for 10^{-7} , 8-QAM, $\alpha = 0.5$

the performance, with the fast rolloff (small α) filters, has been dramatically improved by backing the amplifier down this additional 1 dB. The performance in Figure 6.7.2-8 is actually within about 2.2 dB of theoretical on the basis of receiver E_b/N_0 (the curve in Figure 6.7.2-8 shows 3.2 dB degradation relative to ideal since the 1 dB loss in system margin due to backoff has been added to the plotted signal-to-noise ratio).

Figure 6.7.2-9 shows the system $E_p B/N_0$, where B is backoff, necessary to achieve 10^{-7} symbol error rate for an $\alpha = 0.5$ shaping filter. The best backoff point is seen to be at 0.5 dB less than reference peak power.

6.7.3 Comparison Between Butterworth Waveguide Filtering and Baseband Filtering When the Ford Linear Amplifier Is Used

Here, we compare on a peak power basis, the performance obtained with 5-pole Butterworth waveguide filtering of square pulse M-QAM followed by receiver equalization and the performance obtained with baseband square root raised-cosine filtered M-QAM using the Ford linear amplifier.

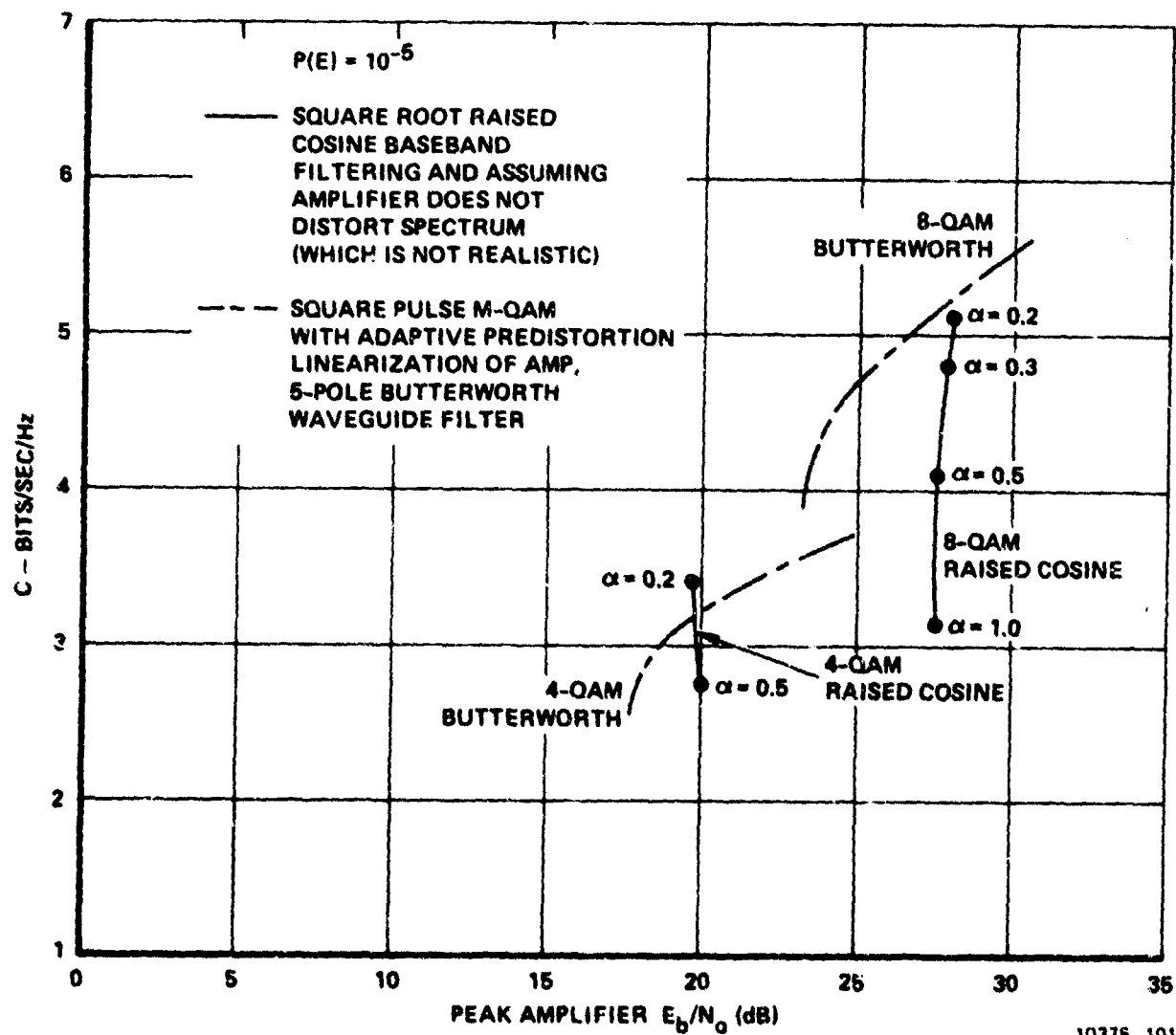
With the square pulse M-QAM, scheme, we assume that the adaptive predistortion scheme to be described in Paragraph 6.8 is used to truly linearize the amplifier and allow peak power output at the saturation power level. With the baseband filtering scheme, we assume that the amplifier does not distort the input signal spectrum. The amplifier does, of course, distort the spectrum and in a practical scheme, either additional waveguide filtering would be required to reduce the distortion-caused spectral side lobes to comply with FCC 19311, or additional power amplifier backoff would have to be employed. This spectral distortion is discussed further in Paragraph 6.8.4.3. Because of the assumption that the amplifier does not distort the spectrum in the baseband-filtered case, the curves plotted here for this case are somewhat optimistic from a practical viewpoint.

The curves for the Butterworth filtered case are taken from Figure 6.6.2-2 given previously. The curves for the baseband filtered case are taken from the error rate versus E_p/N_0 curves plotted in the previous section. In the baseband filtered case, 4-QAM with 0 dB backoff from reference power is used, and with 8-QAM, 1 dB backoff from reference power is used. For the baseband filter case, the parameter, E_p/N_0 , is converted to peak amplifier E_b/N_0 by deducting $10 \log_{10}$ (bits/symbol) from the parameter E_p/N_0 used in the previous section. Thus, 7.8 dB must be subtracted for 8-QAM since there are 6 bits/symbol, and 6 dB must be subtracted for 4-QAM which carries 4 bits/symbol.

Since the amplifier reference output power at "0 dB" backoff in the previous section is actually 2.5 dB below saturated output power, we must in addition add 2.5 dB to the baseband filtered results for comparison with the square pulse M-QAM scheme capable of running at saturation on peaks. The overall correction to the baseband filtered results in terms of BE_p/N_0 for 8-QAM is, therefore, $-7.8 + 2.5 = -5.3$ dB and for 4-QAM is $-6 + 2.5 = -3.5$ dB.

The comparisons for the Butterworth waveguide and the baseband filtered cases are shown in Figure 6.7.3 for symbol error probability = 10^{-5} . As seen in Figure 6.7.3, for 4-QAM signaling at 3 bits/sec/Hz, the Butterworth waveguide filter technique is a little more than 1 dB better than the baseband filter technique. For 8-QAM, the improvement of the Butterworth waveguide technique over the baseband filter technique is more dramatic in the region of 4 to 5 bits-sec-Hz. For example, at 4.5 bits/sec/Hz, the waveguide filter scheme is about 3.5 dB better than the baseband filter scheme.

From the results presented in Figure 6.7.3, we conclude that the waveguide filtered approach offers a significant advantage over the baseband filtered approach in terms of the efficiency of using the Ford linear amplifier peak power output capability. This conclusion is even



10376-101

Figure 6.7.3. Comparison Between M-QAM Schemes Using Ford
Linear AMP $P(E) = 10^{-5}$

more strongly reinforced when one considers that the spectral distortion created by the amplifier still must be reckoned with in the baseband filtered case. That is, for the baseband filter case, FCC Docket 19311 spectral compliance will not be obtained without further amplifier backoff (hence, loss in system margin) or installment of a waveguide filter (hence, loss in system margin due to performance degradation).

As a result of the foregoing comparisons, we have concluded that even the capabilities of an amplifier carefully designed to provide "linear" operation are more efficiently exploited by the use of square pulse M-QAM using the adaptive predistortion amplifier linearization scheme (to be described in the following section). The power and desirability of the adaptive linearization scheme is further enhanced when we consider that even TWT's with their severe AM/AM and AM/PM conversion characteristics can be used as if they were truly linear amplifiers. The development of the adaptive linearization scheme to be described essentially removes the requirement that extremely linear amplifiers be developed for digital microwave signalling - even for the high spectral efficiency regions of capacity where the multi-amplitude signalling formats are required for maximum power efficiency. We now turn to a description of this adaptive linearization technique.

6.8 Adaptive Predistortion Linearization of Power Amplifiers for Digital Signaling

6.8.1 Introduction

The primary impediment to reliable spectrally-efficient digital signaling through microwave power amplifiers is the distortion produced by such amplifiers. This distortion arises as a direct result of the widely known AM/AM and AM/PM conversion characteristics of such power amplifiers.³¹⁻³³ The AM/AM characteristic is usually displayed by plotting power output versus power input and shows the nonlinear manner in which sinusoidal amplitude output depends upon sinusoidal amplitude input. The AM/PM characteristic is usually displayed by plotting the phase shift incurred in passing a sinusoid through the amplifier versus the input sinusoid power. A typical set of AM/AM and AM/PM characteristics for a TWT amplifier is shown in Figure 6.8.1.

These curves are ordinarily used in computer simulations to determine effects produced by the nonideal amplifier by simply determining the instantaneous input amplitude and from this input determining the instantaneous output amplitude and instantaneous phase shift to provide an instantaneous output amplitude and phase. These types of computer models imply that the nonlinearities produced by the amplifier are memoryless operations. Computer simulations based upon this model are justified in that they produce predictions matched well to experiment.

We note that if the input signal is of constant envelope, there is no distortion produced by the amplifier since the nonlinearities depend upon amplitude fluctuations to produce distortion. Thus, with digital modulation one could entirely avoid the problems created by microwave amplifier distortion by using only constant envelope signal designs such as unfiltered PSK or FSK. However, as pointed out in prior sections, such signal designs generally require a good deal more signal-to-noise ratio for a given level of performance than signal designs that also use amplitude as a degree of freedom. The performance disparity between constant and nonconstant amplitude signals becomes greater as the number of bits/sec/Hz is increased.

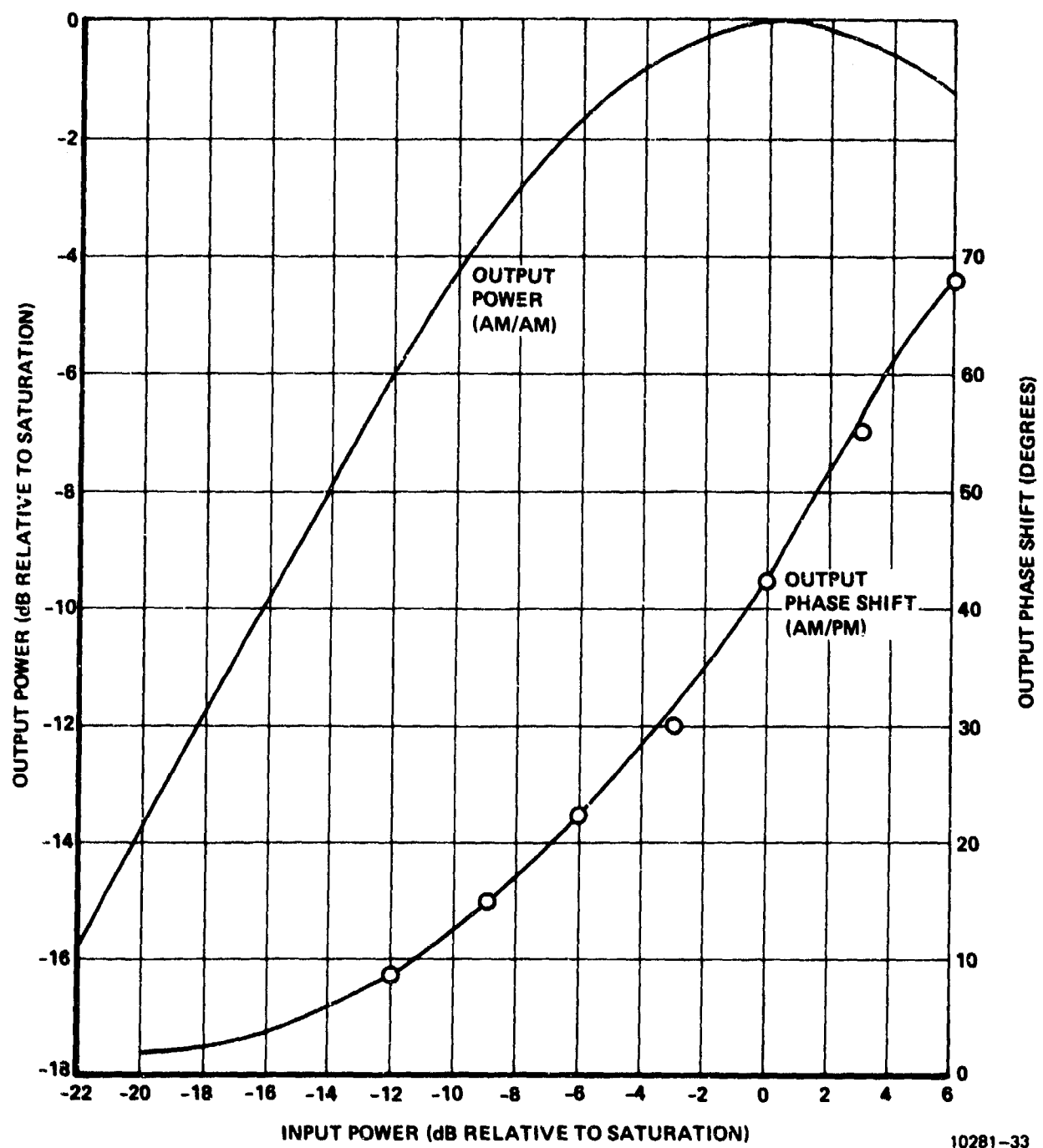


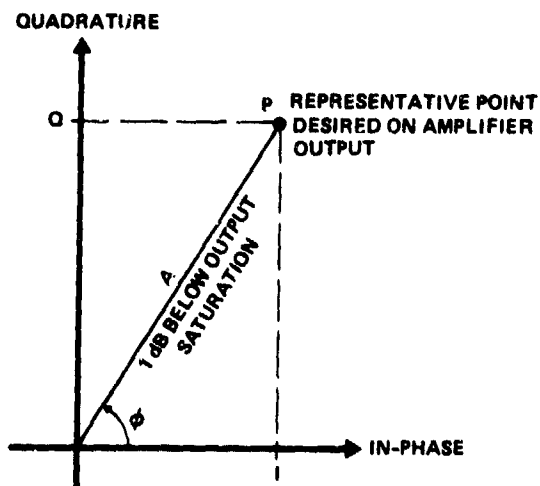
Figure 6.8.1. Model Nonlinear TWT Amplifier Input-Output Characteristics

Therefore, if one is to obtain the performance efficiency of nonconstant amplitude signal designs, the AM/AM and AM/PM distortions must be reckoned with. One brute force technique for reducing the effects of such distortion is to reduce the drive level into the amplifier such that the amplifier output power is considerably below saturation (power amplifier backoff) where the magnitudes of the distortions are tolerable. This technique is a valid and valuable one that has been widely employed with TWT amplifiers. However, this technique loses a great deal of its appeal if the amplifier has to be backed off excessively to obtain acceptable distortion levels since every dB of backoff is a dB lost in link margin. For the spectral efficiencies of interest in this study, acceptable distortion levels are generally in the 35 to 50 dB down region and in order to obtain these distortion levels, the amplifier generally has to be backed off excessively.

In the remainder of this section, we describe a technique that allows one to use multi-amplitude signaling schemes with microwave amplifiers by adapting to the nonlinearities present in the amplifier without resorting to the technique of power output backoff. We will show that the scheme is effective with even the severe AM/AM and AM/PM conversion characteristics of TWT amplifiers.

6.8.2 The Effect of AM/AM and AM/PM Conversion

Figure 6.8.2-1 shows a representative signal space point, P, to be transmitted in a digital modulation format. The point is located



10281-23

Figure 6.8.2-1. A Representative Digital Modulation Signal Point
6-146

by its amplitude A , and its relative phase, ϕ , in the two-dimensional signal space. Alternatively, it is located by its inphase component, I , and its quadrature component, Q . For the purpose of this example, let us suppose that this point is to be produced on the output of an amplifier having the AM/AM and AM/PM characteristics shown in Figure 6.8.1. Further, suppose that we desire that the output amplitude from the amplifier be 1 dB below saturation when this signal point is produced. From the AM/AM curve of Figure 6.8.1 we find that the input amplitude required for this to occur is approximately 4 dB below input saturation. Further, from the AM/PM characteristic of Figure 6.8.1, we note that a signal having input power 4 dB below saturation input incurs $+28^\circ$ of phase shift in passing through the amplifier. Thus, to offset this 28° of phase shift and produce the output point of Figure 6.8.2-1, we must retard the phase of the input signal by 28° . This leads to a "predistorted" input signal as shown in Figure 6.8.2-2. When this signal

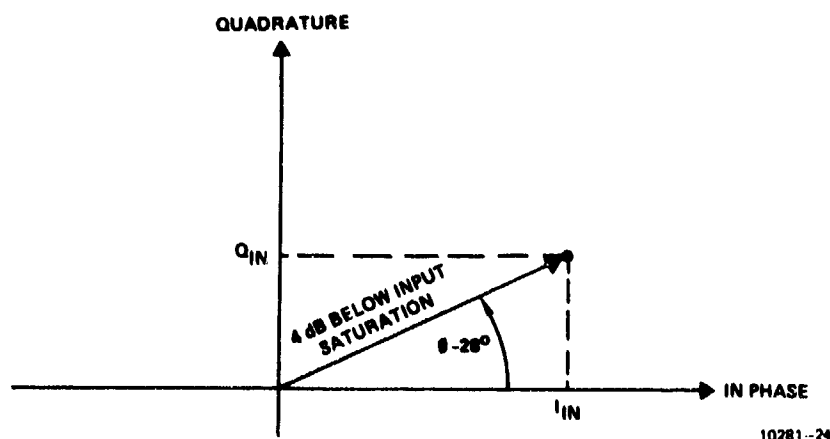


Figure 6.8.2-2. Predistorted Input Signal Point

point is input to the amplifier, the output signal point of Figure 6.8.2-1 is produced. Thus, for this representative digital signal point there exists a combination of input amplitude and phase or - alternatively - an input inphase and quadrature component to have the nonlinear amplifier produce the desired signal in its output.

In a like manner, the required input for each digital signal point in a two-dimensional signal design can be found.

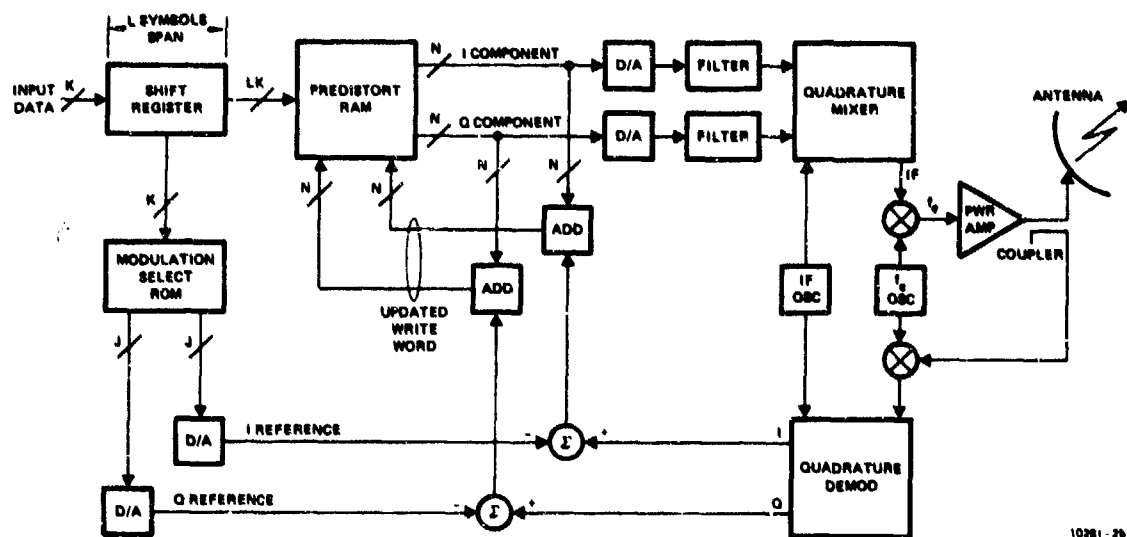
In this manner, by predistorting the input signal space, the output signal space can be rendered free of amplifier distortion at the sampling times.

One means of accomplishing this predistortion would be to simply store fixed distorted input inphase and quadrature components for each of the discrete points in the signal design. Then, as each symbol is chosen at the modulator, the appropriate pair of components could be accessed from a memory. The only problem with such a fixed predistortion scheme is that if the AM/AM and AM/PM amplifier characteristics change, the fixed predistortion is no longer appropriate and severe degradation in performance can result, especially for the multiple bits/sec/Hz signal designs of interest in this study. A scheme that is more attractive from practical standpoints would include a means to adaptively learn the appropriate predistortions to employ with the amplifier - and preferably the adaptation should be of a continuously operating nature in order to track variations in the amplifier characteristics. In the following section a technique for performing such a continuous adaptation is presented.

6.8.3 Implementing an Adaptive Predistortion Digital Modulator

In the previous section we have seen how it is conceptually possible to determine distorted inphase and quadrature components for each digital signal design point to produce undistorted signal points from an amplifier having severely distorting AM/AM and AM/PM characteristics. In this section we show the block diagram for and describe a modulator which accomplishes the predistortion in a continuously adaptive manner.

Figure 6.8.3 shows the basic diagram of an adaptive predistortion modulator developed here at Harris during this study. The technique has the capability of removing both linear and nonlinear distortion effects on the amplifier output at symbol rate sampling times. These distortion effects are caused by power amplifier AM/AM and AM/PM conversion and system filtering.



10261-26 A

Figure 6.8.3. Adaptive Power Amplifier Linearization Scheme for Digital AM/PM Modulator

The quadrature components at the power amplifier output at symbol times are forced, by adaptive predistortion of the input signal, to reproduce any desired points in the two-dimensional output signal space.

As shown in Figure 6.8.3, K data bits are input each symbol time. The K data bits are used to access two J -bit words in a "Modulation Select Read-Only Memory" (ROM). These two words are programmed into the ROM to indicate the two desired quadrature components for the selected digital modulation signal format. These words are D/A'd to form an inphase (I) and quadrature (Q) reference voltage with which to compare the respective components produced on the output of the amplifier. The error signals produced from the comparisons are used to update digital words stored in the "Predistortion Random Access Memory (RAM)" in such a direction as to reduce the error.

As displayed in Figure 6.8.3 a sliding L -symbol span of data bits (for a total of LK bits) are used to access the Predistort RAM for an N -bit inphase component word and an N -bit quadrature component word each symbol time. There are reasons, which we discuss later, why L should be one symbol long (not the least of the reasons is the required Predistort RAM size). The L -span is shown in Figure 6.8.3 primarily for the sake of completeness. If there are memoryful linear distortions occurring due to system filtering, L has to be longer than one in general, but we argue later for not doing significant system filtering prior to the signal coupler following the power amplifier. When such filtering is not included, L need be only one to remove the essentially memoryless AM/AM and AM/PM conversion nonlinearities.

The accessed N -bit quadrature component words are then D/A'd and passed to a quadrature mixer which upconverts the two components with inphase and quadrature IF oscillator signals and then sums the two mixer outputs. This produces the modulator IF interface signal to the microwave radio. The IF signal is then upconverted by mixing with a microwave oscillator and the resultant signal is subsequently amplified

by the power amplifier for transmission. A small amount of the signal from the power amplifier is coupled off by a directional coupler and is coherently downconverted to IF by mixing with the same oscillator that performed the upconversion from IF to microwave. This IF signal is further coherently downconverted from IF to baseband I and Q components by mixing with the quadrature components of the IF oscillator originally used to upconvert from baseband to IF in the forward signal path. As a result of these coherent up/down conversions, we have produced I and Q components occurring on the amplifier output. These components are compared against the reference I and Q components to determine error signals which are then used to force the words stored in the Predistort RAM to move toward values which result in no error.

In the steady state, the words stored in the Predistort RAM will be such that each K-bit RF symbol desired will be produced with no distortion at the output of the power amplifier. The possibility is thus provided for employing amplifiers with very poor AM/AM and AM/PM conversion characteristics with peak input drive levels near saturation without incurring significant performance degradation. Such a scheme would avoid the link margin losses associated with the widespread practice of operating power amplifiers at greatly reduced power levels in order to obtain appropriately low distortion.

A more detailed description of a hardware implementation of the adaptive predistortion modulator is contained in the companion Design Plan document.³⁶

6.8.4 Results Obtained for the Adaptive Predistortion Amplifier Linearization Scheme

6.8.4.1 Introduction

The adaptive predistortion scheme for linearizing a highly nonlinear power amplifier which was presented in the previous section was simulated on a computer during the course of this contract for the purpose of evaluating its potential merit. Its use with two different power amplifiers was simulated. The first amplifier employed was a typical TWT having the AM/AM and AM/PM characteristics shown previously in Figure 6.8.1. This amplifier was used to obtain some feel for the scheme's effectiveness at linearizing severe distortions. The second amplifier used in these simulations was Ford's Linear Amplifier³⁴ which has the AM/AM and AM/PM characteristics previously shown in Figures 6.7-2 and 6.7-3. These latter curves were considered representative of state of the art "linear" microwave amplifier development. They were obtained from the Technical Report, "Experimental Linear Solid State Communications Amplifier," generated by Ford Aerospace and Communications Corporation on a study for Rome Air Development Center (Contract F30602-76-C-0271). This amplifier is the same used in the performance simulations reported in Paragraph 6.7.

6.8.4.2 Signal Space Predistortion Results

The computer program was used to adapt to the TWT amplifier nonlinearity at various levels of peak power output backoff relative to saturated power output. We present some of the results in this section. In these results 4-ary PAM square signalling was employed on each of the quadrature modulator (mixer) inputs in Figure 6.8.3. No baseband or IF filtering is included to spectrally shape the IF signal. After adapting the square pulse quadrature input levels, the output of the power amplifier was found to have the desired 4 x 4 array of square pulse quadrature components shown in Figure 6.8.4.2-1. After adaptation, it

was found that the ideal 4×4 array of quadrature components shown in Figure 6.8.4.2-1 was always obtained - independent of the peak power backoff. The predistorted input quadrature components were, of course, a function of the amount of peak power backoff. Figure 6.8.4.2-2 shows the predistorted input components found necessary by the computer simulation for 0.5 dB peak output power backoff for the TWT amplifier. When these distorted 16 points are passed through the TWT power amplifier, the undistorted 16 points of Figure 6.8.4.2-1 are produced. We note that, with the ideal signalling format of Figure 6.8.4.2-1, there are three discrete amplitude levels. Each of these three amplitude levels experiences a different phase shift in passing through the amplifier as dictated by the AM/PM characteristic of Figure 6.8.1. Similarly, each of the three amplitude levels incurs a different amplitude distortion in passing through the amplifier, as dictated by the AM/AM curve of Figure 6.8.1. Conceptually, then the predistortion points shown in Figure 6.8.4.2-2 represent an adjustment of amplitude for each of the three input amplitude levels to produce linear output amplitude followed by a different phase rotation for each amplitude required to offset the different phase shifts incurred in the amplifier.

For comparison we show in Figure 6.8.4.2-3 the output signal points that would be produced on the TWT amplifier output if predistortion is not employed, for a peak power output backoff of 0.5 dB. Comparing Figure 6.8.4.2-3 with the ideal of Figure 6.8.4.2-1, one can see the rather severe distortion that results when predistortion is not used. The dominant distortive effect displayed in Figure 6.8.4.2-3 is an overall counterclockwise phase rotation of the signal set in comparison with Figure 6.8.4.2-1. But even for a best choice of average signal set phase rotation (which by itself would not degrade performance) rather severe distortion remains.

Figure 6.8.4.2-4 shows the predistorted quadrature inputs necessary to offset TWT amplifier distortion for 0.1 dB of peak power backoff. These distorted components were found by the computer

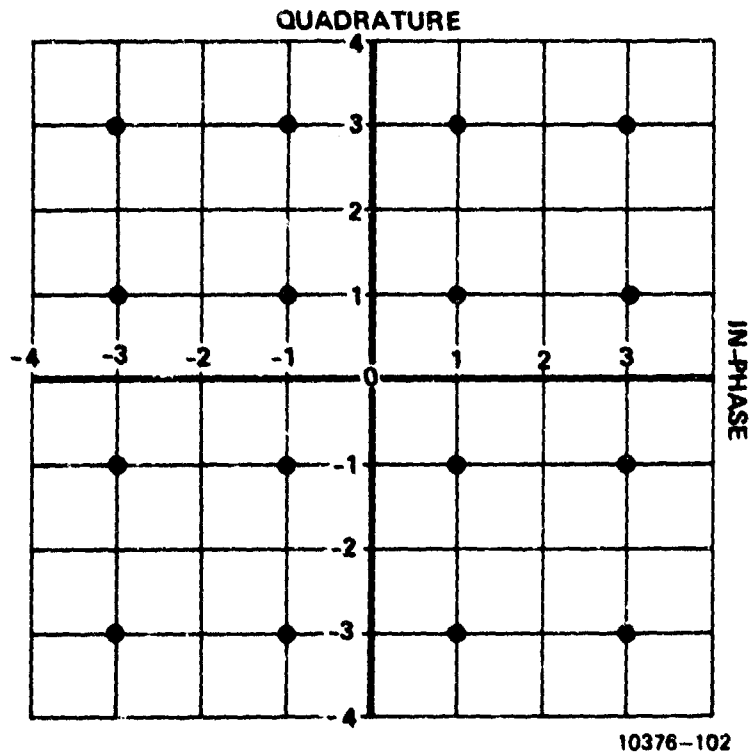
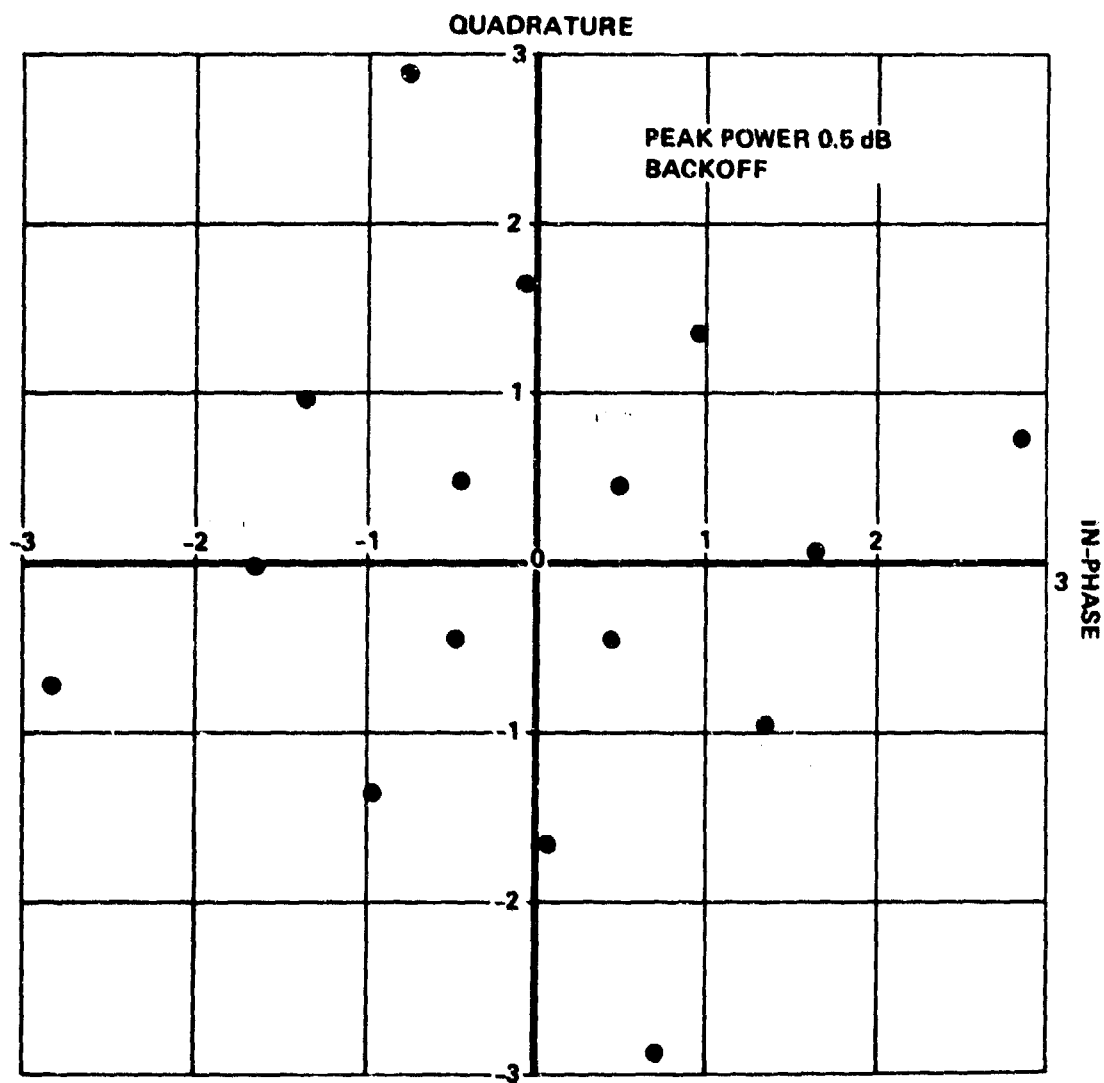
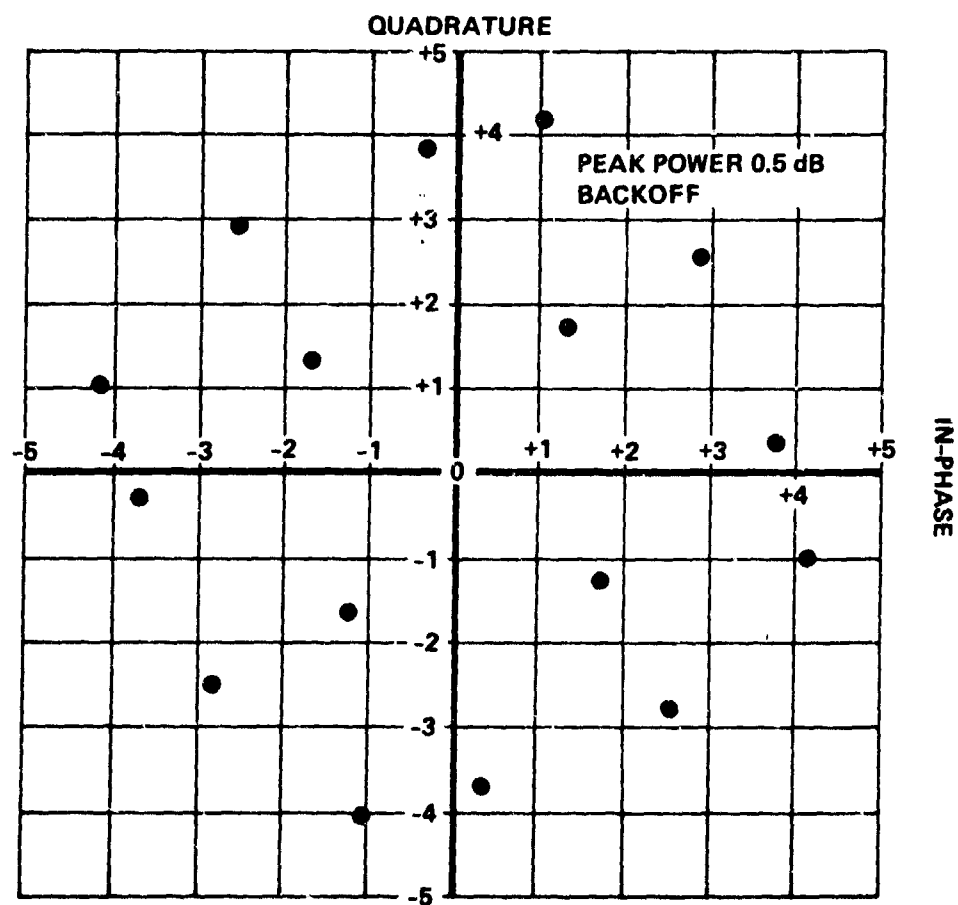


Figure 6.8.4.2-1. TWT Output Signal Points with Predistortion Correction - Arbitrary Peak Power Backoff



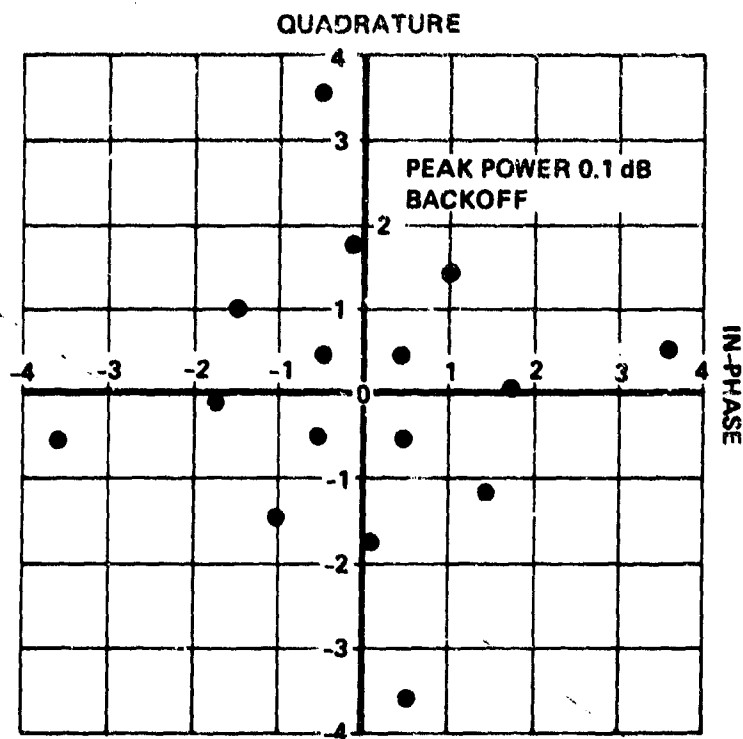
10376-103

Figure 6.8.4.2-2. TWT Predistorted Inputs to Produce No Distortion on Output



10376-104

Figure 6.8.4.2-3. TWT Output Signal Points With
No Predistortion Correction



10376-105

Figure 6.8.4.2-4. TWT Predistorted Input for Zero Output Distortion

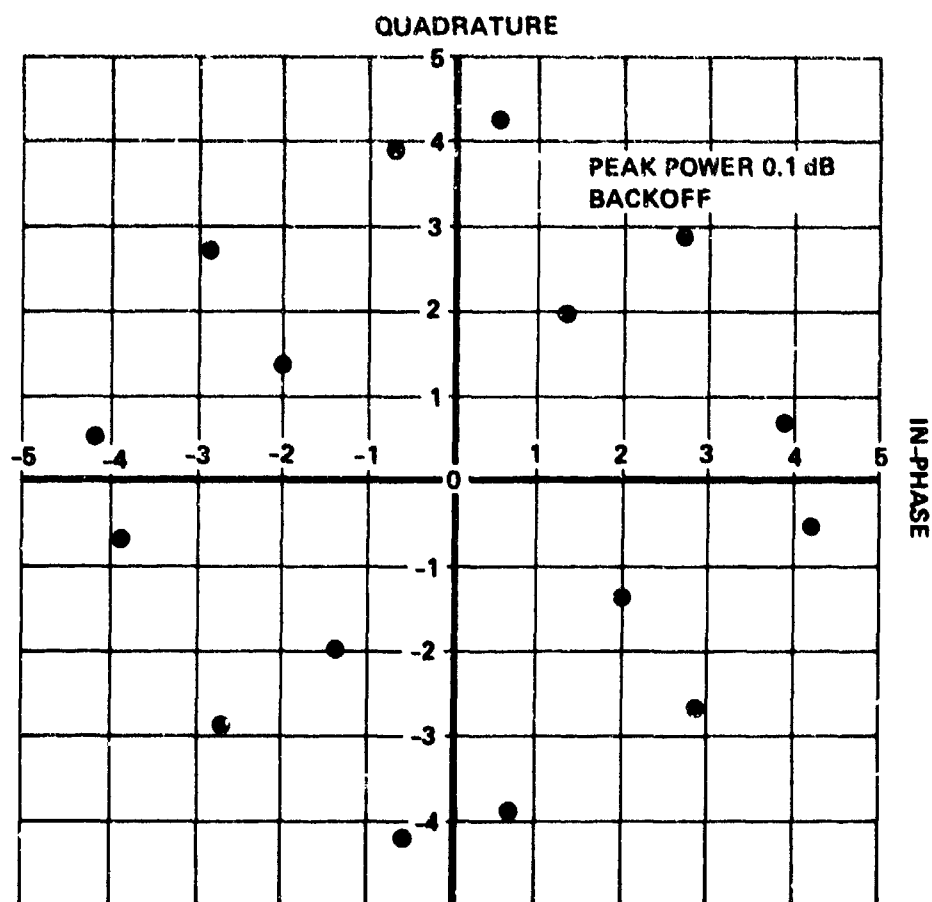
simulation to produce the undistorted components of Figure 6.8.4.2-1. Without the predistortion, the 16 digital signal points of Figure 6.8.4.2-5 would be produced for 0.1 dB backoff. Again, severe distortion is corrected by the predistortion scheme, even for a peak drive level into the TWT amplifier within 0.1 dB of saturation.

Similar results have been obtained using the Ford linear amplifier having the AM/AM and AM/PM conversion characteristics previously shown in Figures 6.7-2 and 6.7-3. That is, near-perfect compensation through the use of adaptive predistortion has been achieved independent of amplifier backoff.

6.8.4.3 Effect of Predistortion on Spectrum

With the ideal output signal points of Figure 6.8.4.2-1, independent of the amplifier backoff, the spectrum produced at the amplifier output with the square pulse signaling used there will be the familiar sinc function spectrum displayed in Figure 6.8.4.3-1. The first side lobe for such a spectrum is only 13 dB below the main lobe and the side lobes reduce at a rate of 6 dB/octave away from the center frequency. Such an amplifier output spectrum will obviously require RF waveguide filtering to reduce the side lobes sufficiently to meet the spectral mask requirements of FCC Docket 19311. Paragraph 6.5.3 details the performance and spectral properties of a signaling scheme involving transmitter filtering of this spectrum to meet FCC 19311 followed by equalization at the receiver to eliminate intersymbol interference created by the transmit filter. This technique has been selected as most desirable for meeting the goals of this study as discussed in Paragraph 6.6.2.

The dependence upon a waveguide filter for spectral containment - while theoretically attractive - has some practical drawbacks that one would like to avoid. Not the least of these drawbacks is the high loaded Q required of these waveguide filters for the 4 and 8 GHz microwave bands of interest in this study - especially for the smallest authorized bandwidth of interest in each band (3.5 MHz for 4 GHz



10376-108

Figure 6.8.4.2-5. TWT Output Signal Points With No Predistortion Correction

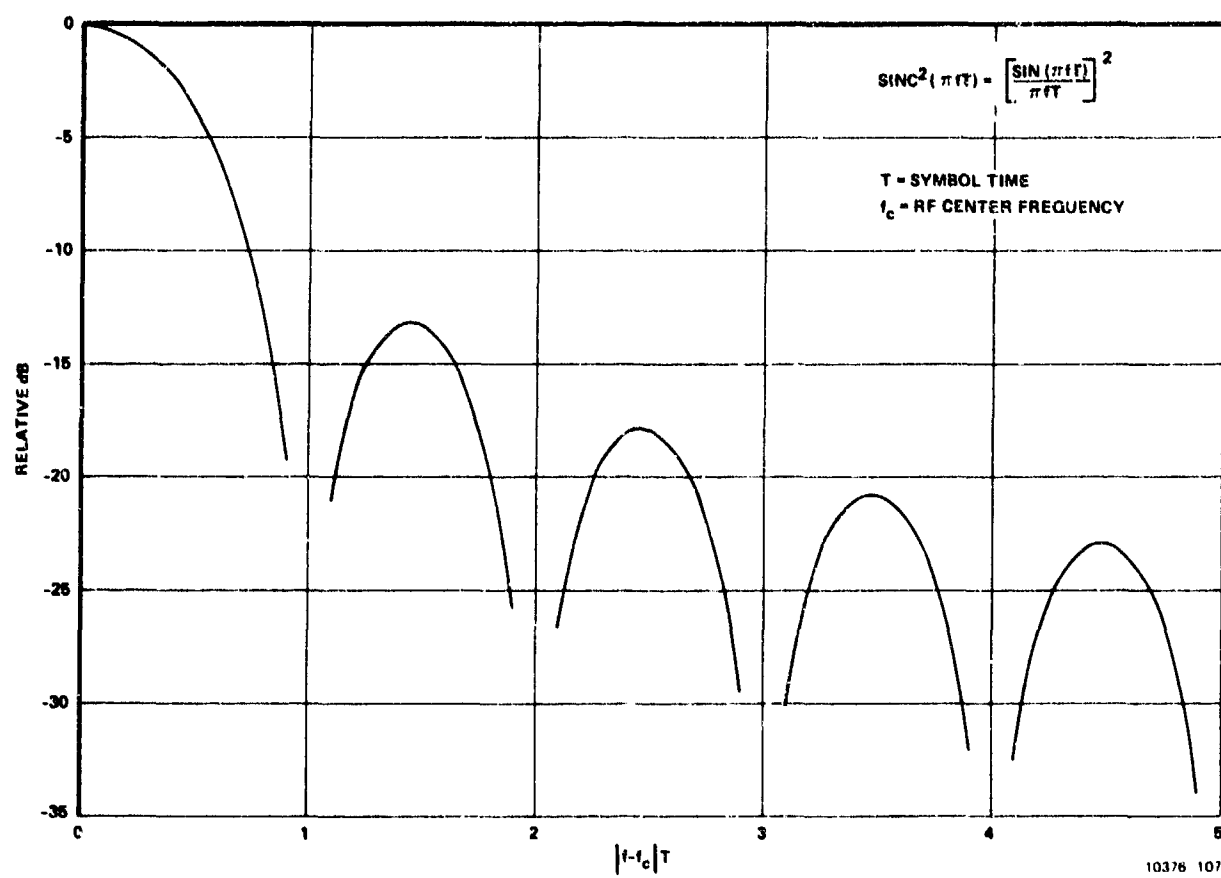


Figure 6.8.4.3-1. Sinc Spectrum

band and 7.0 MHz for the 8 GHz band). With the fixed realizable unloaded Q's available with such filters, the insertion loss increases as the bandwidth is reduced. Discussions with one waveguide filter manufacturer (Microwave Development Laboratories, Needham Heights, Mass.) have indicated that insertion losses for 5-pole filters at 4 and 8 GHz will be as shown in Figure 6.8.4.3-2 as a function of filter 3 dB bandwidth. These insertion losses are achieved by utilizing extremely high unloaded Q ($\sim 18,000$) circular cavities in the waveguide filter design. These curves indicate that for the smallest authorized bandwidths in each band, filters having insertion losses in the neighborhood of 2.5 to 3.0 dB will be required (filter 3 dB bandwidth = 75% of authorized bandwidth). Even with this amount of insertion loss, however, the waveguide filter technique is still attractive relative to alternative approaches to achieving FCC 19311 spectrum compliance as we discuss later in this section.

Another practical problem with the waveguide filter approach for the minimum authorized bandwidths is that filter center frequency detuning with temperature because of thermal expansion and contraction of the filter metal can degrade the performance of the digital modem. This problem is alleviated to some degree by using INVAR material to construct the filter. At 8 GHz carrier frequencies, INVAR filters display approximately 16 kHz of detuning per degree Centigrade temperature variation. At 4 GHz center frequencies, the detuning is approximately 8 kHz/ $^{\circ}$ C. It is conceivable that the use of such filters for the 3.5 and 7.0 MHz authorized bandwidths might require that the filter be in a controlled temperature environment or that some type of closed loop scheme be employed to keep the signal centered in the narrow filter.

With these practical drawbacks to employing waveguide filtering for FCC 19311 spectral compliance in mind, an investigation of an alternative scheme not requiring a waveguide filter was undertaken. The scheme investigated was the use of baseband filtering in a QAM modulator in an attempt to achieve FCC 19311 spectrum compliance. The

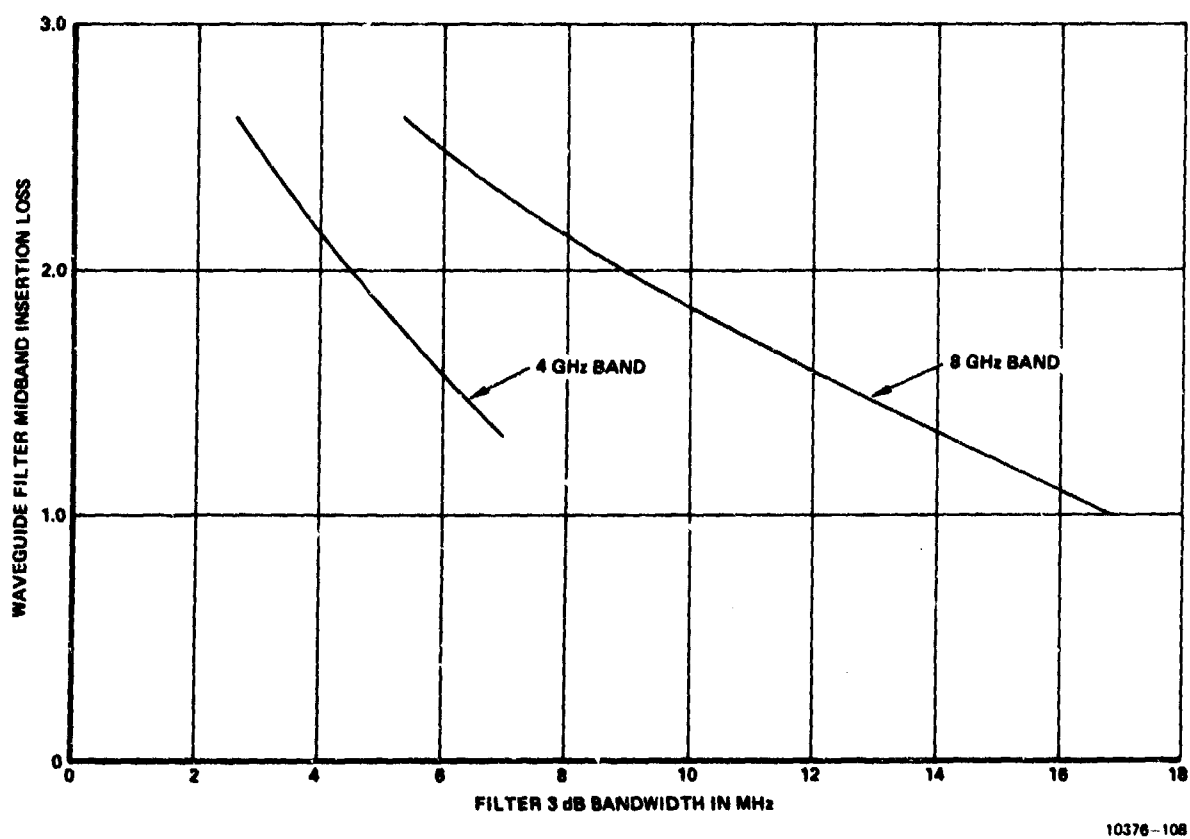


Figure 6.8.4.3-2. Five-Pole Waveguide Filter Insertion Loss

particular scheme examined presumed that the baseband filters were full Nyquist, $\alpha = 0.5$ rolloff parameter, raised cosine filter having the frequency response shown previously in Figure 6.2-2. Further, it was assumed that the baseband filter inputs were weighted M-ary impulses at the symbol rate. Two cases were attempted - one, where the impulse weights were adapted to power amplifier nonlinearity using adaptive predistortion, and another, where no adaptation was used.

If the power amplifier were linear, the spectrum at its output would be bandlimited. For $\alpha = 0.5$ raised cosine filtering, the spectrum goes to zero for frequencies removed by more than 75 percent of the symbol rate from center frequency. For real amplifiers having nonlinear distortion effects, however, there will in general be output spectral content at these frequencies even though none was present on the amplifier input. Figure 6.8.4.3-3 shows the amplifier output spectrum for the Ford linear amplifier having the AM/AM and AM/PM characteristics shown in Figures 6.7-2 and 6.7-3 and for a peak power output of 35.6 dBm (peak "linear" power). In Figure 6.8.4.3-3, the nonlinearity has been adapted to by predistorting the impulse weights into the baseband filters so that no distortion occurs at symbol sampling times on the amplifier output. We stress the point here that the nonlinear effects are removed only at the symbol sampling times to provide at the amplifier output an ideal set of quadrature signal points such as that shown in Figure 6.8.4.2-1 previously. In general, the transition from one sample point to another in the amplifier output signal space occurs in a highly nonlinear manner even with the adaptive predistortion. Consequently, nonlinear distortion effects cause the side-lobe levels on the amplifier output to be finite at frequencies where the input spectrum was zero in the present example as shown in Figure 6.8.4.3-3. The side-lobe level shown there is only 35 dB below the main lobe and would create problems for FCC 19311 compliance in a reasonable bandwidth. Figure 6.8.4.3-4 shows the "linear" power amplifier output spectrum if predistortion is not used. Comparing Figures 6.8.4.3-3 and 6.8.4.3-4, we conclude that the adaptive predistortion technique to linearize the power amplifier at

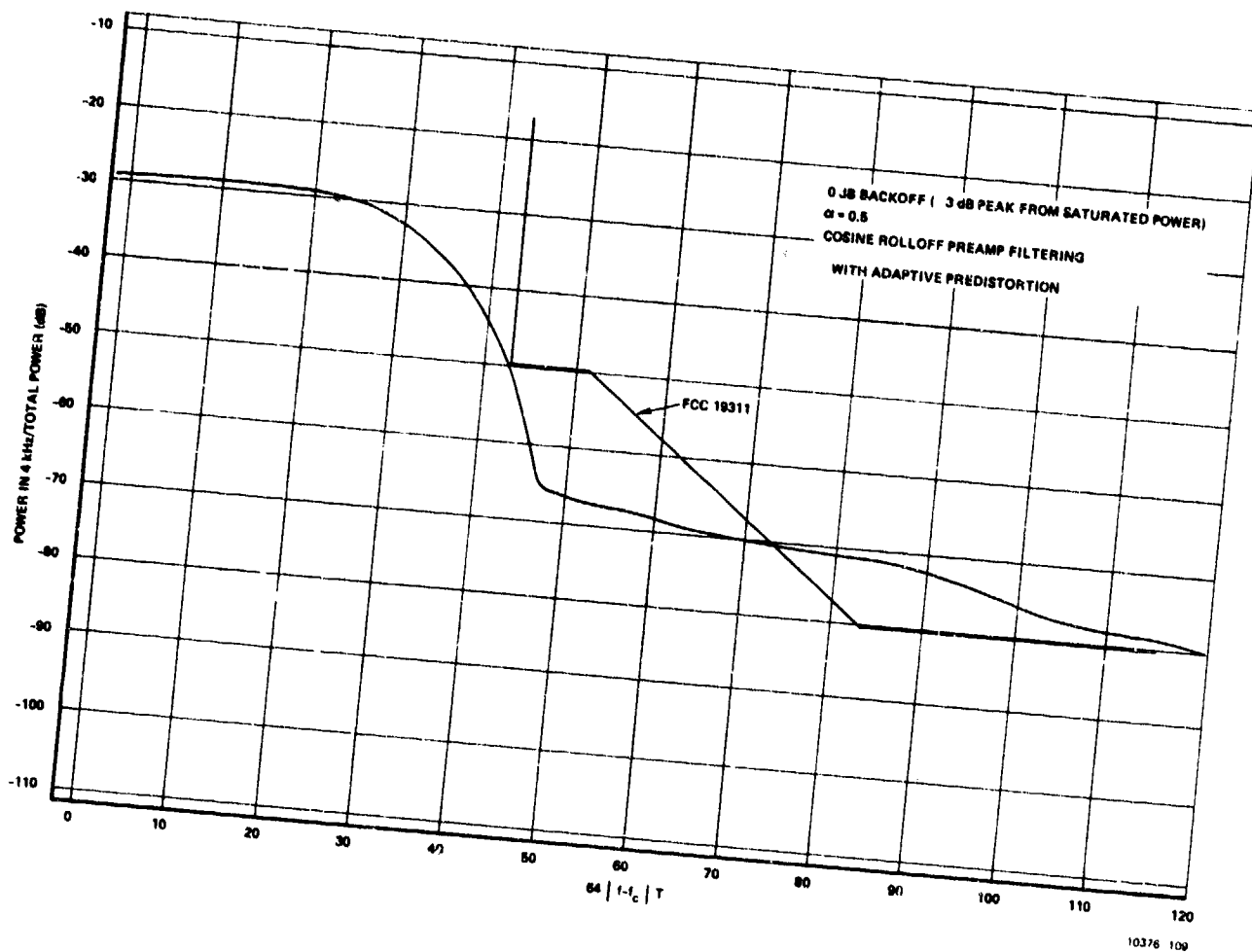


Figure 6.8.4.3-3. Ford Linear Amp

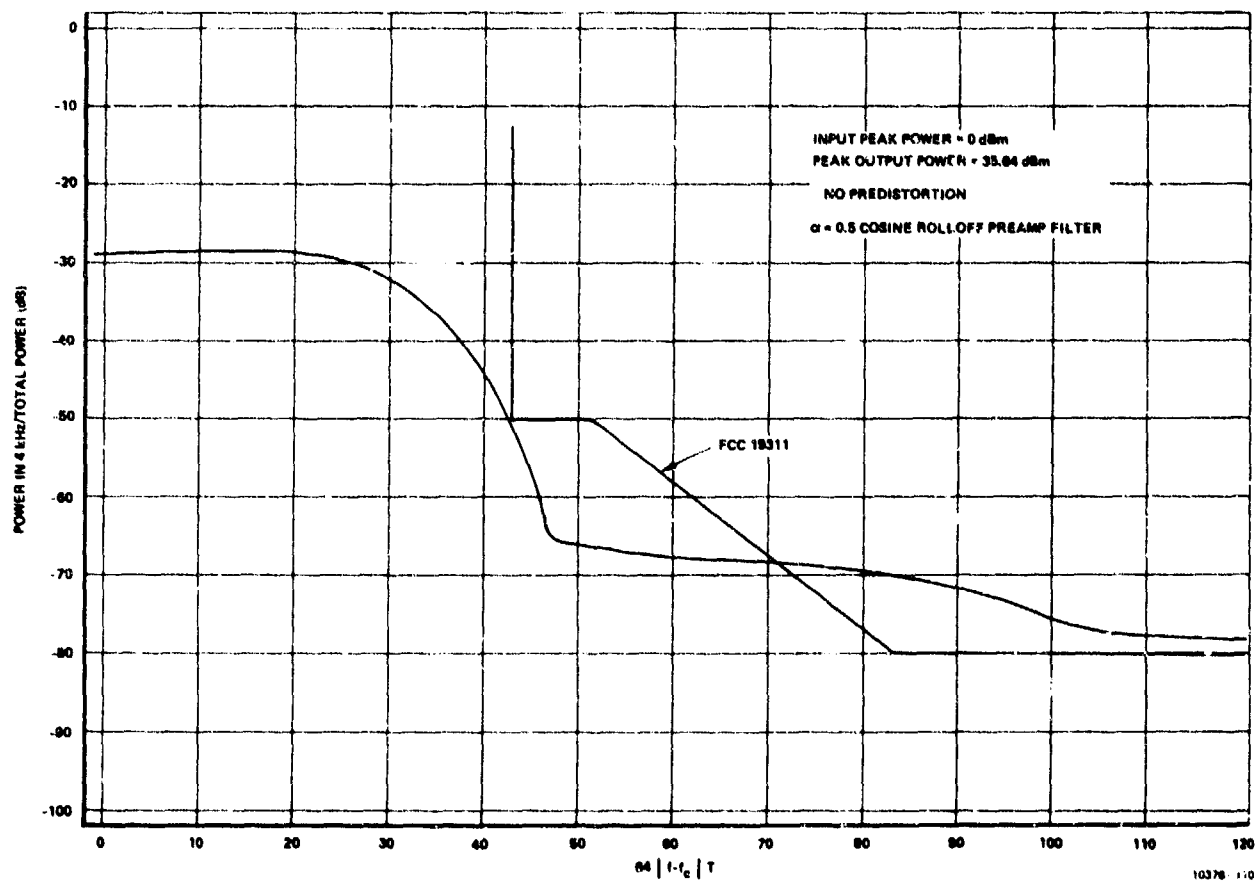


Figure 6.8.4.3-4. Ford Linear Amp

symbol sampling times does not significantly reduce the overall spectrum side lobes at the power amplifier output.

Figures 6.8.4.3-5 and 6.8.4.3-6 show the spectra produced for two other drive levels. The peak power output in Figure 6.8.4.3-5 is 37.6 dBm (about 0.5 dB below single signal saturation) and the peak power output in Figure 6.8.4.3-6 is 31.6 dBm (about 6.5 dB below saturation). Even at the greatly reduced drive level of Figure 6.8.4.3-6, the amplifier has not been rendered sufficiently linear to allow efficient compliance with FCC 19311 (by "efficient compliance," it is meant that an authorized bandwidth that is a small multiple of the symbol rate be required).

The side-lobe levels of Figure 6.8.4.3-6 are still only 35 dB down relative to the main lobe, whereas FCC 19311 compliance requires side-lobe levels approximately 50 dB down relative to the main lobe. (This approximately 50 dB down requirement is needed to get under the FCC 19311 requirement of -80 dB power in 4 kHz in the far side lobes since for the bandwidths of interest here, 4 kHz power in the main lobe is typically around -30 dB relative to total power.) In order to keep the nonlinearity-produced (intermod distortion) side lobes 50 dB down relative to the main lobe, it is conceivable that the power amplifier might have to be operated at low enough drive level to achieve 50 dB down intermod distortion - just to comply with FCC 19311 when using baseband or IF filtering to perform main lobe spectral shaping filtering. In the 3 and 4 bits/sec/Hz region of spectral efficiency, the requirement for such low distortion levels means that the limiting factor determining how hard the amplifier can be driven is FCC 19311 spectral compliance and not performance degradation. Thus, one avoids the use of a waveguide filter for spectral shaping at the expense to the overall link budget of many dB of power amplifier backoff. For example, peak power amplifier backoff of 6.5 dB below saturation in Figure 6.8.4.3-6 has still failed to produce efficient compliance to FCC 19311. If the intermod distortion producing the side lobes of Figure 6.8.4.3-6 is primarily of third order, another 7

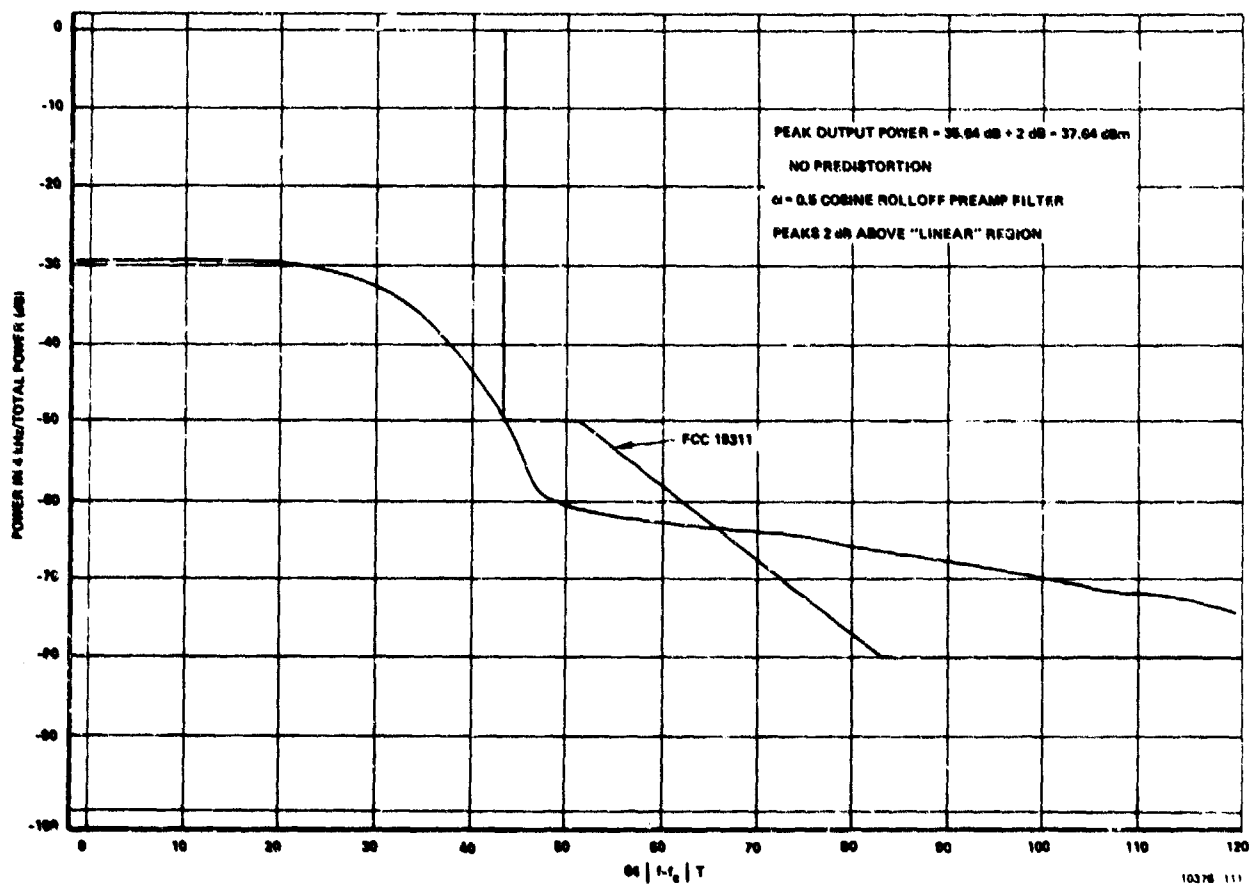


Figure 6.8.4.3-5. Ford Linear Amp

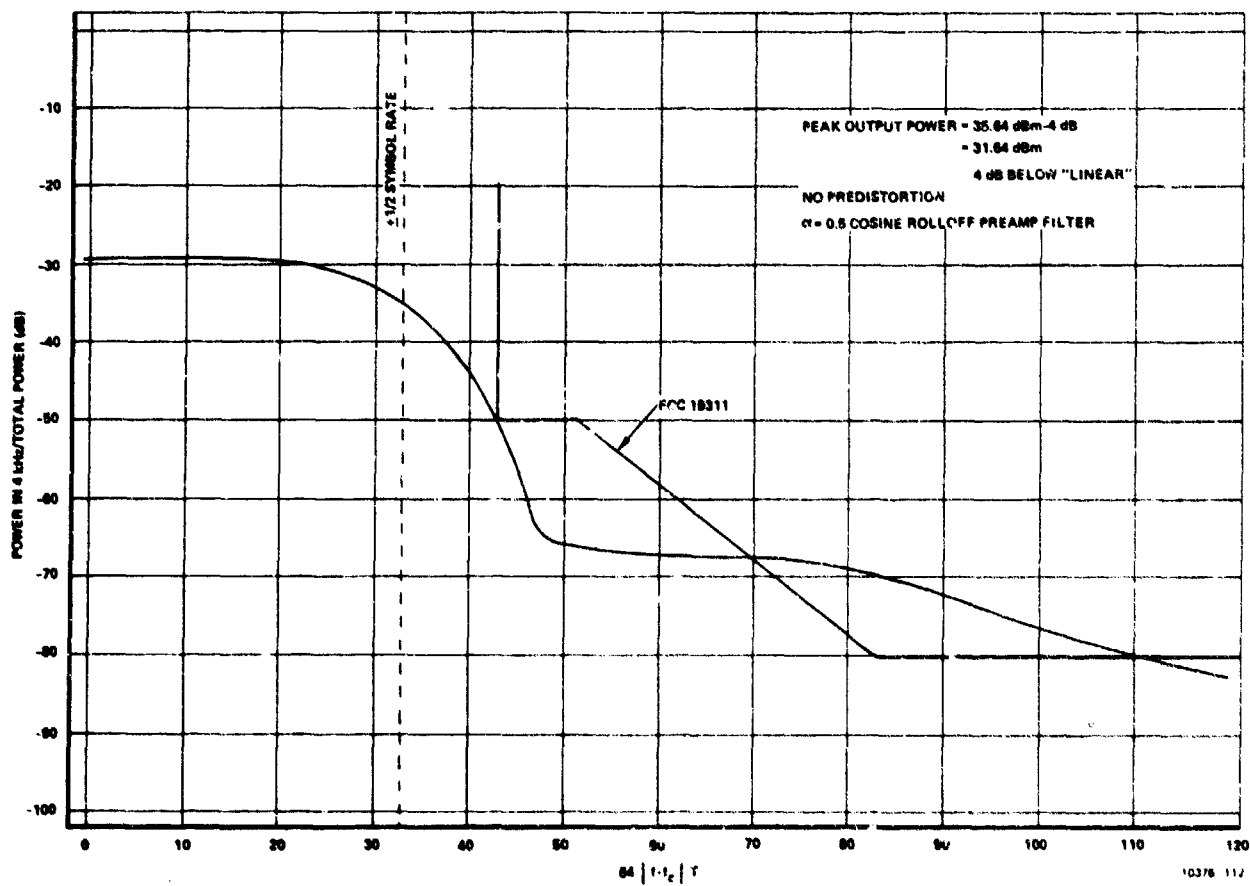


Figure 6.8.4.3-6. Ford Linear Amp

dB of backoff might be necessary to get from the 36 dB down side lobes to 50 dB down side lobes. At this point the peak power amplifier output would be 13.5 dB below saturation.

Spectrum results similar to those shown for the "linear" amplifier were also obtained for the TWT amplifier. Again with the TWT amplifier, even 10 dB of backoff failed to provide efficient compliance with the FCC 19311 spectral mask.

The conclusion from the spectral results is that the use of only baseband or IF filtering for complying with the FCC 19311 spectral mask leads to a requirement for excessive power amplifier backoff just to keep the intermod distortion side lobes under the mask. A better alternative for complying with FCC 19311 from overall link budget standpoints is to use waveguide filtering. The use of such filtering for spectral containment in conjunction with the adaptive predistortion scheme for eliminating degrading nonlinear effects provides a system capable of meeting FCC 19311 wherein the power amplifier is being driven near saturation power on peaks even while transmitting multi-amplitude digital signals.

From the simulations performed, it has been found that the adaptive predistortion scheme, used in conjunction with square pulse multilevel PAM quadrature digital modulation schemes, virtually totally removes the power amplifier nonlinearities as a degrading influence. The waveguide filter necessary to further shape the sinc-type spectrum resulting at the power amplifier output creates linear distortion on the radiated signal, for the elimination of which there are well-known linear equalizer techniques to be employed at the receiver.

Once the transmit power amplifier is linearized, the analysis of the equalized receiver performance presented in Paragraph 6.5.3 applies and provides goals toward which to work in terms of E_b/N_0 required for a given error rate performance.

6.9 Computer Simulations of M-QAM Modem Performance

6.9.1 Introduction

The simulations showing the effectiveness of the adaptive predistortion linearization technique at preventing signal format distortion for the M-QAM modulator have been presented in Paragraph 6.8.4. Here, we shall concentrate on the M-QAM demodulation technique developed on this contract. First, the demodulation technique will be described and then computer simulations of the modem performance will be presented.

6.9.2 M-QAM Demodulator Description

One of the more novel aspects of the M-QAM demodulation technique we have developed is the manner in which adaptive equalization is accomplished at the receiver. This receiver equalization is necessary because of the intersymbol interference created by the waveguide filter at the transmitter. The waveguide filter that has been selected for obtaining FCC 19311 spectral mask compliance for a 14 MHz authorized bandwidth is nominally a 5-pole Butterworth design having RF 3 dB bandwidth of 10.5 MHz (which is the M-QAM symbol rate). This filter creates both amplitude and group delay distortion which must be equalized at the receiver. We have adopted the viewpoint that this equalization must be automatically adaptive as opposed to some form of fixed equalization. The reason for this viewpoint is that modems with high b/s/Hz spectral efficiencies are very sensitive to imperfect equalization. Therefore, it is felt that equalization must automatically track any variations in overall link parameters (e.g., variations of filters with time and temperature) in order to provide a more robust practical modem in an operational environment.

6.9.2.1 Adaptive Equalization Technique

During the phase of this study which has concentrated on implementation techniques for the M-QAM modem, we initially were going to use some form of IF adaptive equalizer.²⁷ Based upon first cut parts counts and cost figures for a hardware realization of an IF equalizer including all the adaptive complex weights and control circuitry, it was concluded that the most expensive element of the demodulator was the IF equalizer. Consequently, an effort was undertaken to eliminate it by replacing it with a form of baseband equalization. This effort was successful and resulted in the technique to be described below. The technique developed has the merit that the equalization is reduced to a relatively simple logic processing of quadrature baseband components. The effectiveness of the technique has been demonstrated by computer simulation.

The block diagram for the M-QAM demodulator is shown in Figure 6.9.2.1. The 70 MHz IF signal from the radio is input to the demodulator where IF filtering and fixed nominal equalization are first performed. The purpose of the fixed equalization is to nominally correct for distortion occurring in the transmit waveguide filter. In computer simulations, only second order all pass network phase compensation for the Butterworth waveguide filter was included. No amplitude equalization was included. Somewhat better performance might be expected for R-QAM for 1 to 2 dB of adjustable parabolic amplitude response boost across a 14 MHz bandwidth.

After the filtering and fixed equalization, the signal is passed to a standard M-QAM demodulator where the signal is downconverted to baseband quadrature components. The in-phase and quadrature legs of the mixers are sampled at the symbol rate of 10.5 MHz and A/D converted to 8 bits accuracy. These two raw quadrature component output words could be fed to M-ary slicers for the required M-level decisions if the

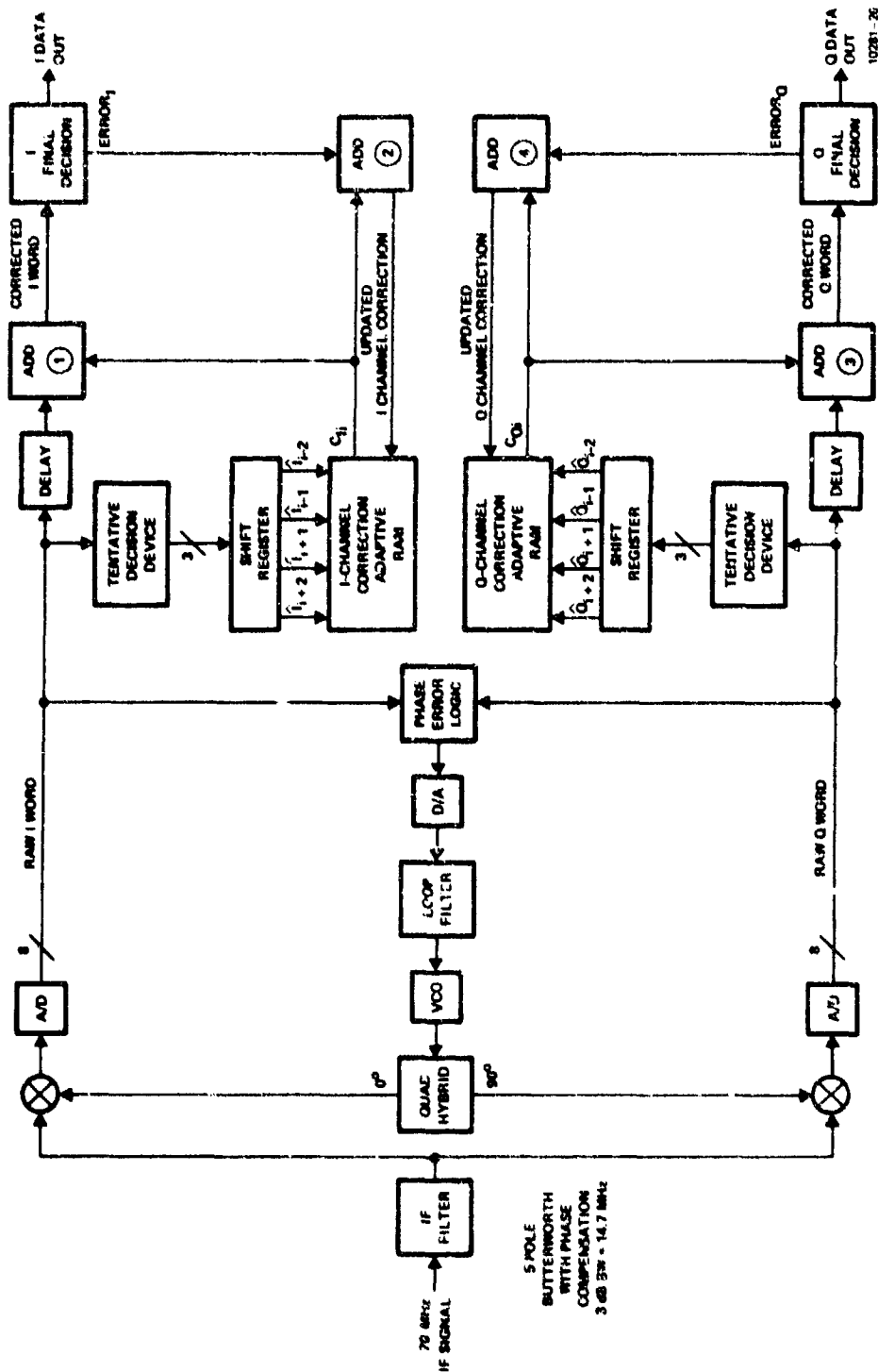


Figure 6.9.2.1. M-QAM Demodulator With Adaptive RAM Equalization

fixed equalization could be relied upon to be stable and accurate and if the overall link conditions remained fixed. In order to track system variations and to provide a more robust demodulator for primarily the 8-QAM signaling format, we have developed and included the adaptive baseband equalization hardware shown to the right in Figure 6.9.2.1. We shall now describe the adaptive equalization technique.

Since identical adaptive processing of the raw A/D words is performed for both quadrature components, we shall describe only the I channel processing.

The first step in this baseband adaptive equalization is to input the raw A/D word into a tentative decision device which is simply an M-ary slicer. The 3-bit output (for 8-QAM) of the tentative decision device would be the appropriate output of the modem, if there were no intersymbol interference. These 3-bit tentative decisions are input to a series of shift registers. The tentative decisions stored in this series of shift registers are observed for the two symbol intervals preceding and following the i th interval. These tentative decisions for the I channel are labeled I_{i+2} , I_{i+1} , I_{i-1} , and I_{i-2} in Figure 6.9.2.1. Conceptually, these surrounding tentative decisions provide usable information concerning the intersymbol interference existing on the i th raw I channel word. As shown, the four tentative decisions are used to access a correction word stored in a random access memory, (RAM). This correction word obtained from the RAM is added to the Raw I channel word in ADD (1) producing a corrected I word. This corrected I word is input to an M-ary slicer where a final decision is made on the I channel information which is then output from the modem. When the final decision is made, the error to the nearest ideal M-ary level is also determined and this error (Error $_I$) is fed back to ADD (2) (scaled by a suitable loop constant) to adaptively modify the RAM-stored correction word. Thus, the adaptive loop is closed for forming the correction word. In the steady-state, the RAM-stored corrections home in on the values necessary to make the corrected I word average zero error to the ideal M-ary levels.

We note that this adaptive equalization scheme requires no multiplication and summing of individual tap positions for forming the corrected words as do standard implementations of adaptive transversal equalizers. An adaptively-learned correction word is simply accessed in the RAM and added to the raw channel word. The fact that no multiplication and linear combining is required is important in high-speed digital modems where the time required to perform such operations is a limiting factor.

Another point of departure from standard transversal equalizers with this equalization scheme is that the crosstalk correction is not restricted to be a linear combination of surrounding symbols. As a matter of fact, with the equalization scheme described, the correction word accessed from the RAM can be a highly nonlinear function of the surrounding tentative decisions. (It is whatever function necessary to make the error in the corrected word average zero.) This can have the beneficial effect of correcting for nonlinearities in the quadrature mixers, AGC amplifier, and A/D characteristic, for example. This can, therefore, lead to a more robust performance for the demodulator in the face of these practical imperfections.

This adaptive equalization scheme appears to be new. The author is unaware of references in the literature which describe this type of equalization technique. It does have some characteristics in common with decision feedback equalization,³⁷ namely that the tentative decisions are used to access the correction. But decision feedback equalization usually employs linear combinations of past decisions, whereas this technique is not restricted to linear combinations. Also, unlike decision feedback equalization, this scheme does not require the multiplication necessary to form the linear weighted combination of the decisions. This can be important in a high rate modem.

6.9.2.1.1 Performance Results Obtained With the Adaptive Baseband Equalization Technique

We have simulated the performance obtainable for the modem equalization scheme outlined above and shown schematically in Figure 6.9.2.1. The nominal conditions for the simulated system are given in Table 6.9.2.1.1-1.

Table 6.9.2.1.1-1. Nominal Conditions Simulated (8-QAM)

Modulation:	8-ary PAM on quadrature channels (8-QAM) Symbol Rate = 10.5 MHz
Spectral Efficiency: (FCC 19311)	4.5 b/Hz in 14 MHz authorized bandwidth
Transmit Waveguide Filter:	5 pole Butterworth 3 dB BW = 10.5 MHz
Receiver IF Filter:	5 pole Butterworth - 3 dB BW = 14.7 MHz with two second order ALLPASS phase compensation (One for waveguide filter and one for receiver filter)
Equalization:	The adaptive RAM technique using four tentative decisions as described herein

Figure 6.9.2.1.1-1 shows the results obtained from the simulations. Also shown for reference is the performance curve for ideal nonbandlimited 8-QAM. We note that for the nominal conditions the performance with this equalization scheme is within 1.2 dB of ideal performance. Without the baseband equalizer the performance is at least 7 dB worse than ideal. Also shown are the performances obtained when additional parabolic group delay and amplitude slope distortions are added. As shown, adding 1 dB amplitude slope across 10.5 MHz (symbol rate) band plus 10 percent symbol time parabolic group delay distortion over the same band results in only about 1 dB additional degradation. 2 dB slope distortion across this band causes rather severe degradation (around 7 dB) at the lower error rates. 1 dB slope distortion plus 20 percent symbol time parabolic group delay causes around 2 dB degradation. The tolerances of the technique to these additional distortions over nominal conditions will yield better performance in the face of practical imperfections.

The results obtained for 4-QAM using the baseband equalization technique described above are shown in Figure 6.9.2.1.1-2. The symbol error rate is plotted versus E_b/N_0 . The nominal conditions were as shown in Table 6.9.2.1.1-2.

As shown in Figure 6.9.2.1.1-2, the performance with nominal conditions is within 1 dB of ideal 4-QAM at 10^{-9} error rate. Also shown are the curves for additional distortions across symbol rate (10.5 MHz) bandwidth. For example, 2 dB of amplitude slope distortion across 10.5 MHz causes about 0.6 dB degradation over nominal conditions at 10^{-9} error rate.

6.9.3 M-QAM Simulation Results for Various Implementation Imperfections

Computer simulations were performed to determine the sensitivity of the M-QAM modem to various equipment imperfections. The equipment imperfections considered were:

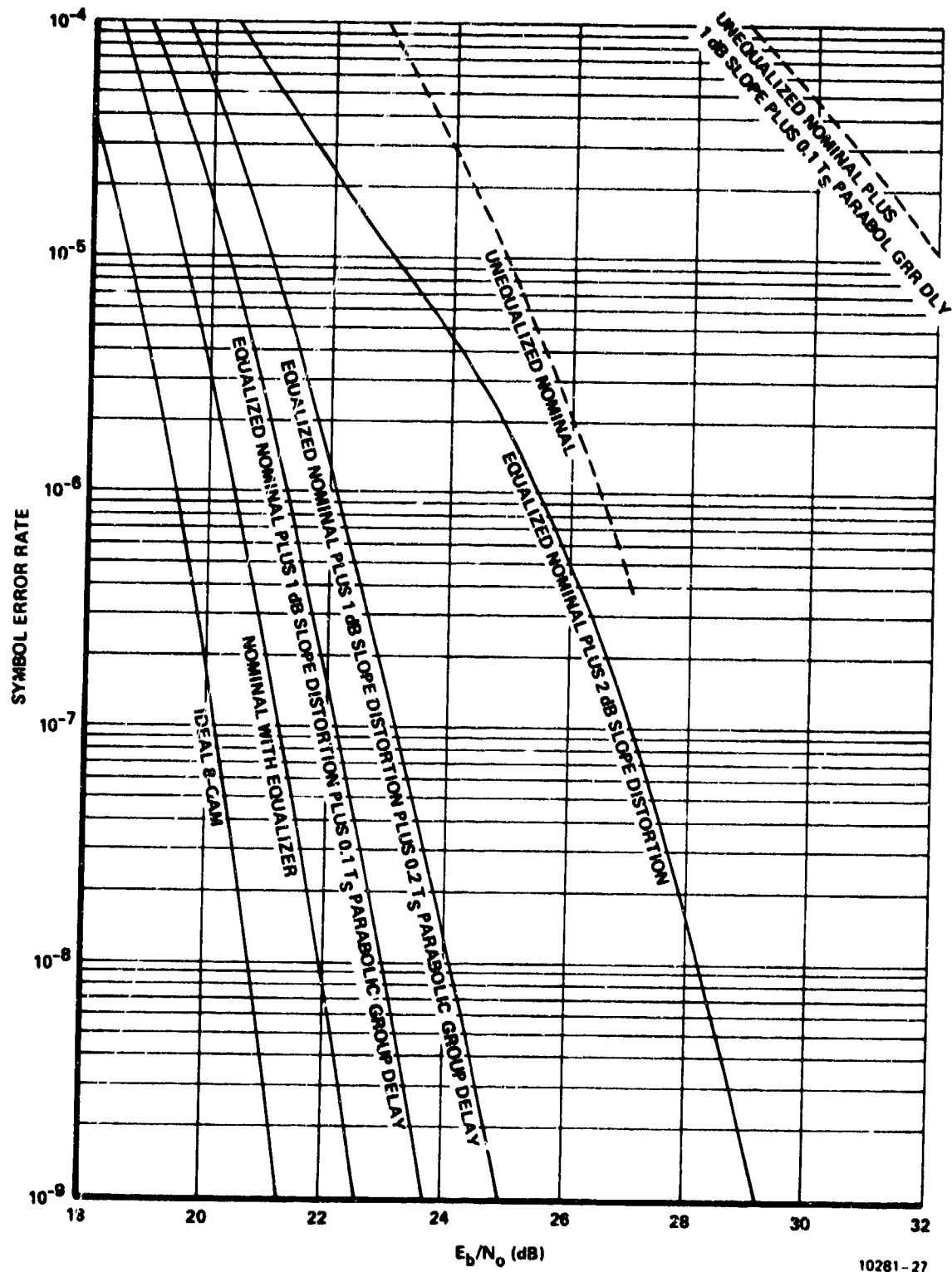


Figure 6.9.2.1.1-1. Performance of 8-QAM Demodulator

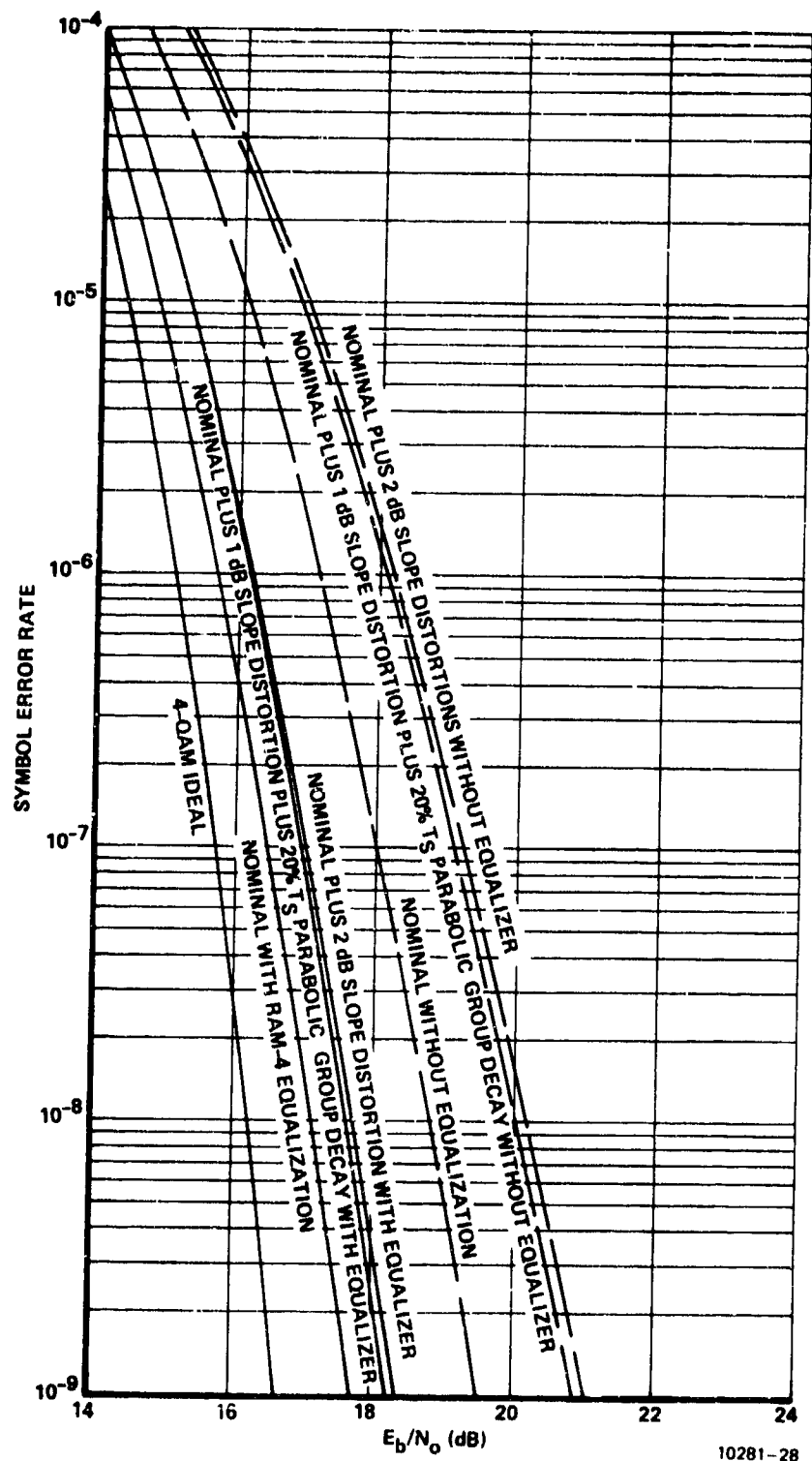


Figure 6.9.2.1.1-2. Performance of 4-QAM Demodulator With Baseband Equalizer

Table 6.9.2.1.1-2. Nominal Conditions Simulated (4-QAM)

Modulation:	4-ary PAM on quadrature channels (4-QAM) Symbol Rate = 10.5 MHz
Spectral Efficiency: (FCC 19311)	3 bits/Hz in 14 MHz authorized bandwidth
Transmit Waveguide Filter:	5 pole Butterworth - 3 dB BW = 10.5 MHz
Receiver IF Filter:	5 pole Butterworth - 3 dB BW = 14.7 MHz with two second order ALLPASS phase compensation (One for waveguide filter and one for receiver filter)
Equalization:	The adaptive RAM technique using four tentative decisions as described above

1. Phase jitter on the receiver coherent reference
2. Variation in symbol timing at the receiver
3. Variation in AGC level at the receiver

The sensitivity of the modem to nonideal filter distortions in both amplitude and phase characteristics was indicated previously in Paragraph 6.9.2.1.1.

For these sensitivity simulations, we assumed an ideal receive IF filter which equalizes the overall frequency response from transmitter to receiver IF output to a raised cosine characteristic having rolloff parameter $\alpha = 0.5$. This IF filter compensates for the 5-pole Butterworth characteristic of the transmit waveguide filter as well as the $\sin x/x$ rolloff of the data spectrum due to square pulse M-QAM signaling. The frequency response for this compensating IF filter is shown in Figure 6.9.3-1.

The performance obtained with this IF filter for 4- and 8-QAM versus average received E_b/N_0 is shown in Figure 6.9.3-2. Note that the use of this IF filter provides performance within 0.7 dB of ideal QAM for 10^{-9} symbol error rate.

The ideal IF filter characteristic shown in Figure 6.9.3-1 required to result in $\alpha = 0.5$ raised cosine overall channel response is not exactly obtainable in practice. However, the results of Paragraph 6.9.2.1.1 show that with practical filters and the baseband equalization scheme, performance within 0.5 dB of this ideally equalized case can be obtained. Therefore, the sensitivity of the M-QAM modem to equipment imperfections to be displayed here are deemed applicable to the realistic IF filter case.

The nominal conditions for the following simulations are shown in Table 6.9.3.

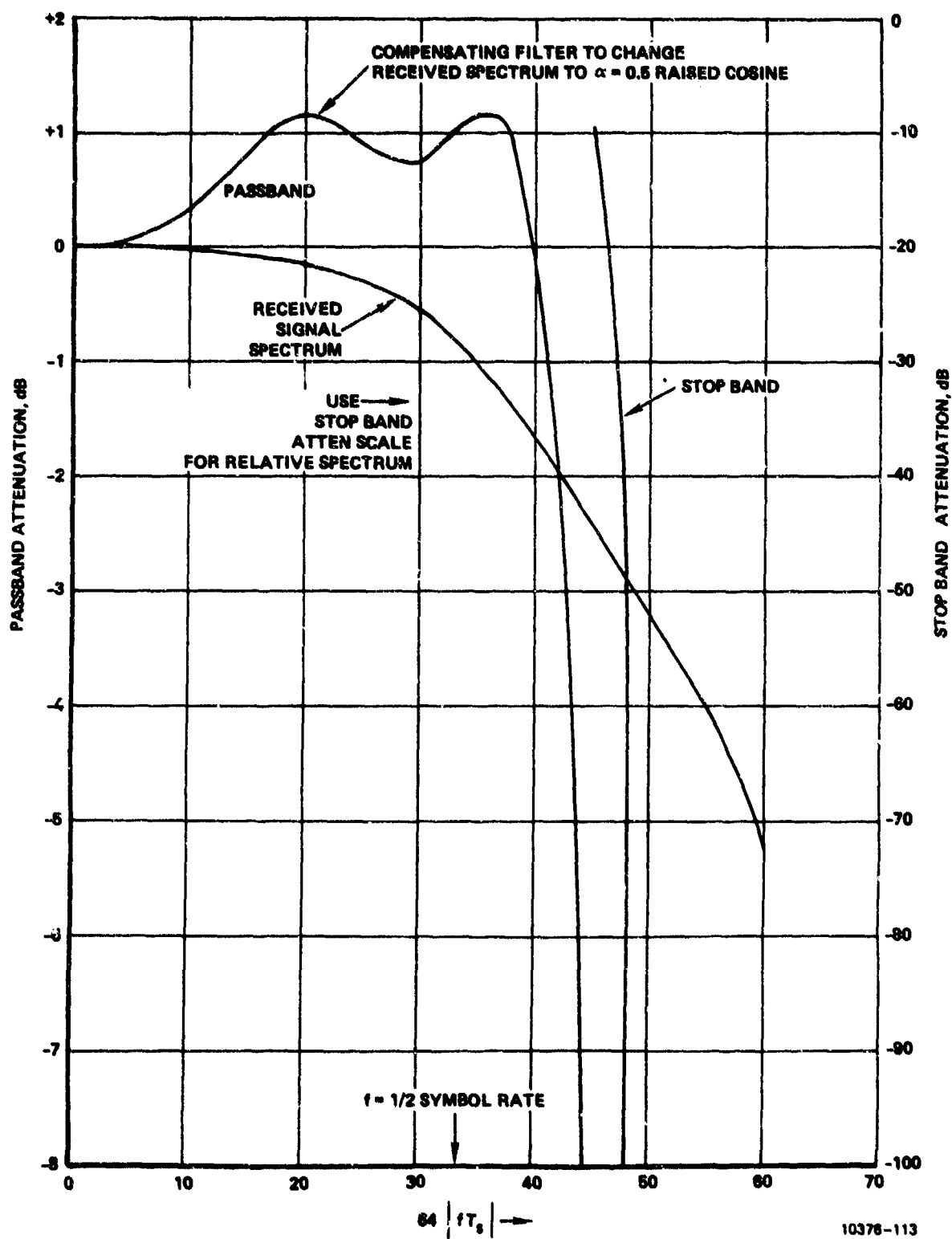


Figure 6.9.3-1. Receiver Equalizer Filter

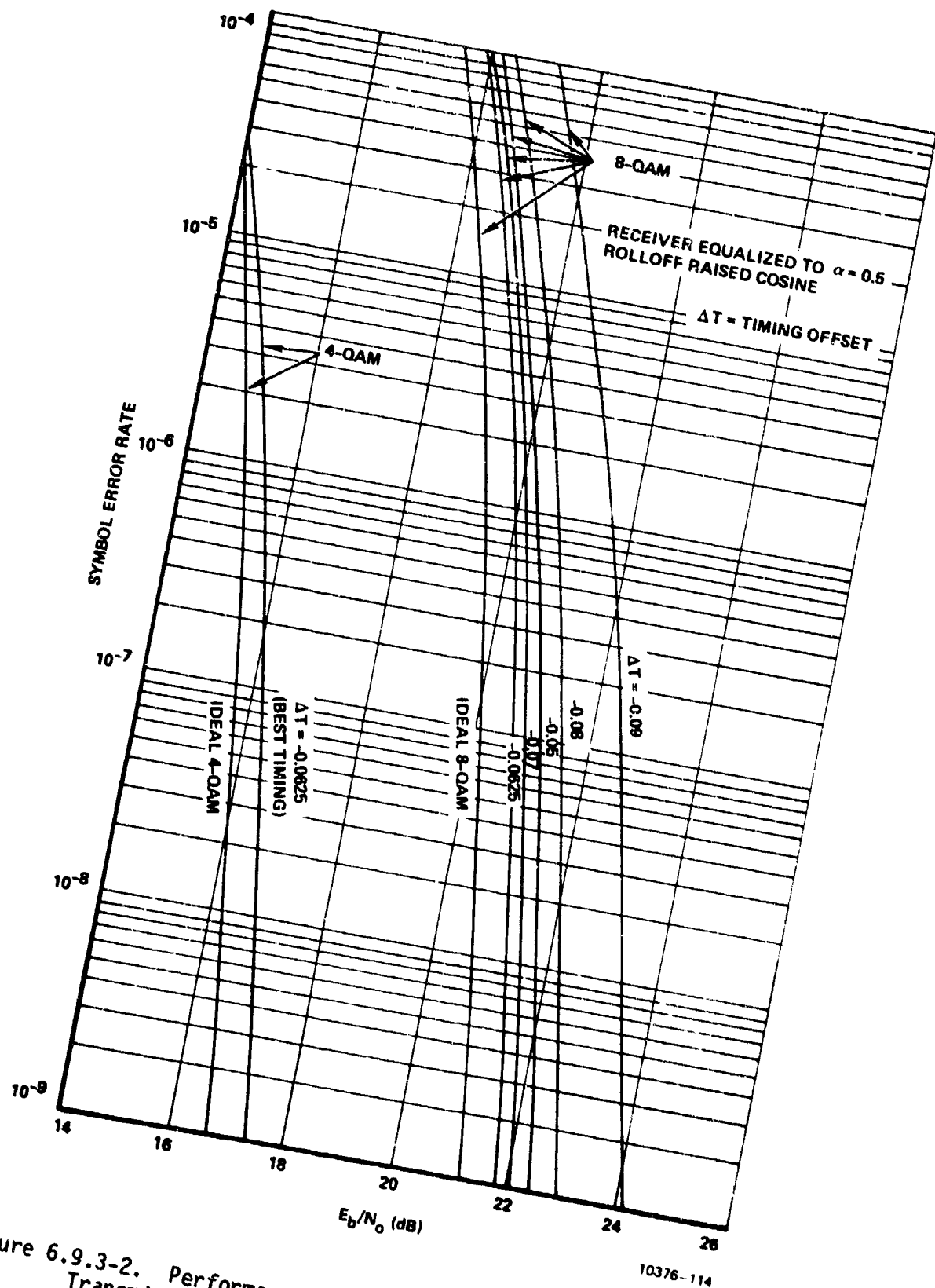


Figure 6.9.3-2. Performance of M-QAM 5-Pole Butterworth Transmitter Filter 3 dB BW = $0.5 \times \text{SR}$

Table 6.9.3. Nominal Conditions for Sensitivity Simulations

Signal Format:	M-QAM, Square Pulse Signaling, Symbol Rate = 10.5 MHz
Transmit Filter:	5 pole Butterworth Waveguide Filter, 3 dB bandwidth = 10.5 MHz
FCC 19311 Authorized Bandwidth:	14 MHz
Receiver IF Filter:	That necessary to equalize overall frequency response to $\alpha = 0.5$ raised cosine (Figure 6.9.3-1)
Demodulation Technique:	Simply an M-ary slicer for the two baseband quadrature components
Phase Reference Jitter:	0 degree rms
Symbol Timing:	Nominal
AGC Level:	Nominal

6.9.3.1 Performance of Nominal M-QAM Modem With TWT Amplifier

Figure 6.9.3.1 shows the performance simulated for the nominal conditions given in Table 6.9.3 for 8-QAM when a TWT having AM/AM and AM/PM characteristics shown previously in Figure 6.8.1 of Paragraph 6.8 is used at the transmitter. The adaptive predistortion linearization technique described in Paragraph 6.8 is used at the transmitter to linearize the TWT. For the results of Figure 6.9.3.1, the TWT was driven on peaks to within 0.5 dB of saturated power output. Comparing the performance in Figure 6.9.3.1 with that in Figure 6.9.3-2 (where the amplifier was linear) one sees that the TWT amplifier provides the same performance as a linear amplifier. This shows the effectiveness of the adaptive predistortion amplifier linearization technique.

6.9.3.2 Performance Sensitivity to Receiver Phase Reference Jitter

Figures 6.9.3.2-1 and 6.9.3.2-2 show the sensitivity of the nominal M-QAM modem to receiver phase reference jitter. All parameters were at the nominal conditions of Table 6.9.3 with the exception of phase jitter. Comparing Figures 6.9.3.2-1 and 6.9.3.2-2 shows that 8-QAM is much more sensitive to phase jitter than 4-QAM, as one would expect.

From these simulations we have concluded that the receiver phase reference loop must be designed to hold the reference jitter below 0.5° rms to avoid severe degradation in the 8-QAM case.

6.9.3.3 Performance Sensitivity to Receiver Symbol Timing

Figures 6.9.3.3-1 and 6.9.3.3-2 show the sensitivity of symbol error rate for 8- and 4-QAM, respectively, to variation in the location of symbol timing at the receiver. The nominal conditions simulated are shown in Table 6.9.3. Again, 8-QAM performance is a much more sensitive function of receiver symbol timing phase than 4-QAM.

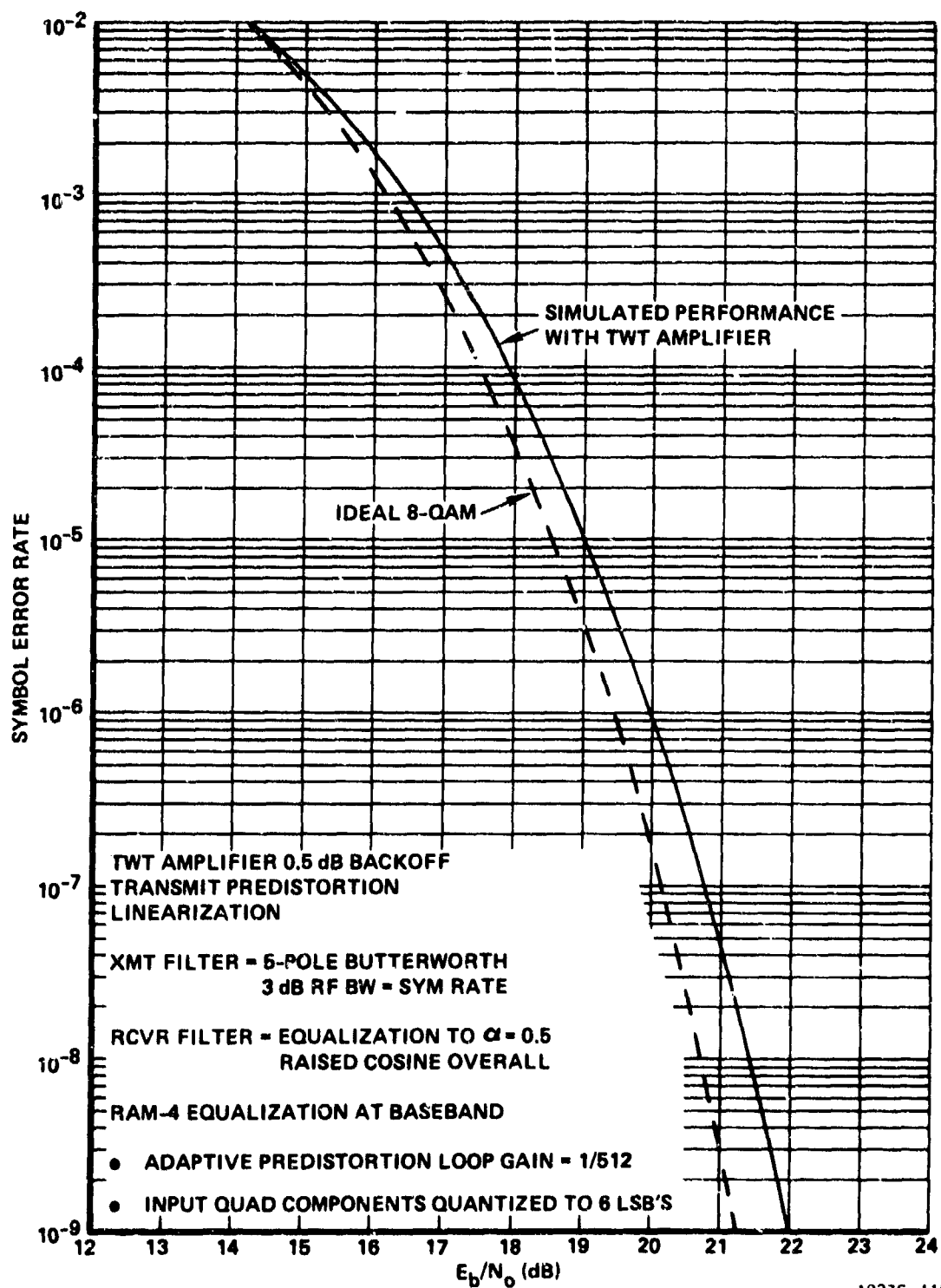
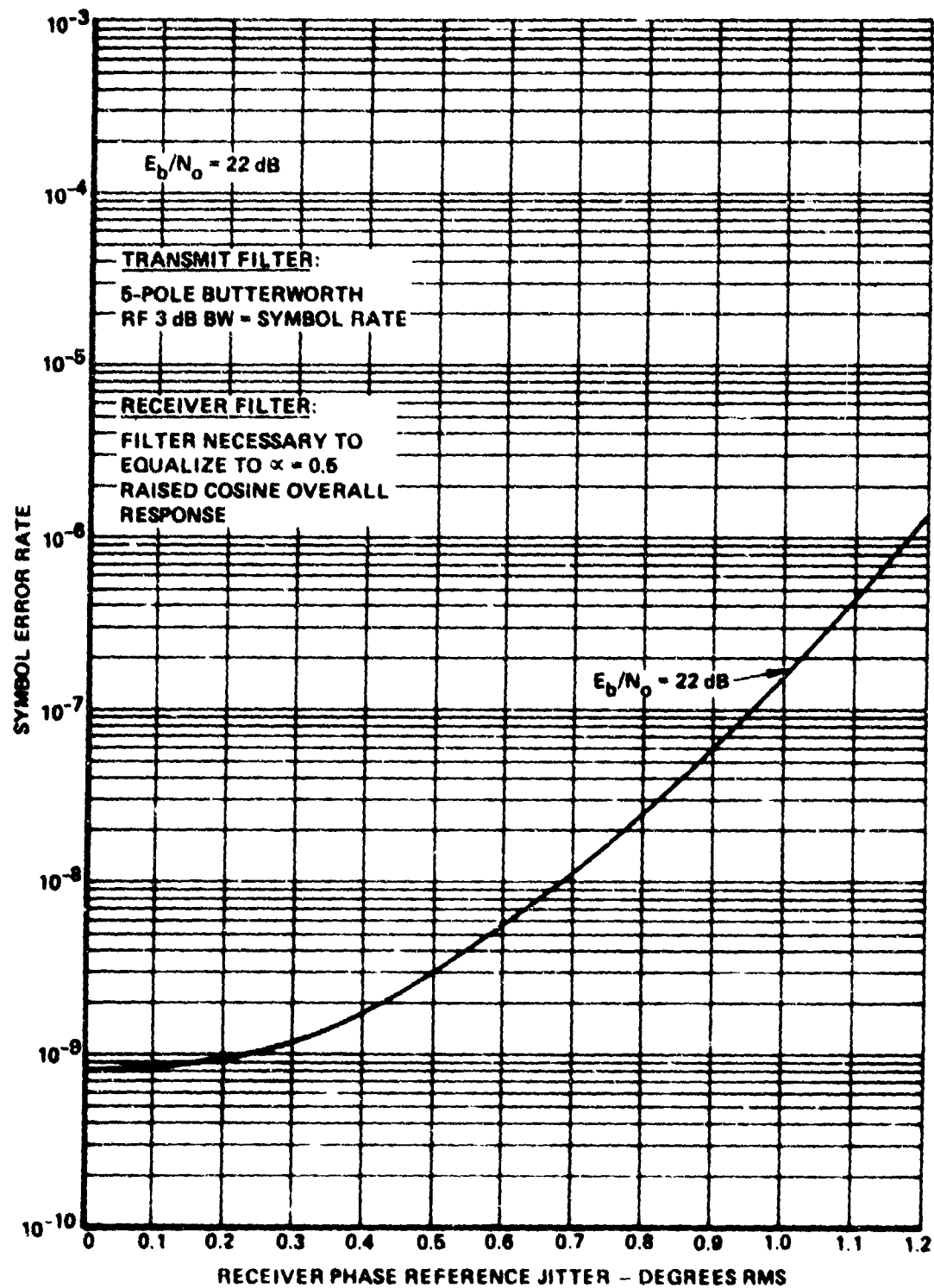


Figure 6.9.3.1. 8-QAM Performance With TWT Amplifier



10376 116

Figure 6.9.3.2-1. 8-QAM Sensitivity to Phase Reference Jitter

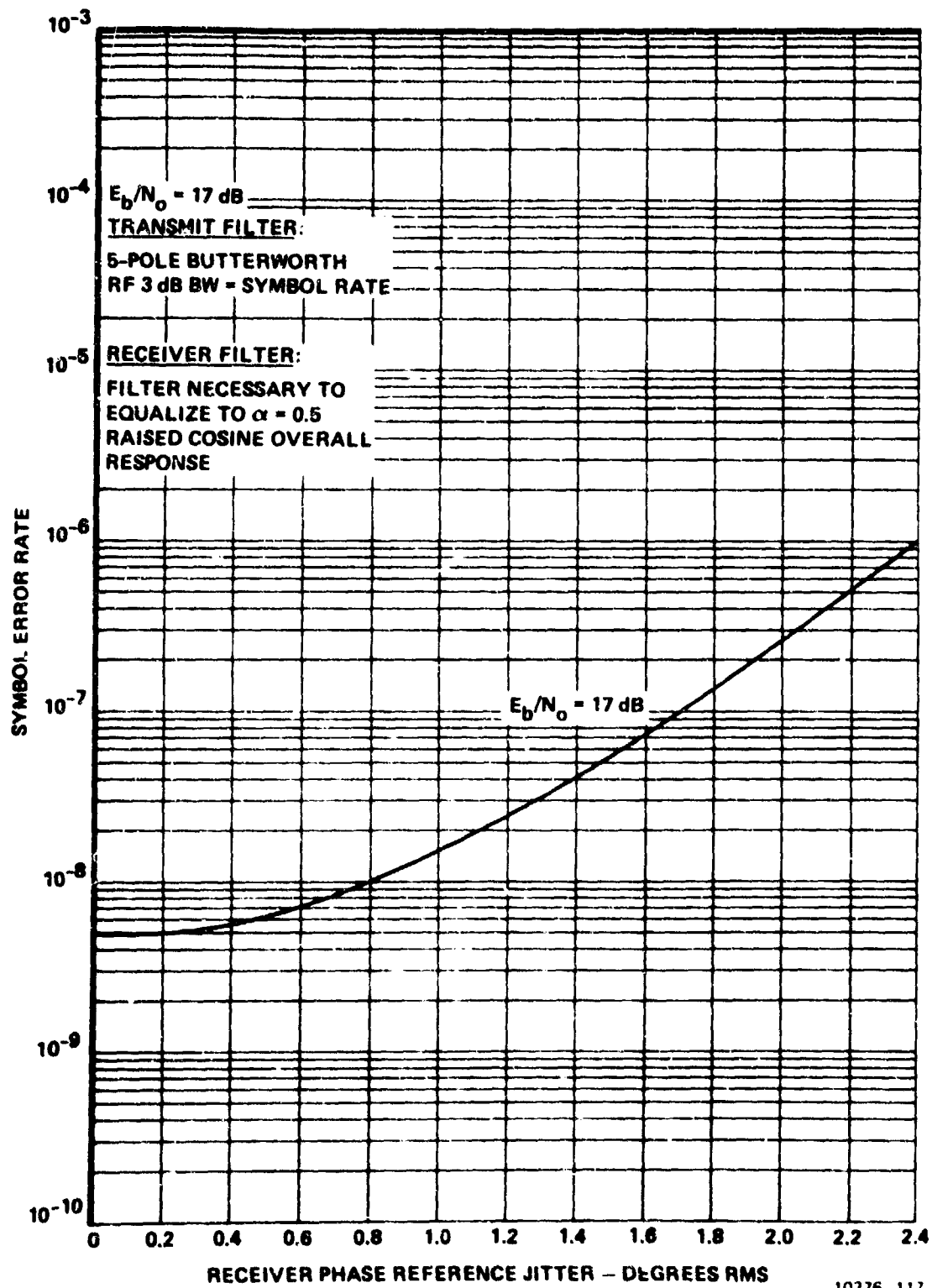


Figure 6.9.3.2-2. 4-QAM Sensitivity to Phase Reference Jitter

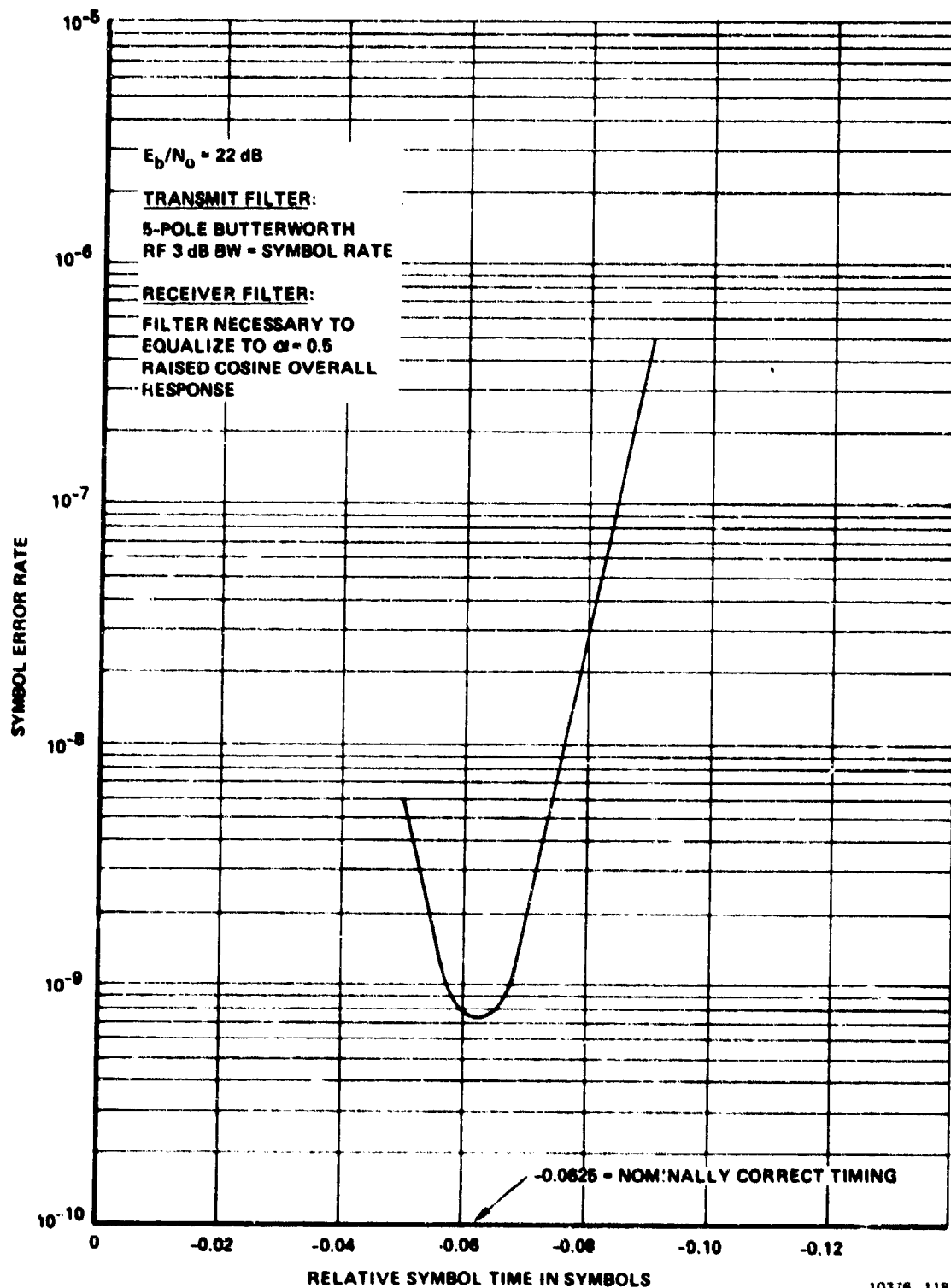


Figure 6.9.3.3-1. 8-QAM Sensitivity to Symbol Timing Variation

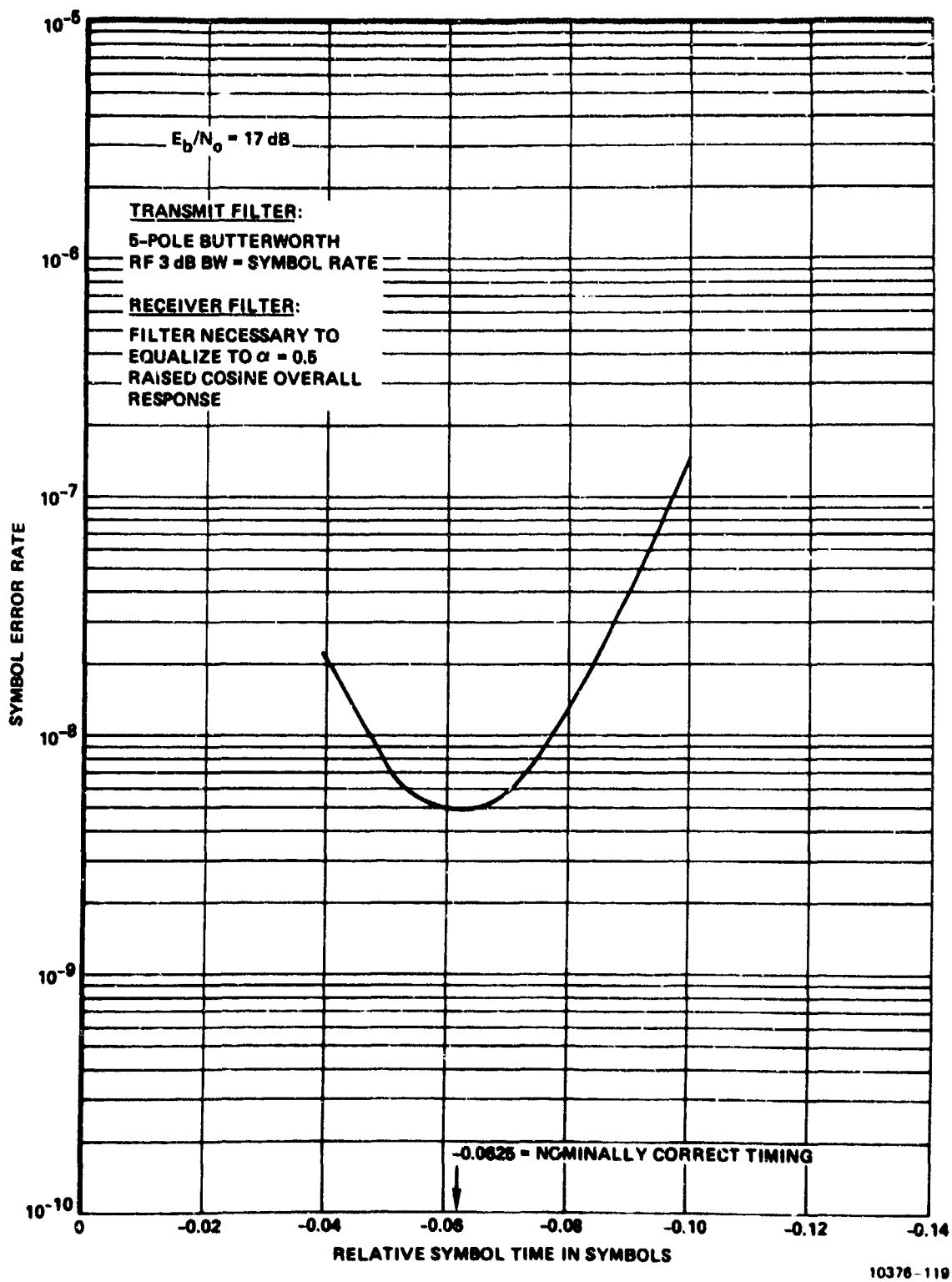


Figure 6.9.3.3-2. 4-QAM Sensitivity to Symbol Timing Variation

From these simulations we have concluded that symbol timing must be obtained having less than 1 percent of symbol rms jitter to avoid significant degradation in the 8-QAM case.

6.9.3.4 Performance Sensitivity to AGC Variation

Figures 6.9.3.4-1 and 6.9.3.4-2 show the sensitivity to AGC level at the receiver for 8- and 4-QAM respectively. Once again, the sensitivity of 8-QAM to the AGC setting is greater than the sensitivity of 4-QAM.

From these simulations we have concluded that the AGC rms variation about nominal should be held to around 1 percent.

6.9.4 Performance of Modem With SAW Device Receive IF Filters

Because of the possibility of buying cheaper and more stable 70 MHz IF filters implemented using Surface Acoustic Wave (SAW) devices as opposed to lumped parameter IF filters, we examined the performance available with the modem using an approximation to a SAW filter. From literature published by SAW filter manufacturers, we concluded that SAW filters were available for 70 MHz IF center frequency which were approximated by an $\alpha = 0.25$ raised cosine frequency response. Such responses are shown in Figure 6.9.4-1 for 13 and 13.5 MHz 3 dB IF bandwidth which are in the range of IF bandwidth required.

Simulations were performed using these $\alpha = 0.25$ raised cosine filters as the IF filter in the modem. In addition, the IF filter modelled in the simulations included a second order all-pass network to phase compensate the five-pole Butterworth transmit waveguide filter. The results obtained using this IF filter are presented below.

Figure 6.9.4-2 shows the variation in symbol error rate versus AGC level for $E_b/N_0 = 22$ dB. This curve is the symbol error rate

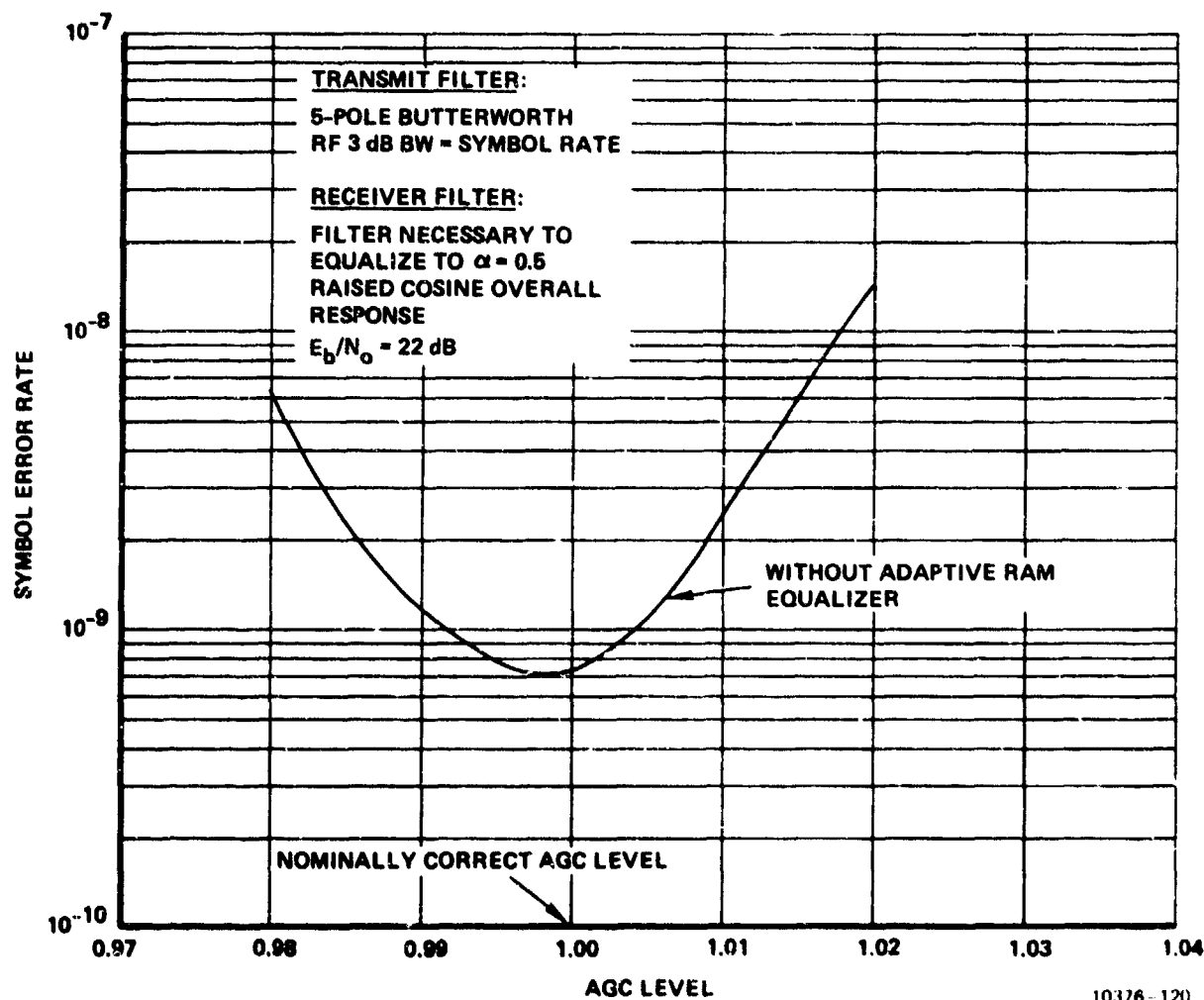
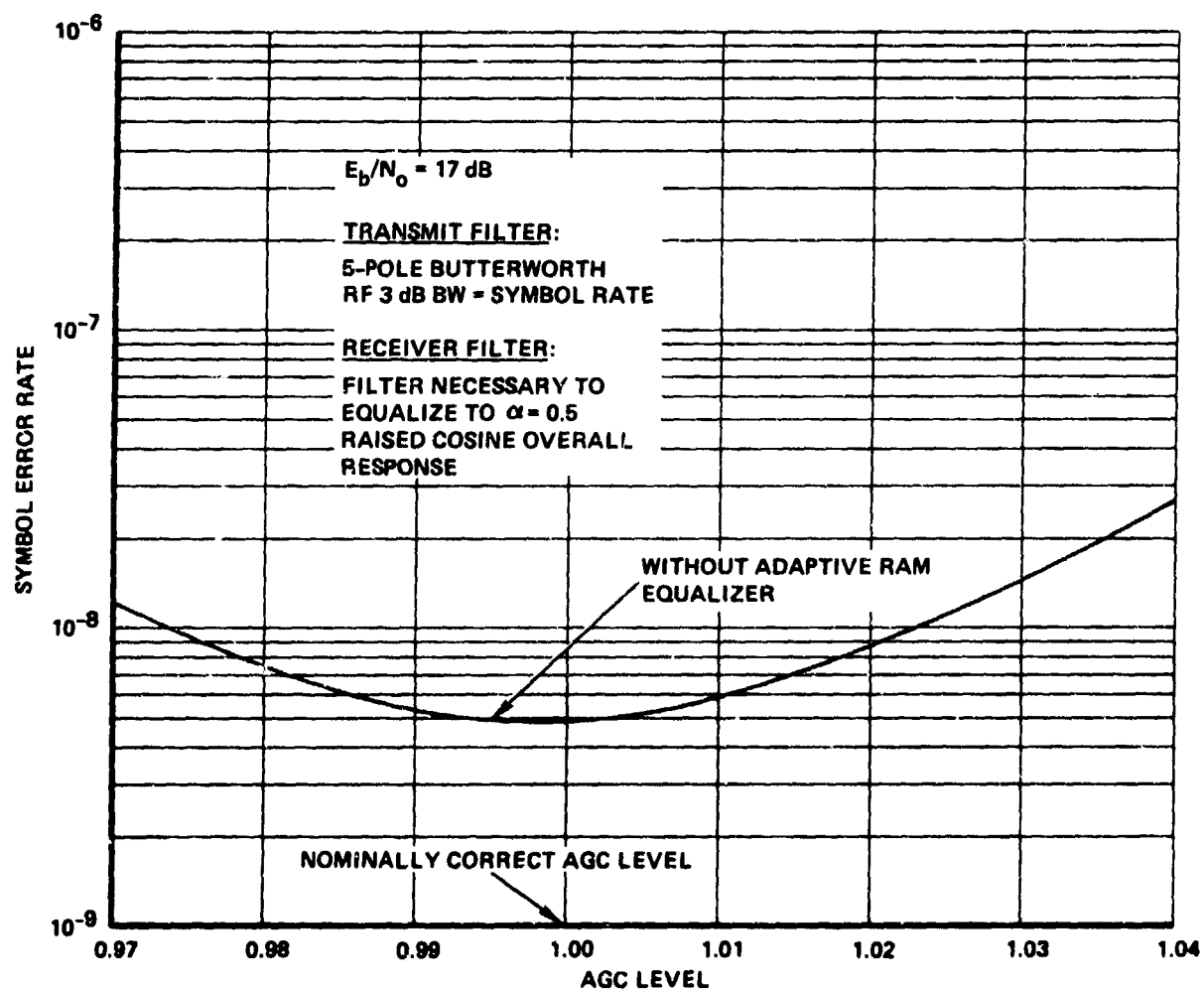
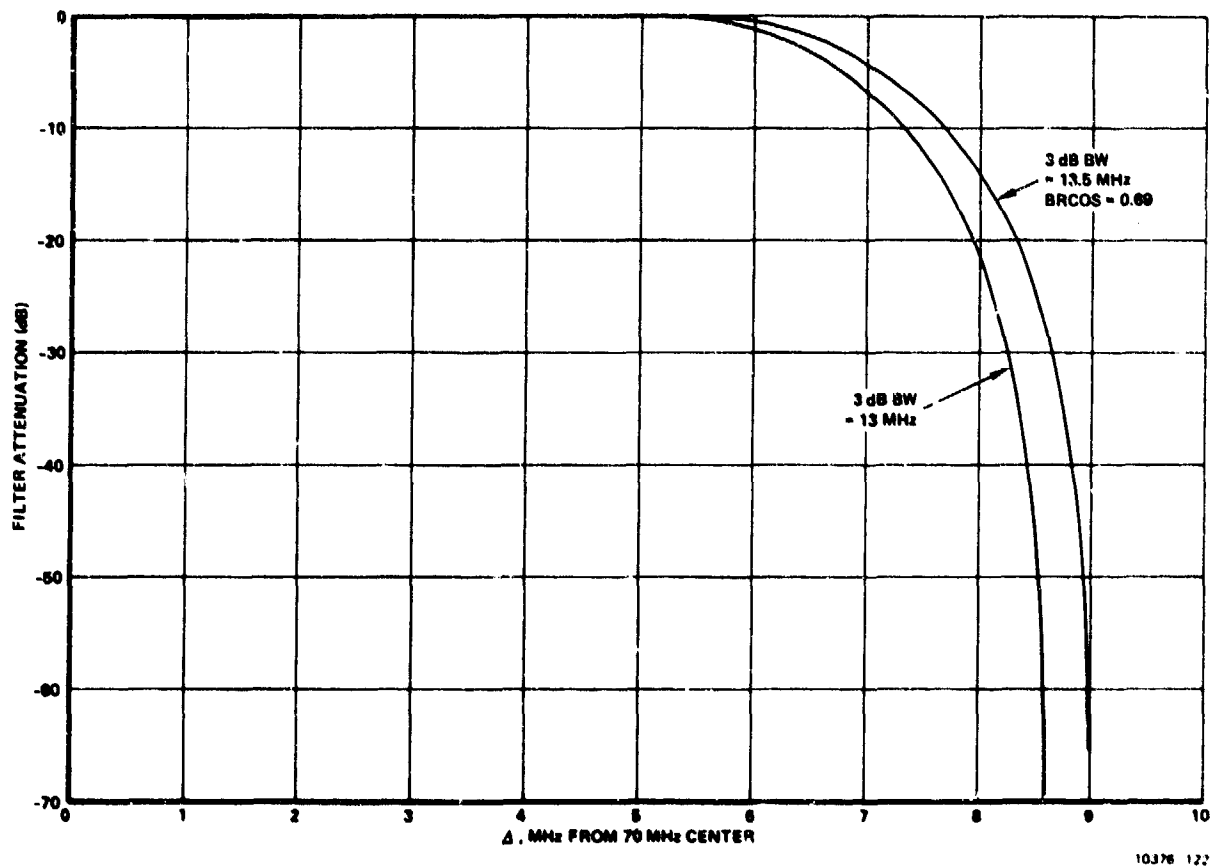


Figure 6.9.3.4-1. 8-QAM Sensitivity to AGC Variation



10376-121

Figure 6.9.3.4-2. 4-QAM Sensitivity to AGC Variation



10376 122

Figure 6.9.4-1. $\alpha = 0.25$ Raised Cosine Frequency Response

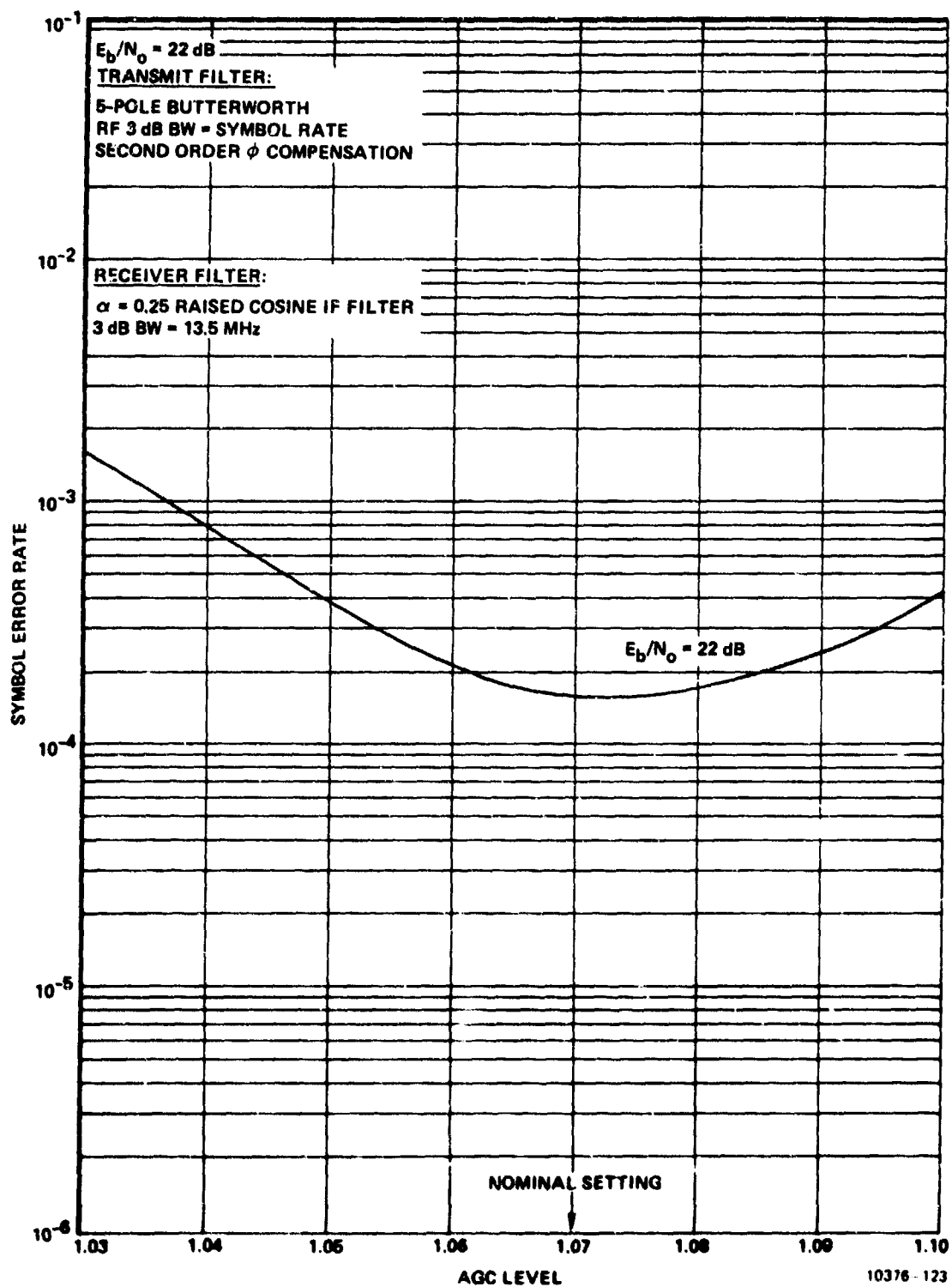


Figure 6.9.4-2. 8-QAM - Sensitivity to AGC

that would result without the use of the baseband equalization scheme described in Paragraph 6.9.2.1. It is also the symbol error rate for the tentative decisions in Figure 6.9.2.1. This curve was produced to determine the best setting for AGC level which, as seen in Figure 6.9.4-2, occurs at AGC level = 1.07. At this setting, the tentative decisions feeding the baseband equalization circuitry have an error rate of 1.5×10^{-4} .

Using this AGC level, the performance of the demodulator using the baseband equalizer was next simulated. Figure 6.9.4-3 shows the resulting performance for the filter with 13.5 MHz 3 dB bandwidth. At 22 dB it is seen that the baseband equalized symbol error rate has been dropped to 8.6×10^{-9} whereas the tentative decision symbol error rate was 1.5×10^{-4} . This shows the effectiveness of the baseband equalization technique. Also, we note that the equalized performance is within 1.5 dB of ideal 8-QAM at 10^{-9} error rate.

Figure 6.9.4-4 shows the baseband equalized performance when the 3 dB bandwidth of the raised cosine filter is reduced to 13 MHz. Performance is still within 1.8 dB of ideal at 10^{-9} error rate. One of the SAW filter manufacturers (Andersen Laboratories, Inc. - BP 70 series) sells an off-the-shelf 13 MHz 3 dB bandwidth 70 MHz IF bandpass filter. From these simulations it appears that this filter can be used to provide performance within 2 dB of ideal at 10^{-9} error rate.

The resulting performance plotted in Figure 6.9.4-4 assumed ideal receiver phase reference and symbol timing. In order to evaluate the effect of nonideal implementation, the simulation was again performed for the 13 MHz 3 dB bandwidth filter assuming 0.5° rms phase jitter and symbol timing offset of 0.75 percent of a symbol from nominal. The performance curve in Figure 6.9.4-5 was the result. Comparing Figures 6.9.4-4 and 6.9.4-5, it can be seen that at 10^{-9} error rate, the additional equipment imperfection degrades performance by about 0.4 dB for 8-QAM. Figure 6.9.4-6 shows the performance for the same conditions

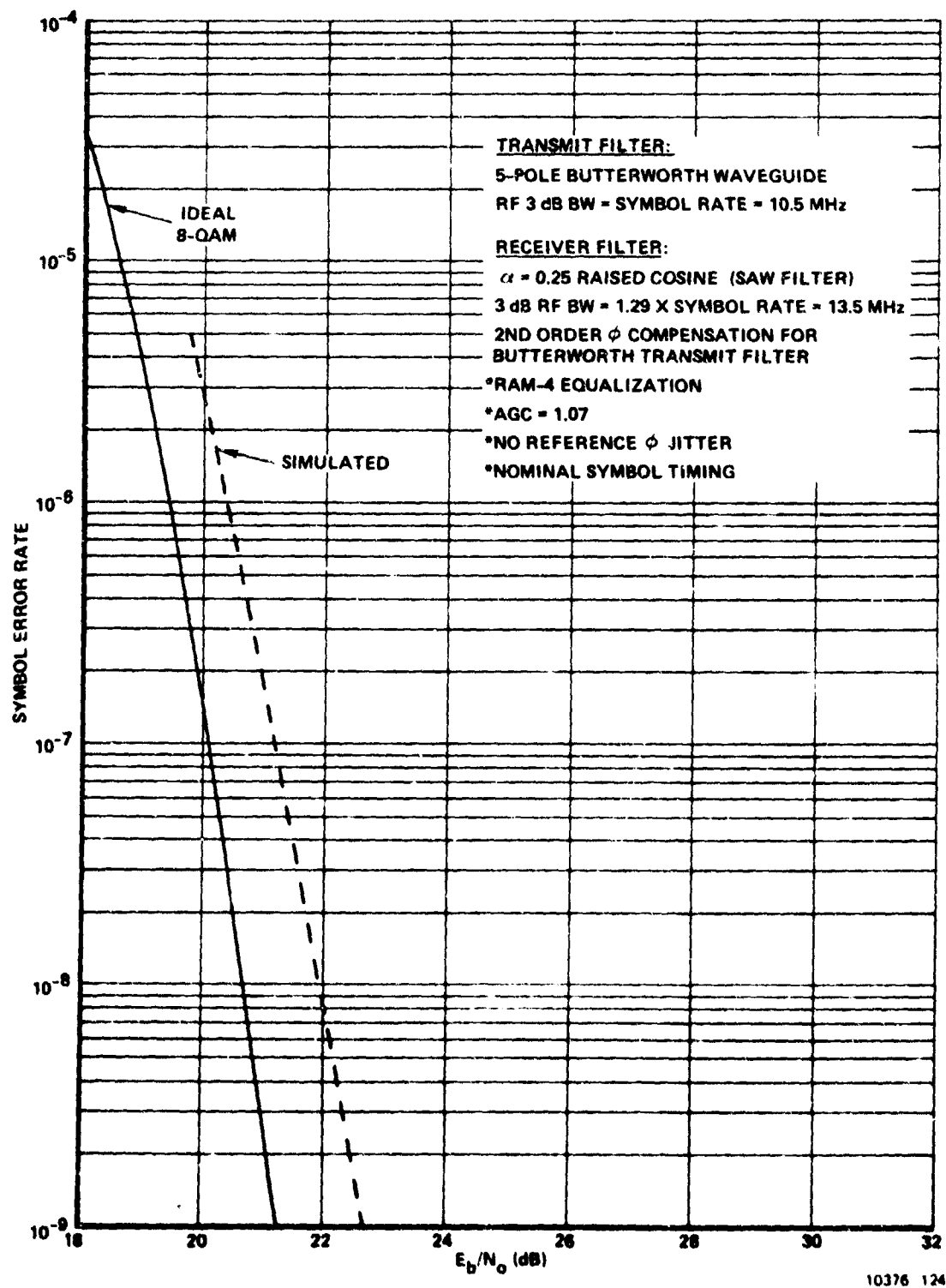


Figure 6.9.4-3. 8-QAM Performance

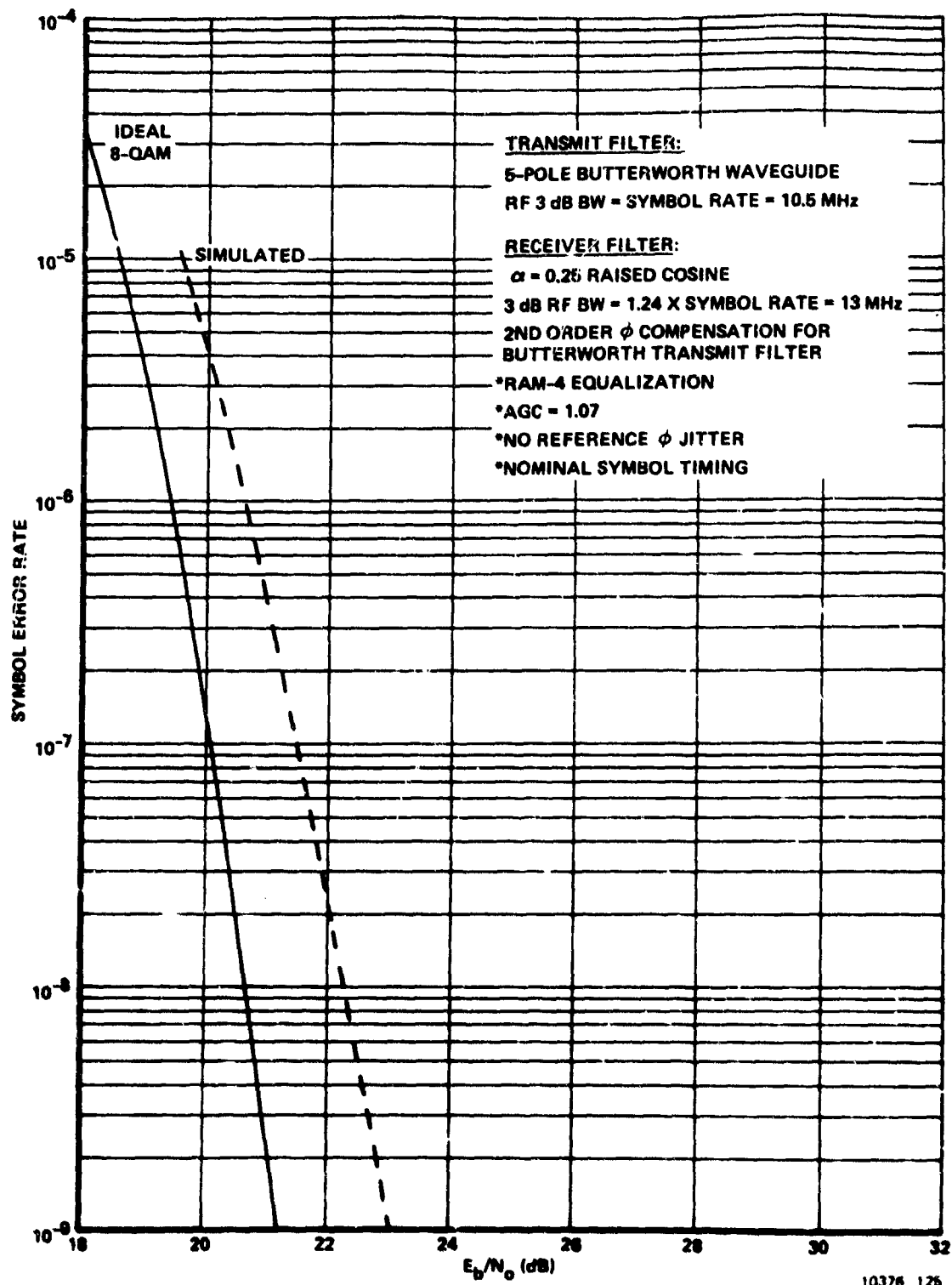


Figure 6.9.4-4. 8-QAM SAW Filter Performance

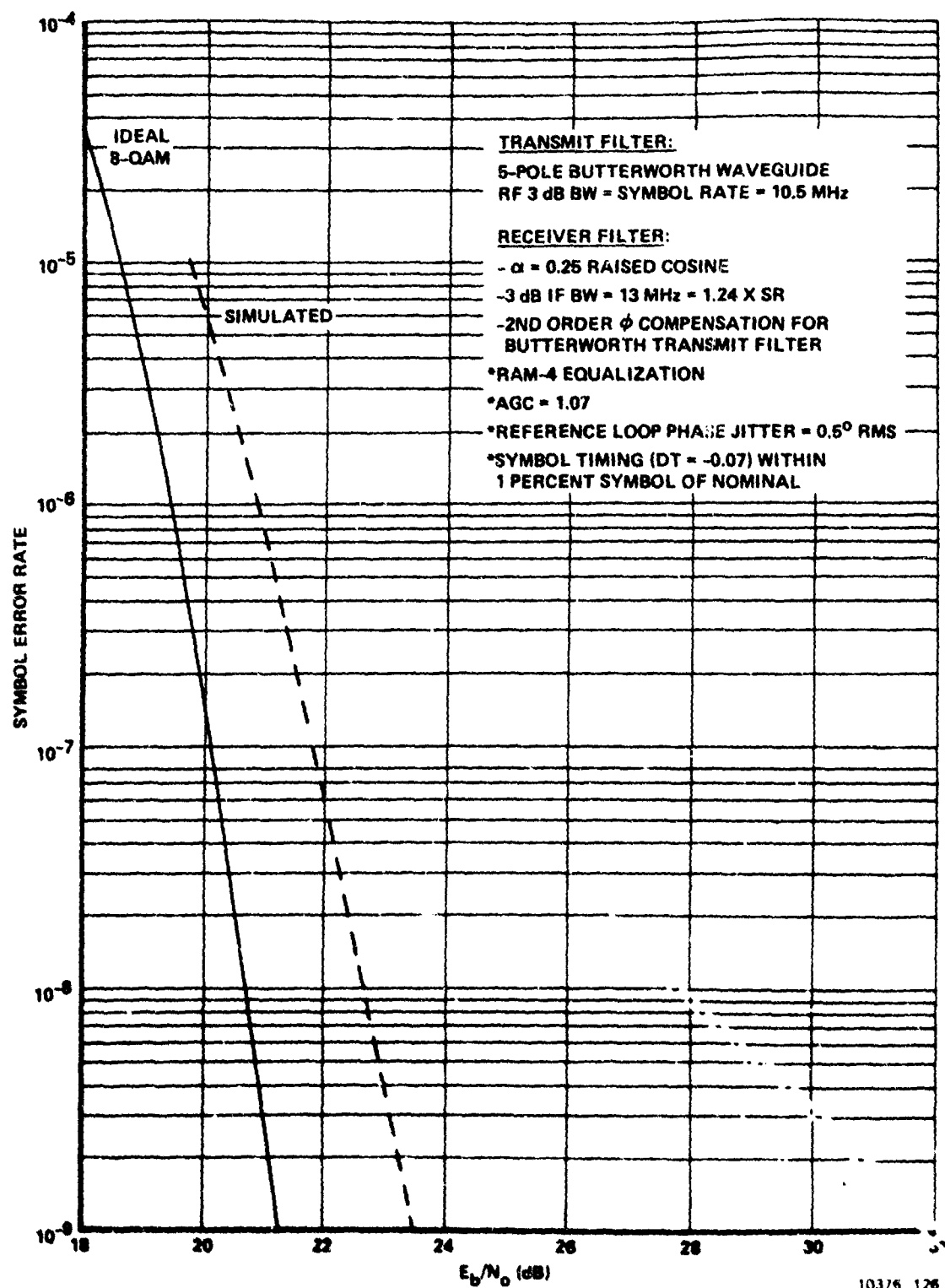


Figure 6.9.4-5. 8-QAM Performance

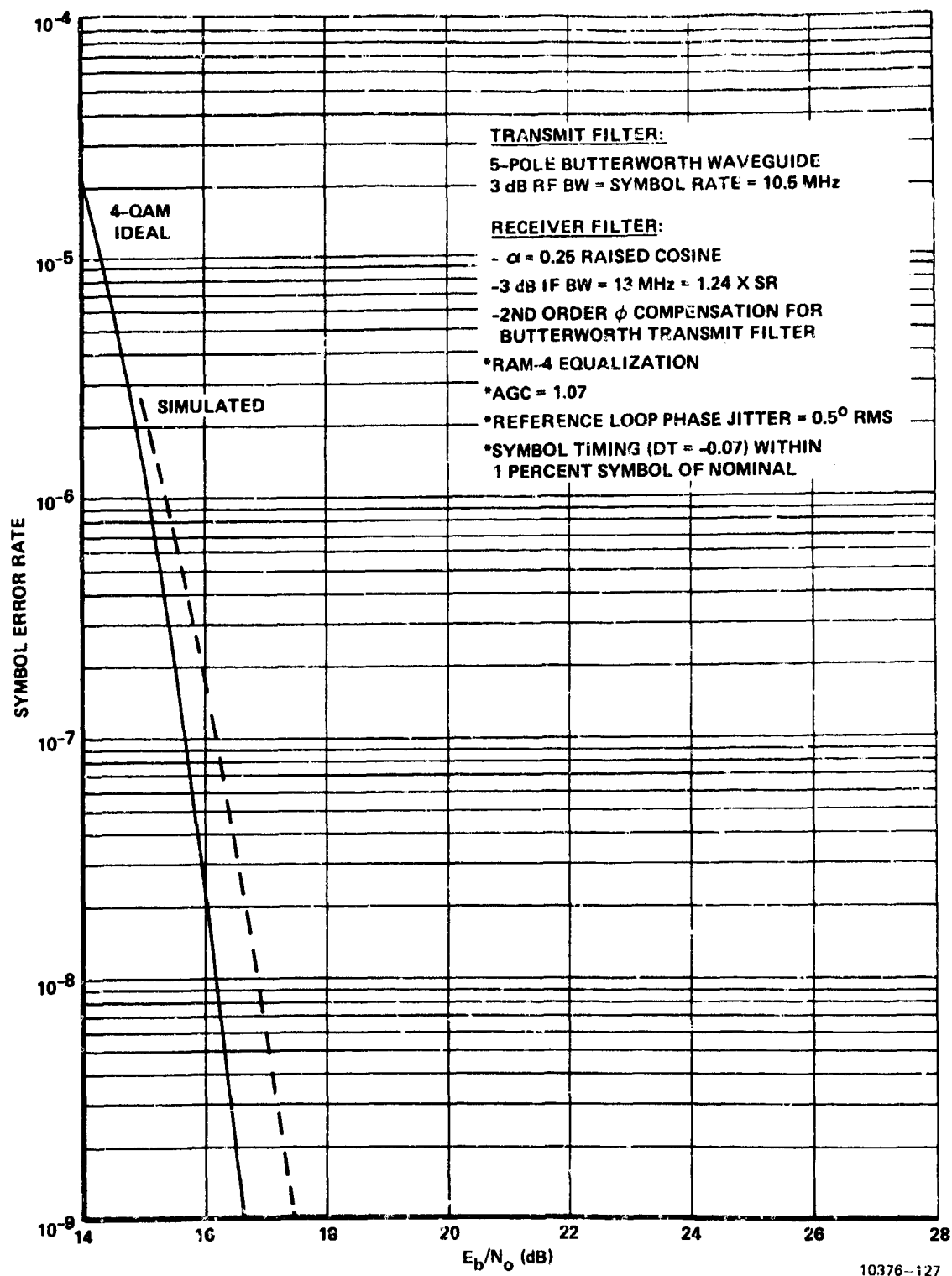


Figure 6.9.4-6. 4-QAM Performance

for 4-QAM. Even with the equipment imperfections, the 4-QAM performance is within 0.8 dB of ideal.

6.9.5 Computer Simulations - Summary and Conclusions

Based upon the computer simulations, the following summary has been formed as the basis for inputs to the hardware designers.

1. The use of the adaptive predistortion technique at the modulator allows the use of the M-QAM signalling format with a TWT amplifier and essentially no degradation occurs relative to use of a truly linear amplifier.
2. A five-pole Butterworth waveguide filter having 3 dB bandwidth of 10.5 MHz provides FCC 19311 spectral compliance in a 14 MHz authorized bandwidth. The symbol rate of the M-QAM modem will be 10.5 MHz.
3. The receiver IF filter can be a five-pole Butterworth filter having 3 dB bandwidth of 14.7 MHz or an off-the-shelf SAW filter having 3 dB bandwidth of 13 MHz. In either case, second order all-pass phase compensation networks should be used to reduce group delay distortion occurring in the transmit and/or receiver IF filter. Although we used no amplitude correction equalization in the simulated IF filters, the provision of such a correction adjustable up to 2 dB of parabolic amplitude boost across a 14 MHz IF bandwidth would be desirable.
4. The hardware phase reference loop must be designed to hold the phase jitter to less than 0.5° rms.
5. The hardware symbol timing loop must be designed to hold timing jitter to less than 1 percent of symbol time rms.

6. The hardware AGC loop must be designed to hold AGC variation to less than 1 percent rms variation about nominal.

The hardware M-QAM modem incorporating these inputs is described in the companion Design Plan document.³⁶

7. AN APPLICATION OF ERROR CORRECTION CODING TECHNIQUES TO A SPECTRALLY-EFFICIENT DIGITAL MODEM

A general discussion of the application of coding to spectrally-efficient modems is contained in Appendix 3. Here we shall be concerned specifically with a particular coding technique applicable to the M-QAM signaling technique.

When one considers the types of errors that occur due to channel noise with a multilevel signaling scheme like M-QAM, he is immediately impressed with the fact that adjacent level errors are by far the dominant type on each of the quadrature channels. This can be seen by considering that the M levels are spaced by Δ volts and that an adjacent level error is made for channel noise greater than $\Delta/2$ volts, whereas for a nonadjacent error, channel noise voltage greater than $(3/2)\Delta$ must occur. The ratio of the two noise voltages is thus seen to be 3, or a power ratio of 9, which corresponds to approximately 9.5 dB. Thus, the probability of a nonadjacent error corresponds to a signal-to-noise ratio which is 9.5 dB higher than for the probability of an adjacent level error. Obviously then, the probability of symbol error is almost totally determined and dominated by the adjacent level errors.

From the fact that adjacent level errors are so dominant for the M-QAM schemes ($M > 2$), it is obvious that it can be very wasteful to use any of the error correction capability of coding to protect against nonadjacent level errors. This fact argues against coding strategies involving the indiscriminate application of coding to the full incoming information bit stream followed by a mapping of the coded bits onto the M-QAM signal states.

An encoding scheme that makes more effective use of the power of coding for multilevel signal alphabets (in that it recognizes that correction of adjacent level errors is what is most needed) is shown in Figure 7-1. Here, we have shown the application of coding to an 8-level

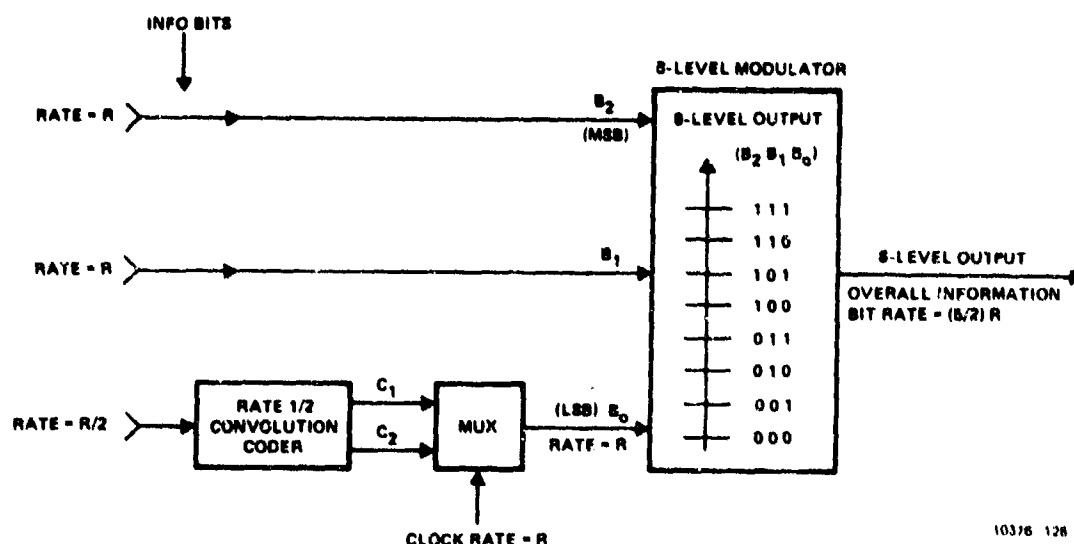


Figure 7-1. Error Correction Coding, Rate = 5/6,
Applied To 8-Level Modulation

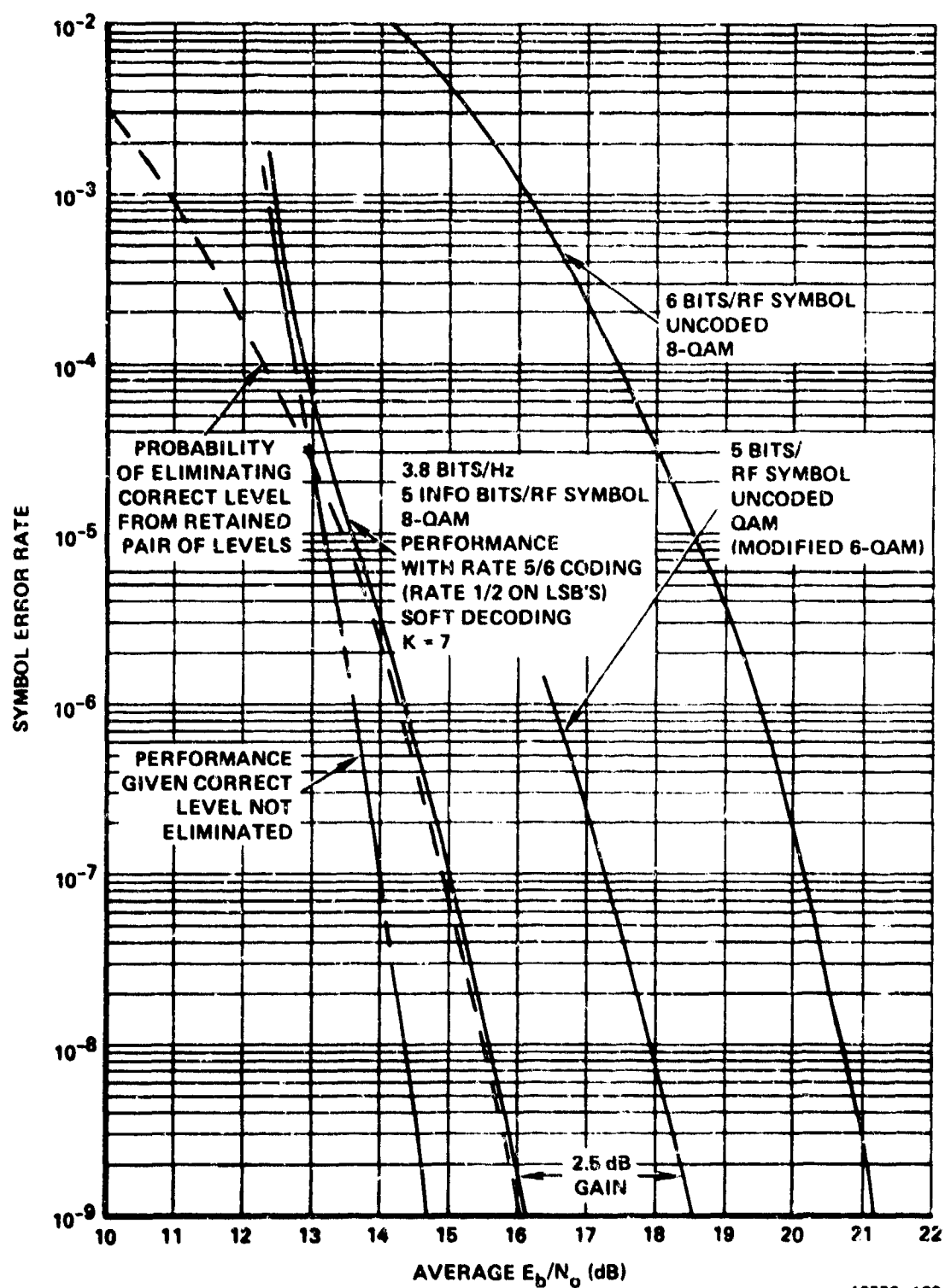
PAM modulator (which could be one of the quadrature channels of an 8-QAM modulator). As shown, the LSB (B_0) input to the 8 level modulator is actually a coded bit from a rate 1/2 coder. The two MSB's (B_1 and B_2) input to the 8-level modulator are uncoded information bits. Thus this encoding scheme carries $2 \frac{1}{2}$ information bits per 8-level symbol as opposed to 3 bits in the uncoded case. The overall coding rate is, therefore $(2.5/3) = 5/6$.

The rate one-half coding in Figure 7-1 has been applied only to the LSB of the 8-level symbol. The basic idea in the decoding scheme envisioned for this encoding strategy is to use the error-correcting capability of the rate one-half code to resolve which of two adjacent 8-ary levels was transmitted. That is, we envision as a first step at the demodulator that only the two 8-ary levels immediately above and

immediately below the received level be retained as decision candidate levels. From the 8-level mapping shown in Figure 7-1, it is seen that one of these two retained levels has a 0 in the LSB position and the other retained level has a 1 in the LSB position. Thus, as far as deciding between the two candidate levels is concerned, a binary decision must be made. The binary rate one-half code, employed in the fashion shown in Figure 7-1 on the LSB (B_0), is ideally suited to making this binary decision. The correlation of the received level with a coded bit "0," which is the candidate level with a "0" in the LSB position; and the correlation with a coded bit "1," which is the candidate level with a "1" in the LSB position, can be computed and fed to a rate one-half decoder for deciding on the LSB, B_0 . Once a decision is made on B_0 , the two corresponding MSB's, B_1 and B_2 , simply "tag along" with the coded LSB and a decision is implicitly made on them at the same time that the decision is made by the decoder on the LSB. Therefore, this scheme follows the suggestion previously made that the power of the error correction code concentrated upon a resolution of adjacent level errors.

The performance improvement obtainable with the coder/decoder strategy outlined above is limited by the probability of eliminating the correct 8-ary level on the initial narrowing down process to select only the closest two 8-ary levels. It can be seen that if the spacing between levels is Δ , then a noise greater than Δ is required to push the transmitted level to a point between two levels - neither of which is the transmitted level. On the other hand, an error is made in the uncoded system for a noise greater than $\Delta/2$. Thus, the possibility exists for obtaining almost 6 dB (less the coding bandwidth loss) of gain over the uncoded 8-level system.

Figure 7-2 shows the performance we have computed for a constraint length 7 rate one-half convolution code applied to the LSB's as in the scheme described above for 8-QAM signaling. A soft decision Viterbi decoder is assumed. We note that with the use of this powerful rate one-half code, the performance is limited by the probability of eliminating the correct level from the retained pair.

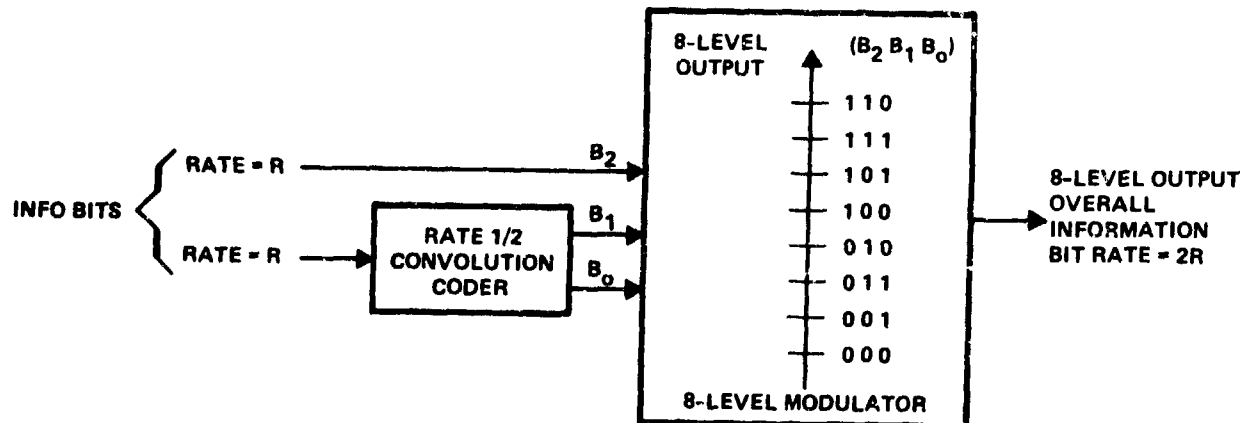


10376-129

Figure 7-2. 8-QAM Performance With Rate 5/6 Coding

The gain relative to the uncoded 8-QAM signal is 5.2 dB at symbol error rate of 10^{-9} . However, since the coded signal carries only 5 information bits per RF symbol, the true coding gain should be computed with reference to a 5 bit/symbol uncoded modulation. Such a signal is modified 6-QAM, described in Paragraph 4.2.1, and the performance of this uncoded modulation is plotted for reference. As shown, the coded system gains 2.5 dB relative to modified 6-QAM uncoded signaling. Both the coded 8-QAM scheme and the uncoded modified 6-QAM scheme operate at 3.8 b/s/Hz in a practical system.

Another coding scheme applicable to an 8-QAM modulator briefly examined on this study is shown in Figure 7-3. Here, one of the information bits, B_2 "tags along" with the two rate one-half coded bits, B_0 and B_1 . The three bits, B_0 , B_1 and B_2 are applied to an 8 level modulator with the level assignments shown in Figure 7-3. Note that with the level assignments shown, any set of four successive



10376-130

Figure 7-3. Rate 4/6 Error Correction Coding Applied to an 8-Level Modulator

8-ary levels contains all four rate 1/2 code branches, i.e., $B_0B_1 = 00, 01, 10, 11$. The idea suggested here is to narrow down at the

receiver to the four levels closest to the received level as decision candidates, and then to let a rate one-half decoder resolve which of the four candidates was actually transmitted. It can be verified that if the spacing between adjacent levels is Δ , then a noise of 2Δ is required to eliminate the correct level from the set of four retained candidates. The 8-level symbol error rate, on the other hand, is dominated by noise exceeding $\Delta/2$, i.e. half the spacing. Thus, the probability of eliminating the correct node on the four-candidate-selection process at the receiver is 12 dB better (less the coding bandwidth loss) than the symbol error rate of the uncoded 8-level scheme. Since the coded scheme described is capable of carrying 2 bits per 8-level symbol, whereas the uncoded scheme carries 3 bits per 8-level symbol, the overall code rate is $2/3$.

A decoder for deciding on the correct one of the four candidate levels like that described in Appendix 3 for 4-PAM signaling is envisioned. Once the bits B_0 and B_1 are decided by the decoder, the associated "tag along" bit, B_2 is also determined.

Application of this 8-level coding strategy to both quadrature legs of an 8-QAM modulator when a constraint length 7, rate one-half encoder is employed, along with a soft decision Viterbi algorithm decoder at the receiver, produces the performance of Figure 7-4. The coded 8-QAM scheme carries 4 information bits per 8-QAM symbol. Comparing the performance at 10^{-9} symbol error rate shows that 5 dB of coding gain is obtained relative to the equivalent-capacity uncoded 4-QAM scheme. Both schemes are capable of 3 bits/sec/Hz under FCC Docket 19311 in a practical modem design.

These coding gains available with reasonable coding strategies further enhance the flexibility and desirability of the selected M-QAM modulation schemes for spectrally efficient digital data transmission. The coding results show that coding can be profitably incorporated at a

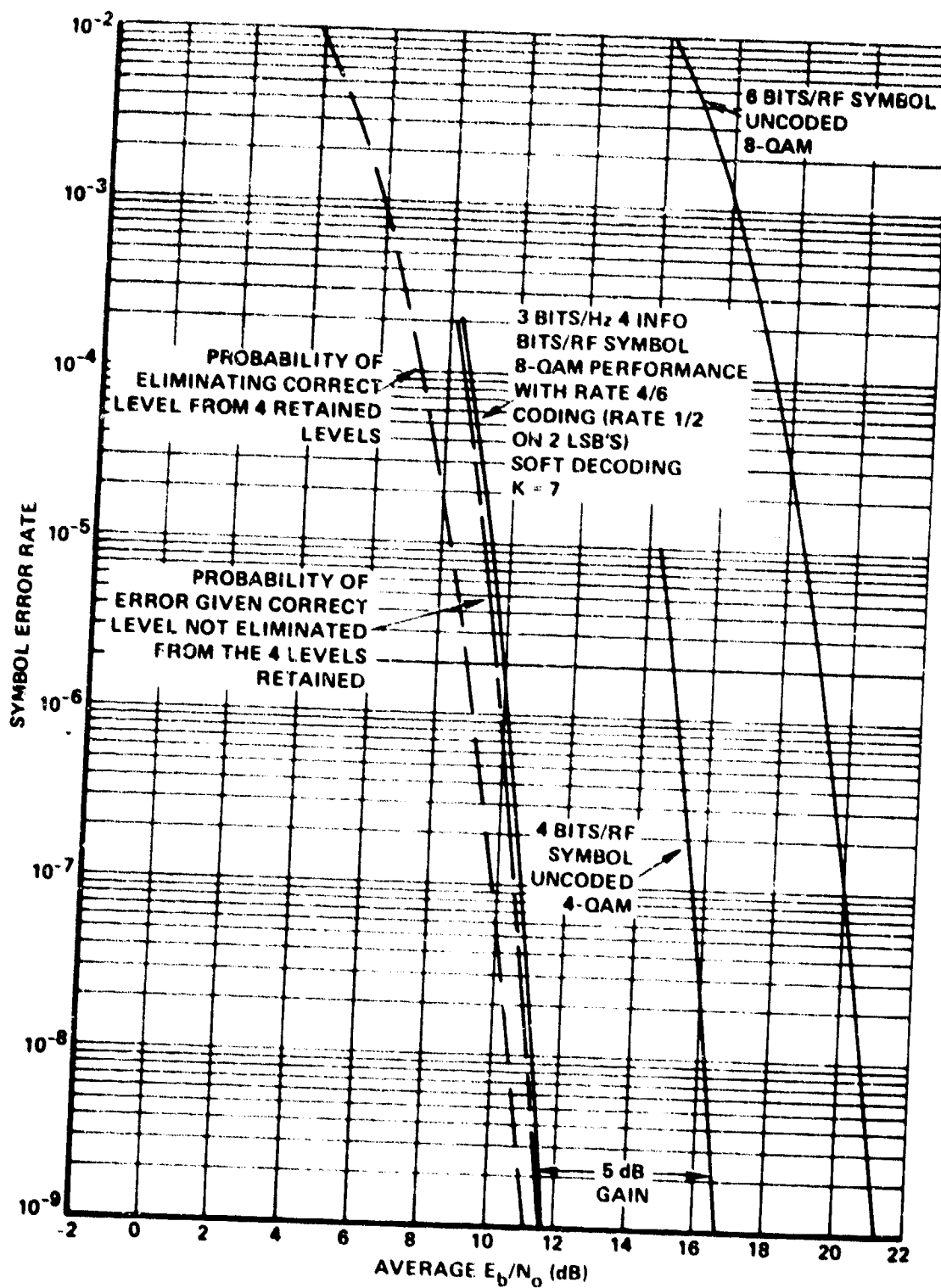


Figure 7-4. Performance of Rate 2/3 Coding With 8-QAM Modulator

10376 131

later date to an uncoded M-QAM modem to obtain improved performance. The schemes outlined above are believed to be new coding strategies for spectrally efficient modems. They concentrate the power of the error correction codes where they are most needed in a spectrally efficient multilevel modem - that is, on the resolution amongst possible levels close to the received level. Possible levels sufficiently removed from a receive level are so unlikely as to be totally disregarded as viable decision candidates. Dramatic gains using relatively simple coder/decoder strategies follow upon the adoption of this viewpoint.

8. SUMMARY AND MAJOR CONCLUSIONS OF THIS STUDY

As a result of the work performed on this study, we have come to the following major conclusions regarding linear modulation techniques for digital microwave:

1. Practical modem designs can achieve spectral efficiencies in the 3 to 5 bits/s/Hz range under the FCC Docket 19311 criterion.
2. Attempts to push the spectral efficiency higher than approximately 5 bits/s/Hz under FCC Docket 19311 should be looked upon with a great deal of skepticism because of the practical difficulties associated with implementing circuitry with the required low imperfection levels. For example, distortion levels in all the receiver IF signal processing chain would need to be 50 dB down (or greater) relative to the signal, for higher spectral efficiencies.
3. Comparisons among various digital modulation schemes should be made on the basis of peak (preferably, saturation) power amplifier output requirement. A scheme requiring the least peak power amplifier capability is best. Comparisons should not be made on the basis of required average received signal-to-noise ratio since this measure does not bear any common relationship among various modulation techniques to the efficiency with which the peak power amplifier capability is being used. The reason no common relationship exists is because different modulation schemes generally have different peak-to-average power ratio requirements at the input to the power amplifier, and/or they involve different spectral truncation power losses in a postamplifier (waveguide)

filter, and/or they require differing amounts of power amplifier backoff.

4. Partial response schemes are generally poorer in performance when peak power limited comparisons are made with signalling schemes not using partial response. If baseband partial response spectral shaping is employed, the ratio of peak-to-average power at the input to the power amplifier is always increased as demonstrated in Paragraph 2.2.2. If, on the other hand, the partial response spectral shaping is effected by a waveguide filter, a similar spectral truncation power loss will be incurred as demonstrated in Paragraph 6.6.3. Over the range of spectral efficiencies from 3 to 5 bits/s/Hz, the peak power comparisons made in this study indicate that the use of M-QAM signalling with no partial response is preferable to the multilevel partial response schemes. Generally, over this spectral efficiency range, increasing the number of levels in the no partial response M-QAM scheme is a more effective way to obtain more bits/s/Hz in a peak power limited situation than by staying with the same number of levels and employing more restrictive filtering to obtain partial response shaping.
5. A linear microwave amplifier such as that developed by Ford can be used with M-QAM signalling format but the peak input drive level must be limited to 2.5 to 3.5 dB below single signal saturation. In addition, waveguide filtering would also be required to limit distortion side lobe levels to below the FCC Docket 19311 spectral mask. It was shown, however, that the Ford linear amplifier peak power capability is more efficiently used with the adaptive predistortion linearization scheme using waveguide filters.

8. SUMMARY AND MAJOR CONCLUSIONS OF THIS STUDY

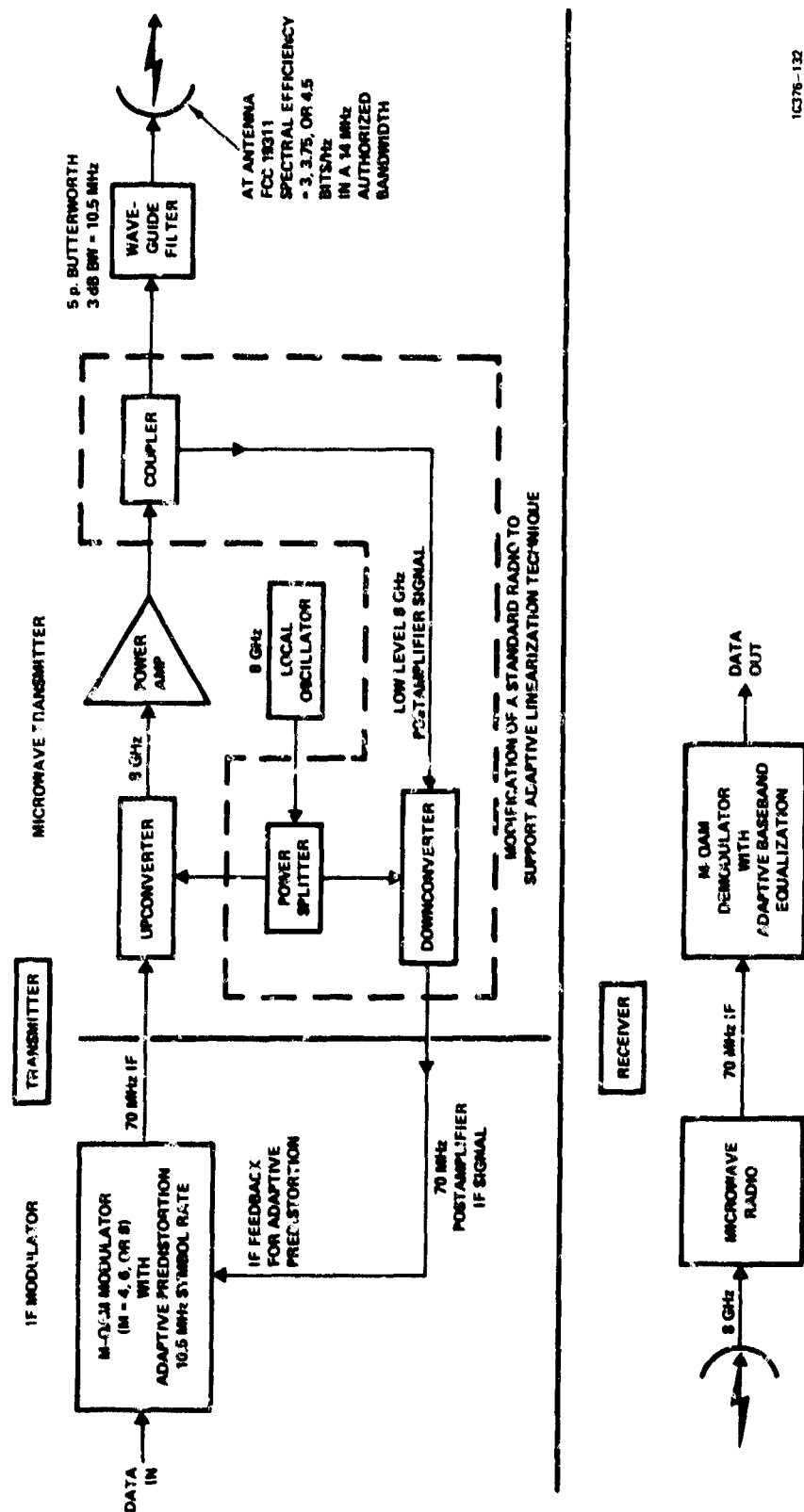
As a result of the work performed on this study, we have come to the following major conclusions regarding linear modulation techniques for digital microwave:

1. Practical modem designs can achieve spectral efficiencies in the 3 to 5 bits/s/Hz range under the FCC Docket 19311 criterion.
2. Attempts to push the spectral efficiency higher than approximately 5 bits/s/Hz under FCC Docket 19311 should be looked upon with a great deal of skepticism because of the practical difficulties associated with implementing circuitry with the required low imperfection levels. For example, distortion levels in all the receiver IF signal processing chain would need to be 50 dB down (or greater) relative to the signal, for higher spectral efficiencies.
3. Comparisons among various digital modulation schemes should be made on the basis of peak (preferably, saturation) power amplifier output requirement. A scheme requiring the least peak power amplifier capability is best. Comparisons should not be made on the basis of required average received signal-to-noise ratio since this measure does not bear any common relationship among various modulation techniques to the efficiency with which the peak power amplifier capability is being used. The reason no common relationship exists is because different modulation schemes generally have different peak-to-average power ratio requirements at the input to the power amplifier, and/or they involve different spectral truncation power losses in a postamplifier (waveguide)

6. The use of baseband or IF filtering alone, with realistic linear amplifiers, in an attempt to avoid the use of a waveguide filter for obtaining FCC Docket 19311 compliance, is a wasteful technique in terms of overall system link margin. The reason for this is that realistic power amplifiers' intermod distortion characteristics require excessive power backoff to obtain the spectral distortion levels needed to remain under the FCC Docket 19311 spectral mask.
7. The discovery on this study of the adaptive predistortion technique for linearizing a power amplifier for digital modulations represents a major development in the spectrally efficient modem area. The use of even TWT's with their relatively severe nonlinearities, which are adaptively and continuously compensated for by the predistortion technique - can now be realistically considered for the multi-amplitude linear modulation signalling techniques. The technique for linearization almost totally removes the amplifier as a degrading influence in the system - even for peak drive levels approaching single signal saturation. The employment of this technique thus allows the use of presently available power amplifiers for high spectral efficiency modems. It can also remove the pressure on microwave amplifier designers to attain increasingly stringent distortion levels in order to support digital signalling at increasing spectral efficiencies.
8. The development on this study of the baseband receiver equalization technique described in Paragraph 6.9.2.1 represents a significant accomplishment for high-speed digital communication. The use of this equalization technique results in a significantly cheaper

implementation than for adaptive IF equalization techniques. From simulation results obtained using the baseband equalization technique, performance within 1 to 2 dB of ideal M-QAM signalling is realistically obtainable with a practical modem design.

9. The use of a postamplifier waveguide filter (as opposed to preamplifier filtering) for effecting the most significant spectral shaping required to comply with FCC Docket 19311 is the most efficient technique for a situation involving a peak power limited amplifier. The theoretical result derived in Paragraph 6.6.3 comparing the relative efficiencies for pre- and post-amplifier filtering approaches supports this conclusion. Also, the peak power comparisons made in Paragraph 6.7.3 provide further simulation evidence that postamplifier filtering is best in the range of spectral efficiencies of most interest (3-5 bits/s/Hz).
10. A practical hardware implementation block diagram for an M-QAM modulator/demodulator has been presented in Figures 6.8.3 and 6.9.2.1. This modem is based upon and incorporates all the major results and conclusions given in 1-9 above. A detail hardware design is included in the companion design plan document³⁶. The modem has been designed to provide 3, 3.75, and 4.5 bits/s/Hz operation under the spectral constraints of FCC Docket 19311 for an authorized bandwidth of 14 MHz. These spectral efficiencies are obtained using 4-QAM, modified 6-QAM, and 8-QAM, respectively. The overall recommended system block diagram using this modem is as shown in Figure 8-1. The transmit spectrum in all spectral efficiency modes is as shown in Figure 8-2. The M-QAM (square-pulse) symbol rate is 10.5 MHz in all spectral efficiency modes. The bit



10376-132

Figure 8-1. Overall LMT System Block Diagram

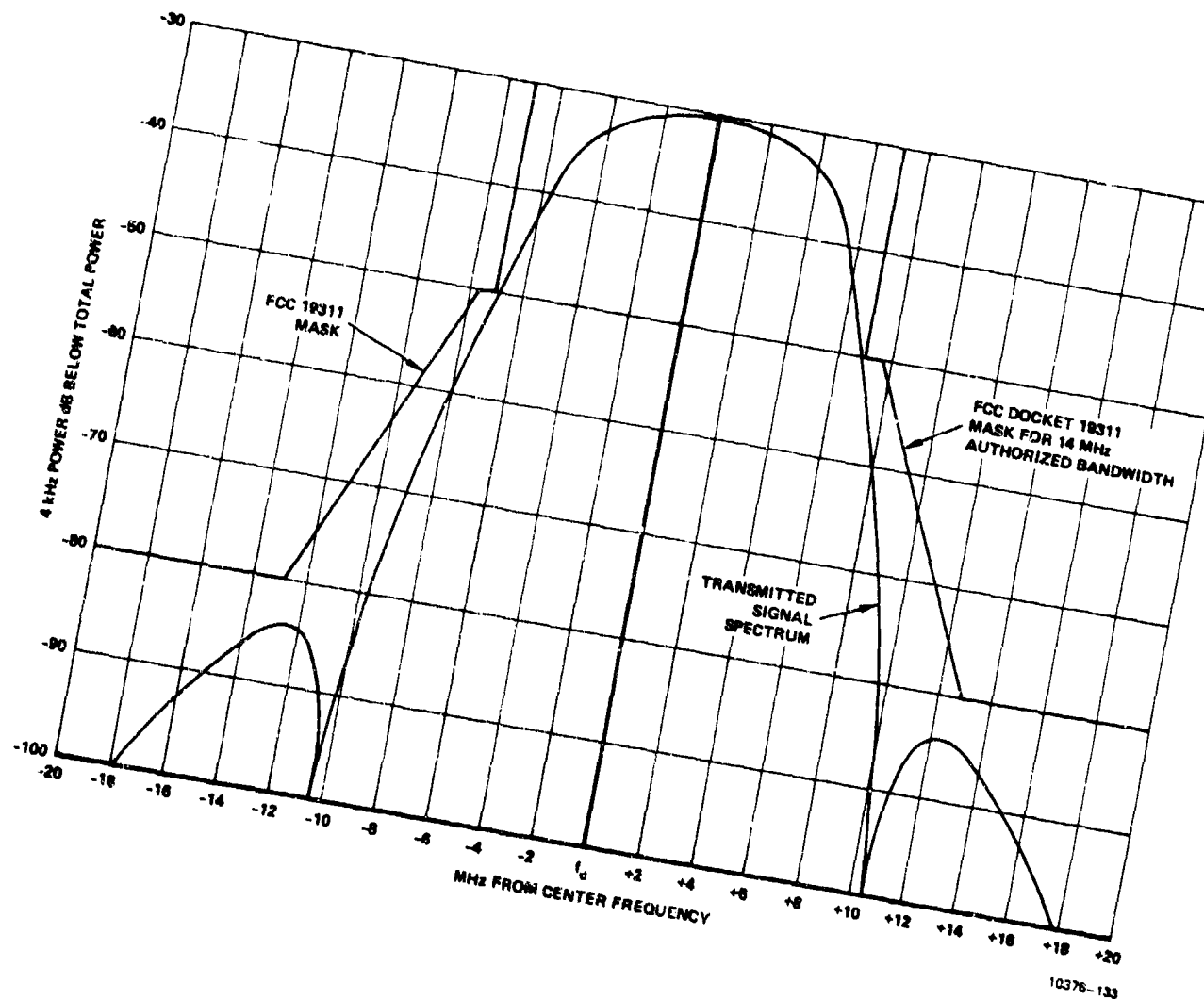


Figure 8-2. LMT Modem Spectrum

rates supported in the 14 MHz authorized bandwidth are 42, 52.5, and 63 Mb/s in the 3, 3.75, and 4.5 bits/s/Hz modes, respectively. As shown in Figure 8-1, the adaptive predistortion linearization technique is used at the transmitter. Thus, the power amplifier need not be a "linear" amplifier with this modem. A TWT amplifier can, in fact, be employed. A symbol rate wide (3 dB) five-pole Butterworth Waveguide filter is installed to trim the $\sin x/x$ spectrum from the power amplifier to obtain compliance with the FCC Docket 19311 mask as shown in Figure 8-2. At the receiver, the M-QAM demodulator with adaptive baseband equalization is used to decode the data. Based upon simulations, the measured performance of the modem will be as shown in Figure 8-3.

In summary, we feel that the M-QAM modem developed, using the conclusions of this study, represents the most desirable and efficient solution for obtaining spectral efficiencies of between 3 and 4.5 bits/s/Hz under FCC Docket 19311 spectral criteria. The modem makes use of several novel advancements in the state of the art of linear modulation/demodulation techniques which were conceived and developed on this contract. We feel that these developments (particularly the amplifier linearization technique) are key elements for opening up the realistic, practical consideration of digital microwave modems having spectral efficiencies in the 4 to 5 bits/s/Hz region under FCC Docket 19311.

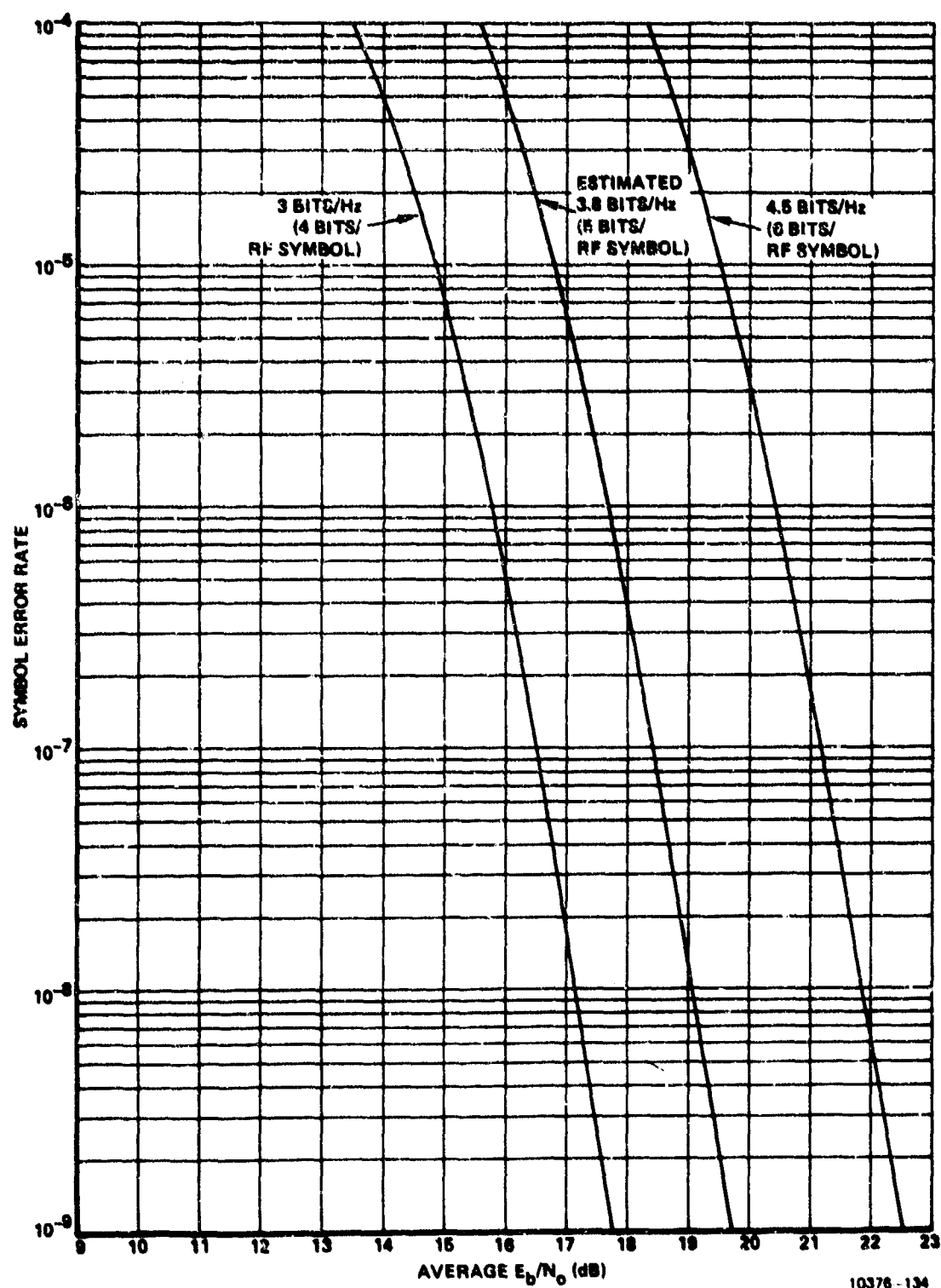


Figure 8-3. LMT Practical Hardware Modem Performance

APPENDIX 1
CHANNEL CAPACITY BOUNDS AND THEIR RELEVANCE
TO SIGNAL DESIGN

APPENDIX 1
CHANNEL CAPACITY BOUNDS AND THEIR RELEVANCE
TO SIGNAL DESIGN

In any analytical effort, it is useful to have theoretical bounds that represent goals for the analytical effort. In our present case the analytical effort which we wish to discuss is the search for an appropriate signal design for use in conjunction with linear power amps on microwave digital data links. The goal of this signal design effort is that signal design which simultaneously optimizes performance and spectral occupancy. The performance objective is to require as small a signal power as possible for a given probability of error. The spectral occupancy objective is to meet the spectral mask delineated in FCC Docket 19311.

Although there exist no theoretical bounds delineating allowable combinations of these exact performance and spectral constraints, there is one which comes close and, therefore, seems relevant to this effort. This theoretical bound is the channel capacity bound first advanced by Shannon.² This bound is also derived and stated in compact form by Wozencraft and Jacobs.³ The theoretical equation for the channel capacity bound is given by

$$C_n = (1/2) \log_2 (1 + 2E_n/N_0) \quad (A1-1)$$

where:

C_n = bits/dimension channel capacity

E_n = Average energy per dimension

N_0 = One-sided white Gaussian noise spectral density

The assumption is made that the transmitted signals are represented by points in an n-dimensional signal space. The "dimensions" of the signal space are simply an orthogonal set of basis waveforms. The transmitted signal is thus a linear combination of the basis waveforms. The channel capacity of Equation (A1-1) is obtained when one derives the maximum number of bits of information per dimension that can be carried by the signal at zero error rate. The bound is obtained as the dimensionality of the signal space tends to infinity. The bound of Equation (A1-1) then represents an unattainable (in practice) limit for an infinitely complex modulator (mapping of an infinity of signal points onto an infinite dimension signal space). It is to be noted that "bandwidth" never explicitly enters into the theoretical derivation of the channel capacity bound. Also note that the bound is not on bit rate in bits/second but rather on "bits/dimension."

Bit rate in bits/second and channel bandwidth in hertz can be forced into the channel capacity equation in an intuitively pleasing way. These concepts enter the capacity equation when one considers how many orthogonal dimensions per second can be accommodated by a channel of "bandwidth" W hertz. If one defines the bandwidth W = equivalent Nyquist^{4, 5} bandwidth of the channel, then the Nyquist theorem states that

$$D = 2W \quad (A1-2)$$

where

D = Orthogonal dimensions (no crosstalk pulses) per second

W = Equivalent Nyquist bandwidth of channel

Thus combining Equations A1-1 and A1-2 one obtains

$$R = C_n D \leq W \log_2 (1 + 2E_n D / N_0 D)$$

or

$$R \leq W \log_2 (1 + \rho) \quad (\text{A1-3})$$

where

R = Bit rate in bits/second

ρ = S/N ratio in Nyquist bandwidth

From Equation (A1-3) we obtain a bound on bits/s/Hz where hertz is Nyquist bandwidth:

$$\frac{R}{W} \text{ (bits/s/Hz)} \leq \log_2 (1 + \rho) = \log_2 \left[1 + \frac{E_b}{N_0} \left(\frac{R}{W} \right) \right] \quad (\text{A1-4})$$

Thus we are left with a bound on bits/s/Hz for zero error rate versus ρ , the S/N in Nyquist bandwidth. Equation (A1-4) is plotted in Figure A1.

For bits/s/Hz of Nyquist bandwidth and ρ , the S/N in the Nyquist bandwidth $\left(\frac{1}{2T} \right)$, this gives limits of systems for zero error rate. Generally, modulation schemes for a fixed error rate will fall to the right and below the channel capacity bound of Figure A1. We show in Figure A1 the combination of R/W and ρ for various M-ary PAM schemes for an error rate of 10^{-5} . Note that these schemes track the capacity bound - being roughly 7 to 8 dB away for all M. Generally, when a particular modulation scheme displays this characteristic of tracking within 7 or 8 dB at 10^{-5} error rate, it is an indication of a very efficient scheme and one that will be difficult to improve upon without the use of some type of error correction encoding.

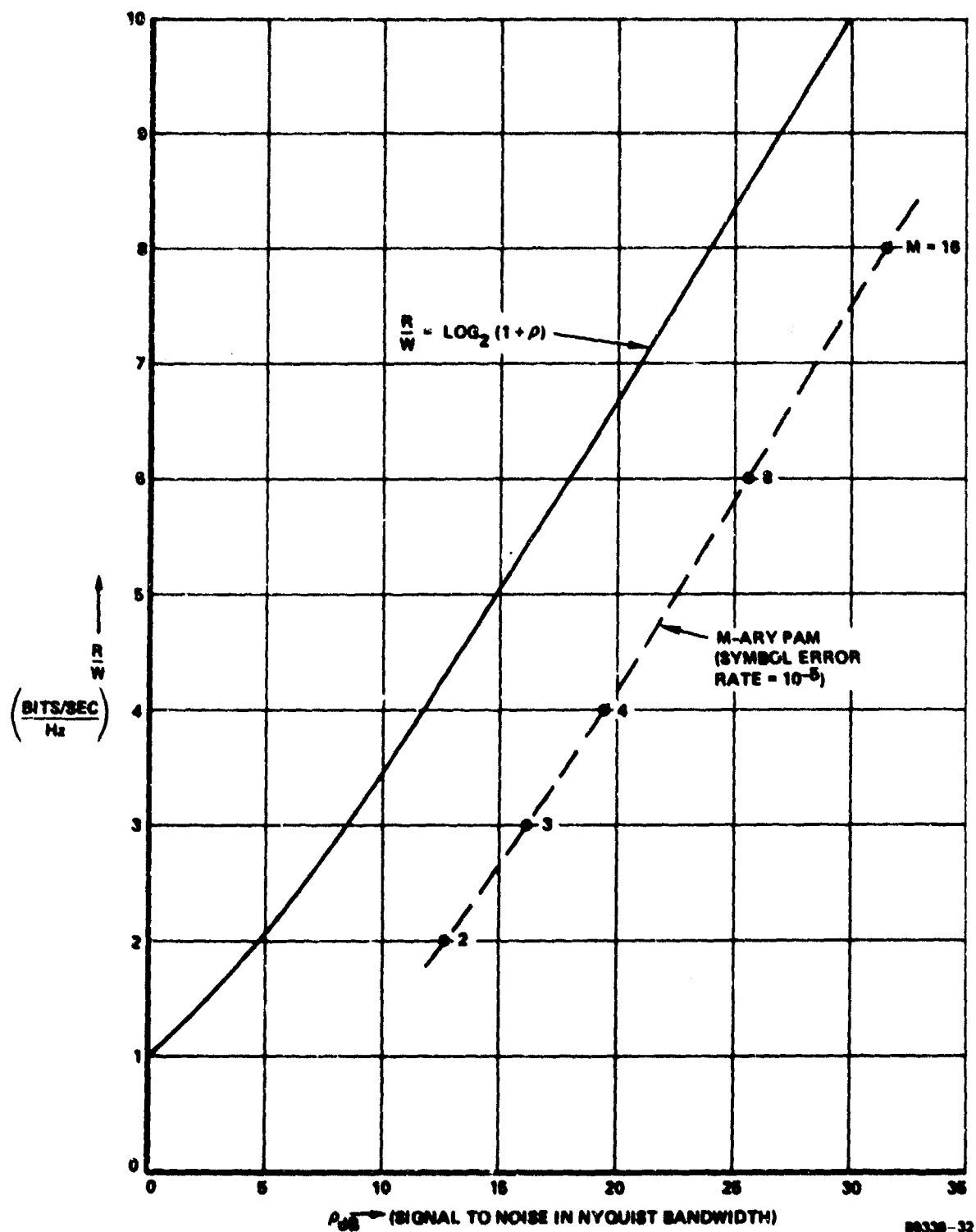


Figure A1. Theoretical Bound $\frac{R}{W}$ Versus ρ

APPENDIX 2
MINIMUM BANDWIDTH PULSE SHAPE

APPENDIX 2

MINIMUM BANDWIDTH PULSE SHAPE

Let us consider the problem of determining a pulse shape which minimizes spectral occupancy. The pulse is to be restricted to an interval of time $\pm T/2$ and is represented by some function of time, $f(t)$, during this interval. We wish to find the function of time, $f(t)$, such that:

$$I = \frac{1}{2\pi} \int_{-\omega_b}^{\omega_b} |\alpha(\omega)|^2 d\omega \quad (A2-1)$$

is maximum where $\omega_b = 2\pi f_b$ and:

$$\alpha(\omega) = \int_{-T/2}^{+T/2} f(t) e^{-j\omega t} dt \quad (A2-2)$$

We wish to maximize I with the constraint that the pulse energy is fixed:

$$\int_{-T/2}^{+T/2} f^2(t) dt = J$$

where J is an arbitrary constant.

By combining Equations (A2-1) and (A2-2) we obtain:

$$\begin{aligned} I &= \frac{1}{2\pi} \int_{-\omega_b}^{\omega_b} \left| \int_{-T/2}^{+T/2} f(t) e^{-j\omega t} dt \right|^2 d\omega \\ &= \frac{1}{2\pi} \int_{-T/2}^{+T/2} \int_{-T/2}^{+T/2} f(t_1) f(t_2) \\ &\quad \left[\int_{-\omega_b}^{\omega_b} e^{j\omega(t_1 - t_2)} d\omega \right] dt_1 dt_2 \end{aligned}$$

Carrying out the integration in brackets we have

$$I = \frac{\omega_b}{\pi} \int_{-T/2}^{+T/2} \int_{-T/2}^{+T/2} f(t_1) f(t_2) \frac{\sin \omega_b (t_1 - t_2)}{\omega_b (t_1 - t_2)} dt_1 dt_2 \quad (A2-3)$$

The standard techniques of variational calculus can now be applied to maximize I under the constraint of a fixed value for J as follows. Consider $I + \lambda J$ where λ is a constant.

$$I + \lambda J = \frac{\omega_b}{\pi} \int_{-T/2}^{+T/2} \int_{-T/2}^{+T/2} f(t_1) f(t_2) \frac{\sin \omega_b (t_1 - t_2)}{\omega_b (t_1 - t_2)} dt_1 dt_2 + \lambda \int_{-T/2}^{+T/2} f^2(t_2) dt_2$$

Let $f = f_0 + \alpha g$ where f_0 is the optimum waveform:

$$I + \lambda J = \frac{\omega_b}{\pi} \int_{-T/2}^{+T/2} \int_{-T/2}^{+T/2} [f_0(t_1) + \alpha g(t_1)] [f_0(t_2) + \alpha g(t_2)] \frac{\sin \omega_b (t_1 - t_2)}{\omega_b (t_1 - t_2)} dt_1 dt_2 + \lambda \int_{-T/2}^{+T/2} [f_0(t_2) + \alpha g(t_2)]^2 dt_2$$

Setting $\frac{d(I + \lambda J)}{d\alpha} = 0$ and $\alpha = 0$

$$0 = \frac{\omega_b}{\pi} \int_{-T/2}^{+T/2} \int_{-T/2}^{+T/2} f_0(t_1) g(t_2) \frac{\sin \omega_b (t_1 - t_2)}{\omega_b (t_1 - t_2)} dt_1 dt_2 + \frac{\omega_b}{\pi} \int_{-T/2}^{+T/2} \int_{-T/2}^{+T/2} f_0(t_2) g(t_1) \frac{\sin \omega_b (t_1 - t_2)}{\omega_b (t_1 - t_2)} dt_1 dt_2 + 2\lambda \int_{-T/2}^{+T/2} f_0(t_2) g(t_2) dt_2$$

Since $\frac{\sin \omega_b (t_1 - t_2)}{\omega_b (t_1 - t_2)} = \frac{\sin \omega_b (t_2 - t_1)}{\omega_b (t_2 - t_1)}$:

$$0 = \frac{2\omega_b}{\pi} \int_{-T/2}^{+T/2} \int_{-T/2}^{+T/2} f_0(t_1)g(t_2) \frac{\sin \omega_b (t_1 - t_2)}{\omega_b (t_1 - t_2)} dt_1 dt_2$$

$$+ 2\lambda \int_{-T/2}^{+T/2} f_0(t_2)g(t_2)dt_2$$

$$0 = \int_{-T/2}^{+T/2} g(t_2) \left[\frac{\omega_b}{\pi} \int_{-T/2}^{+T/2} f_0(t_1) \frac{\sin \omega_b (t_1 - t_2)}{\omega_b (t_1 - t_2)} dt_1 \right. \\ \left. + \lambda f_0(t_2) \right] dt_2$$

For this equation to hold for all $g(t)$, the center bracket must be zero.

Hence:

$$\int_{-T/2}^{+T/2} f_0(t_1) \frac{\sin \omega_b (t - t_1)}{\omega_b (t - t_1)} dt_1 = \frac{-\lambda\pi}{\omega_b} f_0(t) \quad (A2-4)$$

The solution for $f_0(t)$ in Equation (A2-4) is the optimum pulse shape in the time interval from $\pm T/2$. The solutions to the integral Equation (A2-4) are prolate spheroidal wave functions.^{7,8} The energy beyond f_b normalized to the total pulse energy can be obtained by combining Equations (A2-4) and (A2-3). We first write Equation (A2-3) as:

$$I = \frac{\omega_b}{\pi} \int_{-T/2}^{+T/2} f_0(t_1) \left[\int_{-T/2}^{+T/2} f_0(t_2) \frac{\sin \omega_b (t_1 - t_2)}{\omega_b (t_1 - t_2)} dt_2 \right] dt_1$$

Then replacing the term in brackets by its equivalent from Equation (A2-4):

$$I = -\lambda \int_{-T/2}^{+T/2} f_0^2(t_1) dt_1 = -\lambda J$$

Thus the desired ratio is:

$$R = \frac{J - I}{J} = \frac{J + \lambda J}{J} = 1 + \lambda$$

The coefficients $(-\lambda)$, are the eigenvalues of the prolate spheroidal functions. The characteristic value, λ_0 , of the zero order function maximizes R . Hence, the ratio of energies, which is equivalent to the ratio of the spectral power beyond f_b to the total power of a PAM pulse train of such pulses, can be determined directly from determination of λ_0 . Values of λ_0 as a function of $T f_b$ can be obtained from tables of spheroidal functions. The resulting ratio as a function of $T f_b$ is shown in Figure A2-1. The shape of an optimum pulse for 40 dB spectral occupancy ($T f_b = 2$) is given in Figure A2-2.

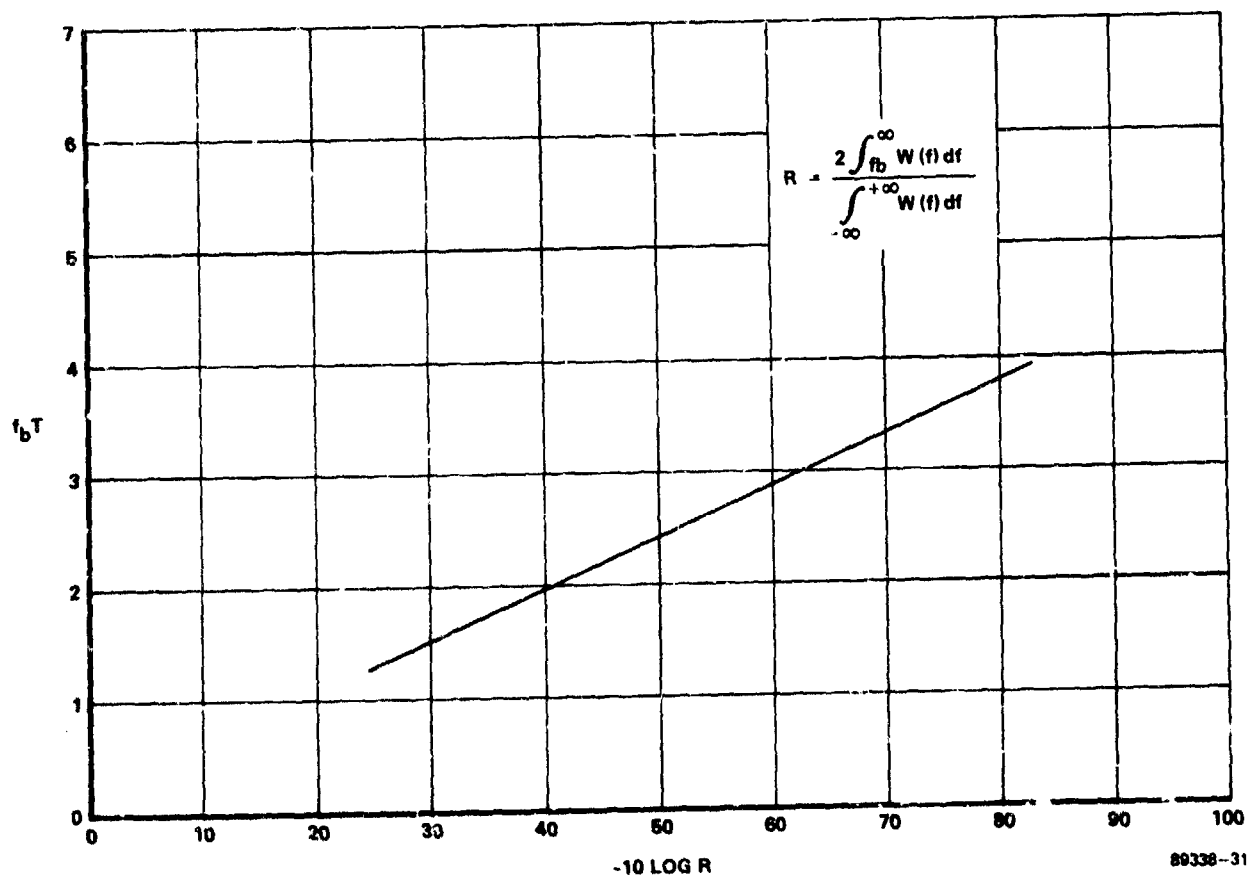


Figure A2-1. Normalized Spectral Occupancy, $f_b T$ Versus R Optimum Pulse

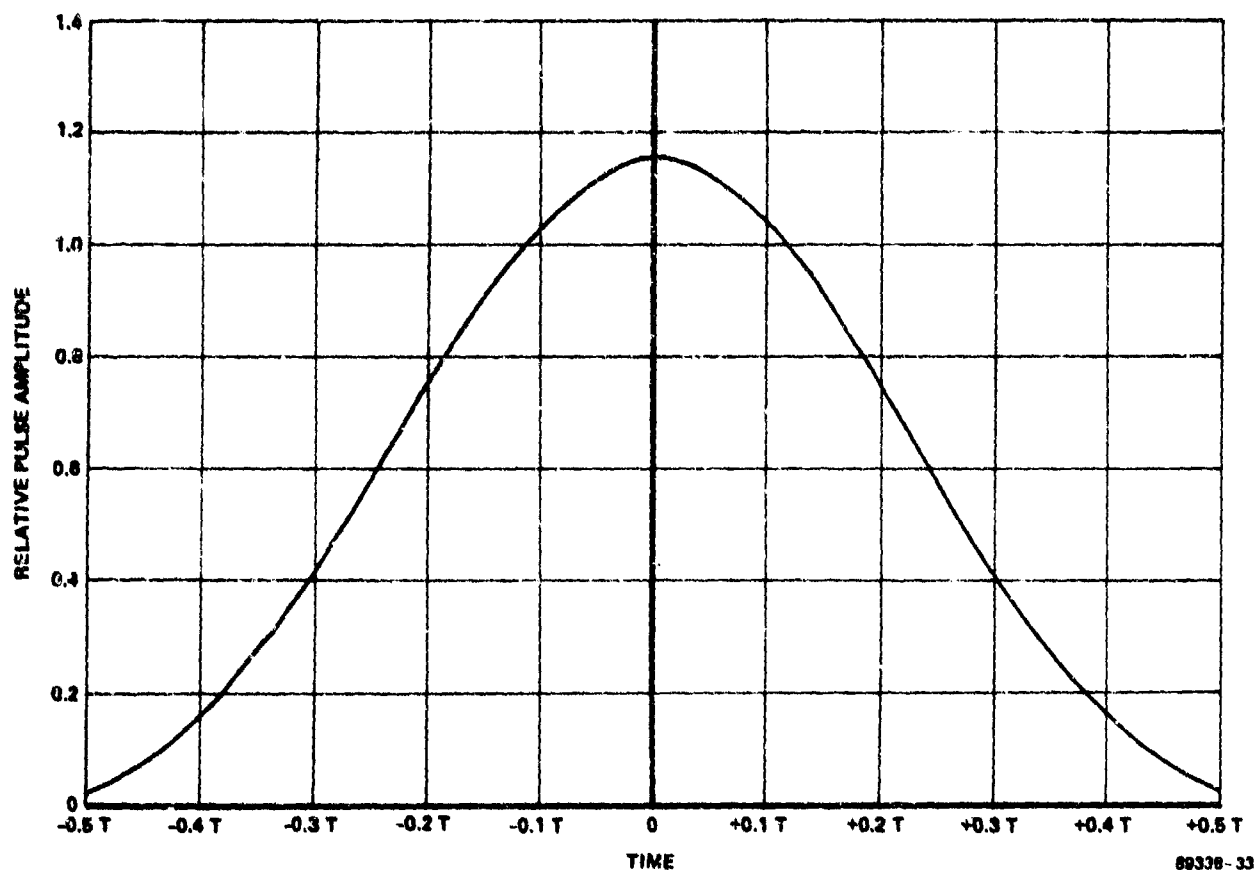


Figure A2-2. Optimum Pulse Shape for 40 dB Spectral Occupancy

We have shown that the truncated prolate spheroidal wave functions are the finite duration PAM pulse shapes for maximally concentrating the spectral power in a selected bandwidth. Figure A2-3 taken from Figure 5 of Reference 7 shows the shape of several of these functions. The optimum finite duration pulse shape to use is one of the shapes truncated to $\pm T/2$. (The functions are even in t .) The function chosen depends upon the bandwidth within which the power is to be maximally concentrated. The parameter c is defined by the relation:

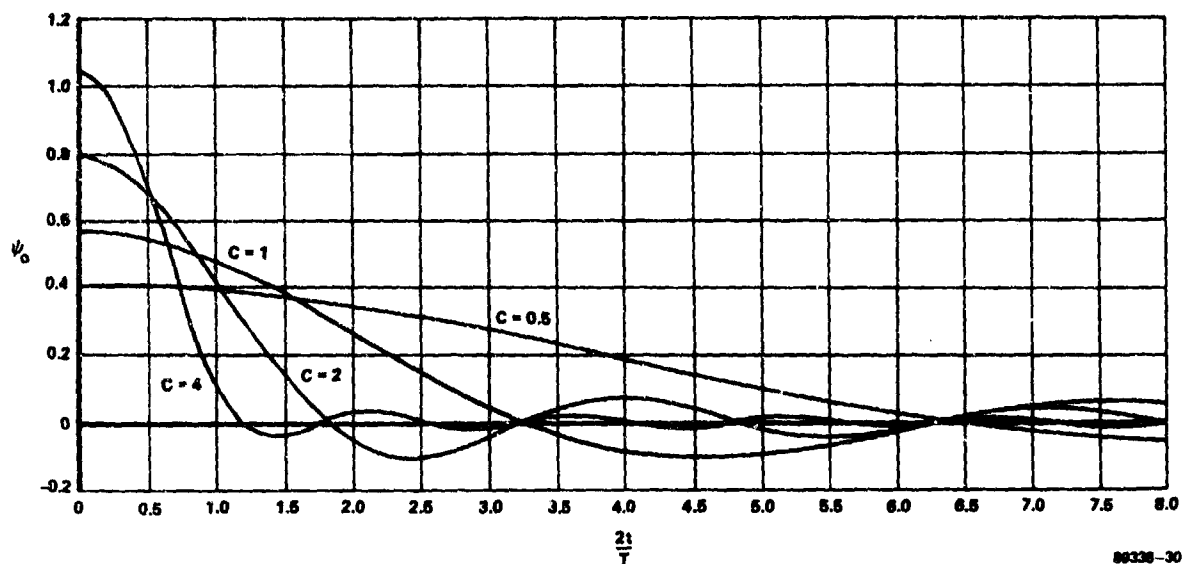


Figure A2-3. Slepian and Pollak's $\psi_0(t)$

$$c = \pi BT \quad (A2-5)$$

where B = the (lowpass) bandwidth within which power is to be maximally concentrated

T = finite duration of the pulse.

There is nothing in the development of these functions as optimal pulse shapes that requires the duration, T , of the pulse to be equal to the symbol time, T_s , in the PAM scheme. If we specify that the pulse last for μ symbol times we have

$$T = \mu T_s \quad (A2-6)$$

(We will not require in general that μ be an integer.) As an example of the implications of the results of Landau, Pollak, and Slepian^{7,8} related to the problem in this study of designing spectrally compact signalling schemes, consider the following. Using Equations (A2-6) in (A2-5) we obtain

$$c = \pi \mu B T_s \quad (A2-7)$$

If we choose B to be $B_A/2$ where B_A is the authorized bandwidth of the microwave link, then Equation (A2-7) becomes

$$c = \frac{\pi}{2} \mu B_A T_s. \quad (A2-8)$$

Equation (A2-8) specifies c (hence a pulse shape from Figure A2-3) of symbol times (μT_s) finite duration which will maximally concentrate signal power in the lowpass band $\pm B_A/2$ (RF bandwidth = B_A). There is no other μT_s finite duration waveshape pulse that will put greater power in the authorized bandwidth. The fraction of total power in band is shown⁷ to be the eigenvalue, $\lambda_0(c)$ associated with the specified prolate spheroidal wave function. Slepian and Pollak⁷ tabulate several of the values of $\lambda_0(c)$ for various c . Thus, for constant c there is a constant percentage power in band. Equation (A2-8) along with the values of $\lambda_0(c)$ allows us to plot the data in Figure A2-4. There, combinations of μ and B_s/B_A (ratio of symbol rate to authorized bandwidth) leading to constant percentage power in band are plotted.

From the data presented in Figure A2-4 one can infer a great deal. For example, if B_s is chosen to equal B_A , then a pulse shape of at least 2.5 symbol times duration must be chosen to place 99.589 percent of total power in the authorized bandwidth. If an optimum pulse shape lasting only a single symbol time is chosen ($B_s = B_A$), then the percent power, p , contained in B_A will certainly be less than 88.056 percent (but more than 57.258 percent). If, on the other hand, the symbol rate is chosen to be $0.4 \times B_A$ then there exists a pulse shape one symbol time long which will make $p = 99.589$ percent and a pulse shape only two symbol times long will make $p > 0.9999$.

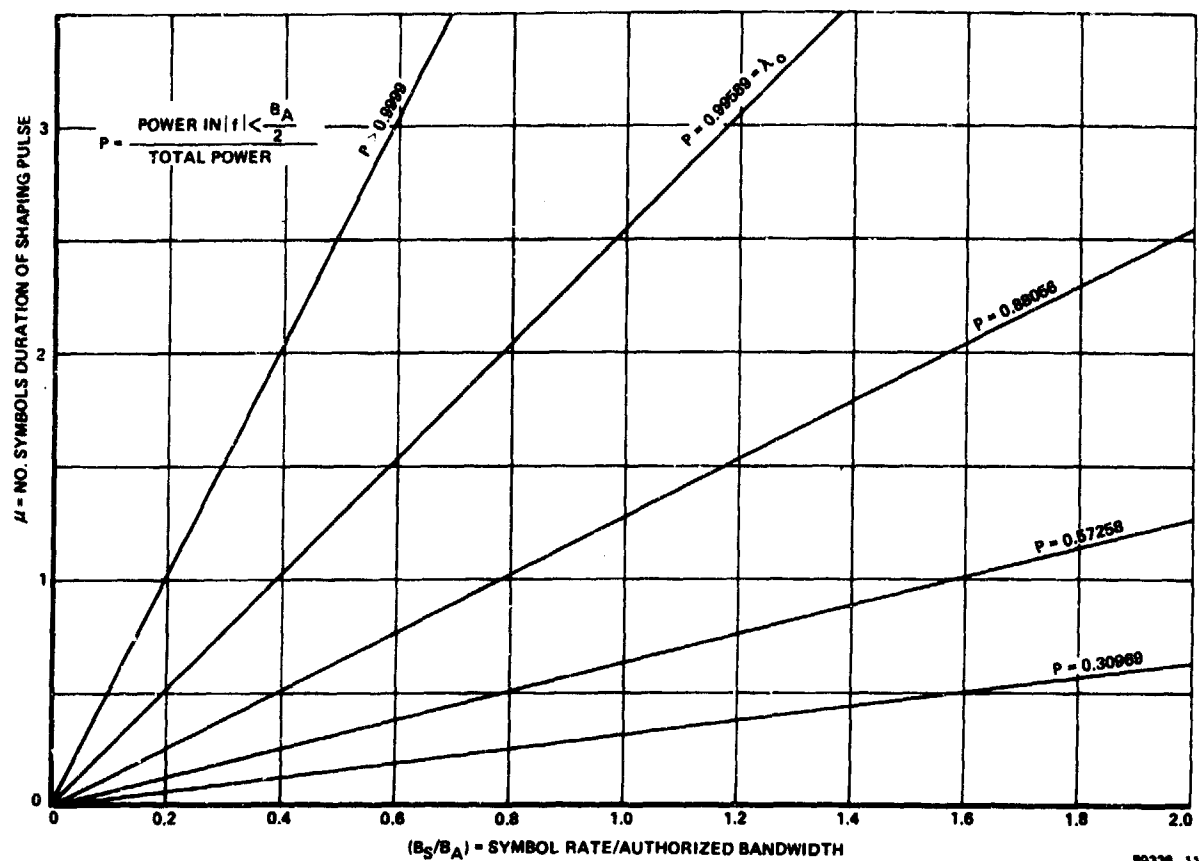


Figure A2-4. μ Versus B_S/B_A for Constant In-Band Power Using Prolate Spheroidal Functions

The data of Figure A2-4 can be presented also as shown in Figure A2-5. Here μ , the length of the pulse in symbol times is held fixed and the minimum possible percentage out-of-band power is plotted versus B_S/B_A .

Admittedly, percent power in-band is not the spectral constraint in this study - FCC 19311 is - but these theoretical bounds for this case should prove useful in guiding the signal design effort to a successful conclusion.

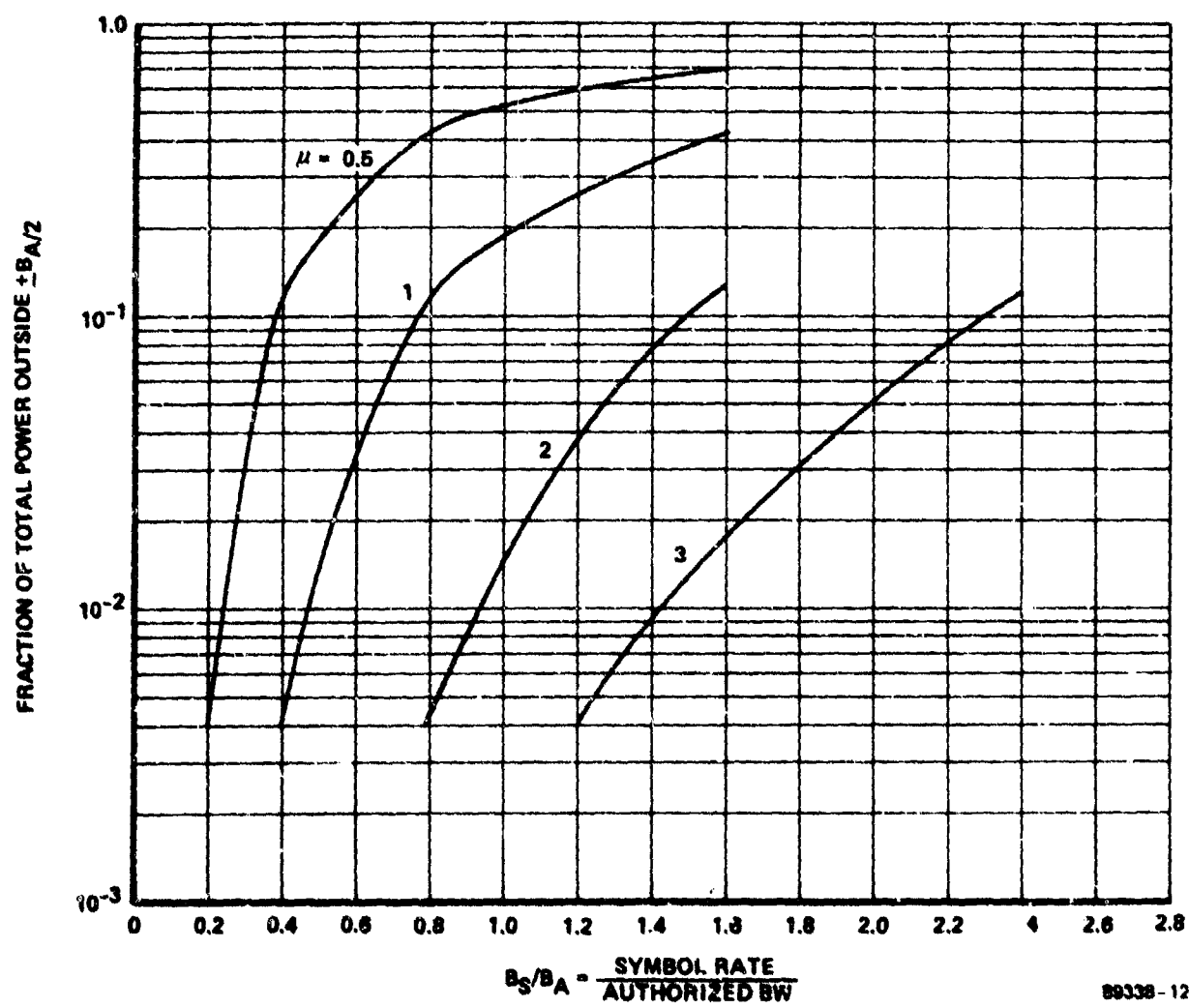


Figure A2-5. Out-of-Band Power Versus B_S/B_A for Constant μ Using Prolate Spheroidal Functions

APPENDIX 3
CODING GAIN FOR HIGH BIT PACKING DENSITY SIGNALLING SCHEMES

APPENDIX 3

CODING GAIN FOR HIGH BIT PACKING DENSITY SIGNALLING SCHEMES

A3.1 Introduction

For the microwave channels of interest in this study, one is generally concerned primarily with the bandwidth-constrained channel communication problem rather than with the power-limited problem. With the microwave channel the problem generally is not with having too low an S/N ratio to support reliable communication. Rather, the concern is with getting a high volume (high bit rate) of traffic through a given bandwidth allocation in such a manner that efficient use is made of the relatively high S/N ratios available.

The problem then on the microwave channels of interest in this study resolves into how to get the highest volume of traffic through a bandwidth-constrained channel while making efficient use of available transmitter power. Generally, then one seeks modulation schemes for those channels which are capable of transmitting at as high as possible a bit rate per Hertz of radiated spectral occupancy (high bit packing density).

A3.2 Channel Capacity

The digital modulation signal design then essentially becomes how to get as many independent (orthogonal) symbols per second through the bandwidth-constrained channel as possible. There are theoretical limits on how many bits of information each of the orthogonal symbols can carry at a given S/N ratio and still obtain arbitrary low error rate. These theoretical limits are referred to as channel capacity bounds and are the result of the work by Shannon².

Figure A3-1 shows plots of channel capacity. These curves plot the maximum possible bits of information carried per transmitted symbol at each S/N ratio on the additive Gaussian noise channel. The S/N

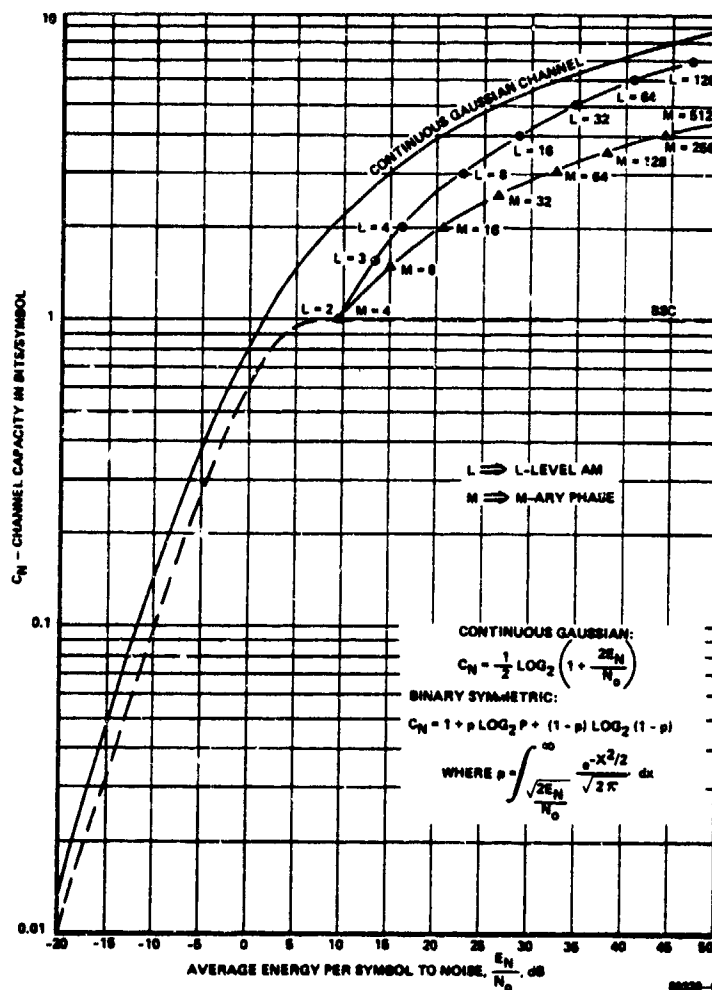


Figure A3-1. Comparison of Capacity Curves With Actual System Performance (Systems Have $P(e) = 10^{-5}$)

ratio plotted is E_n/N_0 which is the average energy per symbol divided by one-sided noise spectral height. E_n/N_0 is therefore S/N ratio in bandwidth equal symbol rate. The continuous Gaussian channel curve is the ultimate limit for unconstrained channel input and output alphabets. The BSC (Binary Symmetric Channel) curve is for binary input and output alphabets. For high bit packing density modulation schemes, we are interested in channel capacities generally above 1-bit/symbol.

We have plotted on Figure A3-1 the performance of L-ary amplitude modulated symbols and M-ary PSK symbols for a 10^{-5} symbol error rate to show their performance relative to the channel capacity

bound. We note that L-ary AM for all L remains within approximately 8 dB of the channel capacity curve while M-ary PSK becomes more inefficient in terms of required E_b/N_0 relative to channel capacity as M increases.

The point in plotting these performances relative to channel capacity is to show that even at high bit packing densities coding gain is available. For L-ary AM the curves show that roughly 8 dB can be had by suitable coding schemes. We are more accustomed to thinking of coding gain in terms of binary transmitted symbols where with code bandspreading we convey less than one information bit per transmitted symbol bit ($C_N < 1\text{-bit/symbol}$). Below we give a simple example of a coding scheme where gain is obtained at an information transfer of 1 bit per transmitted symbol. The concept presented below can be extended to greater bit packing densities in a straightforward manner.

A3.3 One Bit/Symbol Code Example

Suppose one has a transmitter capable of transmitting 4-ary Pulse Amplitude Modulation (PAM). The baseband voltage levels are as shown in Figure A3-2a. If each of the four levels is equally likely the voltages shown produce average energy/symbol = E_s .

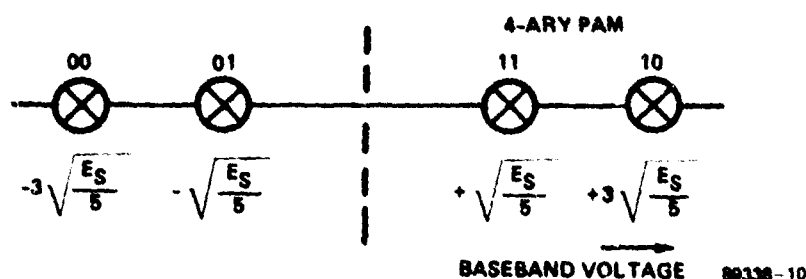
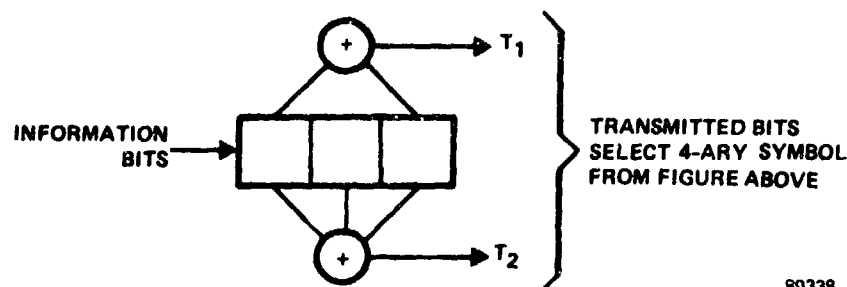


Figure A3-2a. 4-ary PAM Baseband Voltages

In Figure A3-2b we show a constraint length (encoder register length) = 3 rate one-half convolution code. For each information bit inserted into the encoder register, two bits (T_1 and T_2) are produced for channel transmission. What we propose here is to allow T_1 and



89338-10-1

Figure A3-2b. Rate One-Half Constraint Length 3 Convolution Code

T_2 to select one of the four PAM levels of Figure A3-2a to transmit over the channel. Thus, each of the 4-level symbols will convey one information bit to the receiver. E_s in this case will then be equivalent to E_b , the average energy/bit.

The distance structure of the code of Figure A3-2b is such that the minimum distance between two code paths involves two antipodal code branches and one orthogonal coded branch. With the Grey-code encoding of T_1 and T_2 (code branch bits) onto the 4-ary PAM as shown in Figure A3-2a this produces a minimum distance between paths of at least

$$d_{\text{code}}^2 = 2 \left(4 \sqrt{\frac{E_b}{5}} \right)^2 + \left(2 \sqrt{\frac{E_b}{5}} \right)^2 \quad (\text{A3-1})$$

or

$$d_{\text{code}} = 6 \sqrt{\frac{E_b}{5}} \quad (\text{A3-2})$$

For binary PSK, as a standard for comparison, the minimum distance is

$$d_{\text{PSK}} = 2\sqrt{E_b} \quad (\text{A3-3})$$

Comparing Equations (A3-2) and (A3-3) shows the simple coding scheme has a 2.5 dB advantage over binary PSK. Both these schemes are 1-bit/transmitted symbol schemes and would require essentially the same channel bandwidth. The coded scheme would require a constraint length 3 Viterbi decoder with the four branch metrics computed by correlating each received symbol against each of the four possible PAM levels. (As an aside, it can be shown that use of constraint length 7 convolution code will gain 4.5 dB over PSK when employed in the above scheme.)

A3.4 Importance of Considering Coding and Modulation Jointly

The above example can be used to demonstrate the importance of considering the coding and modulation processes jointly. The 4-ary uncoded modulation scheme alone considered above loses approximately 4 dB in terms of E_b/N_0 relative to PSK. The constraint length 3 code gains roughly 1.8 dB on the PSK channel. One might be tempted to conclude on the basis of a cursory examination that the coded scheme described above would lose 2.2 dB relative to PSK when in fact we have shown a gain of 2.5 dB when a mating of code assignments to 4-ary PAM levels is considered.

APPENDIX 4
BIBLIOGRAPHY AND REFERENCES

APPENDIX 4

BIBLIOGRAPHY AND REFERENCES

1. Forney, G. David, Jr., "Maximum-Likelihood Sequence Estimation of Digital Sequences in the Presence of Intersymbol Interference," IEEE Trans. Inform. Theory, Vol. IT-18, May 1972, pp. 363-378.
2. Shannon, C. E., "The Mathematical Theory of Communication," BSTJ, July and October 1948.
3. Hozencraft, J. M. and I. M. Jacobs, Principles of Communication Engineering, Wiley, New York, 1965.
4. Nyquist, H., "Certain Topics in Telegraph Transmission Theory," Trans. AIEE, April 1928.
5. Lucky, R. W., J. Salz, and E. J. Weldon, Jr., Principles of Data Communication, McGraw-Hill, New York, 1968.
6. FCC Docket 19311, Federal Communications Commission, FCC 74-985, 24163, Adopted: September 19, 1974, Released: September 27, 1974.
7. Slepian, D. and H. O. Pollak, "Prolate Spheroidal Wave Functions, Fourier Analysis and Uncertainty-I," BSTJ, January 1961, pp. 43-63.
8. Landau, H. J. and H. O. Pollak, "Prolate Spheroidal Wave Functions, Fourier Analysis and Uncertainty-II," BSTJ, January 1961, pp 65-84.
9. Viterbi, A. J., "Error Bounds for Convolutional Codes and an Asymptotically Optimum Decoding Algorithm," IEEE Trans. Inform. Theory, Vol. IT-13, April 1967, pp. 260-269.
10. Forney, G. David, Jr., "The Viterbi Algorithm," Proc. IEEE, Vol. 61, March 1973, pp. 268-278.
11. Viterbi, A. J., "Convolutional Codes and Their Performance in Communication Systems," IEEE Transactions on Communication Technology, Vol. COM-19, No. 5, October 1971, pp. 751-772.
12. "Broadband Digital Modem," RADC Study by Harris Corporation, Contract Number F30602-74-C-0263, 1975.
13. "Broadband Modem II," RADC Study by Harris Corporation, Contract Number F30602-76-C-0434, 1977.
14. de Buda, R., "Coherent Demodulation of Frequency Shift Keying With Low Deviation Ratio," IEEE Trans. Comm., Vol. COM-20, June 1972, pp. 429-435.
15. Doelz, M. L., and E. H. Heald, "Minimum-Shift Data Communication System," U.S. Patent 2,977,417, March 28, 1961 (assigned to Collins Radio Company).

16. Osborne, William P. and Michael B. Luntz, "Coherent and Noncoherent Detection of CPFSK," IEEE Trans. Comm., Vol. COM-22, August 1974, pp. 1023-1036.
17. Barber, Steve G. and Carl W. Anderson, "Modulation Considerations for the DRS-8 91 Mb/s Digital Radio," IEEE International Conference on Communications, Chicago, June 1977.
18. Brady D. M., "FM-CPSK: Narrowband Digital FM With Coherent Phase Detection," International Conference on Communications, Philadelphia, June 1972.
19. Wood, W. A. H., "Modulation and Filtering Techniques for 3-Bits/Hertz Operation in the 6 GHz Frequency Band," International Conference on Communications, Chicago, June 1977.
20. Smith, J. G., "Spectrally Efficient Modulation," International Conference on Communications, Chicago, June 1977.
21. Hartman, P. R. and E. W. Allen, "Design Considerations for a 3-Bit/Hertz Digital Radio at 6 GHz," International Conference on Communications, Toronto, Canada, June 1978.
22. Simon, M. K., "An MSK Approach to Offset QASK," IEEE Trans. Comm., Vol. COM-24, August 1976, pp. 921-923.
23. Weber, William J., III, Phillip H. Stanton, and Joe T. Sumida, "A Bandwidth Compressive Modulation System Using Multi-Amplitude Minimum Shift Keying (MAMSK)," IEEE Trans. Comm., Vol. COM-26, May 1978, pp. 543-551.
24. Arthurs, E. and H. Dym, "On the Optimum Detection of Digital Signals in the Presence of White Gaussian Noise - A Geometric Interpretation and a Study of Three Basic Data Transmission Systems," IEEE Trans. on Comm. Systems, December 1962, pp. 336-372.
25. Slepian, D. and H. O. Pollak, "Prolate Spheroidal Wave Functions, Fourier Analysis and Uncertainty - I," BSTJ, January 1961, pp. 43-63.
26. Landau H. J. and H. O. Pollak, "Prolate Spheroidal Wave Functions, Fourier Analysis and Uncertainty - II," BSTJ, January 1961, pp. 65-84.
27. "Phase Distortion Study," Final Report, Contract Number DAAB07-76-C-0001, for U.S. Army Satellite Communications Agency, by Magnavox Government and Industrial Electronics Company Advanced Products Division, August 1976.
28. Cox, D. C., "Linear Amplification with Nonlinear Components," IEEE Trans. Commun., Vol. COM-22.
29. Cox, D. C. and R. P. Leck, "Component Signal Separation and Recombination for Linear Amplification with Nonlinear Components," IEEE Trans. Commun., Vol. COM-23, pp. 1281-1287.

30. Cox, D. C. and R. P. Leck, "A VHF Implementation of a LINC Amplifier," IEEE Trans. Commun., pp. 1018-1022.
31. Kunz, W. E., J. J. Foster, and R. F. Lazzarini, "Traveling Wave Tube Amplifier Characteristics for Communications," The Microwave Journal, March 1967.
32. Berman, A. L., and C. E. Mahle, "Nonlinear Phase Shift in Traveling-Wave Tubes as Applied to Multiple Access Communications Satellites," IEEE Trans. on Comm. Tech., Vol. COM-18, No. 1, February 1970.
33. CNR, Inc., "Line-of-Sight Techniques Investigation," RADC-TR-74-330, (AD#A006104), Final Report, January 1975.
34. "Experimental Linear Solid-State Communications Amplifier," Ford Aerospace and Communications Corporation, WDL Division, Technical Report, RADC Contract F30602-76-C-0271, 15 July 1977.
35. Kaplan, Wilfred, Advanced Calculus, Second Edition, Section 2-21, Addison-Wesley Publishing Co.; Reading, Mass., 1973, p. 186.
36. Harris LMT Design Plan Document
37. Austin, M. E., "Decision Feedback Equalization for Digital Communication Over Dispersive Channels," Tech. Report 461, Res. Lab. Electronics, MIT, August 11, 1967.